Role of Disintegrin and Metalloproteinase 17 (ADAM17) in Hypertension and Thoracic Aortic Aneurysm

by

Mengcheng Shen

A dissertation submitted in partial fulfillment of the requirements for the degree of

Doctor of Philosophy

Department of Physiology

University of Alberta

ABSTRACT

Hypertension is a major risk factor for cardiovascular complications such as stroke, myocardial infarction, heart failure, and renal failure, and therefore is an enormous healthcare burden worldwide. The renin-angiotensin system (RAS) is an essential regulator of blood pressure homeostasis, and angiotensin II (Ang II), the primary effector peptide of the RAS, plays a crucial role in acute and long-term regulation of blood pressure predominantly through the Ang II receptor type I (AT1). Although blockade of the RAS has been a mainstay in the treatment for hypertension and its complications, novel candidates in mediating the Ang II-induced hypertension and end-organ damage continue to be discovered.

Thoracic aortic aneurysm (TAA), another vascular complication, is a permanent dilation and structural weakening of the thoracic aorta that predisposes to the fatal consequences of aortic dissection or rupture. Although efforts have been devoted to determining the molecular and pathophysiological characteristics of TAA, the underlying mechanisms for TAA initiation and development are still largely unknown. Currently, there is no treatment available for this disease, and surgical repair is the only option to treat advanced TAA.

A disintegrin and metalloproteinase-17 (ADAM17) is a membrane-bound protease that proteolytically processes a variety of multifunctional cell surface molecules to regulate cell growth, proliferation, migration, differentiation, apoptosis, angiogenesis and neovascularization, inflammation, ECM remodeling, inflammatory cell adhesion, recruitment and transmigration, and vascular barrier integrity.

The research presented in this dissertation identified the role of smooth muscle cell (SMC)- and endothelial cell (EC)-specific ADAM17 in Ang II-induced hypertension and end-organ damage, as well as in the pathogenesis of TAA. *In vitro, Adam17*-deficiency did not alter the cell morphology or basal levels of SMC contractile proteins, but significantly suppressed Ang II-induced proliferation and migration in these cells. By infusing Ang II in SMC-*Adam17*-intact and SMC-*Adam17*-deficient mice for 2 and 4 weeks, we observed a transient protection of Ang II-induced hypertension, cardiac and renal hypertrophy and fibrosis in SMC-*Adam17*-deficient mice, which were abolished with prolonged Ang II infusion. *Ex vivo* vascular function and compliance assessed in mesenteric arteries were comparable between genotypes. Mechanistic studies showed that EGFR signaling from other vascular cell types (e.g., fibroblasts) might compensate for the loss of biological functions of ADAM17 in SMCs.

An optimized periadventitial elastase-injury induced TAA model was used to explore the role of vascular ADAM17 in the progression of TAA. Both SMC- and EC-deficiency of *Adam17* mitigated elastase-induced TAA, however, *in vitro* studies revealed that ADAM17 in SMCs and ECs played distinct roles in the pathogenesis of TAA. In response to elastase-induced injury, *Adam17*-deficiency in SMCs prevented contractile-to-synthetic phenotypic switching in these cells, thereby preventing perivascular fibrosis, inflammation, and adverse aortic remodeling. In comparison, *Adam17*-deficiency in ECs protected the integrity of the intimal barrier by preserving the junction protein complex, which consequently led to the suppression of inflammatory cell infiltration into the aortic wall. In line with the findings observed in genetically modified mice, an ADAM17-selective inhibitor showed protective effects on TAA formation as well as growth.

In summary, the research described in this dissertation demonstrated that *Adam17*-deficiency in SMCs is not sufficient to suppress Ang II-induced hypertension and end-organ damage. Whereas in TAA, ADAM17 plays cell-specific functions in disease progression by promoting pathological remodeling of SMC and impairing the integrity of intimal EC barrier. The protective role of genetic and pharmacological inhibition of ADAM17 in attenuating the progression of TAA highlighted the unique position of this protease as a potential treatment target for TAA.

PREFACE

All of the work presented henceforth was conducted in Dr. Zamaneh Kassiri's laboratory in 474 Heritage Medical Research Center, University of Alberta, Edmonton, AB, Canada. Non-diseased human ascending aortas were procured from donors through the Human Organ Procurement and Exchange program (HOPE) program at the University of Alberta (credit: Dr. Gavin Y. Oudit). Human aneurysmal specimens were procured from the proximal ascending aorta of patients undergoing prophylactic resection as a consequence of bicuspid aortic valve-associated aortopathy at the University of Calgary (credit: Dr. Paul W.M. Fedak). Informed consent was obtained from these patients after Institutional Review Board approval (REB17-0207). The study protocols were approved by the Human Research Ethics Review Process (HERO) at the University of Alberta. All animal procedures were performed according to the ARRIVE (Animal Research: Reporting of *in vivo* Experiments) guidelines, and according to the guidelines of Animal Care and Use Committee (ACUC) at the University of Alberta and the Canadian Council of Animal Care (CCAC). The protocol number for animal studies is AUP1273.

The technical protocols (i.e., primary human and mouse aortic smooth muscle cell isolation, and periadventitial elastase-injury induced thoracic aortic aneurysm) referred to in Chapter 2 were established or optimized by myself in Dr. Z. Kassiri's laboratory. Dr. Jude Morton helped with the *ex vivo* pressure myography experiments. Dr. Xiuhua Wang conducted all the quantitative TaqMan real-time PCR experiments. The plasma concentrations of ADAM17 inhibitor PF-548 were measured by technicians of *Pfizer*, Inc.

A version of Chapter 3 of this dissertation has been published as *Shen M, Morton J, Davidge ST, and Kassiri Z. Loss of smooth muscle cell disintegrin and metalloproteinase 17 transiently suppresses angiotensin II-induced hypertension and end-organ damage. Journal of Molecular and Cellular Cardiology. 2017;103:11-21.* I was responsible for all major areas of concept formation, data collection, and analysis, as well as the majority of manuscript composition. Dr. J. Morton helped with the *ex vivo* pressure myography experiments. Dr. S.T. Davidge contributed to manuscript edits. Dr. Z. Kassiri was the supervisory author and was involved with concept formation and manuscript composition.

A version of Chapter 4 of this dissertation has been published as *Shen M, Hu M, Fedak PWM, Oudit GY, and Kassiri Z. Cell-specific functions of ADAM17 regulate the progression of thoracic aortic aneurysm. Circulation Research. 2018* (doi: 10.1161/CIRCRESAHA.118.313181). I was responsible for all major areas of concept formation, data collection, and analysis, as well as the majority of manuscript composition. M. Hu helped with immunoblotting experiments. Drs. P.W.M. Fedak and G.Y. Oudit provided human aorta

specimens, contributed to data interpretation, and edited the manuscript. Dr. Z. Kassiri was the supervisory author and was involved with concept formation and manuscript composition.

DEDICATIONS

I dedicate this dissertation to my parents Bonian Shen and Zhifeng Liu, who offered me unconditional love and support through the long journey.

ACKNOWLEDGMENTS

First and foremost I want to express my deepest appreciation and gratitude to my supervisor and mentor Dr. Zamaneh Kassiri. I appreciate all her contributions of time, ideas, patience, and funding to make my Ph.D. experience productive and stimulating. The joy and enthusiasm she has for her research were contagious and motivational for me. Without her continuous support, I would never be able to get the chance to learn such diverse and challenging techniques in the laboratory, which I believe will make me stand out of the most in my future career. I am also thankful for the excellent example she has provided as a successful scientist and professor.

I want to express my greatest thanks to my supervisory committee members, Drs. Sandra T. Davidge and Michael Sean McMurtry, each of whom had provided patient advice and guidance throughout my research process. Importantly, both of them were not only unwavering supportive in a scientific sense but also shared with me their valuable insights into the importance of being an optimistic, independent, adventurous, observant, and humble person. Dr. Davidge provided moral support that was paramount in helping motivate me to strive for glitches throughout my Ph.D. program. Dr. McMurtry always encouraged me to evaluate my current position in life, my goals, and the direction I should be headed to attain them. I would also like to thank Dr. Gavin Y. Oudit for the platform he provided in his laboratory, without his help, we would never get the chance to utilize the delicate radiotelemetry technique to complete my first project. It was definitely a great achievement and joy for me to perform such as a technically demanding surgery independently.

I also want to express my deepest gratitude and appreciation to my master's supervisor Dr. Qiang Liu. His mentorship, both in science and life, has helped shape me into the person I am today. It is always helpful to release my pressure by recalling the old days when I was working in his laboratory. I still remember all the efforts he made to make sure I was competitive for the China Scholarship Council (CSC) studentship, which finally made it possible for me to join the University of Alberta to pursue my Ph.D. degree.

The members of the Kassiri group and the Oudit group have contributed immensely to my personal and professional time at the University of Alberta. The group has been a source of friendship as well as good advice and collaboration. I am especially grateful for Dr. Abhijit Takawale's company and support for almost four years. We have now become lifetime friends and

always share ideas and recent advances in cardiovascular research field with each other even after he moved to Montreal Heart Institute for post-doctoral training. I also want to thank all other past and present group members that I have had the pleasure to work with or alongside, you will definitely be a beautiful piece of memory in my entire life. In truth, I could not have achieved my current level of success without a strong support group.

I would like to sincerely thank Dr. Rabban Mangat, who helped me a lot throughout my Ph.D. program. Without her tremendous encouragement and support and constructive advice, I could never make the achievement I have made today.

I would like to extend a special thanks to the Cardiovascular Research Center (CVRC) for their technical assistance. I would also like to gratefully acknowledge the financial support provided by the China Scholarship Council (CSC) and Motyl Graduate Studentship in Cardiac Sciences.

Most importantly, I would like to thank my family for all their unconditional love, encouragement, and understanding. For my parents who raised me with a love of science and supported me in all my pursuits. For my siblings who took great care of my parents when I was far away from home and pursuing my Ph.D. degree. I would like to share the joy of this journey with my family. Thank you so much!

Mengcheng Shen

University of Alberta

April 5th, 2018

TABLE OF CONTENTS

LIST OF TABLES

LIST OF FIGURES

LIST OF ABBREVIATIONS

AAA	Abdominal aortic aneurysm
ACE2	Angiotensin-converting enzyme-2
ACEi	Angiotensin-converting enzyme inhibitor
ACTA2	α-smooth muscle actin
ADAM	A disintegrin and metalloproteinase
ADAM-TS	A disintegrin and metalloproteinase with thrombospondin motif
ALCAM	Activated leukocyte cell adhesion molecule
AMPKAA2	AMPK-activate alpha-2
Ang II	Angiotensin II
ANGPTL4	Angiopoietin-like-4
APLP	APP-like protein
ApoE	Apolipoprotein E
APP	Amyloid precursor protein
ARB	Angiotensin receptor blocker
AT1 & AT2	Angiotensin receptors type1 and type 2
ATCC	American type culture collection
BACE1	β-secretase-1
BAPN	β-aminopropionitrile
BAV	Bicuspid aortic valve
BSA	Bovine serum albumin
BW	Body weight
CCL	(C-C motif) ligand
CCL4L1	C-C chemokine ligand 4-like-1
CCR	C-C chemokine receptor type
CCRC	Cumulative concentration-response curve
CHL1	Close homologue of L1
c-Met	Met proto-oncogene/hepatocytes growth factor receptor
CNTN3	Contactin-3
PKC	Protein kinase C
CSF1	Macrophage colony-stimulating factor-1
CX3CL	Chemokine (C-X3-C motif) ligand
CXCL	(C-X-C motif) ligand
CXCR	C-X-C chemokine receptor
DAB2IP	DAB2 interacting protein
DAPI	4′,6-Diamidino-2-phenylindole dihydrochloride
DDR1	Discoidin domain receptor-1
DLL1	Delta-like-1
DSG2	Desmoglein-2
EC	Endothelial cell
ECM	Extracellular matrix
EGF	Epidermal growth factor
EGFR	Epidermal growth factor receptor
ELK1	E26 ETS-like transcription factor-1
EMT	Epithelial-to-mesenchymal transformation

LIST OF ABBREVIATIONS

eNOS	Endothelial nitric oxide synthases
EpCAM	Epithelial cell adhesion molecule
EPCR	Endothelial protein C receptor
EphA3/B2	Ephrin receptor-A3/B2
ER	Endoplasmic reticulum
ErbB	Avian erythroblastosis oncogene B
ERK	Extracellular signal-regulated kinase
FasL	Fas ligand
FBN1	Fibrillin-1
FGF	Fibroblast growth factor
FGFR2	Fibroblast growth factor receptor-2
FLT1	Fms related tyrosine kinase-1
FLT3L	Fms-related tyrosine kinase-3 ligand
FSTL3	Follistatin-like-3
FCGBP	Fc fragment binding protein
GAL3ST4	Gal-3-sulfotransferase-4
GATA	GATA-binding protein
G-CSF	Granulocyte colony-stimulating factor
GFPT2	Glutamine-fructose-6-phosphate transaminase-2
GH	Growth hormone
GHR	Growth hormone receptor
GM-CSF	Granulocyte-macrophage colony-stimulating factor
GPC1	Glypican-1
GPCR	G-protein coupled receptor
GPIbα	Platelet glycoprotein Ib alpha chain precursor
GPV & GPVI	Glycoproteins V & VI
HAoEC	Human aortic endothelial cell
HB-EGF	Heparin-binding epidermal growth factor-like growth factor
HDL	High-density lipoprotein
HERP1	HES-related repressor protein-1
HILPDA	hypoxia-inducible lipid droplet-associated protein
HOPE	Human organ procurement and exchange
HPRT	Hypoxanthine-guanine phosphoribosyltransferase
HVR	Hypervariable region
ICAM1	Intercellular adhesion molecule-1
IFNγ	Interferon-gamma
IGF	Insulin-like growth factor
IGF2R	Insulin-like growth factor-2 receptor
IGFBP	Insulin-like growth factor-binding protein
IL	Interleukin
IL-1RII	Interleukin-1 receptor II
IL1RN	Interleukin 1 receptor antagonist
IL6R	Interleukin-6 receptor
iRhom 2	Inactive rhomboid-2

LIST OF ABBREVIATIONS

JAM-A	Junctional adhesion molecule-A
JNK	c-Jun N-terminal kinase
KL-1/2	Kit ligand-1/2
KLF4	Krüppel-like factor-4
L1CAM	L1 cell adhesion molecule
LAG3	Lymphocyte activation gene-3
LAR	Leukocyte common antigen-related
LDLR	Low-density lipoprotein receptor
LFA1	Lymphocyte function-associated antigen-1
LOX	Lysyl oxidase
LOX1	Lectin-like oxidized low-density lipoprotein receptor-1
LPA	Lipoprotein (A)
LPS	Lipopolysaccharide
LRP1	LDL receptor-related protein-1
LV	Left ventricle
LYPD3	Ly6/PLAUR domain-containing protein-3
MAPK	Mitogen-activated protein kinase
Mch	Methylcholine
M-CSF	Macrophage colony-stimulating factor
M-CSFR	Macrophage colony-stimulating factor-1 receptor
MDC	Metalloproteinase disintegrin cysteine-rich
MFAP5	Microfibril-associated protein-5
MI	Myocardial infarction
miRNA	MicroRNA
MMP	Matrix metalloproteinase
mRNA	Messenger RNA
MT1-MMP	Membrane-bound MMP type I
MYH11	Myosin heavy chain-11
MYLK	Myosin light chain kinase
MAPK	Mitogen-activated protein kinase
Mch	Methacholine
M-CSF	Macrophage colony-stimulating factor
M-CSFR	Macrophage colony-stimulating factor-1 receptor
MDC	Metalloproteinase disintegrin cysteine-rich
MFAP5	Microfibril-associated protein-5
MI	Myocardial infarction
miRNA	MicroRNA
MMP	Matrix metalloproteinase
mRNA	Messenger RNA
MT1-MMP	Membrane-bound MMP type I
MYH11	Myosin heavy chain-11
MYLK	Myosin light chain kinase
NCAM	Neural cell adhesion molecule
NgR	Nogo-66 receptor

LIST OF ABBREVIATIONS

NOS	Nitric oxide synthase
Nox4	Nicotinamide adenine dinucleotide phosphate oxidase-4
NPR	Neuronal pentraxin receptor
NRG	Neuregulin
OCT4	Octamer-binding transcriptional factor-4
OCT	Optimal cutting temperature
p55/p75 TNFR	p55/p75 tumor necrosis factor receptor
p75NTR	p75 neurotrophin receptor
PAI-1	Plasminogen activator inhibitor type I
PAP	Plasmin-antiplasmin complexes
PAR1	Protease-activated receptor-1
PBS	Phosphate-buffered saline
Pcdhγ	gamma-Protocadherins
PDGF	Platelet-derived growth factor
PE	Phenylephrine
PIIINP	Aminoterminal propeptide of type III procollagen
PICP	Carboxyterminal propeptide of type I procollagen
PLAP	Placental leucine aminopeptidase
PPARγ	Peroxisome proliferator-activated receptor-gamma
Pref1	Preadipocyte factor-1
PRKG1	cGMP-dependent protein kinase type 1
PrPc	Cellular prion protein
PSGL1	P-selectin glycoprotein ligand-1
PSR	Picrosirius red
PSS	Physiological saline solution
PTP	Protein tyrosine phosphatase
Ptprz	Protein tyrosine phosphatase receptor type z
PVDF	Polyvinyl difluoride
RECK	Reversion-inducing-cysteine-rich protein with kazal motif
RIP	Regulated intramembrane proteolysis
Robo	Roundabout guidance receptor
ROS	Reactive oxygen species
RPTPκ	Receptor-like protein tyrosine phosphatase kappa
RT-PCR	Reverse transcription polymerase chain reaction
SCF	Stem cell factor
SDS	Sodium dodecyl sulfate
SH3	Src homology-3 domain
SHPS1	SH2 domain-containing protein tyrosine phosphatase substrate-1
siRNA	Small interfering RNA
SMC	Smooth muscle cell
SM-MHC11	Smooth muscle myosin heavy chain-11
SNP	Single nucleotide polymorphism
SorLA1	Sorting protein-related receptor containing LDLR Class A repeats-1
sPLA2-X	Group X secretory phospholipase A2

LIST OF ABBREVIATIONS

SRPX2	Sushi repeat protein X-linked-2
STAT	Signal transducer and activator of transcription
STC1	Stanniocalcin-1
TAA	Thoracic aortic aneurysm
TACE	Tumor necrosis factor-alpha converting enzyme
TBST	Tris-buffered saline with Tween® 20
TGFα/β	Transforming growth factor alpha/beta
TGFR	Transforming growth factor receptor
TIM3	T cell immunoglobulin and mucin domain-3
TIMP	Tissue inhibitor of matrix metalloproteinase
TLR2/4	Toll-like receptors-2/4
TMEFF2	Tomoregulin-2
TNFα	Tumor necrosis factor-alpha
TNFR	Tumor necrosis factor receptor
tPA	Tissue plasminogen activator
TRANCE	TNF-related activation-induced cytokine
TREM2	Triggering receptor expressed in myeloid cells-2
TrkA	Tropomyosin receptor kinase A
TSP1	Thrombospondin-1
TUNEL	Terminal deoxynucleotidyl transferase (TdT) dUTPNick-End Labeling
uPA	Urokinase plasminogen activator
VCAM1	Vascular cell adhesion molecule-1
VCC	Vibrio cholera cytolysin
VE-cadherin	Vascular endothelial-cadherin
VEGFA	Vascular endothelial growth factor A
VEGFR	Vascular endothelial growth factor receptor
VVG	Verhoeff-van gieson

CHAPTER 1

INTRODUCTION

1.1. Prologue

A disintegrin and metalloprotease-17 (ADAM17) is a type I membrane-bound protease that can proteolytically activate a diverse array of multifunctional cell surface substrates by cleavage of their extracellular domains. Since ADAM cleaves a great number of disease-relevant substrates, such as cytokines, chemokines, adhesion molecules, growth factors and/or their receptors, it is not surprising that ADAM17 is implicated in numerous human diseases including cancer, heart diseases, rheumatoid arthritis, atherosclerosis, diabetes, renal fibrosis, and Alzheimer's disease (1-4). As such, ADAM17 has become an emerging central regulator that may be actively involved in the pathogenesis of different types of diseases, and is a promising target for future treatments (5, 6). However, the role of ADAM17 in diseases of the cardiovascular system remains underexplored.

Hypertension is the most important risk factor involved in almost all different cardiovascular and renal diseases, including cardiac hypertrophy, valvular heart diseases, cardiac arrhythmia, coronary diseases, cerebral stroke, aortic aneurysm, and renal failure (7). Although blood pressure-lowering drugs can effectively alleviate hypertension-associated morbidity and mortality, ongoing effort is continuously being devoted to uncovering novel pathogenic mechanisms of hypertension. It is because the cause of hypertension remains elusive, and a thorough understanding of the etiologies of hypertension will provide us a clearer picture of how to treat hypertension and its complications more efficiently and effectively with minimal side effects. Aortic aneurysm, another vascular complication, is a pathological dilation and structural destruction of the aorta that predisposes to the potentially fatal consequence of aortic rupture. Due to the present lack of an in-depth understanding of the mechanisms involved in the initiation and progression of aortic aneurysm, no pharmacological therapy has been validated through double-blinded randomized clinical trials to limit aneurysm growth or rupture.

Since the physiological and pathological roles of ADAM17 in health and diseases are very complex and highly dependent on the cellular context (8), this literature review will discuss how dysregulated ADAM17 activity may affect the pathogenesis of different types of cardiovascular diseases with special focuses on hypertension and aortic aneurysm. Firstly, the biological functions and categorization of different types of proteases will be briefly outlined. Secondly, a thorough comparison of the differences and similarities of the structures, functions of major domains, and

mechanisms for substrate selectivity, recognition, and activity regulation will be conducted between ADAM17 and its relatives within the ADAM protease family. Thirdly, the so far identified substrates for ADAMs, the developmental phenotypes of somatic ADAM knockout mice and cell-specific *Adam17* knockout mic will be reviewed. Fourthly, recent advances on the role of ADAM17 dysregulation in the onset and/or progression of different cardiovascular diseases will be discussed. Finally, different types of ADAM17 inhibitors that are being tested in preclinical studies and clinical trials will be summarized.

1.2. General biological functions and categorization of proteases

Proteases are a large family of enzymes consisting of 589 members in humans, 673 in mice, and 659 in rats (9). In last few decades, the concepts of proteases have extensively evolved. Although these enzymes were originally recognized as the central executioners that are merely implicated in non-specific dietary proteins catabolism into small peptides and amino acids. It has now been well appreciated that proteases regulate multiple essential biological processes, such as DNA replication, cell cycle progression, cell proliferation, migration and differentiation, morphogenesis and tissue remodeling, immunity, fertilization, neural development, angiogenesis, wound healing, hemostasis, and apoptosis, through proteolytic cleavage of various substrates (10). Conversely, failure in regulation of these proteases underlines the pathogenesis and/or progression of diverse human diseases, including but not limited to inflammatory diseases (e.g., rheumatoid arthritis), cancer (e.g., breast cancer), neurodegenerative diseases (e.g., Alzheimer's disease), and cardiovascular diseases (e.g., cardiac hypertrophy and atherosclerosis) (11).

Proteases can be divided into five classes, namely aspartyl proteases, cysteine proteases, metalloproteases, serine proteases, and threonine proteases based on their mechanisms of catalysis (12, 13). **Figure 1.1** is an illustration of the complete set of proteases from mouse, rat and human origins that are categorized into five catalytic classes as mentioned above. A more comprehensive comparison of the differences between human and mouse proteases is available from the Degradome Database (http://degradome.uniovi.es/hmd.html) generated by The Lopez-Otin Laboratory (9).

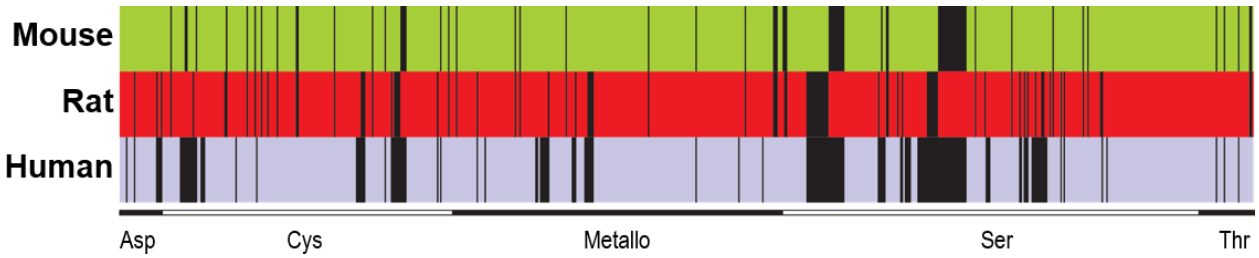

Figure 1.1 A global view of the proteases from mouse, rat, and human origins. The proteases from each species are categorized into five catalytic classes: aspartyl proteases (Asp), cysteine proteases (Cys), metalloproteases (Metallo), serine proteases (Ser), and threonine proteases (Thr). Proteases absent in any species are shown as black bars. The figure is adapted from Puente and Lopez-Otin (12).

Metalloproteases are the most abundant class of proteases that can be further classified into three heterogeneous subfamilies based on their structure and sequence homology, including matrix metalloproteases (MMPs), a disintegrin and metalloproteases (ADAMs) and ADAMs with a thrombospondin domain (ADAM-TSs). While MMPs have been extensively explored in various pathologies including cardiovascular diseases (14-18), the physiological and pathological functions of ADAMs and ADAM-TSs in the cardiovascular system have only started to be investigated in recent years, and their importance as potential therapeutic targets for various cardiovascular diseases is starting to become evident.

1.3. General features and phylogeny of ADAMs

The first ADAMs to be discovered were the two subunits of the heterodimeric sperm protein fertilin (which were renamed as ADAMs 1 and 2) (19, 20). Owing to the advances in genome sequencing, the ADAM family has grown considerably since its constitution in 1995 (21). To date, 40 ADAM genes have been identified in the mammalian genome, of which 34 genes encoding rat ADAMs, 37 genes (8 of them have only been found to date as predictions) encoding mouse ADAMs, and 27 genes (including seven pseudogenes) encoding human ADAMs (**Table 1.1**) (12). ADAMs 1, 3-6, and 25 are pseudogenes in the human genome but are active in mouse and rat genomes (13). A similar scenario is also observed in rats, whose genome lacks three mouse ADAM orthologs (i.e., ADAMs 6B, 38, and 39) that are functional in mice (12). Moreover, ADAM20 is exclusively expressed in the human genome and ADAM6 in the mouse genome, respectively (13).

Based on their catalytic activity, ADAMs can be categorized into two major subfamilies: those contain a catalytic site signature motif (HEXGHXXGXXHD) (X being any amino acid residue, the same as below) in their metalloproteinase domain and therefore are proteolytically active (22);

and those are proteolytically inactive and may be involved in protein folding and protein-protein interactions through their adhesive properties (23). ADAMs 8-10, 12, 15, 17, 19, and 33 are found to be capable of cleaving a variety of membrane-bound molecules, and are expressed broadly in somatic tissues (12, 24). ADAMs 1-3, 5, 18, 24-26, and 32 are solely or predominantly expressed in the mammalian male reproductive organs (e.g., testis) that are involved in spermatogenesis and/or fertilization (25), whereas ADAMs 11, 22, and 23 are mainly expressed in the central nervous system to function as receptors for the secreted leucine-rich glioma inactivated proteins to regulate synaptic transmission (26, 27). A subgroup of ADAMs called testases are exclusively expressed in rodent testis for reproduction, with 7 putative testase genes identified in the rat genome and 9 in the mouse genome (**Table 1.1**) (12).

1.4. Structure of ADAMs

ADAMs, originally named the metalloproteinase disintegrin cysteine-rich (MDC) (28), are Zn^{2+}-dependent, type I transmembrane proteins with homology to snake venom integrin ligands that belong to the adamalysin metalloproteinase family. Adamalysins and the other three Zn^{2+}-dependent metalloprotease families namely astacins, matrixins, and serralysins form the metzincin superfamily (29). As classified based on their highly conserved structural homology, most ADAMs are composed of (from N-terminus to C-terminus): a peptidase unit followed by a metalloprotease domain, a disintegrin domain, a cysteine-rich region, an EGF-like module, a transmembrane domain, and a highly variable cytoplasmic tail (**Figure 1.2**). For the majority of ADAMs, domains downstream of the pro-domain are of similar length and share cysteine alignment. ADAMs 10 and 17, however, are structural varying compared to other ADAMs in several respects, such as the size of metalloprotease domain, features of their cysteine-rich region, and an absence of the EGF-like module.

Table 1.1 ADAMs in human, mouse, and rat genomes

Protease	Synonyms	Mouse gene	Rat gene	Human locus
ADAMDEC1	Decysin	+	+	8p21.2
ADAM1a	FTNAP, PH-30a, Fertilin-α, ADAM1P	+	+	12q24.12
ADAM1b	N/A	+	+	N/A
ADAM2	PH-30b, PH30, CT-15, Fertilin-β	+	+	8p11.22
ADAM3B	CYRN1/2, tMDCI	+	+	8p11.22/16q12.1
ADAM4	tMDCV	+	-	14q24
ADAM4B	N/A	+	+	14q24
ADAM5	tMDCII, ADAM5P	+	+	8p11.22
ADAM6	tMDCIV, CD14orf96	+	+	14q32.33
ADAM6B	N/A	+	-	N/A
ADAM7	GP-83, EAPI	+	-	8p21.2
ADAM8	CD156, MS2, CD156a	+	+	10q26.3
ADAM9	CORD9, MCMP, MDC9, Mltng	+	+	8p11.22
ADAM10	AD10, AD18, CDw156m HsT18717, kuzbanian, MADM, RAK	+	+	15q21.3
ADAM11	MDC	+	+	17q21.31
ADAM12	ADAM12-OT1, CAR10, MCMP, MCMPMltna, MLTN, MLTNA	+	+	10q26.2
ADAM15	MDC15	+	+	1q21.3
ADAM17	CD156B, CSVP, NISBD, NISBD1, TACE	+	+	2p25.1
ADAM18	tMDCIII, ADAM27	+	+	8p11.22
ADAM19	FKSG34, MADDAM, MLTNB	+	-	5q33.3
ADAM20	N/A	-	-	14q24.2
ADAM21	ADAM31	+	+	14q24.2
ADAM22	MDC2	+	+	7q21.12
ADAM23	MDC3	+	+	2q33.3
ADAM24	Testase-1	+	+	N/A
ADAM25	Testase-2	+	+	8p22
ADAM26	Testase-3	+	+	N/A
ADAM28	eMDCII, MDC-Lm, MDC-Ls	+	+	8p21.2
ADAM29	svph1, CT73	+	+	4q34.1
ADAM30	svph4	+	+	1p12
ADAM32	N/A	+	+	8p11.22
ADAM33	C20orf153, DJ964F7.1	+	+	20p13
ADAM34	Testase-4	+	+	N/A
ADAM35	Testase-5	+	-	N/A
ADAM36	Testase-6	+	+	N/A
ADAM37	Testase-7	+	+	N/A
ADAM38	Testase-8	+	-	N/A
ADAM39	Testase-9	+	-	N/A

ADAMs labeled in **bold type** represent pseudogenes in the human genome.
HGNC: https://www.genenames.org/cgi-bin/gene_search?search=ADAM;
NCBI gene: https://www.ncbi.nlm.nih.gov/gene/?term=ADAM;
The Lopez-Otin Laboratory Degradome Database: http://degradome.uniovi.es/met.html.

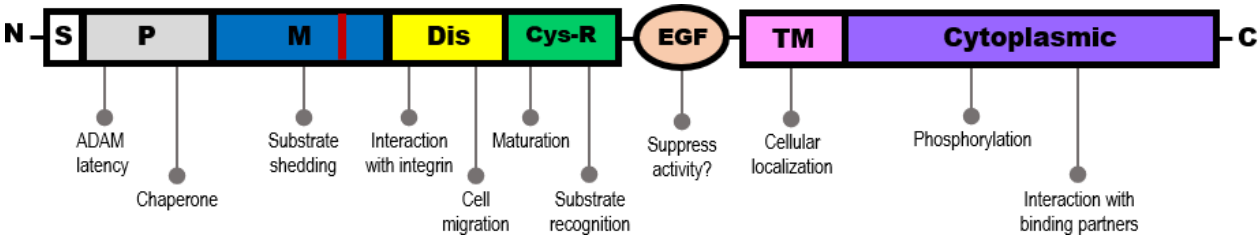

Figure 1.2 A schematic representation of a prototype ADAM showing its primary (linear) structure of different domains with their proposed functions. N, N-terminus; S, signal peptide; P, pro-domain; M, metalloproteinase domain; Dis, disintegrin domain; Cys-R, cysteine-rich region; EGF, EGF-like module; TM, transmembrane domain; Cytoplasmic, cytoplasmic tail; C, C-terminus. Note that ADAMs 10 and 17 are lack of the EGF-like module.

1.4.1. Peptidase unit

The peptidase unit contains a signal peptide and a pro-domain. The pro-domains maintain ADAMs in an inactive state by blocking the metalloproteinase catalytic site via the so-called 'cysteine switch' mechanism, which is defined as 'a conserved cysteine residue in the pro-domain forms a complex with Zn^{2+} in the metalloproteinase domain, thereby blocking the catalytic site' (30-32). However, the conserved cysteine residue of pro-domain in ADAM17 may not be required to keep its precursor form inactive, as mutated cysteine switch does not affect the inhibitory effect of its pro-domain (32, 33). In addition to its inhibitory function, the pro-domain also acts as a chaperone and protects ADAMs from degradation during their biogenesis and transport through the secretory pathway (33). Moreover, the pro-domain also ensures proper folding of ADAMs before entry into the secretory pathway (34). Interestingly, both synthesized or purified pro-domains from different ADAMs can act as potent, selective inhibitors of the mature, active forms of ADAM sheddases (32, 35, 36).

The maturation process of an ADAM is regulated by its signal peptide, which directs correct intracellular trafficking of the stably folded zymogen from the endoplasmic reticulum (ER) to the late Golgi, where its pro-domain is proteolytically removed by furin-like proprotein convertases (37). Interestingly, ADAM8 (38) and ADAM28 (39) have been found to undergo autocatalytic pro-domain removal. ADAMs 8, 9, 12, and 28 can undergo alternative splicing events, giving rise to soluble forms of ADAMs without the transmembrane domain and the cytoplasmic tail (40).

1.4.2. Metalloproteinase domain

The metalloprotease domain is adjacent to the pro-domain. Among the 20 functional human ADAMs, only 12 of them (i.e., ADAMs 8-10, 12, 15, 17, 19-21, 28, 30, and 33) are proteolytically active (22). In contrast, 17 mouse ADAMs are proteolytically active (41). The catalytic Zn^{2+} is coordinated by the three histidines (H) in the consensus sequence (HEXGHXXGXXHD). Glutamic acid (G) is highly conserved in the signature motif and polarizes the zinc-associated water molecule for the nucleophilic attack towards the target peptide bond. The use of cell-based shedding experiments, *in vitro* cleavage assays, or genetic approaches (e.g., knockout mice) has allowed a clear advance in our knowledge of the repertoire of substrates (which is also known as the degradome (10)) for different ADAMs. A list of proteolytically active ADAMs with their substrates ranging from cell adhesion molecules to growth factors, cytokines, and/or their receptors is available in **Table 1.2**. Since ADAM17 is the target ADAM in this dissertation, the most up-to-date version of degradome of ADAM17 is further summarized in **Table 1.3**. While the majority of known ADAM substrates are membrane-anchored, some are soluble (e.g., insulin-like growth factor-binding protein/IGFBPs 3 and 5 (42)) or are components of the extracellular matrix (ECM) (e.g., fibronectin, collagen IV, and gelatin) (43) (See also in **Tables 1.2 and 1.3**). However, it is noteworthy to point out that most of the substrates for ADAMs were identified based on *in vitro* shedding assays using soluble protein recombinants and model synthetic peptides. Therefore, these approaches sometimes lead to less consistent results and may not accurately reflect the *in vivo* functions of these enzymes because of the yet to be fully understood substrate recognition mechanisms by ADAMs (will be discussed in more detail in **Chapter 1.6**). As such, the results obtained from cell-free systems should be interpreted cautiously, and further verification of these 'theoretical' substrates using genetic approaches is warranted.

Table 1.2 Proteolytically active ADAMs and their substrates

ADAMs	Substrates
ADAM8	APP, CD16, CD23, CD62L/L-selectin, CHL1, c-Kit, CX3CL1, FLRG, KL-1, IL-1RII, L-selectin, NCAM140/180, Pro-ADAM8, Pro-amphiregulin, Pro-betacellulin, Pro-EGF, Pro-HB-EGF, Pro-TNFα, p55 TNFR, SCF, VCAM-1
ADAM9	APP, c-Kit, Collagen XVII, DLL1, FGF2 (IIIb), Fibronectin, IGFBP-5, KL-1, Laminin, Oxytocinase/P-LAP, Pro-EGF, Pro-HB-EGF, Pro-TNFα, p75 Neurotrophin receptor (NTR), p75 TNFR, VCAM-1, VE-cadherin
ADAM10	APP, APLP2, Axl, BACE1, CD23, CD30, CD42b-α/GPIbα, CD44, CD162/PSGL-1, CD223/LAG3, Collagen IV, Collagen XVII, Corin, CX3CL1, CXCL16, DLK1, DSG2, E-cadherin, Ephrin A2/A5, EphB2, ErbB2/HER2, FasL, GPV, GPVI, IL-6R, Jagged, L1CAM, N-cadherin, NCAM140/180, Notch, Pcdhγ, PrPc, Pro-amphiregulin, Pro-betacellulin, Pro-EGF, Pro-epiregulin, Pro-HB-EGF, Pro-TGFα, Pro-TNFα, RPTPκ, Serrate, Slit, Sortilin/NTR3, TRANCE, VE-cadherin,VEGFR2
ADAM12	Collagen IV, DLL1, FGFR2IIIb, Fibronectin, FLRG, Follistatin, Gelatin, IGFBP-3/5, Oxytocinase/P-LAP, Pro-betacellulin, Pro-EGF, Pro-HB-EGF
ADAM13	ADAM 13 (cysteine-rich domain), Fibronectin
ADAM15	CD23, Collagen IV, Pro-amphiregulin, Pro-HB-EGF, Pro-TGFα
ADAM17*	ACE2, APLP2, APP, Axl, Carbonic anhydrase IX, CD30, CD40, CD42b-α/GPIbα, CD44, CD62L/L-selectin, CD71, CD166, CD223/LAG3, CD227/Mucin-1, c-Kit, c-Met, Collagen XVII, CX3CL1, CXCL16, DLK1, DSG2, Ebola virus glycoprotein, EPCR, Epigen, ErbB4/HER4, GHR, GPV, GPVI, Jagged, KL-1/2, ICAM-1, IL-1RII, IL-6R, L1CAM, LDLR, LRP1B, M-CSFR, Mephrine-β, NCAM140/180, Nectin-4, NgR, Notch1, PAR1, Pro-amphiregulin, Pro-epiregulin, Pro-betacellulin, Pro-EGF, Pro-HB-EGF, Pro-neuregulin, p75NTR, p55 TNFR, p75 TNFR, Pro-TGFα, Pro-TNFα, PTP-LAR, PrPc, Semaphorin 4D, SHPS-1, SorLA-1, TRANCE, TrkA, Type II NRGα/β, VCAM-1, VVC
ADAM19	ADAM 19 (cysteine-rich domain), APP, α2-macroglobulin, c-Kit, KL-1, Neuregulin, Pro-betacellulin, Pro-EGF, Pro-HB-EGF, Pro-neuregulin, Pro-TNFα (in TACE deficient cells), TRANCE
ADAM 23	β-APP, KL-1
ADAM28	Pro-ADAM 28, CD23, IGFBP-3
ADAM33	APP, CD23, Insulin B Chain, c-Kit, KL-1, TRANCE

*****A complete list of substrates identified so far for ADAM17 is available in Table 1.3.

Abbreviations: APLP, APP-like Protein; APP, Amyloid Precursor Protein; BACE1, β-secretase1; CHL1, Close Homologue of L1, CX3CL, Chemokine (C-X3-C motif) Ligand; c-Met, Met Proto-oncogene/Hepatocytes Growth Factor Receptor; DLK1, Delta like 1; DSG2, Desmoglein 2/Desmosomal Cadherin; EGF, Epidermal Growth Factor; EphA3/B2, Ephrin Receptor A3/B2; EPCR, Endothelial Protein C Receptor; ErbB2/4, v-erb-b2 erythroblastic leukemia viral oncogene homolog 2/4; FasL, Fas Ligand; FGF, Fibroblast Growth Factor; FSTL3, Follistatin-like 3; GPV, Glycoprotein V (platelets); GPVI, Glycoprotein VI (platelets); HB-EGF, Heparin-binding Epidermal Growth Factor; IGFBP, Insulin-like Growth Factor Binding Protein; IL, Interleukin; KL-1/2, Kit ligand-1/2; LAR, Leukocyte Common Antigen Related; L1CAM, L1 Cell Adhesion Molecule; LAG3, Lymphocyte Activation Gene 3; LDLR, Low Density Lipoprotein Receptor; LRP1B, LDL Receptor Related Protein 1B; M-CSFR Macrophage Colony-stimulating Factor 1 Receptor; NCAM, Neural Cell Adhesion Molecule; NgR, Nogo-66 Receptor; NRG, Neuregulin; p75NTR, p75 Neurotrophin Receptor; PAR1, Protease-activated Receptor 1; Pcdhγ, γ-Protocadherins; P-LAP, Placental Leucine Aminopeptidase; PTP, Protein Tyrosine Phosphatase; PrPc, Cellular Prion Protein; PSGL, P-selectin Glycoprotein Ligand; RPTPκ, Receptor-like protein tyrosine phosphatase κ; SCF, Stem Cell Factor; SHPS-1, Src homology 2 (SH2) domain-containing Protein Tyrosine Phosphatase Substrate 1; SorLA-1, Sorting Protein-Related Receptor Containing LDLR Class A Repeats 1; TNF, Tumor Necrosis Factor; TNFR, Tumor Necrosis Factor Receptor; TRANCE, TNF-related Activation-induced Cytokine; TrkA, Tropomyosin Receptor Kinase A; VCAM1, Vascular Cell Adhesion Molecule 1; VCC, Vibrio Cholera Cytolysin.

Primary references can be found in Seals and Courtneidge (31); Becherer and Blobel (44); White (23); Dreymueller, et al. (45); and Kleino (46).

Table 1.3 ADAM17 substrates

Substrate	Refs	Substrate	Refs	Substrate	Refs	Substrate	Refs
Cytokines and chemokines		**Growth factors**			**Receptors**		
CD154	(47)	Amphiregulin	(48)	CD30/TNFRSF8	(49)	M6P	(50)
CX3CL1/Fractalkine	(51)	Betacellulin	(41)	CD40/TNFRSF5	(52)	M-CSFR	(53)
CXCL16	(54)	CSF1	(55)	CD71	(56)	NPR	(57)
KL1/2	(58)	DLK1	(59)	CD89/FcαR	(60)	Notch1	(61)
MICA/B	(62)	EGF	(41)	CD163	(63)	Neogenin	(64)
Jagged1	(65)	Epigen	(66)	CD223/LAG3	(67)	NgR	(68)
TNFα	(69)	Epiregulin	(41)	c-Kit	(70)	p75NTR	(71)
Lymphotoxin αβ	(72)	FLT3L	(73)	c-Mer	(53, 74)	p55 TNFR	(75)
TMEFF2	(76)	HB-EGF	(41)	EPCR	(77)	p75 TNFR	(75)
TRANCE	(78)	Neuregulin1	(79)	ErbB4/HER4	(80)	PAR1	(81)
Adhesion molecules		Pref1	(82)	GHR	(83)	PTP-LAR	(84)
CD166/ALCAM	(56)	Semaphorin 4D	(85)	GPIbα	(86)	Ptprz	(87)
CD44	(88)	TGFα	(41)	GPV	(89)	PTPα	(90)
CD54/ICAM1	(91)			GPVI	(92)	TIM3	(93)
CD62L/L-selectin	(94)	**ECM**		IGF2R	(50)	TLR2/4	(95, 96)
CD137/4-1BB	(97)	GPC1	(98)	IL-1RII	(53, 99, 100)	TrkA	(101)
CD227/Mucin1	(102)	Syndecan-1	(103)	IL-6R	(53, 100, 104)	TREM2	(105)
Claudin5	(106)	Syndecan-4	(103)	IL23R	(107)	SHPS1	(53)
Collagen XVII	(108)			LOX1	(109)	SorLA1	(53)
DSG2	(56)	**Enzymes**		LDLR	(53)	VEGFR1/FLT1	(110)
EpCAM	(111)	ACE2	(112)	LRP1	(113)	VEGFR2	(114)
JAM-A	(115)	Carbonic anhydrase IX	(116)		**Other effector proteins**		
L1CAM	(88, 117)	MERTK	(118)	APLP2	(119)	PrPc	(120)
Nectin4	(121)			APP	(122)	PMEL17/GP100	(123)
Neuroligin3	(124)	**Receptors**		C4.4A/LYPD3	(36)	Trop2	(125)
NCAM140/180	(126)	Axl	(53, 118)	Ebola Glycoprotein	(127)	Vasorin	(128)
VCAM1	(129)	CD16/FcγRIIIA	(130)	Klotho	(131)	VVC	(132)

The table shows ADAM17 substrates verified by *in vivo* and *in vitro* mechanistic evidence.

Abbreviations: ACE2, Angiotensin Converting Enzyme 2; ALCAM, Activated Leukocyte Cell Adhesion Molecule; APLP, APP-like Protein; APP, Amyloid Precursor Protein; CX3CL, Chemokine (C-X3-C motif) Ligand; c-Met, Met Proto-oncogene/Hepatocytes Growth Factor Receptor; CSF1, Macrophage Colony-stimulating Factor 1 Precursor; DLK1, Delta like 1; DSG2, Desmoglein 2/Desmosomal Cadherin; EGF, Epidermal Growth Factor; EPCR, Endothelial Protein C Receptor; EpCAM, Epithelial Cell Adhesion Molecule; ErbB4, v-erb-b2 erythroblastic leukemia viral oncogene homolog 4; FLT1, Fms Related Tyrosine Kinase 1 FLT3L, Fms-related Tyrosine Kinase 3 Ligand; GHR, Growth Hormone Receptor; GPC1, Glypican-1; GPIbα, Platelet Glycoprotein Ib alpha Chain Precursor; GPV, glycoprotein V (platelets); GPVI, glycoprotein VI (platelets); HB-EGF, Heparin-binding Epidermal Growth Factor; ICAM-1, Intracellular Adhesion Molecule; IGF2R, Insulin Like Growth Factor 2 Receptor; IL, Interleukin; JAM-A, Junctional Adhesion Molecule-A; KL1/2, Kit ligand-1/2; LAR, Leukocyte Common Antigen Related; L1CAM, L1 Cell Adhesion Molecule; LAG3, Lymphocyte Activation Gene 3; LDLR, Low Density Lipoprotein Receptor; LOX1, Lectin-like Oxidized Low Density Lipoprotein Receptor 1; LRP1, LDL Receptor Related Protein 1; LYPD3, Ly6/PLAUR domain-containing Protein 3; M-CSFR Macrophage Colony-stimulating Factor 1 Receptor; NCAM, Neural Cell Adhesion Molecule; NgR, Nogo-66 Receptor; NPR, Neuronal Pentraxin Receptor; NRG, Neuregulin; p75NTR, p75 Neurotrophin Receptor; PAR1, Protease-activated Receptor 1; PTP, Protein Tyrosine Phosphatase; PrPC, Cellular Prion Protein; Ptprz, Protein Tyrosine Phosphatase Receptor Type Z; Pref1: Preadipocyte Factor 1; SHPS1, Src Homology 2 (SH2) Domain-containing Protein Tyrosine Phosphatase Substrate 1; SorLA1, Sorting Protein-Related Receptor Containing LDLR Class A Repeats 1; TIM3, T Cell Immunoglobulin and Mucin Domain-3; TLR2/4, Toll-Like Receptor 2/4; TMEFF2, Tomoregulin-2; TNF, Tumor Necrosis Factor; TNFR, Tumor Necrosis Factor Receptor; TRANCE, TNF-related Activation-induced Cytokine; TREM2, Triggering Receptor Expressed in Myeloid Cells; TrkA, Tropomyosin Receptor Kinase A; VCAM1, Vascular Cell Adhesion Molecule 1; VCC, Vibrio Cholera Cytolysin; VEGFR1/2, Vascular Endothelial Growth Factor Receptor 1/2.

1.4.3. Disintegrin domain

Disintegrins are small soluble proteins which were originally found to inhibit platelet activation and aggregation by blocking integrin binding to fibrinogen (133). The disintegrin domain makes ADAMs unique among membrane-anchored proteins by interacting with integrins through a disintegrin loop (134). While most ADAM disintegrin loops contain 14 amino acids with the 'canonical' disintegrin loop motif (CRXXXXXCDXXEXC), ADAM10 and ADAM17 contain distinct motifs (135). Studies have revealed that the disintegrin domain of an ADAM can interact with various integrins (136), and different residues within the disintegrin loop appear to predominate in interactions with different integrins (137), thereby achieving the regulation of cell adhesion, cytoskeleton reorganization, and cell polarity (138). A detailed description of ADAM-integrin pairs is summarized elsewhere by Kleino (46). However, it remains obscure that whether and how the interactions between disintegrin domains and integrins observed *in vitro* are related to *in vivo* functions, since ADAMs are much smaller proteins than integrins, the integrins must either be tilted along the membrane or they must be in a bent conformation to bind to the ADAM disintegrin-cysteine-rich domains on the same membrane. Integrins are thought to be inactive when in bent conformation and straightening has been suggested to be the prerequisite for binding and signaling (139). On the other hand, in all known structures the disintegrin loops are buried deep inside of disintegrin domain and therefore are not readily for integrin binding (140). In addition to the accessibility of integrins to the disintegrin domain, it is also important to understand the sequence requirements for integrin selectively, to gain cell-specific regulation of ADAM disintegrin-integrin interactions, and to determine the critical consequences of ADAM disintegrin-integrin pairing.

1.4.4. Cysteine-rich region

All ADAMs contain a cysteine-rich region. However, the cysteine spacing of ADAM10 and ADAM17 deviate from the highly conserved sequence observed in other ADAMs, which therefore partially diverges their structures from those of other ADAMs (141). Although it is not fully understood whether all ADAMs share a similar mechanism to recognize certain substrates, the cysteine-rich region is found to be important for the recognition of interleukin-1 receptor II (IL-1RII) but not of tumor necrosis factor alpha (TNFα) or p75 TNFR by ADAM17 (99). It has been

suggested that the cysteine-rich region is also important for biological functions such as integrin-dependent cell spreading (142, 143), cell adhesion (144), and protease activity (145).

1.4.5. EGF-like module

Most ADAMs, except ADAM10 and ADAM17, have an EGF-like module between the cysteine-rich region and the transmembrane region. In ADAMs 10 and 17, their cysteine-rich domain is followed by a membrane-proximal domain and a small stalk region (140, 146). Although the precise function of EGF-like module remains unknown, it has been suggested that this domain serves as a bridge to form a C-shaped arm by connecting the metalloproteinase domain, disintegrin domain, cysteine-rich region and the hypervariable region (HVR) (140). The C-shaped structure of ADAMs allows for an interplay between the proteolytic and the adhesion domain that could act as a mechanism for substrate recognition. For proteolytically inactive ADAMs, the HVR may work to modulate cell-cell and cell-matrix interactions (140). Curiously, ADAMs 10 and 17 are the most effective sheddases, suggesting that the existence of EGF-like module may hinder the shedding activity of ADAMs.

1.4.6. Cytoplasmic tail

The cytoplasmic tails of ADAMs are heterogeneous in terms of their lengths and compositions. The cytoplasmic tails of many ADAMs contain one or more Src homology 3 domain (SH3) binding sites or sites for serine, threonine or tyrosine phosphorylation (31). A variety of adapter proteins have emerged as ADAM cytoplasmic tail binding partners to affect overall protease activity, intracellular transport, localization, and cell signaling (22). A detailed list of binding partners for each ADAM has been summarized by White*, et al.* (147). Phosphorylation of, or binding of adapter proteins to, the cytoplasmic tail could regulate ADAM maturation, trafficking, membrane localization, proteolytic activity, etc. (31). However, studies showed that phosphorylation of the cytoplasmic tail is not necessary for ADAM17-dependent shedding activity: the phosphorylation status of the cytoplasmic tail of ADAM17 does not affect cleavage of pro-transforming growth factor-alpha (TGFα) in response to growth factor stimulation (148), and cytoplasmic domain-truncated ADAM17 shows comparable shedding activity versus intact ADAM17 (149).

1.5. Regulation of ADAM activity

Although the expression levels of ADAMs have been reported to change in pathological conditions such as arthritis, acute myocardial infarction, and cancer as a result of increased circulating cytokines and/or growth factors (150, 151), it is accepted that the activities of ADAMs are predominantly regulated by rapid posttranslational mechanisms. It is because the increase in gene expression and protease synthesis are rather slow regulators of shedding activity. Post-translational regulation of ADAM shedding activity occurs at various levels, including ADAM maturation, cytoplasmic tail modification (phosphorylation or interacting with adaptor proteins); protease redistribution at the cell surface; conformational changes; and different types of endogenous inhibitory and regulatory mechanisms.

1.5.1. ADAM activation

As mentioned in **Chapter 1.4.1**, ADAM maturation requires proteolytic separation of the pro-domain from its metalloproteinase domain. However, at steady state, the vast majority of ADAM 10 (152) and ADAM17 (153) are retained in the ER or Golgi apparatus, and binding partners such as tetraspanin and inactive rhomboid (iRhom) 2 are required to bind to ADAM10 (154) and ADAM17 (155), respectively, to promote protease maturation and translocation to the plasma membrane.

A lot of studies have also shown that ADAMs can shed their substrates either constitutively or in regulated conditions. Accumulating evidence further suggests that the constitutive shedding is mainly regulated through the mitogen-activated protein kinases (MAPKs) p38 pathway, whereas regulated shedding is usually activated by the extracellular signal-regulated kinase (Erk) pathway (31). Interestingly, ADAM10 and ADAM17 are proved to be sheddases for amyloid precursor protein (APP) (156), C-X3-C motif chemokine ligand-1 (CX3CL1) (51, 157) and interleukin-6 receptor (IL6R) (158). While ADAM10 cleaves these substrates constitutively, ADAM17 sheds them in a regulated manner. The simplest explanation for this observation is that ADAM10 and ADAM17 preferentially respond to different triggers: while the former is more sensitive to intracellular calcium elevation, the latter is more sensitive to phorbol esters (the activator for protein kinase C/PKC pathway, which has been proven to be upstream of the Erk pathway (149)).

Regulated ectodomain shedding by ADAMs requires exposure of cells to one or a few physiological or non-physiological stimuli, including cytokines and growth factors (159, 160), reactive oxygen species (ROS) (161), G-protein coupled receptor (GPCR) agonists (e.g., angiotensin II/Ang II, endothelin-1, thrombin, carbachol, and lysophosphatidic acid) (149), calcium ionophores (162), lipopolysaccharide (LPS) (160), and phorbol esters (163). It has been shown that these stimuli could promote the maturation of ADAMs through removing their pro-domains, which is followed by translocation of these proteases to the plasma membrane where ectodomain shedding usually occurs. However, it has been shown that physiological stimuli do not alter the abundance of the mature ADAM17 on the cell surface or the speed of its turnover (83, 153, 164-166).

The cytoplasmic tails of most ADAMs have at least three motifs putatively involved in protein-protein interaction that would regulate ADAM action: SH3-binding domains, phosphorylation sites, and a PDZ domain. ADAM activation by GPCR ligands is thought to be achieved by phosphorylation at their cytoplasmic tails. Several lines of evidence indicate that phosphorylation of the cytoplasmic domain of ADAM17 is indispensable for GPCR-mediated epidermal growth factor receptor (EGFR) transactivation (22, 41, 167-172). ADAMs 10 (41, 169, 173, 174), 12 (175), and 15 (169) have also been implicated in a number of GPCR-EGFR transactivation events. However, Le Gall, *et al.* (149) showed that the transmembrane domain, rather than the cytoplasmic tail, is essential for ADAM17 activation, as both intact and cytoplasmic tail-truncated constructs (i.e., phosphorylation site removed ADAM17) exerted comparable responses to the stimulation of thrombin, epidermal growth factor (EGF), lysophosphatidic acid, and TNFα. In agreement with this finding, Fan, *et al.* (148) demonstrated that several mutations at the phosphorylation site of ADAM17 did not compromise the shedding of pro-TGFα induced by growth factors. Similarly, stimulus-mediated shedding by ADAM19 has also been observed to occur independently from its cytoplasmic domain, and was only dependent on its transmembrane domain (176). Interestingly, Le Gall, *et al.* (149) further demonstrated in the same study that ADAM17 activation seems to be more conformational change-related (i.e., to only expose the catalytic domain), and was independent of pro-domain removal.

Adaptor proteins which can bind to the SH3 domains or PDZ domain may either activate or deactivate an ADAM by regulating its scaffolding, sorting, ER retention, endocytosis, etc. A list of identified adaptor proteins for different ADAMs is summarized by Kleino (46).

1.5.2. ADAM inhibition

ADAM activity can also be regulated by tissue inhibitors of metalloproteinases (TIMPs), a four-membered family that are best known for their function as endogenous inhibitors to form tight, non-covalent complexes with active MMPs in a 1:1 stoichiometry (15). While the inhibitory function of TIMPs against MMPs is broadly overlapping, TIMPs show a much greater specificity in inhibiting ADAMs. Studies showed that TIMP3 is the only TIMP that physiologically inhibits ADAM17 activity by binding to its dimer at the cell surface (177). Erk or p38-dependent phosphorylation of the cytoplasmic domain decrease the abundance of ADAM17 dimers (178). Since ADAM17 monomer has lower affinity than the dimer for TIMP3, the suppression of ADAM17 activity by TIMP3 is withdrawn when the dimers are dissociated. ADAM10 is susceptible to the inhibition by TIMPs 1 and 3 (179). The proteolytic activity of other ADAMs (except ADAMs 8 and 9 (180)) can also be inhibited by various TIMPs (reviewed in (1, 46)).

Other inhibitors of ADAMs include the reversion-inducing cysteine-rich protein with kazal motif (RECK) which has been reported to inhibit ADAM10 activity during cortical neurogenesis (181). Isolated pro-domains from some ADAMs can also act as their own potent and selective inhibitors as documented for ADAM10 (182) and ADAM17 (32) through a mechanism independent of the 'cysteine-switch' mechanism. Indeed, a recent study showed that the pro-domain of ADAM17 was an effective inhibitor which robustly suppressed ADAM17 activity in a murine model of kidney fibrosis (183). Moreover, a furin cleavage-resistant version of ADAM17 pro-domain (referred to as 4mut) was generated, and exhibited potent, selective inhibitory effects on ADAM17 (184, 185). The profound inhibitory effects of 4mut have further been verified in a few inflammatory disease models such as LPS-induced sepsis and collagen-induced arthritis (184). Owing to the great performance of 4mut in ameliorating inflammation phenotypes in murine models, patients who are suffering from Crohn's disease, ulcerative colitis, septic shock, rheumatoid arthritis, systemic lupus erythematosus, and type II diabetes are currently being recruited for clinical trials to test the efficacy of this ADAM17-selective inhibitor in different types

of inflammatory diseases (184, 185). In addition, a great number of synthetic inhibitors (either showing broad-spectrum inhibitory effects on metalloproteinases or selective inhibitory effects on one or two ADAMs) and monoclonal antibodies for ADAMs have been developed by pharmaceutical companies and are being subjected to clinical trials for cancers and inflammatory diseases (2, 186-188). The implications and future directions of different types of ADAM17 inhibitors in cardiovascular diseases will be discussed in more detail in **Chapter 1.12**. A better understanding of the mechanisms of ADAM inhibition may shed light on the development of effective inhibitors that can specifically attenuate or block pathological signals as a result of dysregulated ADAMs in different human diseases.

Redistribution of mature ADAMs within the plasma membrane also affects the activity of these sheddases, and it may be associated with 'sheddase-substrate interaction' or substrate accessibility to a target ADAM sheddase. Recent data showed that active ADAM17 is localized separately from its substrate in cholesterol-rich membrane domains, namely lipid rafts, which can thus spatially restrict its activity (189), whereas depletion of cellular cholesterol and lipid rafts increased the shedding of IL6R (158) and CD30 (190) by ADAM17. Similarly, depleting cellular cholesterol and disrupting lipid rafts can also trigger ADAM10-dependent ectodomain shedding of IL6R (158). In contrast, ectodomain shedding of neuregulin by ADAM19 was enhanced when both the sheddase and the substrate were within the lipid rafts (176).

1.5.3. ADAM regulation

In addition to phosphorylation of the cytosolic domain, glycosylation, another posttranslational regulator, plays important roles in regulating the structure and function of ADAMs. ADAM8 possesses three sites of *N*-glycosylation, and each of them exhibits specific function, namely proper processing, exit from Golgi and ER, and cell surface localization (191). ADAM9 glycosylation is found in both membrane-anchored and secreted isoforms in breast cancer cells (192). *N*-glycosylation of ADAM12 has been reported in human glioblastomas (193), and ADAM15 has been identified to contain 5 potential *N*-linked glycosylation sites (194). However, no functional significance has yet been attributed to glycosylation of ADAM12 or ADAM15. ADAM17 glycosylation has been reported to suppress its shedding activity through interfering with its catalytic domain (195). Moreover, it has also been reported that ADAMs 8, 9, 10, 12, and 17 show much lower affinity to their glycosylated substrates (196).

Epigenetic regulations mainly through DNA methylation and histone modifications have also been implicated in regulating ADAM activities, although available findings are all currently observed in cancer cells. For example, inhibition of histone deacetylation upregulates ADAM19 mRNA expression (197), whereas histone deacetylation has been reported to underline transforming growth factor beta-1 (TGFβ1)-induced ADAM19 expression in ovarian cancer (198). Expression of ADAM33 has also been shown to be tightly regulated by a methylation site in its promoter region (199). Epigenetic silencing of ADAM12 by Z-DNA silencer was observed in breast cancer (200), while epigenetic suppression of microRNA-122 (miR-122) could indirectly impact its target ADAMs, ADAM10 and ADAM17, in hepatocytes (201). Although the significance of epigenetic regulation of ADAMs in cardiovascular diseases is so far unexplored, the findings in cancer studies provide new insight into additional regulatory mechanisms for these proteases.

Furthermore, the interaction between ADAMs and MMPs has been found to impact ADAM functions. For example, in breast cancer cells, ADAM12 can regulate the recruitment of MT1-MMP (membrane-bound MMP type I or MMP14) to the cell surface where they form a ternary complex with integrin $\alpha_v\beta_3$, thereby leading to activation of MT1-MMP and suppression of tumor cells from apoptosis (202). MMP7 is required to process pro-ADAM28 before its active form can shed IGFBP3 (203). Moreover, MT1-MMP has been reported to form a complex with fibroblast growth factor receptor-2 (FGFR2) and ADAM9 to proteolytically inactivate ADAM9, thereby preventing ectodomain shedding of FGFR2 by this ADAM (204). In line with this observation, depletion of ADAM9 in *Mmp14*-deficient mice rescued the defective calvarial bone growth via restoring fibroblast growth factor (FGF) signaling (204).

In addition to their direct interaction, indirect interactions between ADAMs and MMPs have also been reported. ADAM12 was identified as the mediator of Ang II-mediated cardiac hypertrophy downstream of MMP7 (205). The crosstalk between ADAM17 and MMP2 was also found in Ang II-induced cardiac hypertrophy and fibrosis (206). ADAM17 can contribute to androgen-independent prostate cancer cell invasion by shedding of TGFβ1, which subsequently activates the EGFR-Ras-Raf-MEK-Erk signaling axis, leading to overexpression of MMP2 and MMP9 (207). Lentiviral RNAi targeting of ADAM17 downregulated LPS-induced MMP9 expression in lung epithelial cells via inhibition of TNFα/NF-κB signaling (208). The compelling

evidence suggests that mutual regulation of ADAMs and MMPs occurs at transcriptional as well as posttranscriptional (proteolysis) levels. Further studies of the interplays between ADAMs and MMPs are largely warranted to provide novel insights into their mechanisms of actions in health and disease conditions. Moreover, when considering the application of ADAM-selective inhibitors in clinical applications, the potential impacts of these inhibitors on MMP activities are also required to be fully examined.

1.6. Substrate recognition by ADAMs

ADAM17 was the first ADAM implicated in ectodomain shedding since its identification as the tumor necrosis factor-alpha converting enzyme (TACE) in 1997 (164, 209). Since then the list of substrates for ADAM17 has expanded rapidly. So far, there are more than 80 membrane-tethered molecules (6,7) identified as substrates for ADAM17 (**Table 1.3**). Although ADAM17 was initially recognized as an essential sheddase in embryonic development, the highly heterogeneity of the function and structure of its substrates makes ADAM17 as a central regulator for other critical physiological events such as immune response, inflammation, cell growth, proliferation and adhesion, wound healing, ECM remodeling, and angiogenesis (4-6, 210-214). In this regard, as the best-characterized member of the ADAM family, ADAM17 is now being used as a prototype sheddase to understand the functions of other ADAMs.

It is clear now that ADAMs show an unusually wide substrate specificity, which raises a crucial question of how ADAMs recognize their substrates. Since only a small portion of cell surface proteins can be shed by ADAMs, there should be a common feature shared by their substrates. However, we are still far from understanding the property of this 'common feature'. Nevertheless, it is widely accepted that ADAMs show promiscuity in substrate recognition, and therefore, it is difficult to establish a consensus cleavage motif for all known substrates for ADAMs. Interestingly, it has been shown that mutagenesis of residues around or even at the cleavage sites had limited effects on ADAM17-mediated ectodomain shedding of substrates such as p55 TNFR (215), L-selectin (216), IL6R (217), TGFα, and β-APP (218). In contrast, deletion of more than 10 amino acids from the extracellular juxtamembrane region of pro-TNFα blocked the release of soluble TNFα (219). However, replacement of 14 amino acids at the cleavage sites (which are spatially close to the plasma membrane) for TGFα and β-APP with a non-cleavable amino acid fragment

did not affect ADAM-mediated ectodomain shedding (218). Indeed, there is no common recognizable pattern found around the cleave sites of substrates for ADAM17, as summarized elsewhere by Arribas and Esselens (2). Therefore, the proximity (usually within the length of 15 amino acids) of the cleavage site of a substrate to the cell membrane rather than the amino acid sequence may be the determinant for ADAM-mediated substrate recognition and cleavage.

Despite the lack of a consensus cleavage motif, studies using small peptide substrates demonstrated that ADAM17 prefers to cleave substrates carrying aliphatic residues at the P1' site (immediately downstream of the cleavage site of the substrate) (220) and basic amino acids at the P2' site (221). It has also been suggested that substrate recognition is dependent on the tertiary structures of substrates (222) and the accessibility of their cleavage sites by ADAMs (223). Therefore, it is unsurprising that secreted (soluble) ADAMs preferentially cleave different substrates than their full-length counterparts since membrane-anchored ADAMs have limited access to their substrates on the same cell membrane (176). It is also important to note that, with only one reported exception (146), ADAM-mediated ectodomain shedding occurs in *cis* and not in *trans*, meaning that substrate and protease have to be expressed on the same cell. However, more studies need to be conducted to understand how ADAM domains coordinate and organize in three dimensions such that the metalloprotease domain can access different cleavage sites (149).

Interestingly, some studies observed that ADAM17 cleaves some peptide mimetics for native membrane-anchored substrates far less efficiently, suggesting sequence distal to the cleavage site may also be important for substrate recognition (221). Several pieces of evidence suggest that the formation of stable complexes between ADAMs and the sequence outside the juxtamembrane region of its substrates may also present a way to mediate substrate recognition. For instance, the transient formation of a complex between ADAM17 and growth hormone receptor (GHR) leads to the shedding of the latter, whereas the interaction between ADAM17 and GHR can be blocked by the presence of growth hormone (GH) (224). Complexes between ADAM17 and pro-TNFα have also been identified (225). However, it is unlikely that the sequences distal to the juxtamembrane region can be a common feature that ADAMs recognize their substrates, giving the structural diversity of the substrates for ADAMs.

1.7. Substrate selectivity by ADAMs

In addition to the short of knowledge of the mechanisms by which ADAMs recognize their substrates, it is also largely unknown that why ADAMs show differential substrate selectivity, regardless some ADAMs share a small portion of substrates with each other. ADAMs 9, 10, 12, 15, 17, and 19 are all involved in the EGFR signaling. However, they preferentially shed different cognate ligands for EGFR (**Table 1.2**) even within the same cell type (41, 168, 169). As compared to other ADAMs, ADAM10 shares a much higher structural homology with ADAM17 (**Figure 1.2**). However, it has been shown that while ADAM10 preferentially sheds betacellulin and EGF, ADAM17 preferentially sheds TGFα, amphiregulin, epiregulin, and HB-EGF (41). Interestingly, *Adam17*-null mice demonstrated development defects that are reminiscent of those seen in mice lacking TGFα (226, 227), HB-EGF (228, 229), or EGFR (230, 231), which is not surprising since ADAM17 is found to be the major sheddase for most EGFR ligands, and activated EGFR signaling is considered to play a critical role in embryonic development (168, 232). In contrast, *Adam10*-deficient mice die at day 9.5 of embryogenesis due to multiple defects in nervous and cardiovascular systems development as a result of downregulated Notch signaling (233) but not of disrupted EGFR signaling observed in *Adam17*-deficient mice. *Adam9* (234) and *Adam15* (235) knockout mice develop normally, whereas *Adam12* knockout mice display minor development defects (236). Moreover, triple knockout mice lacking *Adams 9, 12* and *15* are viable and fertile without apparent pathological abnormalities (41). Overall, these studies have suggested that the other ADAMs play less prominent roles in EGFR signaling or probably elicit limited functions only in adult tissues.

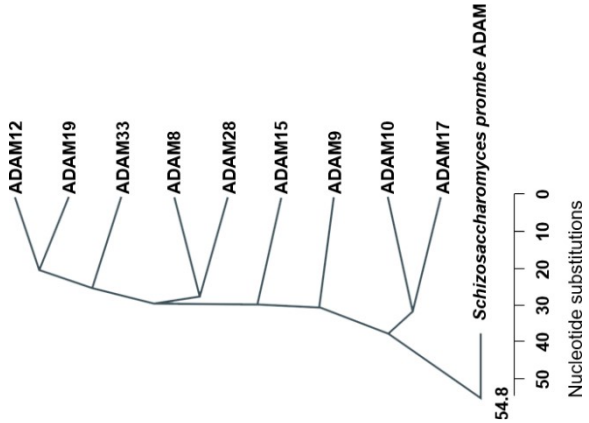

Figure 1.3 The phylogenetic relationship of ectodomains of proteolytically active ADAMs and an ADAM from *Schizosaccharomyces prombe*. The phylogenetic tree is generated by the DNA Star Clustal alignment program. The figure is adapted from Blobel (232).

Since ADAM17 has the largest repertoire of substrates among all ADAMs (**Table 1.3**), it is inevitable that some other ADAMs share a small fraction of substrates with ADAM17 and may exert functional redundancy. However, ADAM17 seems to be the principal sheddase that mediates ectodomain shedding of some biologically important substrates to execute critical cellular signals. For example, ADAM17, as well as ADAMs 9 and 10, can release the ectodomain of pro-TNFα (31). However, only *Adam17*-deficient mice showed significantly reduced pro-TNFα shedding, indicating that ADAM17 is the predominant sheddase for pro-TNFα and is involved in proinflammatory responses (69). Similarly, *Adam17*-intact but not *Adam17*-deficient cells can generate soluble APP, although ADAMs 8, 9, 10, 19, and 33 are also found to be able to release soluble APP (**Table 1.2**). Moreover, the recent studies also demonstrated that iRhom2, a binding partner for ADAM17, is not only necessary for ADAM17 maturation but also affects the protease's substrate specificity. Genetic deletion of iRhom2 prevents ectodomain shedding of TNFα and some EGFR ligands (e.g., HB-EGF and amphiregulin) but not of TGFα, L-selectin or intercellular adhesion molecule-1/ICAM1 by ADAM17 (155, 237). Furthermore, double knockout of iRhom2 and its isoform iRhom1 abolished all ADAM17-dependent shedding events (238), suggesting the critical role of the two iRhom isoforms in substrate selectivity by ADAM17.

Accumulating evidence suggests that ADAM-mediated ectodomain shedding of different substrates within the same cells or shedding of the same substrate in different cell types might exert opposite and/or parallel signals, especially those associated with inflammation. ADAMs are known to shed a group of chemokines and cytokines to regulate chemotactic cell migration and inflammatory responses, and ADAMs 10, 17, and 19 are found to be the principal sheddases for chemokines and cytokines, whereas other ADAMs show less prominent shedding capability on these substrates (**Tables 1.2 and 1.3**). In non-immune cells such as smooth muscle cells (SMCs) and endothelial cells (ECs), soluble chemokines and cytokines induce complex responses, which vary from apoptosis to proliferation, growth, and migration (239, 240). However, it is interesting that some ADAMs such as ADAM17 can shed both pro-TNFα and its receptors. While soluble TNFα can trigger a pro-inflammatory or anti-inflammatory response in cells once binding to its cognate receptors (i.e., p55 TNFR or p75 TNFR (75)), cleaved TNF receptors can serve as a decoy to suppress this pathological event by sequestering soluble TNFα (212). Interestingly, ADAM17-mediated shedding of the p55 TNFR or p75 TNFR may regulate different signaling pathways, since it has been shown that p55 TNFR activation suppresses EC migration and angiogenesis, whereas

p75 TNFR activation shows the opposite effects (241). Although it remains elusive how and when ADAM17 acts regulatory effects by shedding pro-TNFα and its cognate receptors under the same condition, it is believed that ADAM17-mediated shedding events are regulated in a spatiotemporal manner and is tightly balanced under normal physiological conditions (3, 164). The property that ADAM17 can cleave both pro-TNFα and its cognate receptors can also be considered as a self-protective mechanism during prolonged immune stimulation (242). Once this balance is disrupted, dysregulated ADAM17 shedding activity will contribute to various pathological conditions.

In addition to the antagonism effect caused by ADAM-mediated shedding of ligand and its cognate receptor, other examples of released antagonists are found within the family of adhesion molecules, which are usually involved in the process of leukocyte recruitment. Soluble L-selectin (243) and junctional adhesion molecule-A/JAM-A (115) have been shown to block P-selectin glycoprotein ligand-1/PSGL1 and lymphocyte function-associated antigen-1/LFA1 on ECs and leukocytes, respectively, and thereby suppress the adhesion of leukocytes to ECs and reduce subsequent transmigration. Moreover, ADAM-mediated shedding can also downregulate the expression levels of adhesion molecules (e.g., vascular cell adhesion molecule-1/VCAM1 and L-selectin) and chemokines (e.g., CX3CL1) and thereby decrease the adhesiveness of the endothelial surface for leukocytes (244, 245).

Cell-cell and cell-matrix interactions influence signal transduction in all multicellular organisms (246). ADAMs can also shed a great number of cell adhesion molecules and ECM components (**Tables 1.2 and 1.3**) to mediate or regulate cell migration, sorting, survival, and differentiation. These processes are critical for tissue and organ development and are equally important for the maintenance of tissue and organ homeostasis and morphology in adults. ADAMs 8, 10, and 17 are the prominent sheddases associated with ectodomain shedding of various cell adhesion molecules (**Tables 1.2 and 1.3**). While the majority of ADAM10 substrates are ubiquitously expressed in different cell types and are thought to be involved in the regulation of tissue morphogenesis (233), cell migration (247) and axon guidance (248), many substrates for ADAM8 or ADAM17 are important for platelet, neuronal, and endothelial cell functions (247).

The shedding consequences of a given ADAM are usually cell type- and substrate-dependent. In the context of ADAM-mediated ectodomain shedding in leukocyte recruitment into the inflamed

tissue, the functions of a given ADAM during this process seem to be contradictory across literature and the conclusions can be completely different depending on which angle (e.g., cell types and substrates) it was looked at. It has been shown that ADAM10 but not ADAM17 on leukocytes is essential for chemokine-induced cell adhesion, stress fiber rearrangement, and cell migration (249). In contrast, L-selectin on neutrophils shed by ADAM17 has been shown to downregulate neutrophil adhesiveness and recruitment to inflammatory sites, and the same study also showed that *Adam17*-deficient monocytes display no acceleration of infiltration into the inflammatory sites (250). Moreover, Tsubota*, et al.* (251) demonstrated that monocyte ADAM17 but not ADAM10 promotes diapedesis during transendothelial migration through ectodomain shedding of Mac-1. Therefore, it remains challenging to decipher the question of how an ADAM precisely cleaves which biologically relevant substrates in which cells at which stages of development or pathological process.

1.8. ADAMs mediate diverse biological functions through proteolytical cleavage of their substrates at different subcellular compartments

ADAMs comprise the major sheddase family. As mentioned above, the main function of proteolytically active ADAMs is the ectodomain shedding (a process defined as cleavage of the juxtamembrane region of a transmembrane protein to release its nearly entire extracellular region or ectodomain into the extracellular space) (252) from the cell surface of a group of structurally and functionally diverse membrane-bound precursors. A lot of studies have shown that ectodomain shedding plays an essential role in regulating the function of cleaved substrates. However, the consequences of ectodomain shedding can vary, depending on the function of substrate protein (22, 45, 253). Moreover, secreted ADAMs have been shown to shed substrates that are not attached to the cell membranes. For example, IGFBPs 3 and 5 inhibit the activity of insulin-like growth factor (IGF). ADAM-mediated processing of IGFBPs, therefore, activates the IGF signaling (42).

After ADAM-mediated ectodomain shedding, the remaining membrane-bound stub in some cases can undergo regulated intramembrane proteolysis (RIP) to generate an intracellular signaling molecule by intramembrane proteases such as γ-secretase, which can subsequently translocate into the nucleus to activate or repress the expression levels of specific target genes (254). ADAMs 10 and 17 are the most prominent sheddases involved in the RIP process. Most of the known substrates

for ADAM10 and a significant fraction of substrates for ADAM17 have found to be the targets for intracellular proteolysis, which is important for many physiological processes, such as embryonic development, hematopoiesis and normal functioning of the nervous system and the immune system (255). Interestingly, HB-EGF (256) and neuregulin-1 (257) are also found to be subjected to RIP, and their proteolytically released cytoplasmic domains exert distinct functions rather than activating the EGFR and ErbB4 signaling, respectively. A detailed list of substrates for ADAMs that are targeted to the RIP pathway is available as described elsewhere (46).

As a consequence of their ability to shed such a variety of multifunctional substrates, ADAMs elicit a number of endocrine, paracrine, juxtacrine or autocrine cellular signaling events at several levels, including cell growth, proliferation, differentiation, migration and adhesion; cell survival, apoptosis, senescence and autophagy; and angiogenesis (10). However, the precise functions of an individual ADAM are highly dependent on the cell type-specific expression pattern and the subcellular localization of its substrates. Since most of the events mentioned above are essential during embryonic development as well as in physiological processes of adult organisms, dysregulation of properly regulated shedding activities by ADAMs may contribute to the development of various human pathologies.

1.9. The roles of ADAMs in embryonic development

1.9.1. ADAMs exert differential functions during embryonic development

The critical roles of proteolytic active ADAMs in embryonic development can be appreciated by examining the phenotypes of ADAM loss- and gain-of-function mouse models. **Table 1.4** provides an overview of the diverse phenotypes (under physiological conditions and disease models) in mice with somatic deletion or overexpression of one or more ADAMs. Based on these knockout studies, it clearly shows that mice lacking ADAM10, ADAM17, or ADAM19 are embryonically or postnatally lethal, suggesting their indispensable role in fertilization, neurogenesis, myogenesis, bone development, lung branching morphogenesis, and heart development (232, 233, 258-261). In contrast, mice lacking *Adams 8* (262), *9* (234) or *15* (235) develop normally, whereas *Adam12*-null mice show minor defects during development (236). A comprehensive ADAM gene knockout experiment conducted by Sahin, *et al.* (41) demonstrated that knocking out *Adams 9*, *12* or *15* alone or in combination have no defective effects on

development. The absence of obvious pathological phenotype in mice deficient of *Adam 9*, *12* or *15* may indicate functional compensation contributed by ADAMs 10 and 17.

1.9.2. Biological functions of individual ADAM in the cardiovascular system

Since pathological cardiac remodeling is usually associated with re-expression of fetal genes in the cardiomyocytes, and vascular remodeling is associated with contractile-to-synthetic phenotypic switching in the SMCs, it is necessary to learn about the biological functions of individual ADAM in the cardiovascular system before we can understand how dysregulated ADAM activities contribute to the pathogenesis of different types of cardiovascular diseases.

ADAM8. ADAM8 is primarily expressed in hematopoietic cells and can be detected in spleen, bone, brain, lungs, and spinal cord under physiology conditions. Although *Adam8*-deficient mice develop normally with no evident spontaneous pathological or developmental phenotypes (262), ADAM8 could contribute to cardiac inflammation as its levels have been reported to be elevated in the peri-infarct myocardium following myocardial infarction (MI) (263) which is often associated with infiltration of inflammatory cells. *In vitro, Adam8*-deficiency attenuates the capacity of inflammatory cells to invade ECM similar to the observations made in cells expressing inactive ADAM8 (264). Therefore, it seems that the proteolytic activity of ADAM8 is required to mediate cell migration. Although there is no direct evidence showing the role of ADAM8 in vasculogenesis, SMC ADAM8 was shown to be upregulated under the condition of airway inflammation (265), and endothelial ADAM8 promoted angiogenesis in mouse models of retinopathy (266) and spinal cord injury (267).

ADAM9. ADAM9 is primarily expressed in ECs, skeletal muscle cells, fibroblasts, and SMCs, and is a member of the Meltrin family that was originally identified to mediate fusion of muscle cells during development, and therefore was implicated in myogenesis and formation of myotubes, including cardiac myocardium (234). Moreover, evidence showed that ADAM9, together with ADAM19, participates in endocardial cushion development (268). However, *Adam9*-null mice develop normally, and are viable and fertile with no defects in muscle formation (234). ADAM9 inhibition suppresses vascular SMC migration as a result of abolished HB-EGF-EGFR signaling (269). Using mouse embryonic cells lacking ADAM9, it showed that this ADAM protease could mediate shedding of angiogenesis-related proteins such as CD40, Tie2, EphB4, vascular

endothelial growth factor receptor-2 (VEGFR2), VE-cadherin, and VCAM1, suggesting its role in vascularization process (270). Indeed, *Adam9*-deficient mice showed significantly reduced neovascularization upon oxygen-induced retinopathy (270).

ADAM10. ADAM10 is the principal ADAM sheddase expressed in embryonic fibroblasts, ECs, and cardiomyocytes, and is involved in RIP-mediated Notch/Delta signaling, which is a key pathway involved in different aspects of embryonic development. This notion is evident by embryonically lethality of *Adam10*$^{-/-}$ mice around ED 9.5. These knockout mice show multiple defects in the developing central nervous system, cardiovascular system, and somites, which closely resemble those seen in mice deficient in Notch/Delta signaling (233). Mice lacking ADAM10 in the ECs die after ED 10 due to multiple cardiac and vascular defects similar to *Notch1* mutant mice (271). *In vitro* studies showed that ADAM10 regulates EC and SMC migration through shedding diverse substrates, such as N-cadherin, discoidin domain receptor-1 (DDR1), and Notch (reviewed in (247)).

ADAM12. During development, the ADAM12 transcript is mainly expressed in skeletal muscle and bone (272). ADAM12 expression has been reported in fibroblasts, SMCs, and brain, but is almost absent in ECs (144). ADAM12 was originally thought to be involved in myogenesis during embryonic development along with ADAM9 and ADAM19 (273). However, *Adam12*$^{-/-}$ mice are viable with no obvious developmental defects or pathologies, although 30% mortality in *Adam12*$^{-/-}$ pups within the first week has been reported (236). *Adams 9/12/15*-triple knockout mice have been reported to be viable, fertile, and generated in correct Mendelian ratios (41). Similarly, *Adams 9/12/15/19* quadruple knockout embryos show no apparent defect in muscle development (268). The normal muscle development found in the three types of gene knockout mice raises the possibility of compensation mechanism by other Meltrins in myogenesis. Endothelial ADAM12 has been suggested to involve in limiting new vessel sprouting by shedding of VEGFR2 (274).

Table 1.4 Phenotypes in mice with somatic ADAM-deficiency or overexpression

Genotype	Phenotypes	Refs
***Adam8*$^{-/-}$**	Viable, fertile, no evident spontaneous pathological or developmental phenotypes; reduced neovascularization after retinopathy and spinal cord injury; thymic hyper cellularity; decreased the development of experimental asthma due to loss of T cell expressed ADAM8 and associated with decreased T cell infiltration into the lungs	(262, 266, 267, 275, 276)
***Adam9*$^{-/-}$**	Viable, fertile, no evident spontaneous pathological or developmental phenotypes; reduced pathological neovascularization in the retina; accelerated wound healing without affecting inflammatory cell recruitment	(234, 270, 277)
***Adam10*$^{-/-}$**	Embryonic lethal (E9.5), defective heart and central nervous system development, vasculogenesis and somitogenesis; resembles Notch1 knockout phenotype	(233)
***Adam10* overexpression**	Increased secretion of APP; reduced β-amyloid and amyloid plaque formation; impaired long-term potentiation and cognitive deficits alleviated	(258)
Dominant-negative *Adam10* overexpression	Increased number and size of amyloid plaques in the brains	(258)
***Adam12*$^{-/-}$**	Viable, fertile, grossly normal; 30% postnatally lethality within one week; minor brown fat and neck muscle hypotrophy; reduced myogenesis and adipogenesis; enhanced wound repair by keratinocyte migration; reduced cardiac hypertrophy	(205, 236, 278)
***Adam12* overexpression**	Dystrophic pathology alleviated in *mdx* mice. Increased expression and redistribution of α7B	(279)
***Adam15*$^{-/-}$**	Viable, healthy, no obvious pathology; decreased neovascularization in proliferative retinopathy; accelerated development of osteoarthritic lesions in aged knockout mice	(235, 280)
***Adam17*$^{-/-}$**	Perinatal to newborn lethal; general epithelial dysgenesis; defective heart and lung development; deficient ectodomain shedding	(229, 252, 281-283)
***Adam17*$^{\Delta Zn/\Delta Zn}$**	Postnatal lethal in two weeks; underdeveloped pulmonary vascular network; abnormal vascular branching; increased hemorrhage; lean hypermetabolic phenotype with normal adipocyte differentiation and reduced energy store	(252, 284)
***Adam19*$^{-/-}$**	80% postnatal lethality 1-3 days after birth; ventricular septal defect; immature valves; abnormal development of artery and pulmonary valves and the cardiac vasculature; reduced angiogenesis; impaired growth and differentiation of the endocardial cushion	(259, 260)
***Adam9/15*$^{-/-}$**	Viable, fertile, no obvious pathology	(41)
***Adam9/12/15*$^{-/-}$**	Viable, fertile, no obvious pathology	(41)
***Adam9/12/15/17*$^{-/-}$**	Similar to *Adam17*$^{-/-}$ phenotype with slightly higher embryonic lethality	(41)
***Adam33*$^{-/-}$**	Viable, fertile, no evident spontaneous pathological or developmental phenotypes; induction of angiogenic sprouting; enhanced blood vessel formation in human embryonic lung explants; expression correlated with asthma and airway hyperresponsiveness	(285, 286)

ADAM15. ADAM15 is widely expressed in brain, lymphoid cells, and vascular cells, and is a unique sheddase that cannot be activated by phorbol esters or calcium ionophores, two common activators of ADAMs. ADAM15 has been suggested to be involved in a number of inflammatory conditions including atherosclerotic lesions (287). Moreover, ADAM15 has also been associated with pathological neovascularization in proliferative retinopathy which was suppressed in *Adam15*$^{-/-}$ mice (235), but not in mice carrying a loss-of-function point mutation in the catalytic domain of ADAM15 (288). This was attributed to the very limited target substrates for this ADAM protease, and highlights the importance of non-catalytic functions of ADAM15 in neovascularization. ADAM15 is highly expressed in ECs and can upregulate the expression of vascular endothelial growth factor-A (VEGFA) and its cognate receptors, VEGFR1 and VEGFR2, under ischemic conditions (289), which strongly supports its proangiogenic function. These studies highlight the significance of ADAM15 function in disease conditions despite its apparent lack of contribution to embryonic development. ADAM15 has been shown to inhibit SMC migration by affecting integrin β_1 (290), but promote angiogenesis in a mouse model of retinopathy (235).

ADAM17. ADAM17 has been shown to be one of the indispensable ADAM sheddases involved embryonic development, and is expressed mainly in embryonic fibroblasts, cardiomyocytes, and SMCs. Although *Adam17*$^{-/-}$ mice are embryonically lethal, they do not show any defects in Notch signaling (252). However, due to the disrupted EGFR signaling, *Adam17*$^{-/-}$ embryos exhibit thickened and malformed heart valves that resemble those of mice lacking HB-EGF (229, 282, 291, 292). *Adam17*$^{\Delta Zn/\Delta Zn}$ mice showed underdeveloped pulmonary vasculature network, abnormal vascular branching, and increased hemorrhage (284). *In vitro,* ADAM17 promotes SMC migration through transactivation of the EGFR signaling pathway by various CPGR agonists (214, 293). Endothelial ADAM17 has been implicated in promoting or inhibiting cell migration and angiogenesis, depending on which substrate is cleaved (reviewed in (247))

ADAM19. ADAM19 is highly expressed in ECs, epithelial cells, fibroblasts, and cardiomyocytes (294). *Adam19*$^{-/-}$ mice show ventricular septum defects, abnormal formation of heart valves, and some neuronal abnormalities. Therefore, most mice die within 1-3 days after birth (295). ADAM19 has been suggested to participate in the development of the endocardial cushion. During this process, epithelial-to-mesenchymal transformation (EMT) of endocardial epithelial cells generates most of the cushion mesenchymes that constitute the main components of the septa

and valves. In the endocardial cushion, ADAM19 is expressed in both epithelial and mesenchymal cells which are originating from the neural crest cells. Overexpression of ADAM19 in neural crest cells, but not in ECs, was crucial for the proper formation of ventricular septum and valves. This study further demonstrated that while *Adam19*-deficient neural crest cells migrated into the heart normally, they could not properly fuse the right and left ridges of the cushion tissues in the proximal outflow tract, and therefore led to defects in the assembly of the outflow tract and the atrioventricular cushions that would form the ventricular septum (260). Embryonic fibroblasts from *Adam19*$^{-/-}$ mice exhibit aberrant ectodomain shedding of neuregulin-1, one of the ErbB ligands expressed in ECs, which could explain the impaired differentiation of the endocardial cushion during the development of the heart, highlighting the critical role of ADAM19 in proteolytic regulation of ErbB signaling (295). ADAM19-mediated shedding of neuregulin was reported to stimulate proliferation and angiogenesis of ECs in an autocrine manner (296). However, ADAM19 cleaves HB-EGF only in the absence of ADAM17 (268), suggesting this protease may not be important in regulating cardiac development process through the EGFR signaling. The blood vessels within the myocardium of *Adam19*$^{-/-}$ mice appeared abnormal, with disrupted SMC ensheathment. In contrast, perivascular edema in capillaries and extensive vacuolization of ECs were observed in the myocardium (297).

ADAM33. ADAM33 is a widely expressed member of the ADAM family, and is proposed to contribute to airway inflammation, such as asthma and bronchial hyperreactivity in a genome-wide association study (298). However, the genetic study failed to show phenotypic differences between WT and *Adam33*$^{-/-}$ mice in established models of airway inflammation (285). Interestingly, although no information is available in terms of the role of ADAM33 in cardiovascular development, it has been shown that ADAM33 was upregulated in human atherosclerotic plaques, mainly dominated by SMCs and inflammatory cells. *In vitro* study also confirmed the inhibitory role of ADAM33 in SMC migration. Moreover, an ADAM33 single nucleotide polymorphism (rs574174) is positively correlated with atherosclerosis severity (299). The purified catalytic domain of ADAM33 has been shown to cause rapid induction of EC differentiation *in vitro*, and neovascularization *ex vivo* and *in vivo* (286).

1.10. ADAM dysregulation is associated with miscellaneous human diseases

In most cases, augmented expression of ADAMs are linked to miscellaneous pathological conditions, such as diseases of respiratory system (e.g., ADAM33) (298), central nervous system (e.g., ADAM8 (38)), liver (e.g., ADAM17 (212)), kidneys (e.g, ADAM17 (183, 300)), muscles (e.g., ADAM12 (236)), and joints (e.g., ADAM17 (221)). Conversely, overexpression of some ADAMs may elicit protective effects on several diseases. A typical example for this case is that ADAM10, as the predominant α-secretase (301), can cleave APP and prevent the production and aggregation of neurotoxic β-amyloid peptides (302), thereby ameliorating the progression of Alzheimer's disease. This protective role of ADAM10 in neurodegenerative diseases is corroborated by the observation that overexpression of ADAM10 alleviates the symptom in a mouse model of Alzheimer's disease (258).

1.11. ADAM17 in cardiovascular diseases

Since the role of ADAM17 in hypertension and the associated cardiovascular pathologies (end-organ damage) and aortic aneurysm are the main focuses of this dissertation, the involvement of ADAM17 in hypertension and the associated concentric cardiac hypertrophy and renal dysfunction, as well as aortic aneurysm, will be addressed.

1.11.1. Augmented ADAM17 expression contributes to diseases of the cardiovascular system

Although tremendous efforts have been devoted to mechanistic studies and drug development, diseases of the cardiovascular system remain the primary cause of human morbidity and mortality worldwide. It has been widely accepted that ADAM17-dependent ectodomain shedding of substrates such as EGFR ligands, TNFα and its receptors, interleukin 6 receptor (IL6R), VEGFR2, L-selectin, ICAM-1, VCAM-1, CX3CL1, C-X-C motif ligand 16/CXCL16, JAM-A and vascular endothelial (VE)-cadherin can directly or indirectly regulate a series of biological processes such as cell growth, proliferation, migration, differentiation, and apoptosis, angiogenesis and neovascularization, ECM remodeling, inflammatory cell adhesion, recruitment, and transmigration, and vascular barrier integrity, of all which are closely associated with the etiologies of many types of pathological conditions, such as cancer, inflammatory diseases, and cardiovascular diseases. To date, the pathological roles of ADAM17 in cancer and inflammatory

diseases have been extensively investigated (4, 46, 303-306), and numerous synthetic inhibitors or antibodies targeting ADAM17 have been developed and are being tested in preclinical and clinical studies to evaluate their efficacy in suppressing tumorigenesis and inflammation (188, 247, 307) (see also in **Chapter 1.12** for more detailed description). Within the cardiovascular system, ADAMs 8, 9, 10, 12, 15, 17, 19, 28, and 33 are expressed at basal levels. However, the role of ADAM17 and other ADAMs in the cardiovascular physiology and pathology remain underexplored.

1.11.2. ADAM17 in hypertension

Longstanding hypertension is the primary cause of hypertensive cardiac remodeling (308) and nephropathy (309). Although the precise mechanisms underline the pathogenesis of hypertension remains elusive, diverse factors such as genetic mutations and single nucleotide polymorphisms (SNPs), stress, obesity, diabetes, as well as environmental factors predispose to hypertension and subsequent end-organ damage.

However, studies on the role of ADAM17 in hypertension are scarce, with one study showing that global inhibition of ADAM17 failed to suppress systolic blood pressure increase in the spontaneously hypertensive rat model (310), and another study showing SMC-specific deficiency of *Adam17* had no effect on hypertension (endpoint recording) after 2 weeks of Ang II infusion (311).

1.11.3. ADAM17 in cardiac hypertrophy

Accumulating evidence shows that ADAM17 is involved in GPCR agonists-induced EGFR transactivation, which propagates the downstream MAPK and PI3K pathways and contributes to cardiovascular complications including hypertension and cardiovascular remodeling (312). In the heart, activated signaling through MAPK and PI3K pathways drives transcriptional and posttranscriptional regulation of immediate-early genes and the re-expression of fetal genes (e.g., α-skeletal actin and β-myosin heavy chain) to promote the growth of cardiomyocytes and subsequently the development of cardiac hypertrophy. Meanwhile, ECM components such as fibronectin-1 and collagen type I and III, are also upregulated, which contribute to cardiac fibrosis (313).

By examining ADAM17 expression patterns in human healthy and hypertrophic heart specimens, it revealed that ADAM17 was increased in the hearts of patients with dilated cardiomyopathy (DCM) and obstructive cardiac hypertrophy (314). In contrast, elevated levels of ADAM12 were only observed in hypertrophic hearts (314).

In animal models, Asakura, *et al.* (175) firstly reported that ADAM12 inhibition attenuated cardiac hypertrophy and subsequent dilation in mice through either induction of pressure overload or administration of GPCR agonists, Ang II and phenylephrine (PE). The authors further demonstrated *in vitro* that Ang II, endothelin-1, and PE could transactivate EGFR signaling to promote cardiomyocyte hypertrophy through ADAM12-mediated shedding of HB-EGF. Pharmacological inhibition of ADAM12 activity using a metalloproteinase inhibitor or a neutralizing antibody against HB-EGF abrogated protein synthesis in cardiomyocytes in response to PE or Ang II treatment. Interestingly, suppressed ADAM12-HB-EGF-EGFR signaling also improved cardiac contractility. A followed study further showed that MMP7-ADAM12 axis was involved in Ang II-induced hypertension, and inhibition of MMP7 not only attenuated blood pressure increase and cardiac hypertrophy, but also suppressed ADAM12 overexpression (205).

Interestingly, ADAM17 seems to function upstream of ADAM12 as well, since inhibition of this ADAM protease blocked cardiac hypertrophy and fibrosis in rodent models of spontaneous hypertension and Ang II-induced hypertension through regulating ADAM12 and MMP2 activities (310). The central role of ADAM17 in Ang II-mediated cardiac hypertrophy was further corroborated by the finding that this pathological process can be regulated through the activated nicotinamide adenine dinucleotide phosphate oxidase 4 (Nox4)-ADAM17-HB-EGF-EGFR signaling axis (315).

It has long been observed that Ang II can trigger a hypertrophic but not hyperplastic response in cultured SMCs (316). However, the underlying mechanism was obscure until ADAM17 was found to be involved in Ang II-mediated EGFR transactivation through the shedding of HB-EGF in SMCs. The activated EGFR signaling was subsequently responsible for protein synthesis in VSMCs (172, 317). A recent study reported that a short-term (2 weeks) infusion of Ang II was protective against the development of cardiac and renal hypertrophy and fibrosis (311). However, our study (the key findings in **Chapter 3**) revealed that this effect of ADAM17 is rather transient and *Adam17*-deficiency in SMCs does not offer long-term protection (214).

Surprisingly, it has been shown that genetic deletion of *Adam17* specifically in cardiomyocytes exacerbated pressure overload-induced cardiac hypertrophy and systolic dysfunction, mainly due to upregulated integrin β_1 levels (318). It is well-established that mechanical stress induces the expression of integrin β_1, the cell surface sensor for stress/strain that activates the intracellular pro-hypertrophic signaling pathways (319). While this function of integrin β_1 is required for induction of compensatory hypertrophy, an augmentation of its membrane-bound level can exacerbate the hypertrophic response leading to early onset of decompensation and dilated cardiomyopathy. Therefore, upregulated ADAM17 in cardiomyocytes may facilitate the shedding of the ectodomain of integrin β_1, thereby disrupting its connection with the ECM and limiting the extent of the resulting hypertrophy (318). Intriguingly, this function of cardiomyocyte ADAM17 was limited to hypertrophy secondary to mechanical stress, but not to Ang II-induced hypertrophy (318). Therefore, it suggests that cardiomyocyte ADAM17 might regulate cardiac hypertrophy only upon mechanical stress but not GPCR agonists. Overall, these findings suggest that cell type-specific ADAM17 may play different roles in the pathogenesis of cardiac hypertrophy triggered by different stimuli.

1.11.4. ADAMs in renal diseases

There are a limited number of studies exploring the role of ADAM17 in renal diseases. ADAM17 has been found to mediate prolonged Ang II infusion-induced chronic renal disease, where elevated shedding of TGFα activated the EGFR signaling and subsequently led to renal lesion and fibrosis (300).

In addition to the detrimental role of ADAM17 in hypertensive nephropathy, a recent study showed that renal proximal tubule-specific ADAM17 was responsible for renal inflammation and fibrosis through cleavage of pro-TNFα and one of the EGFR ligands, amphiregulin, in a mouse model of renal fibrosis (183).

1.11.5. ADAMs in vascular remodeling

ADAM17-mediated shedding events, such as activation of the inflammatory response, an increase in permeability, leukocyte adhesion and recruitment, inflammation resolution, vascular repair, and neovascularization, can be implicated in several vascular pathophysiological processes.

Therefore, inflammation is a common feature observed in these processes, and activated ADAM17 is found to regulate leukocyte rolling, adhesion, intraluminal crawling, transendothelial extravasation, and proliferation through a well-orchestrated ADAM17-mediated shedding events at the right time and the right place through cleavage of PSGL-1 and CD44 on leukocytes (320); of selectins (e.g., P-selectin and E-selectin) (321, 322), adhesion molecules (e.g., VCAM-1 and ICAM-1) (323), chemokines (e.g., CX3CL1 and CXCL16) (157), adherens junctions (e.g., VE-cadherin) (324), and tight junctions (e.g., JAM-A (115) and claudin (106)) on activated ECs; of ECM components (e.g., collagen IV, the major structural protein in the basal membrane) in the extracellular space; and of growth factor ligands from themselves or neighboring cells (41, 232).

ADAM17 has been shown to increase predominantly in the macrophage-positive regions of human atherosclerotic plaques compared to healthy arteries (325, 326). In patients with coronary artery diseases, the ADAM17 level was drastically elevated in the infarcted area of the heart post-acute MI (327).

Animal studies revealed that the ADAM17-mediated inflammation is associated with atherogenesis. It was reported by Canault*, et al.* (328) that ADAM17 expression in aortic lesions showed a time-dependent elevation in atherosclerosis-prone *Apoe*$^{-/-}$ mice fed a high-fat diet with different durations. However, it does not seem to be the case that broad inhibition of ADAM17 could rescue or at least attenuate this pathological phenotype. A recent study showed that global inhibition of ADAM17 exacerbated the progression of atherosclerosis mainly through constitutive activation of TNFR2 (or p75 TNFR) signaling, which could promote inflammatory cell proliferation and suppress apoptosis (329). Interestingly, accumulating evidence suggests that cell-specific ADAM17 plays different roles in atherogenesis. For example, myeloid *Adam17*-deficient mice developed larger but more stable atherosclerotic plaques compared to the control mice (330). In contrast, endothelial *Adam17*-deficient mice showed significantly less plaque formation (330). Peritoneal macrophage *Adam17*-deficiency led to an anti-atherogenic phenotype through enhanced apoptotic cell phagocytosis (efferocytosis) (211).

ADAM17 has been shown to play a pivotal role in angiogenesis in different disease models. *In vitro,* inhibition of ADAM17 in cultured ECs suppressed cell invasion in a 3D Matrigel, whereas overexpression of ADAM17 resulted in significant outgrowth of endothelial sprouts (331, 332).

Therefore, increased endothelial ADAM17 expression can compromise the structural stability of advanced plaques as a result of enhanced angiogenesis (333, 334). In contrast, endothelial *Adam17*-deficiency has been shown to attenuate pathological neovascularization in oxygen-induced retinopathy through the suppressed ADAM17-dependent VEGFA-VEGFR2-Erk signal cascade (335). Cardiomyocyte-specific *Adam17*-deficiency exacerbated left ventricle dilation and dysfunction post-MI due to reduced angiogenesis in the infarcted myocardium (336). The compromised angiogenesis was not because of reduced shedding of VEGFA, but rather due to reduced expression and activation of its receptor, VEGFR2, under ischemic conditions (336). This finding also suggests a role for ADAM17 in the crosstalk between cardiomyocytes and ECs in the myocardium. However, it should be noted that while ADAM17-mediated angiogenesis worsens the progression of retinopathy, it improves heart functions post-MI.

In addition to regulating angiogenesis through the VEGF-dependent pathway, endothelial ADAM17 inversely regulates the expression level of thrombospondin-1 (TSP1), a potent anti-angiogenic adhesive glycoprotein (337). A recent study has shown that inhibition of TSP1 attenuated re-endothelialization and exacerbated neointimal formation post vascular injury in mice (338).

Overall, these findings not only demonstrate distinct functions of ADAM17 in an organ- and disease-dependent fashion, but also indicate that cell type-specific ADAM17 exerts differential functions even under the same pathological condition. Therefore, a thorough understanding of cell-specific functions of ADAM17 in the cardiovascular system is the prerequisite to the development of effective and specific drugs targeting cardiovascular diseases with minimal side effects. Moreover, global overexpression or inhibition of ADAM17 may not be a suitable approach to treat these diseases (will discuss in more detail in **Chapter 1.12**).

1.11.6. ADAMs in aortic aneurysm

1.11.6.1. Definition, epidemiology, and etiologies of aortic aneurysm

Aortic aneurysm, which is defined as a focal dilation and weakening of the aortic wall that is at least 50% larger than the normal diameter, is the second most frequent aortopathy after atherosclerosis. Based on the location of aortic dilation along the vascular tree, aortic aneurysm can be termed as thoracic aortic aneurysm (TAA) and abdominal aortic aneurysm (AAA). While

human AAA is usually found at the infrarenal aorta, TAA can be found at different locations along the thoracic aorta. Specifically, approximately 60% of TAAs occur in the root or ascending aorta, 10% in the aortic arch, 40% in the descending aorta, and 10% in the thoracoabdominal aorta, with some aneurysms developing in multiple sites (339). In addition, TAA may present in 10%-15% of AAA patients (340).

Overall, AAA is more commonly found than TAA in the general population. The prevalence rates for TAA and AAA are 0.16% to 0.34% (341, 342) and 1.7% to 7.2% (343-345), respectively. However, TAA rupture-associated mortality rate is about two to three times higher than that of AAA (346).

It is also noteworthy to point out that patients with aortic aneurysm are at increased risk of cardiovascular events that are unrelated to the aneurysm *per se*, but plausibly related to common risk factors such as hypertension and inflammation. Indeed, the 10-year risk of mortality from any other cardiovascular cause (e.g., MI or stroke) may be 15 times higher in risk than that of aortopathy-related death in patients with AAA (347). Currently, there are no pharmacological interventions available for aortic aneurysm, and surgical repair is the only option for this disease. However, patients remain at increased risk for cardiovascular events even after their aneurysms are successfully repaired (348). Considering ADAM17-mediated shedding can affect all these pathological processes during the development of aortic aneurysm, inhibition of ADAM17 may represent a promising therapeutic strategy for this vascular disease. Therefore, the advances in exploring the expression patterns and functional role of ADAM17 in different types of aortic aneurysms from human specimens and animal models will be highlighted, respectively.

It has been widely recognized that TAA and AAA are distinct pathologies, according to the differential anatomical locations, functional and structural characteristics, as well as embryonic origins of SMCs between the thoracic and abdominal aorta (349). The recent advances indicate that the initiation of AAA is multifactorial with a strong genetic element. Smoking has been shown to be the most important risk factor associated with AAA, which is followed by age, hypertension, hyperlipidemia, atherosclerosis, and male sex (350). Indeed, AAA is more commonly found in elders, and displays a strong sex-dependent prevalence discrepancy, with men being 6 times more affected than women. Interestingly, a large cross-sectional study suggests that genetic component

is actually the second most important risk factor in AAA development (350). Candidate gene and genome-wide approaches have identified robust associations between AAA and variants in or nearby the *SORT1*, *LDLR*, *DAB2IP*, *LRP1*, *ELN*, *CRP*, *TGFB,* and various *MMP* genes, suggesting that aberration of lipid metabolism and proteolytic pathways are the key contributors to AAA (**Table 1.5**). As such, there is a strong atherosclerotic background behind AAA formation, partly because AAA shares exactly the same major predisposing factors as atherosclerosis. However, many of the genes predisposing to atherosclerosis have not been shown to be implicated in AAA formation. Due to its higher prevalence in the general population, AAA is more extensively investigated than TAA, and steady progress has been made in understanding pathophysiological mechanisms underlying AAA (reviewed in (351-355)).

In comparison, TAA can occur at a young age due to strong hereditary influence. However, no overt sex propensity (male:female≈1.7:1) is observed in TAA. The etiologies underlying TAA are diverse and are associated with a complex interaction between genetic factors and hemodynamics (356). To date, a great number of genes causing TAA have been identified and these genetic forms of TAA can be grouped into syndromic and familial forms. Sporadic TAA is a collective term for non-syndromic and non-familial TAA and comprises the largest portion of TAA. The well-defined characteristics of the structure and function of the normal aortic wall, coupled with the discovery of genetic mutations in key regulatory molecules, could contribute to a better understanding of the pathophysiology of syndromic, familial, and sporadic TAAs.

Due to the diverse etiologies, the onset and rate of progression of aortic dilation among the three forms of TAAs are highly variable. Patients with familial TAA generally present at an earlier age (56.8 years) than those with sporadic TAA (64.3 years) (357), since the aneurysmal aorta expands faster in patients with familial TAA (0.21 cm/year *vs.* 0.16 cm/year) (358). In contrast, patients with syndromic TAA present with aortic disease at a much younger age as a result of rapid aortic expansion. Marfan aortas grow at 0.1 cm/year, whereas TAAs of the Loeys-Dietz syndrome can grow faster than 1.0 cm/year, resulting in an average age of death at 26 years (358).

Typically, syndromic TAAs are associated with certain inherited connective tissue disorders, such as Marfan syndrome (mutations in *FBN1*), Loeys-Dietz syndrome (mutations in *COL3A1*), and Ehler-Danols syndrome (mutations in *TGFBRI*, *TGFBRII, SMD3, TGFB2, or TGFB3*). The

genetic basis of familial syndromic TAAs is heterogeneous. Since most of the mutated genes are inherited in an autosomal-dominant manner with variable clinical presentation and incomplete penetrance, about 20% of TAAs have a strong family history (359). So far, a total of 6 mutated genes are identified to cause familial TAAs, and these genes are responsible for coding components of the SMC contractile apparatus (i.e., *MYH11*, *ACTA2*, *MLCK*, and *PRKG1*) or their modifying enzymes (i.e., *MFAP5* and *MAT2A*) (**Table 1.5**). Of note, the six currently identified genes can only explain <20% of all familial TAAs, indicating that there should be more genes to be identified to contribute to this type of TAAs. However, hereditary studies showed that some syndromic TAA-associated genetic mutations are also observed in a subset of patients with familial TAAs, such as *FBN1* in Marfan syndrome and *TGFBRI*, *TGFBRII*, *SMD3*, *TGFB2*, and *TGFB3* in Loeys-Dietz syndrome. In addition, some chromosomal copy number variations and SNPs have emerged as genetic variants that might predispose to familial TAAs and sporadic TAAs (reviewed in (360)). An up-to-date compendium of human aortic aneurysm genes and mutations is available at www.omim.org.

Bicuspid aortic valve (BAV) disease is the most common congenital heart defect that affects approximately 1.3% of the general population, with men being 3 times more commonly affected than women (361, 362). Patients with BAV have degenerative changes in the media of the ascending aorta, including reduced and fragmented elastic fibers and SMC abnormalities, which could lead to maladaptive ECM remodeling and aortic dilation and ultimately TAA. Moreover, asymmetric blood flow applied to the ascending aorta and proximal aortic arch also contributes to TAA formation. BAV-associated TAA accounts for about 14% of patients with TAA (363). A genetic mutation in *NOTCH1* has been identified in a small portion of patients with BAV-TAA (364). Patients with BAV-TAA present at an averaged age of 56 years. Although a sex-dependent TAA prevalence pattern is not observed in BAV patients, TIMP2 levels, SMC density, and collagen content were higher in female aneurysmal samples, suggesting a milder aneurysm phenotype in female patients (365).

Sporadic TAAs occur in isolation and do not show any syndromic or familial transmission. However, sporadic TAAs share the common features of TAAs, which are generally characterized by apoptosis and disarray of VSMCs, fragmentation of elastic fiber, collagen deposition, inflammatory cell infiltration, and upregulation of metalloproteinases. Since sporadic TAAs encompass a wide range of causative etiologies, the precise cellular and molecular mechanisms remain poorly understood. Therefore, using genetic, molecular, cellular, and engineering techniques in conjunction with appropriate animal models for TAA will help generate a much more cohesive understanding of the pathophysiological mechanisms of sporadic TAAs.

1.11.6.2. Mouse models of thoracic and abdominal aortic aneurysm

At the pathological level, TAA is characterized as a degenerative disease, and shows medial cystic necrosis, elastin fragmentation, SMC proliferation, and less prominent leukocyte infiltration. In comparison, AAA is usually linked to atherosclerosis, and displays destructive ECM remodeling, SMC apoptosis, neovascularization, and marked inflammatory cell infiltration (**Table 1.5**).

Table 1.5 Comparison of the pathogenesis of thoracic and abdominal aortic aneurysm AAA

	TAA	AAA
Risk factors	Hypertension, BAV	Hypertension, smoking, hypercholesterolemia, obesity, aging, male sex
Sex-dependent prevalence (male-to-female ratio)	1.7:1	6:1
Average age	65 years for overall TAAs; 26 years for syndromic TAA; 56.8 years for familial TAA; and 64.3 for sporadic TAA	75 years of age
Pathological characteristics	Cystic medial necrosis, elastic fiber fragmentation, SMC apoptosis, proteoglycan accumulation, less extent of inflammation	Elastic fiber degradation, SMC loss, neovascularization, chronic inflammation
Inflammatory phenotype	Th1-predominant immune response	Th1- & Th2-predominant immune responses
Predominantly elevated cytokines	IFNγ	IFNγ, IL4, IL10, and IL17
Genetic predisposition	*ACTA2, FBN1, MFAP5, MYH11, MYLK, NOTCH1, PRKG1, SMD3, TGFBRI, TGFBRII*	*19q13 (AAA1), 4q31 (AAA2), ACE, AGTR1, CDKN2B-AS1, CNTN3, DAB2IP, IL1RN, IL6R, LPA, LRP1, LDLR, SORT1*

Abbreviations: AAA, abdominal aortic aneurysm; ACE, angiotensin converting enzyme; ACTA2, α-smooth muscle actin; AGTR1, Angiotensin II receptor type 1; CNTN3, contactin-3; DAB2IP, DAB2 interacting protein; FBN1, fibrillin-1; IFNγ, interferon gamma; IL1RN, interleukin 1 receptor antagonist; IL6R, interlukin-6 receptor;LDLR, low-density lipoprotein receptor; LPA, lipoprotein (A); LRP1, low-density lipoprotein receptor-related protein 1; MFAP5, microfibril-associated protein 5; MYH11, myosin heavy chain 11; MYLK, myosin light chain kinase; PRKG1, cGMP-dependent protein kinase type 1; SORT1, sortilin-1; TAA, thoracic aortic aneurysm; TGFBR, transforming growth factor β receptor.

*Primary references can be found in Luyckx, et al. (360);Saratzis and Bown (366);*and *Brownstein, et al. (367).*

Theoretically, monitoring the changes at cellular and molecular levels during the initiation, maturation, and rupture of human aortic aneurysm would help target critical molecules that are involved in the pathogenesis of aneurysm more precisely. By the nature of the disease, acquisition of human aneurysmal tissues in these formative phases of the disease is not a practical option. Most of the human aneurysmal biopsies acquired during surgical repair are at the advanced stage of the disease, and as such, these precious human tissues can only provide very limited insight into the pathological characteristics of aortic aneurysm at the late stage of the disease.

In this regard, it is important to establish animal models that could recapitulate key features of human TAA or AAA before we can better understand the cellular and biochemical changes during the progression of the two distinct vascular diseases. Due to the complexity of the etiologies of both aneurysms, a number of mouse models for TAA and AAA have been successfully developed and are being used to explore the underlying mechanism for the pathogenesis of aortic aneurysm. Since AAA is more extensively investigated than TAA, a greater number of mouse models (e.g., calcium chloride, elastase, Ang II, and transgenic mice) are available for this type of aneurysm. In comparison, mouse models for TAA are relatively limited. Transgenic mice with known causative or suspicious genetic mutations are used to imitate the mechanisms of different types of aortic aneurysms. Calcium chloride and elastase models were developed recently and are being used to elucidate the role of the protein of interest in the pathogenesis of sporadic TAAs by knocking out the target gene. Ang II and a lysyl oxidase (LOX) inhibitor, β-aminopropionitrile (BAPN), are used in combination to induce TAA, thoracic aortic dissection, or AAA in mice. Although most of the mouse models reproduce inflammation, ECM destruction, cell apoptosis, and aortic dilation, all of which are proposed to be determinants in aortic aneurysm development in humans, they cannot completely mirror the pathological conditions in human aortic aneurysm. The variety of injuries applied to the aorta to trigger experimental aortic dilation reflects the multiplicity of pathways that may be triggered or compromised during the pathogenesis of aortic aneurysm. Therefore, contradictory results can be observed when different disease models are applied to the same genotype. For example, *Mmp12*-deficiency suppresses $CaCl_2$-induce AAA formation (368), but does not affect elastase-induced AAA formation (369). A summary of commonly used mouse models for TAA and AAA is available in **Table 1.6**. Large animal models for aortic aneurysm are primarily developed for interventional testing, and the commonly used AAA models in large animals have been reviewed elsewhere (370, 371).

The calcium chloride model. Periadventitial application of calcium chloride ($CaCl_2$) was the first report to induce aneurysm in rabbit common carotid artery by Gertz*, et al.* (372). Later, Chiou*, et al.* (373) reported the first reproducible AAA model in mice by placing a cotton gauze soaked in $CaCl_2$ topically to the infrarenal aorta for 10-15 min. The $CaCl_2$ concentration used for AAA vary in reported literature, ranging from 0.25 M to 1.0 M (374). Moreover, it usually takes 2-12 weeks to achieve an aortic dilation of more than 50% than the baseline value with an incidence of 50%-93% (374). In order to accelerate the development of AAA, $CaCl_2$ and phosphate-buffered saline (PBS) were sequentially applied to the abdominal aorta to form $CaPO_4$ nanoparticles, and an average increase in aortic diameter than 50% has been reported to occur as early as one week following the intervention (375). The effect of sex on $CaCl_2$-induced AAA has not been reported. Nevertheless, $CaCl_2$-induced experimental aortic aneurysm demonstrates the following pathological characteristics typically observed in human aneurysmal biopsies, including calcification, inflammatory cell infiltration, oxidative stress, neovascularization, elastin degradation, and SMC apoptosis. However, $CaCl_2$-induced experimental aortic aneurysm shows no thrombus or rupture. A number of mechanistic studies showed that a few key molecules such as c-Jun N-terminal kinase (JNK), peroxisome proliferator-activated receptor-γ (PPARγ), MMPs, CCL2, group X secretory phospholipase A2 (sPLA2-X), and plasminogen are involved in $CaCl_2$-induced AAA (reviewed in (374)).

Similarly, this method was adapted to induce TAA by incubating mouse thoracic aorta with 0.5 M of $CaCl_2$ for 15 min (376-378). However, $CaCl_2$-induced dilation in the thoracic aorta is mild, and only an average dilation of 25%-45% after 4 weeks of treatment was reported (376, 378). Moreover, the reproducibility is also relatively low (376-378). In our hands, $CaCl_2$/PBS combination did not induce TAA even after 4 weeks of treatment, as it only triggered fibrosis in the periadventitial region (unpublished data). In addition, $CaCl_2$-induced TAA is associated with a high operative mortality rate (>30%) due to pulmonary complications, since $CaCl_2$ spillage can cause acute lung failure.

The elastase model. The elastase model is used to induce both TAA and AAA. Elastase was initially used to induce AAA by perfusing the abdominal aorta intraluminally with diluted porcine pancreatic elastase type I. Briefly, the procedure is performed in anesthetized mice via a midline abdominal incision. The abdominal aorta is dissected from the vena cava and atraumatic clamps or

temporal suture ligations are positioned distal to the renal arteries and proximal to the iliac bifurcation. The isolated abdominal aorta is perfused with 0.4 U/ml of elastase at 100 mmHg for 5 min through a catheter. After the perfusion is completed, the catheter is removed, and the blood flow is restored before the incision on the abdominal aorta is closed (379). Since this procedure is extremely technically demanding, Bhamidipati*, et al.* (380) modified this model and induced AAA by incubating the adventitial layer of abdominal aorta with undiluted elastase for 5 min. This periadventitial elastase model was then adapted to induce TAA (381), considering the low reproducibility and high mortality by using the $CaCl_2$ model. After acute exposure to elastase, mice can develop TAA or AAA in 2 weeks, and present multiple histological phenotypes that resemble those in human tissues, including diminished and fragmentation of elastic fiber, SMC loss, and inflammatory infiltration (predominantly found in the adventitia). Further molecular analysis revealed that elastase-induced aortic aneurysm shows a drastic activation of MMP2 and MMP9. However, elastase-induced aortic aneurysm does not display thrombus, atherosclerosis, and rupture, which are classical features of human AAA. Interestingly, a recent study showed that a combination of oral administration of BAPN and periadventitial elastase application induced a chronic, advanced-stage AAA with characteristics of persistent aneurysm growth, thrombus, and spontaneous rupture (382). Compared to the periadventitial application model, the intra-luminal perfusion model can result in a macroscopic dilation right after the catheter is withdrawn from the abdominal aorta. The mechanical stress can make the aorta dilate more than 50% than its intimal diameter even when the heat-deactivated elastase is used. Therefore, in this model the threshold of aortic dilation that can be referred to as AAA is usually set to above 100%, which is somewhat against the definition of aortic aneurysm. Interestingly, the elastase perfusion model was used to test sex differences in AAA development, with female mice being more protected against AAA formation (383).

Table 1.6 Mouse models of thoracic and abdominal aortic aneurysm

Mode of TAA induction	Comments	Refs
Genetically modified		
Blotchy	Genetic abnormality on X chromosome, defective collagen and elastin cross-linking due to an underlying defect in copper metabolism	(384)
***Fbn1*$^{C1039G/+}$, *Fbn1*$^{mgR/mgR}$**	Fibrillin-1 deficient, mimics Marfan syndrome	(385, 386)
***Tgfbr1*$^{+/-}$, *Tgfbr2*$^{+/-}$, *Tgfbr1*$^{M318R/+}$, *Tgfbr2*$^{G357W/+}$**	Mimics Loeys-Dietz syndrome	(387)
***Smad3*$^{-/-}$**	Mimics familial TAA, TAA development due to increased GM-CSF expression and inflammatory cell infiltration	(388)
***Smad4*$^{\Delta SMC}$**	Mice develop TAA spontaneously due to upregulated cathepsin S and MMP12 and inflammatory cell infiltration triggered by chemokines released by *Smad4*-deficient SMCs	(389)
***Notch1*$^{+/-}$, *Nos3*$^{-/-}$, *Gata4*$^{+/-}$, *Gata5*$^{-/-}$, *Nkx2.5*$^{+/-}$, *Robo1*$^{-/-}$; *Robo2*$^{-/-}$**	Mimic BAV-associated TAA	(390)
Chemically induced		
$CaCl_2$	Peri-adventitial application of 0.5 M $CaCl_2$ for 15 min, and mice develop TAA in 4 weeks. TAA development is associated with calcification, MMP activation and inflammatory cell infiltration.	(376-378, 391, 392)
Elastase	Peri-adventitial application of undiluted porcine pancreatic elastase for 5 min, and mice develop TAA in 2 wks.	(381, 393)
Deoxycorticosterone acetate+salt or aldosterone+salt	Established a role for mineralocorticoid receptor agonist and high salt in the pathogenesis of TAA and AAA	(394)
Ang II	Ang II infusion for 4 weeks, triggers ECM remodeling, SMC dysfunction, and inflammation.	(378, 395-397)
Ang II+BAPN	3 days of Ang II infusion right after 3 weeks of BAPN infusion. Acute aortic dissection due to infiltration of neutrophil into the aorta.	(398)
Mode of AAA induction	**Comments**	**Refs**
Genetically modified		
***Lox*$^{-/-}$**	Elastin and collagen cross-linking defect with death from aneurysmal rupture in full-term fetus	(399)
Ldlr-/-	Aneurysms localized to the suprarenal segment in mice fed diets enriched with saturated fat, cholesterol, and cholate	(400)
Tsukuba hypertensive mice	Mice overproduce Ang II, rupture of abdominal and thoracic aorta aneurysms within 10 days of increased salt intake	(401)
Chemically induced		
$CaCl_2$	Peri-adventitial application of 0.25 M-1.0 M $CaCl_2$ for 10-15 min, and mice develop TAA in 2 -12 weeks. TAA development is associated with calcification, MMP activation and inflammatory cell infiltration.	(373, 374)
$CaCl_2$/PBS	Infrarenal AAA. Peri-adventitial application of 0.5 M $CaCl_2$ for 10 min and PBS for 5 min, and mice develop AAA in one week. AAA development is associated with calcification, inflammation, and SMC apoptosis.	(375)
Elastase intraluminal perfusion	After temporary obstruction of the infrarenal aortic segment, an arterectomy is performed and elastase is perfused at 100 mmHg for 5 min. Dilation occurs in 1 week.	(379)
Elastase periadventitial incubation	After the infrarenal aortic segment is exposed, a piece of gauze soaked in undiluted elastase is covered on the aorta for 5 min. AAA develops in 2 weeks.	(380)
Elastase + BAPN	Oral administration of BAPN and peri-adventitial elastase application induces a chronic, advanced-stage AAA with characteristics of persistent aneurysm growth, thrombus, and spontaneous rupture.	(382)
Ang II-hyperlipidemic mice	Ang II infusion for 4 weeks to induce suprarenal AAA in *Apoe*$^{-/-}$ or *Ldlr*$^{-/-}$ mice	(402)
Ang II-hyperlipidemic mice with an extra genetic mutation	Intercrossing of mice into hyperlipidemic background is time-consuming and expensive. Ang II infusion for 4 weeks to induce suprarenal AAA.	(403-406)
Ang II-normolipidemic mice with a genetic mutation	Ang II infusion for 4 weeks to induce suprarenal AAA	(407-413)
Ang II+BAPN	Mice are infused with BAPN for the first 2 weeks and Ang II for 4 weeks to induce suprarenal AAA. The phenotype may be genotype-dependent.	(414)

Abbreviation: AAA, abdominal aortic aneurysm; Ang II, angiotensin II; Apoe, apolipoprotein E; BAPN, β-aminopropionitrile; Fbn1, fibrillin-1;Gata, GATA-binding protein; GM-CSF, granulocyte-macrophage colony-stimulating factor; Ldlr, low density lipoprotein receptor; Lox, lysyl oxidase; MMP, matrix metalloproteinase; Nos, nitric oxide synthase; PBS, phosphate-buffered saline; Robo, roundabout guidance receptor; TAA, thoracic aortic aneurysm; Tgfbr; transforming growth factor β receptor.

The Ang II model. Ang II infusion in mice with a hyperlipidemic background (*Apoe*$^{-/-}$ or *Ldlr*$^{-/-}$) is the most widely used AAA model (402). Typically, after 4 weeks of Ang II infusion, these mice develop suprarenal AAA independent of blood pressure increase (403). However, normolipidemic mice can also develop AAA at a lower frequency than hyperlipidemic mice after Ang II infusion (39% *vs.* 100%) (415), suggesting that hyperlipidemia is not required but promotes AAA development. Ang II-induced AAA shows the following characteristics: medial hypertrophy, inflammatory cell infiltration, elastic fiber fragmentation, SMC loss, hemorrhage, and thrombosis. In order to explore whether a gene of interest is involved in AAA development, researchers usually generate targeted genetic knockout mice at a hyperlipidemic background, and test the susceptibility of the double knockout mice to Ang II-induced AAA (403-406). Ang II can also trigger AAA in mice with a single genetic mutation at a normolipidemic background (407-413). Similar to what was observed in the elastase model, Ang II triggered a higher incidence of AAA in male mice (416). Ang II infusion has also been reported to induce TAA in normolipidemic genetic knockout mice (378, 396, 397), suggesting Ang II-dependent GPCR signaling is involved in the pathogenesis of TAA. Moreover, the combination of Ang II and BAPN has been implicated in the development of thoracic aortic dissection (398) or AAA (414), depending on the infusion sequence and duration of the two compounds.

Spontaneously mutated and genetically engineered mice. As mentioned in **Chapter 1.11.6.1.**, genetic variants in the human genome contribute to a large portion of TAA and AAA. Therefore, transgenic mouse models with definitive gene deletion will be the best tool for understanding the functions of the specific genes in the pathogenesis of aortic aneurysm. Similar to those genetic mutations associated with syndromic TAAs and familial TAAs (**Table 1.5**), some single gene mutations in mice have been found to cause spontaneous aortic aneurysm development. The blotchy mouse is a strain containing a spontaneous mutation on the X chromosome which leads to abnormal intestinal copper metabolism. These mice show defective collagen and elastin cross-linking, and most mice develop aortic aneurysm mainly in the aortic arch, thoracic aorta, and occasionally in the abdominal aorta (384). Mice lacking *Smad4* in SMCs are also reported to spontaneously develop TAA due to an upregulation of cathepsin S and MMP12 and inflammation (389). However, the two above mentioned genetic mutations have not been reported in humans with aortic aneurysm. With the increasing use of genetic analysis tools such as genome-wide linkage analyses and genome-wide association studies, more genetic mutations are being or will be

discovered to be associated with human aortic aneurysm. It is more evident than ever that the causes of aortic dilation and subsequent aneurysm are multifactorial, and future studies should include well-characterized populations to adjust for environmental interactions. In addition, more attention should be given on epigenetics and gene expression analyses(417).

Although mouse models for aortic aneurysms are ideal tools to explore specific pathological mechanisms involved in such a complex disease and to enable the development of potential therapeutic targets, there are some inherent limitations that may hinder the translational relevance from mouse models to clinical practice. Firstly, aortic dilation in humans can take decades to form an aneurysm, whereas in mouse models, this occurs within days or weeks after application of the trigger(s). As such, the role of inflammation and proteolytic activity may be overplayed in animal models in terms of their contributions to the progression of aortic aneurysm. Moreover, a rapid stabilization of aortic diameter is followed by healing process in some animal studies because of cessation of the initial stimulus, which is rarely found in human aortic aneurysms. Therefore, mechanisms that may be important to the chronic remodeling of aneurysms in humans are probably poorly represented in animal models. Secondly, thrombus, atherosclerosis (more relevant to AAA), and rupture are commonly found in human aortic aneurysms. These phenotypes are mostly absent in all mouse models. Thirdly, the aorta has been proven to be a heterogeneous organ (349), and the etiologies for TAA and AAA are different. Therefore, aortic aneurysms at both regions that are induced by the same triggers (e.g., elastase, calcium chloride, and Ang II) may not be able to represent the regional-specific pathological mechanisms for TAA and AAA in humans. Lastly, accumulating evidence shows that the pathological events at early (initiation) and late (chronic progression) stages of aortic aneurysm are different. Therefore, the acute aortic aneurysm phenotypes observed in animal models may only reflect the signaling patterns when the disease initiates. This could partially explain why some drugs that are shown to be very effective in animal models but show no effects in clinical trials. A typical example of this notion is doxycycline, a broad-spectrum MMP inhibitor that was shown to suppress experimental AAA in mice but accelerated AAA progression in human patients (418). Overall, there is still great potential for animal models to improve our understanding of the pathogenesis of aortic aneurysm, with the scope of improving current therapeutic strategies. However, caution should be taken when interpreting findings observed in animal models and linking it to clinical practice. On the other hand, more

efforts are required to optimize the currently used animal models for aortic aneurysm to make them more representative of the aneurysmal phenotypes observed in humans.

1.11.6.3. Pathophysiology of aortic aneurysm

Due to the paucity of knowledge on mechanisms of aneurysmal initiation, progression, and rupture, validated medications to slow down or stop aneurysm growth remain lacking. However, progress in understanding aberrant signaling pathways that contribute to aortic aneurysm pathogenesis has been made. Based on characterization of human aneurysmal biopsies and intensive mechanistic studies conducted on genetically engineered and chemically induced animal models, many potential therapeutic targets have been identified and some of them are currently under clinical evaluations (reviewed in (355)). In general, several biological processes have been identified that contribute to the pathogenesis of TAA and AAA, such as inflammation, oxidative stress, elevated proteolysis, SMC apoptosis, EC dysfunction, and ECM degradation.

Renin-angiotensin system (RAS). A positive relationship between the RAS and aneurysm development has been established based on the Ang II infusion model applied in hyperlipidemic or normolipidemic mice (**Table 1.6**). Evidence shows that Ang II induces AAA formation through stimulation of angiotensin receptor type I (AT1), as demonstrated by whole body depletion of *At1* (419). However, cell-specific deletion of *At1* in either SMCs or ECs, the two major cell types in the aortic wall, failed to exert any protective effects on Ang II-induced AAA (420). Additionally, angiotensin-converting enzyme inhibitors (ACEi) (421) and angiotensin receptor blockers (ARB) (422) have been shown to be effective to suppress experimental AAA. The role of RAS in the pathogenesis of TAA may be associated with TGFβ1 signaling, which subsequently affects protease activation and ECM protein degradation (423). Pharmacological inhibition of the AT1 receptor has been shown to suppress TAA in mice with *Fbn1* (424) or *Fbln4* deficiency (425). In contrast, the AT2 receptor has been shown to suppress TAA development in a mouse model of Marfan syndrome through inhibition of the TGFβ1-Erk signaling axis (426). Whole body and EC-specific deletion but not SMC- or leukocyte-specific deletion of *At1* ablated the formation of Ang II-induced TAA (427). Interestingly, Ang II infusion can also promote aortic dilation at the ascending region in C57Bl/6 mice, probably through Ang II-mediated SMC hypertrophy and MMP activation (428). Regardless of the genetic background, the restricted dilation to the ascending aorta in response to Ang II infusion may be attributed to the distinct embryonic origins of SMCs in the

ascending and descending aorta, since evidence shows that the two types of SMCs respond differently to the same stimulus (will discuss in more detail below). Based on the positive findings in animal models of TAA and AAA, alternative strategies such as reducing blood pressure, cardiac inotropy, and shear stress on the aneurysmal aortic segment are proposed to lower the risk of aortic rupture. Disappointingly, clinical trials showed that ACEi, ARBs, β-blockers, and statins all failed to demonstrate a therapeutic reduction of diameter growth compared with placebo (reviewed in (429-431)).

Inflammation. Chronic inflammation is the hallmark of both TAA and AAA, which is a net outcome of infiltration of mononuclear cells, upregulation of cytokines and proteases, and presence of immunoglobulins in the vascular wall. Immunohistochemical analysis of aneurysmal samples showing that macrophages and T lymphocytes are the prominent cell types accumulated in the adventitia and media of both TAAs (432) and AAAs (433). Although compelling evidence shows that macrophages are critical for aneurysm development, it is currently unclear whether specific targeting of macrophage functions would attenuate aneurysm expansion in humans. Since abundant T lymphocytes and immunoglobulins are detected in aneurysmal tissues, the role of autoimmunity in aneurysm formation has been increasingly recognized (reviewed in (434, 435)). It has been proposed that proinflammatory cytokines such as IL2, IFNγ, and TNFα produced by T lymphocytes may have a substantial influence on macrophage production of MMPs and other matrix-degrading proteases, which subsequently lead to ECM degradation and SMC apoptosis. Proinflammatory cytokines associated with Th1 immune responses are enhanced in the blood and aneurysmal specimens from patients with AAA (436), and circulating levels of IFNγ positively correlate with aneurysm expansion (437). Interestingly, it seems that there is a Th1- to Th2-predominant immune response transition between early and late stages of AAA, since it has been reported that Th2-associated cytokines, particularly IL4 and IL10, are elaborated in advanced AAA specimens (438). Since ILs 4 and 10 are anti-inflammatory cytokines and can suppress MMP9 expression (439), the Th2-predominant immune responses might help restrain aneurysm growth and degeneration. TAA has been reported to be associated with the Th1-predominant immune response and increased expression of IFNγ in the aneurysmal tissue. Th2 cytokines, however, were undetectable (440).

Neutrophils and mast cells are also detectable in aneurysmal tissues to a lesser extent. Trafficking of neutrophils from the bloodstream to the vascular wall is mediated by shedding of

adhesion molecules such as L-selectin by ADAMs. Pharmacological inhibition and genetic deletion of L-selectin have been shown to attenuate experimental AAA induced by elastase (441). Mast cell can synthesize and release various inflammatory factors and proteases, which are believed to contribute to the progression of aortic aneurysm (442). Pharmacological inhibition and genetic deletion of mast cells prevented AAA formation in rodent models (443).

Oxidative stress. Low levels of ROS are essential to maintaining normal cellular functions such as mechano-stress signal transduction, physiological angiogenesis, and permeability of ECs, as well as the differentiation and contraction of SMCs. However, excessive oxidative stress secondary to inflammation promotes ECM degradation and SMC apoptosis, which ultimately contribute to the development of aortic aneurysm. Indeed, a marked overproduction of ROS can be detected in human aneurysmal specimens from the thoracic (444, 445) and abdominal aorta (446, 447). Mechanistic studies using transgenic mice or ROS inhibitors revealed a critical role of ROS in the pathogenesis of TAA (444, 445) and AAA (reviewed in (448-450)).

Despite the promising results from animal models, the wide range of upregulated oxidative stress pathways and interactions between them make it extremely difficult to design interventions which can effectively reduce oxidative stress in the diseased aorta. A clinical trial failed to show any beneficial effects of antioxidant therapies on preventing AAA from expansion or rupture (451). Since statistic power and the dose and efficacy of the antioxidants used in this trial would compromise the data interpretation (448), the possibility of a beneficial effect of a better designed antioxidant regimen on AAA cannot be ruled out. Pilot studies using various antioxidant cocktail regimens preoperatively in patients scheduled for elective AAA repair are required to decide which regimen is the most effective one that could reduce oxidative stress in the AAA tissues. Once an effective antioxidant regimen has been verified, a randomized clinical trial could be designed to test the role of oxidative stress in the pathogenesis of AAA in humans. Currently, there is no report available regarding the clinical values of antioxidants in ameliorating TAA in humans.

MMPs. Collagen and elastin are key structural proteins that maintain the tensile strength and recoil property of the aortic wall. Matrix proteolysis is one of the hallmarks of aortic aneurysm. Whereas healthy aortic tissue shows negligible expression of MMPs, increased MMP expression levels are consistently observed in aneurysmal tissues. MMPs can be produced by many cell types,

including vascular cells (e.g., SMCs and fibroblasts) and inflammatory cells (e.g., macrophages and neutrophils) in response to inflammation, oxidative stress, matrix degradation fragments, or enhanced TGFβ1 activity. A very informative profile of activated MMPs in both human TAA and AAA specimens are reviewed elsewhere (452). Signaling pathways such as JNK, JAK/signal transducer and activator of transcription (STAT), osteopontin, and AMPK-activate alpha-2 (AMPKAA2) are shown to lead to MMP activation. Notably, compared to healthy control aortas, MMPs 1, 2, 9, 12, and 14 are elevated in TAA specimens, whereas MMPs 1, 2,3, 9, 12, and 13 are elevated in AAA specimens. Mechanistic studies using transgenic mice showed that *Mmp2*- or *Mmp9*-deficiency could ameliorate or exacerbate aneurysm phenotypes, depending on which animal model was used. For example, *Mmp2*- and *Mmp9*-deficient mice have been reported to protect against $CaCl_2$- or elastase-induce TAA (378, 391) and AAA (369, 453), suggesting that MMPs 2- and 9-dependent ECM degradation plays an important role in the pathogenesis of aortic aneurysm. Surprisingly, a study by our group demonstrated that Ang II infusion resulted in TAA formation in mice with *Mmp2*-deficiency. We further found that MMP2 is not only responsible for ECM degradation but is also crucial in regulating *de novo* biosynthesis of ECM proteins through modulating the bioactivity of TGFβ1 (378). These data suggest that both augmented degradation and impaired synthesis of ECM proteins in the medial layer could contribute to the development of aortic aneurysm.

In addition to MMP2 and MMP9, the role of several other MMPs have been investigated in the development of aortic aneurysm as well. For example, *Mmp12*-deficiency attenuated $CaCl_2$-induced (368) but not elastase-induced AAA (369). *Mmp14*-deficiency promoted Ang II infusion-induced TAA due to suppressed VSMC maturation and disrupted ECM integrity (397).

TIMPs. As the endogenous inhibitors for MMPs, transgenic mice studies showed that deletion of TIMPs could also protect against or promote aneurysm formation. For example, deficiency of *Timp1* promoted the development of $CaCl_2$-induced TAA (392) and elastase-induced AAA (454), respectively. As a cofactor involved in MMP2 activation, *Timp2*-deficiency protected against $CaCl_2$-induced TAA by suppressing MMP2 maturation (455). Mice deficient in *Timp3* developed AAA after Ang II infusion (408). So far, no information is available in the role of TIMP4 in either TAA or AAA development.

Smooth muscle cells. SMCs are the major cell type in the aorta, and show a region-specific diversity of embryological origins. While SMCs in the ascending aorta is from neural ectoderm-derived progenitors of the cardiac neural crest, the cells in the abdominal aorta originate from the paraxial mesoderm-derived somites. It has been shown that the two types of vascular SMCs demonstrate unique responses to various cytokines and growth factors. For instance, homocysteine was only able to stimulate proliferation of neural crest-derived VSMCs, but not of mesodermal VSMCs (456). When treated with TGFβ1, neural crest-derived VSMCs showed elevated DNA synthesis, cell proliferation, PKC pathway activation, and collagen production, while parallel stimulation on mesodermal VSMCs failed to show same responses (457). Therefore, the intrinsic properties of SMCs of different embryonic origins partially explain the distinct etiologies of TAA and AAA.

Under physiological conditions, SMCs can interact directly with different ECM components through cell surface integrin receptors and GPCRs. Therefore, a fundamental unit of cytoskeleton-cell surface receptor-ECM complex regulates intracellular and extracellular signals within the vessels. As mentioned above, four definitive mutations in SMC contractile proteins (i.e., *MYH11*, *ACTA2*, *MLCK*, and *PRKG1*) have been associated with familial TAAs, probably through a disruption of the direct feedback mechanism which subsequently leads to SMC apoptosis and disarray and ECM degradation.

One of the important characteristics of SMCs is that they are not terminally differentiated cells and show high plasticity: mature SMCs can shift reversibly along a continuum from a quiescent and contractile phenotype to a proliferative and synthetic phenotype in response to various stimuli, such as growth factors, mitogens, inflammatory cytokines and chemokines, and mechanical stretch. Each phenotypic state is characterized by expression of a unique profile of structural and functional proteins that correlate with varying patterns of gene expression (458-460). Of note, even under physiological conditions, SMCs possess important secretory properties which ensure the synthesis and repair of various ECM components (e.g., collagen, elastin, and fibrillin) that regulate the structure of the vascular wall. The role of SMC phenotypic switching to a synthetic, proteolytic, and proinflammatory phenotype in the development of aortic aneurysm has been confirmed in animal models (396, 445, 461, 462). Therefore, preserving the contractile phenotype of SMCs under pathological conditions could be a therapeutic target to suppress the development of aortic

aneurysm. Alternatively, reversing SMCs from the synthetic phenotype to the contractile phenotype through the development of tissue-engineered scaffold system may represent a more promising and effective strategy to treat aortic aneurysm and other vascular diseases (460).

Endothelial cells. Owing to their main regulatory function in vascular integrity, inflammatory cell adhesion and transmigration, angiogenesis, and vascular tone, ECs have been increasingly recognized to play an important role in the pathogenesis of aortic aneurysm. Since ECs lie between the bloodstream and the medial layer, blood flow and stimuli such as inflammatory cytokines, Ang II, nitric oxide, and TGFβ1 allow ECs to directly or indirectly interact with contractile SMCs to regulate vessel homeostasis. Vascular remodeling is induced by increased shear stress on ECs (463). Under such conditions, apoptosis or proliferation, inflammation, permeability, expression of adhesion molecules are increased in ECs (464). Moreover, *in vitro* coculture system showed that shear stress applied to ECs could impact the contractile/synthetic phenotypes of the underlying SMCs (465).

Chronic infusion of Ang II has been shown to trigger TAA and AAA in hyperlipidemic mice through the AT1 receptor functions. Cell-specific deletion of *At1* demonstrated that endothelial AT1 plays a critical role in Ang II-induced aneurysm formation in the thoracic aorta (427) but not in the abdominal aorta (420). ECs are the major source for nitric oxide, and studies have shown that dysregulated endothelial NO signaling in aneurysm development (466). For example, a mouse model with uncoupled endothelial nitric oxide synthases (eNOS) rapidly developed AAA upon Ang II infusion, whereas recoupling of eNOS rescued the phenotype (467). EC-specific overexpression of NADPH oxidase-2, a member of ROS, led to aortic dissection in mice infused with Ang II (468). The crucial role of endothelial TGFβ1 can be corroborated by the fact that EC-specific deletion of this protein is embryonically lethal (469). In ECs, TGFβ1 signaling can either inhibit or stimulate the cell growth and function through distinct pathways, and opposing effects enable functional vasculogenesis (469). Indeed, it has been shown *in vitro* that endothelial TGFβ1 could promote a contractile phenotype in SMCs. In contrast, when cultured alone, the SMCs showed a synthetic phenotype in response to TGFβ1 (470).

Infiltration of inflammatory cell into the aortic wall is a hallmark of aortic aneurysm. The role of ECs in mediating inflammatory cell infiltration through upregulation of cell surface expression

of adhesion molecules, activation of proteases, downregulation of junction proteins has been reviewed elsewhere (354, 471-474). Moreover, increased adventitial vasculogenesis is considered to be associated with increased inflammatory cell infiltration, since the newly generated immature vessels can serve as conduits for inflammatory cell transport to promote chronic inflammation in aneurysmal aortas (475).

1.11.6.4. ADAMs in aortic aneurysm

As mentioned above, ADAM-mediated proteolytic shedding of membrane-bound cytokines, chemokines, growth factors and their receptors, and adhesion molecules can activate various signaling pathways which are involved in the pathogenesis of aortic aneurysm. In other words, ADAM can serve as the upstream regulator for almost all the pathological processes observed in aortic aneurysm, and may represent a promising therapeutic target for this disease. However, studies on the ADAM expression pattern in human aortic aneurysm are quite limited, and all the published literature mainly documented elevated ADAM10 and ADAM17 in the aortic specimens from patients with AAA (476, 477). A genetic study showed that ADAM17 polymorphism-associated protease activity increase makes patients more susceptible to sporadic AAAs (478). In contrast, no information is currently available regarding the expression levels of ADAMs in human TAA tissues.

However, studies in animal models have shown an upregulation of ADAMs 10 and 17 together with MMPs 2 and 9 in a rat model of TAA induced by $CaCl_2$ (479). A similar ADAM and MMP expression pattern was observed in a mouse model of AAA induced by $CaCl_2$, whereas temporal inhibition of ADAM17 has been shown to attenuate the aneurysmal phenotype (480). A recent study showed that SMC-specific deletion or pharmacological inhibition of ADAM17 suppressed Ang II and BAPN co-infusion induced AAA development (414). However, no animal data are available on the role of other ADAMs, such as ADAMs 10, 12, 15, and 19 in the pathogenesis of aortic aneurysm. When I started my Ph.D. studies, it was not yet known whether ADAM17 would exert a cell type-specific function in aortic aneurysm, nor was the causative role of ADAM17 in TAA explored.

1.11.6.5. Potential biomarkers and therapeutic targets for aortic aneurysm

To date, no FDA-approved drugs are available for aortic aneurysm treatment, and elective surgical repair is the only option when the aneurysm reaches the threshold diameter or if the aneurysm is rapidly progressing. According to the Law of Laplace, when the aneurysm expands until aortic wall tension drives sac expansion, pharmaceutical therapy will no longer be effective in aneurysm treatment, and surgical aortic reconstruction will be required. Therefore, any pharmaceutical intervention must target the aneurysm while the diameter is still conserved and before wall tension overwhelmingly drives sac expansion. The early identification of patients at risk of aneurysm development is crucial to the success of nonsurgical treatment.

Most aortic aneurysms are asymptomatic, but medical imaging is very effective in the identification of TAA and AAA at their early stage before catastrophic aortic rupture or dissection happens. Currently, there are no recommendations about large-scale screening of populations for TAA due to its low prevalence. In contrast, several randomized trials of AAA ultrasonography screening conducted in the UK, Denmark, and Australia demonstrated a reduction in AAA-related mortality (481), which led to the adoption of ultrasonographic screening programs by the National Health Service in England and Scotland, and by Medicare in the US (482). Although it has been recommended that all individuals aged >60 years and for those aged >50 with a family history of AAA should undergo ultrasonography screening for AAA (483), if validated biomarkers for both TAA and AAA exist, it will not only make the screening procedure much easier and more cost-effective, but will also substantially improve detection rates of both forms of aneurysm in the general population. Moreover, specific biomarkers for aortic aneurysm could be useful to evaluate the status of disease progression during follow-up, potentially predicting adverse events like aortic enlargement, rupture, or dissection.

Several potential biomarkers such as MMPs (e.g., MMPs 2 and 9), cysteine and serine proteases (e.g., plasmin-antiplasmin complexes/PAP, plasminogen activator inhibitor type I/PAI-1, urokinase/uPA, and tissue plasminogen activator/tPA), lipoprotein(a), homocysteine, elastin peptides, collagen fragments (e.g., carboxyterminal propeptide of type I procollagen/PICP and aminoterminal propeptide of type III procollagen/PIIINP), elastase (e.g., α1-antitrypsin/A1AT), cytokines (e.g., IFNγ, TNF, TGFβ1, macrophage migration inhibitory factor/MIF, and osteoprotegerin), and osteopontin have been proposed to serve as biomarkers for diagnosis of

aneurysm and/or for prediction of growth or rupture. Some of these biomarkers are specific for TAA or AAA, and the rest of them can be shared for both forms of aneurysm. The detailed application of these biomarkers in clinical practice has been reviewed elsewhere (353, 354, 484). Interestingly, a recent study reported that a few genes can be upregulated specifically in large AAA (hypoxia-inducible lipid droplet-associated protein/HILPDA, angiopoietin-like-4/ANGPTL4, LOX, sushi repeat protein X-linked-2/SRPX2, Fc fragment binding protein/FCGBP) and ruptured AAA (ADAMTS9, stanniocalcin-1/STC1, glutamine-fructose-6-phosphate transaminase-2/GFPT2, Gal-3-sulfotransferase-4/GAL3ST4, C-C chemokine ligand 4-like-1/CCL4L1), and activation of hypoxia-inducible factor-1α signaling is associated with upregulation of these genes (485). Therefore, this finding may be used as a specific molecular fingerprint to help surgeons make decisions when the large AAA should undergo elective surgery.

Owing to the recent advances in the understanding of the pathophysiology of TAA and AAA, several potential therapeutic targets that have been confirmed to be effective in different animal models for aortic aneurysm may be further translated to clinical practice. Synthetic chemical compounds or monoclonal antibodies that target chemokine receptors on inflammatory cells (e.g., C-C chemokine receptor type 2/CCR2 and C-X-C chemokine receptor type 4/CXCR4), cytokines (e.g., IL, TNF, IFNγ), critical signaling molecules involved in cellular functions (e.g., c-JNK, TGFβ1, and PPARγ), proteases (e.g., MMPs, cysteine proteases, and serine proteases), microRNAs (e.g., miR-21, miR-29b, and miR-712), ROS (e.g., cyclooxygenase-2 and 5-lipoxygenase), and ECM components (e.g., GxxPG fragment) may suppress inflammation, proteolysis, cell apoptosis, and oxidative stress that are involved in the pathogenesis of aortic aneurysm (355, 486).

1.12. Genetic and pharmacological inhibition of ADAM17 in cardiovascular diseases

Upregulation of ADAMs in diseases of the cardiovascular system has been well documented (306, 487). ADAMs 10 and 17 are the two members of the protease family that are actively involved in inflammation through ectodomain shedding of a variety of proinflammatory mediators, receptors, and adhesion molecules (**Tables 1.2 and 1.3**). Moreover, ADAMs 10 and 17 have been implicated in the regulation of vascular permeability by shedding adherens junction proteins (e.g., VE-cadherin, JAM-A, and claudin) expressed on ECs. As such, targeting ADAM proteases might serve to suppress inflammation in a number of chronic diseases such as rheumatoid arthritis,

inflammatory bowel diseases, septic shock, and cardiovascular diseases. The ultimate goal of understanding the biological functions of ADAMs is to figure out whether it will be feasible to design pharmacological inhibitors of specific ADAMs that could aid in combating some of the aforementioned diseases without disturbing normal physiological processes. Since the role of ADAM17 in cardiovascular diseases is the focus of this dissertation, the potential therapeutic values of ADAM17 pharmacological inhibitors in this type of diseases will be discussed.

Table 1.7 Phenotypes in mice with cell-specific ADAM deficiency

Genotype	Targeted tissues/cells	Phenotype	Refs
Adam17$^{f/f}$/Mx1$^{Cre/+}$	Liver, bone marrow, spleen, and thymus	Viable, fertile, no evident abnormalities; temporal ADAM17 deletion; protected against endotoxin (LPS)-induced lethality and $CaCl_2$-induced abdominal aortic aneurysms; improved insulin resistance and energy homeostasis on a high-fat diet; developed severe dextran sulfate sodium-induced colitis	(283, 480, 488)
Adam17$^{f/f}$/LysM$^{Cre/+}$	Myeloid cells	Viable, fertile, no evident abnormalities, protected against endotoxin-induced lethality; no effects on dextran sulfate sodium-induced colitis	(283, 488)
Adam17$^{f/f}$/LysM$^{Cre/+}$/Apoe$^{-/-}$	Myeloid cells	Viable, fertile, no evident abnormalities; enhanced atherosclerosis development with more stable lesions	(489)
Adam17$^{f/f}$/Sox9$^{Cre/+}$	Bone, cartilage, skin, lung, pancreas, intestine, brain and kidney	Viable for 5 months; born with open eyelids; growth retardation; defects in the heart, skin, and hair; osteoporosis; dysregulated lymphopoiesis and granulopoiesis; splenomegaly; increased myelopoiesis	(490)
Adam17$^{f/f}$/Vav1$^{Cre/+}$	Leukocytes	Viable, fertile, protected from *E. coli* -induced peritonitis, rapid/transient neutrophil infiltration to inflamed sites; impaired L-selectin and TNFα shedding; transiently increased neutrophils and monocytes in alveolar space in response to LPS stimulation	(249, 491)
Adam17$^{f/f}$/Tie2$^{Cre/+}$	Endothelial cells	Viable, fertile; reduced pathological retinal neovascularization; reduced tissue damage in acute lung inflammation; reduced growth of B16 melanoma cells;	(335, 492)
Adam17$^{f/f}$/Bmx$^{Cre/+}$/Apoe$^{-/-}$	Endothelial cells	Viable, fertile; reduced atherosclerosis development	(489)
Adam17$^{f/f}$/Sm22α$^{Cre/+}$	Smooth muscle cells	Viable, fertile; no effects on pathological retinal neovascularization and growth of B16 melanoma cells; suppressed SMC proliferation and migration; transiently reduced angiotensin II-induced hypertension and end-organ damage; attenuated abdominal aortic aneurysm formation in response to angiotensin II and β-aminopropionitrile co-perfusion	(214, 311, 335, 414)
Adam17$^{f/f}$/Alb$^{Cre/+}$	Hepatocytes	Viable, fertile; increased sensitivity to Fas-induced hepatotoxicity	(493)
Adam17$^{f/f}$/HB9$^{Cre/+}$	Motor neurons	Viable, fertile; increased Schwann cell myelination	(494)
Adam17$^{f/f}$/Krt14$^{Cre/+}$	Keratinocytes	Viable, fertile; Notch signal inhibition; spontaneous atopic dermatitis and myeloproliferative disease in adults	(495, 496)
Adam17$^{f/f}$/Villin$^{Cre/+}$	Intestinal epithelium	Viable, fertile; blocked EGFR transactivation	(497)
Adam17$^{f/f}$/Ptf1a$^{Cre/+}$	Pancreas	Viable, fertile; inhibited EGFR signaling; protected against pancreatitis; inhibition of Kras driven tumorigenesis	(498)
Adam17$^{f/f}$/Slc34a1$^{Cre/+}$	Kidney proximal tubule	Viable, fertile; protected against renal fibrosis after bilateral ischemia-reperfusion injury	(183)
Adam17$^{f/f}$/MHCα$^{Cre/+}$	Cardiomyocytes	Viable, fertile; increased pressure overload-induced cardiac hypertrophy, fibrosis and systolic dysfunction; reduced cleavage of integrin β1	(318)
Adam17$^{f/f}$/NKX2.5$^{Cre/+}$	Cardiomyocytes	Viable, fertile, no evident abnormalities	(499)
Adam17$^{f/f}$/SPC-rtTA/TetO$^{Cre/+}$	Lung epithelial cells	Viable, fertile; impaired saccular formation, proliferation, differentiation and pulmonary capillary formation	(499)
Adam17$^{f/f}$/Dermol$^{Cre/+}$	Mesenchymal cells	Viable, fertile, no evident abnormalities	(499)
Adam17$^{f/f}$/Foxn1$^{Cre/+}$	Thymic epithelial cells	Viable, fertile; no effects on T cell development and thymic epithelial cell differentiation	(500)

As mentioned above, genetic deletion of ADAM17 in different cell types showed either protective or detrimental effects towards pathological stimuli applied to the heart (318, 336) or the aorta (329, 330, 414), indicating ADAM17 (or probably other ADAMs) in different cell types fulfill unique housekeeping functions (**Table 1.7**). As such, instead of inhibiting ADAMs chronically and globally, strategies aiming to suppress ADAM17 activity must be tailored to target this protease in a proper spatial (cell type-specific targeting) and temporal (time frame-specific targeting) manner. Additionally, an optional dosage will be very important to limit excess of pathologic ADAM17 activity but leaving a residual activity for physiological functions such as tissue homeostasis and repair. In other words, an ideal ADAM inhibitor would only suppress the pathological activity of the protease above the baseline, so the normal shedding events by the protease would not be compromised.

In order to select an appropriate inhibitor for diseases, high potency and high selectivity of this target protease are warranted. As discussed in **Chapter 1.5**, ADAM activity can be regulated at several levels ranging from transcription, maturation, and activation of the protease to proteolytic activity regulation and substrate recognition. Therefore, targeted siRNA can be used to regulate the expression level of ADAM17, and intravenous delivery of *ADAM17* siRNAs can be an optional route to predominantly target vascular ADAM17. The pro-domain (32) and binding protein iRhom2 (237) of ADAM17 have been shown to regulate the maturation of this protease. Although the pro-domain represents a promising target, its stability in cells should be modified, probably by coupling it with polyethylene glycol. In contrast, iRhom2 is more critical for ADAM17 maturation in leukocytes and can even confer to substrate selectivity potentially by affecting trafficking of the protease to selected substrates (237). ADAM17 activity can be regulated by a number of kinases such as p38, Erk, and PKC. However, these signaling pathways are actively involved in other cellular responses such as transcription and proliferation, and therefore, this approach may not represent a specific strategy. Since it has been reported that ADAM17 activity is also affected by conformational changes (139), the generation of specific antibodies that only targeting the active form of ADAM17 could be a promising strategy (501, 502). Since the activity of ADAM17 is dependent on the catalytic domain, a few small molecules have been developed to either suppress the catalytic domain or interfere with the substrate-specificity determining structure of ADAM17. However, some of these small molecule compounds may lack complete specificity, considering the high structural homology of most ADAMs and MMPs. A few of these small molecule

compounds have entered clinical trials for inflammatory diseases such as endotoxemia and rheumatoid arthritis (reviewed in (2, 186-188)). Since TIMP3 is the endogenous inhibitor for both ADAM17 (177) and other MMPs, its low specificity limits the use of this inhibitor as a recombinant therapeutic protein.

Although all the strategies mentioned above may exert potent inhibitory effects on ADAM17 *in vivo*, the high similarity of the active sites of different ADAMs makes it unlikely that a panel of small molecule, potent and highly selective inhibitors of each of the ADAMs will emerge in the near future. Therefore, a better understanding of which ADAM sheds which key substrate in specific biological contexts and deciphering mechanisms that regulate the ADAM protease will help us find an optimal strategy to specifically inhibit the activity of ADAMs in a spatiotemporal-regulated manner, thereby ameliorating the pathological effects as a result of overactivity of the ADAMs.

1.13. Hypothesis

The literature review presented in this chapter led us to the following working hypothesis: deletion of *Adam17* in vascular cells will protect against vascular pathologies such as hypertension and aortic aneurysm through distinct functions in smooth muscle cells versus endothelial cells in the arterial wall.

1.14. Objectives

Objective 1: To characterize the structure and functions of SMCs lacking ADAM17 *in vitro*.

Objective 2: To assess Ang II-induced blood pressure changes in SMC or EC *Adam17*-intact and -deficient mice for 4 weeks.

Objective 3: To evaluate the impact of short-term (2 weeks) and long-term (4 weeks) of Ang II infusion on cardiac and renal hypertrophy and fibrosis in SMC *Adam17*-intact and -deficient mice.

Objective 4: To establish a producible TAA model which can more pathologically resemble the hallmarks of human TAA.

Objective 5: To evaluate the effects of deletion of *Adam17* in SMCs versus ECs on the progression of experimental TAA, and to further dissect the underlying mechanisms for the observed phenotypes using *in vitro* studies.

Objective 6: If genetic inhibition of ADAM17 is protective against the pathogenesis of experimental TAA, use an ADAM17-selective inhibitor to test the effects of ADAM17 inhibition on prevention and treatment of TAA.

CHAPTER 2

MATERIALS AND METHODS

2.1. Antibodies

All the antibodies used for immunohistochemistry, immunocytochemistry, and immunoblotting are listed in **Table 2.1**. Dilution ratio was provided for each application.

Table 2.1 Primary antibody dilution in different applications

Antibody	Catalogue no.	Supplier	Dilution ratio /Application(s)
ADAM17	sc-390859	Santa Cruz	1:1000/IB
ADAM17	sc-13973	Santa Cruz	1:500/IB
ADAM17	AB19027	EMD Millipore	1:500/IHC
β-Actin	4967S	Cell Signaling	1:2000/IB
p-Akt^{Ser473}	9271S	Cell Signaling	1:1000/IB
Akt	9272S	Cell Signaling	1:1000/IB
BrdU	ab74545	Abcam	1:1000/ICC
Calponin	ab46794	Abcam	1:5000/WB; 1:500/IHC & ICC
α-Catenin	sc-9988	Santa Cruz	1:500/IB
β-Catenin$^{Ser33/Ser37}$	sc-57535	Santa Cruz	1:500/IB
β-Catenin	ab79089	Santa Cruz	1:500/IB
γ-Catenin	sc-514115	Santa Cruz	1:500/IB
p120 Catenin	sc-23873	Santa Cruz	1:500/IB
CD31	550274	BD Pharmingen™	1:50/IHC
CD68	MCA1957GA	Bio-Rad	1:50/IHC
Claudin-5	sc-374221	Santa Cruz	1:500/IB
Collagen 1α1	NBP1-30054	Novus Biologicals	1:2000/IB
Collagen 3α1	ab7778	Abcam	1:1000/IB
p-Erk1/2$^{Thr202/Tyr204}$	9101S	Cell Signaling	1:1000/IB
Erk1/2	9102S	Cell Signaling	1:1000/IB
p-EGFR^{Tyr1608}	3777S	Cell Signaling	1:1000/IB
EGFR	2232S	Cell Signaling	1:1000/IB
p-FAK^{Tyr397}	3283S	Cell Signaling	1:1000/IB
FAK	3285S	Cell Signaling	1:1000/IB
HB-EGF	ab185555	Cell Signaling	1:1000/IB
JAM-A	sc-53623	Santa Cruz	1:200/IB
Ly6G	127602	BioLegend	1:500/IHC
p-Paxillin^{Tyr118}	sc-365020	Santa Cruz	1:500/IB
Paxillin	sc-365379	Santa Cruz	1:500/IB
SMA	ab5649	Abcam	1:2000/IB; 1:500/ICC
SM-MHC11	ab53219	Abcam	1:5000/IB; 1:100/ICC
Sm22α	ab144272	Abcam	1:2000/IB; 1:100/ICC
Smoothelin	sc-376902	Santa Cruz	1:1000/IB
TIMP3	NBP1-19662	Novus Biologicals	1:500/IB
α-Tubulin	2144S	Cell Signaling	1:2000/IB
VE-cadherin	2500S	Cell Signaling	1:1000/IB; 1:400/ICC
Vinculin	sc-73614	Santa Cruz	1:500/IB

Abbreviations: IB, immunoblotting, IHC, immunohistochemistry; and ICC, immunocytochemistry.

2.2. Other reagents

Anti-mouse IgG, HRP-linked (7076S), and anti-rabbit IgG, HRP-linked (7074S) were purchased from Cell Signaling Technology. Alexa Fluor 488 Phalloidin (A12379), Alexa Fluor Plus 555 goat anti-rabbit secondary antibody (A32732), Alexa Fluor 594 goat-anti-rabbit (R37117), Cyanine3 goat anti-rat secondary antibody (A10522), and TRIzol™ reagent (15596026) were purchased from Thermo Fisher Scientific. BrdU (5-bromo-2'-deoxyuridine, ab142567) was purchased from Abcam. Staurosporine (sc-3510) was obtained from Santa Cruz Biotechnology, Inc. DMEM/F-12, HEPES (11330057), HBSS (no calcium, no magnesium, and no phenol red) (14175095), L-Glutamine (200 mM, 25030081), Fetal Bovine Serum (FBS, Canadian Origin, 12483020), Amphotericin B (Fungizone, 15290018), and Penicillin-Streptomycin Solution (15140122) were purchased from Gibco. Human Aortic Endothelial Cells (HAoECs, PCS-100-011), Vascular Cell Basal Medium (PCS-100-030) and Endothelial Cell Growth Kit-VEGF (PCS-100-04) were obtained from the American Type Culture Collection (ATCC). Accutase Cell Detachment Solution (SCR005) and Human Plasma Fibronectin Purified Protein (FC010) were purchased from EMD Millipore. PROTOCOL™ 10% Buffered Formalin (23-245684) was purchased from Fisher Scientific. Porcine Pancreatic Elastase Type I (E1250), Evans Blue (E2129), Corn Oil (C8267), Tamoxifen (T5648), Paraformaldehyde (P6148), Angiotensin II (A9525), and Celltyic M Lysis Buffer (C2978) was purchased from Sigma-Aldrich. Human Fibronectin was purchased from Corning (C356008). Collagenase type II (LS004174), Elastase (LS002279), and Soybean Trypsin Inhibitor (LS003570) were obtained from Worthington Biochemical for primary human and mouse smooth muscle cell isolation. Bovine serum albumin (BSA, BAH66-1000) was purchased from Equitech-Bio, Inc. RIPA Lysis and Extraction buffer (89900), Pierce™ Reversible Protein Stain Kit for PVDF Membranes (24585), Restore™ PLUS Western Blot Stripping Buffer (46430), and Pre-stained Spectra Multicolor Broad Range Protein Ladder (26623) were purchased from Thermo Fisher Scientific. Amersham ECL Prime Western Blotting Detection Reagent (RPN2232) was purchased from GE Healthcare, and Clarity Max™ Western ECL Substrate (1705062) was purchased from Bio-Rad. PE Annexin V Apoptosis Detection Kit I (559763) was obtained from BD Biosciences. *In vitro* Vascular Permeability Assay (24-well) Kit (ECM644) was purchased from EMD Millipore. Quantikine ELISA Human VE-cadherin Immunoassay kit (DCADV0), Mca-Pro-Leu-Ala-Gln-Ala-Val-Dpa-Arg-Ser-Ser-Ser-Arg-NH2 fluorogenic peptide substrate III (ES003), and recombinant mouse ADAM17 (2978-AD) were obtained from R & D

systems. Mca-Pro-Leu-OH (M-1975) was purchased from Bachem. Elastic Stain Kit (HT25A) was purchased from Sigma-Aldrich. DeadEnd™ Fluorometric TUNEL System (G3250) was purchased from Promega. ADAM17-selective inhibitor (PF-5480090, PF-548) is a gift from *Pfizer* Inc. through the Compound Transfer Program.

2.3. Human control (non-diseased) and aneurysmal thoracic aorta specimen procurement

Human aneurysmal samples were procured from the proximal ascending aorta of patients (n=5 for each sex) undergoing prophylactic resection as a consequence of bicuspid aortic valve (BAV) associated aortopathy. Informed consent was obtained for these patients after Institutional Review Board approval (REB17-0207). Patients with aortic dissection were excluded. Control samples (n=5 for each sex) were non-aneurysmal healthy ascending aortas obtained from donors through the HOPE (Human Organ Procurement and Exchange) Program at the University of Alberta. The study protocols were approved by the Human Research Ethics Review Process (HERO) at the University of Alberta. Aortic samples were either flash-frozen in liquid nitrogen and stored at -80 °C for molecule studies or fixed in 10 % buffered formalin for histological analyses. The demographic information of healthy and BAV-associated TAA patients are available in **Table 2.2**.

Table 2.2 Demographic information of healthy control and BAV-associated TAA patients

Healthy		**BAV-TAA**	
Sex	Age	Sex	Age
M	47	M	41
M	29	M	47
M	47	M	50
M	38	M	41
M	38	M	37
F	65	F	59
F	21	F	48
F	68	F	56
F	42	F	63
F	48	F	34

2.4. Animals

All animal procedures were performed according to the ARRIVE (Animal Research: Reporting of *in vivo* Experiments) guidelines, and according to the guidelines of Animal Care and Use Committee (ACUC) at the University of Alberta and the Canadian Council of Animal Care (CCAC). *Adam17*$^{flox/flox}$ mice (*Adam17*$^{tm1.2Bbl}$*/J, Adam17*$^{f/f}$, Stock#009597) and *Sm22α-Cre*-expressing (*Tg(Tagln-cre)1Her*, Stock#017491) mice were purchased from the Jackson Laboratory. Mice with smooth muscle cell deficiency of *Adam17* (*Adam17*$^{f/f}$*/Sm22*$^{Cre/+}$) were generated by cross-breeding *Adam17*$^{flox/flox}$ mice with *Sm22α-Cre*-expressing mice. Mice with endothelial cell *Adam17*-deficiency (*Adam17*$^{f/f}$*/Tie2*$^{Cre/+}$) were generated by cross-breeding *Adam17*$^{flox/flox}$ mice with *Tie2-CreER*^{T2}-expressing (*Tie2-MerCreMer*) mice with a tamoxifen-inducible *CreER*^{T2}-recombinase (503). Activation of the inducible *CreER*^{T2}-recombinase in *Adam17*$^{f/f}$*/Tie2*$^{Cre/+}$ mice was achieved by three days of tamoxifen (prepared as working solution of 20 mg/ml in corn oil) treatment at 6 weeks of age (80 mg/kg/d, *p.o.*) as described (503). The control littermates (*Adam17*$^{f/f}$) also received tamoxifen in an identical manner. Animals were allowed 3 weeks to recover from the side-effects of tamoxifen before TAA induction. We used the inducible *Tie2-MerCreMer* recombinase to delete ADAM17 in the endothelial cells in adult mice rather than using the constitutively active *Tie2-Cre* recombinase to avoid the non-specific effects of *Tie2-Cre* on non-endothelial cells during embryonic development. The constitutively active *Tie2-Cre* recombinase targets hematopoietic cells in addition to endothelial cells (504, 505), which would further impact the immune system of the animals.

Genotyping protocols and primers used for each reaction are listed in **Tables 2.1** and **2.2**. Representative genotyping results for *Adam17-flox* (*Adam17*$^{wt/wt}$, *Adam17*$^{flox/wt}$, *Adam17*$^{flox/flox}$), *Sm22α-Cre* (*Sm22*$^{Cre/+}$), and *Tie2-MerCreMer* (*Tie2*$^{Cre/+}$) are shown in **Figure 2.1**. Mice of both genders were used in this study. All experimental mice were in a C57BL/6 genetic background and were genotyped by PCR conducted on genomic DNA extracted from toe clip samples.

Table 2.3 Genotyping protocol for *flox*, *Sm22-Cre*, and *Tie2-MerCreMer* mutations

	Flox reaction		Sm22-Cre reaction		Tie2MerCreMer reaction	
1	94 °C	8 min	94 °C	8 min	95 °C	10 min
2	94 °C	20 s	94 °C	30 s	95 °C	30 s
3	65 °C	30 s	51.7 °C	1 min	48 °C	30 s
	-0.5 °C/cycle					
4	68 °C	40 s	72 °C	1 min	72 °C	90 s
5	Go to 2, 10 times		Go to 2, 35 times		Go to 2, 45 times	
6	94 °C	15 s	72 °C	2 min	72 °C	10 min
7	60 °C	30 s	4 °C	Forever	4 °C	Forever
8	72 °C	40 s	END		END	
9	Go to 6, 28 times					
10	72 °C	2 min				
11	4 °C	Forever				
12	END					

Table 2.4 Primers for *flox*, *Sm22-Cre*, and *Tie2-MerCreMer* PCR reactions

Primer name	Sequence 5'→3'	Primer type	Targets	Target size (bp)
13799	TCC CCC AGC TAG ATT GTT TG	Forward	Flox	Mutant 650 & WT 537
13800	AGG ACC CAG GTT CAG TTC CT	Reverse	Flox	
oIMR1084	GCG GTC TGG CAG TAA AAA CTA TC	Forward	Cre	100
oIMR1085	GTG AAA CAG CAT TGC TGT CAC TT	Reverse	Cre	
oIMR7338	CTA GGC CAC AGA ATT GAA AGA TCT	Forward	WT	324
oIMR7339	GTA GGT GGA AAT TCT AGC ATC ATC C	Reverse	WT	
T1	CGA GTG ATG AGG TTC GCA AG	Forward	Tie2	390
T2	TGA GTG AAC GAA CCT GGT CG	Reverse	Tie2	

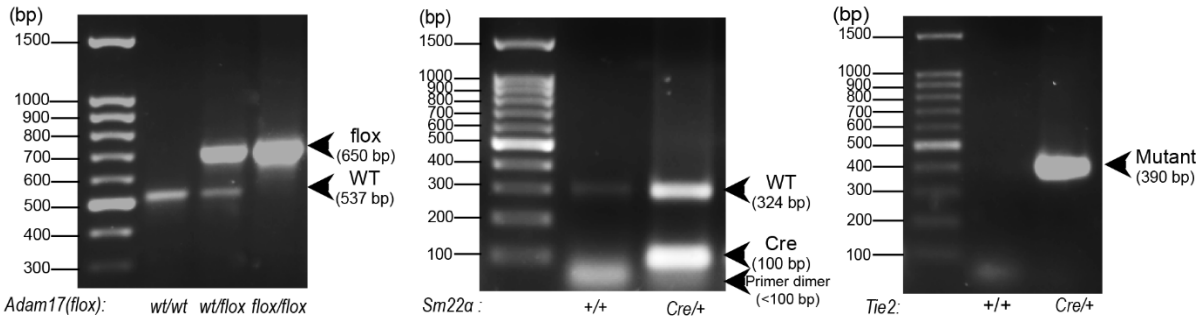

Figure 2.1 PCR genotyping results of toe clip samples from indicated genotypes. LoxP flanked ADAM17 allele was detected at 650 bp, and WT-ADAM17 band was detected at 537 bp (Left Panel). DNA PCR gel shows the band for *Sm22α-Cre* allele ($Sm22^{Cre/+}$) and its WT allele ($Sm22^{+/+}$) (Middle Panel), and for *Tie2-CreER*^{T2} allele ($Tie2^{Cre/+}$) and its WT allele ($Tie2^{+/+}$).

ADAM17 levels in the smooth muscle cells of *Adam17$^{f/f}$* and *Adam17$^{f/f}$/Sm22$^{Cre/+}$* mice were confirmed by real time-PCR and immunoblotting in aortic tunica media as well as in cultured primary aortic smooth muscle cells. Tamoxifen-induced *Adam17* knockdown efficiency in endothelial cells was evaluated by comparing ADAM17 protein levels in the lung homogenates of *Adam17$^{f/f}$* and *Adam17$^{f/f}$/Tie2$^{Cre/+}$* mice at least two weeks post tamoxifen treatment. Control genotypes included *Sm22α-Cre* mice and *Tie2-CreER^{T2}* (+tamoxifen) mice.

2.5. Angiotensin II pump implantation

Alzet micro-osmotic pumps (Model 1004, Durect Co.) were implanted subcutaneously in 10- to 12-week-old male mice to deliver 1.5 mg/kg/day of angiotensin II or vehicle (saline) for two or four weeks as before (378).

2.6. Telemetric blood pressure measurement

Telemetry transmitter (model PA-C10; Data Sciences International, St. Paul, MN) was implanted in 12 weeks old male mice as follows. Mice were anesthetized using 4% isoflurane in oxygen and maintained with 2% isoflurane for the duration of the telemeter implantation procedure. Mice were placed in the supine position on a circulating water warming pad (38 °C, VWR International), and the thorax was shaved and disinfected with 4% Stanhexidine solution (Omega Laboratories, Montreal, Quebec). A small skin incision was made to expose the left common carotid artery by gentle blunt dissection. Telemeter catheter (model PA-C10; Data Sciences International, St. Paul, MN) was cannulated into the left common carotid artery and advanced to reach the aortic arch. The catheter was secured with three silk sutures. The body of the telemeter was placed in a subcutaneous pocket in the left flank of the animal. The incision was then closed with continuous stitching with 6-0 silk suture. Meloxicam (0.2 mg/kg, *i.p.*) was administered to provide post-operative analgesia every 24 hours for two days. Mice were allowed to recover for one week before obtaining baseline blood pressure recordings. After three consecutive days of baseline recordings, micro-osmotic pumps containing Ang II were implanted, and blood pressure was recorded over the following 28 days. To reflect the impact of circadian rhythms on blood pressure changes, recordings were carried out consistently from 10 AM to 12 PM and from 10 PM to 12 AM. Systolic, diastolic, and mean blood pressure were recorded at a sampling rate of 500 Hz from data collected for 3 seconds at 30-second intervals using the Ponemah Physiology Platform

P3 Plus software (version 5.2, Data Sciences International, St. Paul, MN). Telemeter calibration was performed before implantation and following explanation, and the recorded blood pressure values were corrected for any drift in calibration over the 6-week period (from implantation to the end of 4-week recording) (506). The average offset drift for PA-C10 telemeters in our study was 1.8 ± 0.3 mmHg (Mean ± SD) over 6 weeks of telemeter implantation.

2.7. *Ex vivo* pressure myography

After 2 weeks of saline or Ang II infusion, second-order mesenteric arteries from either genotype was used for *ex vivo* pressure myography assessment as before (507). Tissue dissections were performed in ice-cold physiological saline solution (PSS), composition (in mmol/l) 10 HEPES, 5.5 glucose, 1.56 $CaCl_2$, 4.7 KCl, 142 NaCl, 1.17 $MgSO_4$, 1.18 KH_2PO_4, pH 7.5. Mesenteric arteries were cleaned of all surrounding adipose and connective tissues and mounted on two glass cannulae in a two-bath pressure myograph (Living Systems, Burlington, VT). Vessels were orientated such that flow of PSS through the lumen was applied in the same direction as blood flow *in vivo*. Vessels were given a 40-minute equilibration period during which they were exposed to a stepwise increase in pressure from 60 to 80 mmHg with regular changes of the PSS bathing solution. The pressure was set to 60 mmHg for measurement of active experimental responses, a level which was chosen since it did not cause myogenic responses. Following the equilibration period, a cumulative concentration-response curve (CCRC) was constructed to increasing concentrations of the adrenergic agonist phenylephrine (PE, 0.001 µmol/l to 100 µmol/l). To investigate vasodilator responses to methacholine (MCh), a second CCRC (0.0001 µmol/l to 100 µmol/l) was constructed in the presence of PE (1 µmol/l) constriction. To evaluate the effects of SMC-specific *Adam17* knockdown and chronic Ang II infusion on vascular passive characteristics, mesenteric arteries were equilibrated in Ca^{2+}-free PSS in the presence of papaverine (0.1 µmol/l) to initiate complete dilation. Passive characteristics were then assessed using pressures from 0 mmHg to 140 mmHg. Corresponding circumferential wall stress was calculated using the equation: circumferential stress (dyne/cm^2) = (P×D)/2T, where P = transmural pressure (mN/mm^2, 1 mmHg = 0.133 mN/mm^2), D = internal diameter (mm), and T = wall thickness (mm). Corresponding circumferential wall strain was calculated using the equation: circumferential strain = $(D_f - D_0)/D_0$, where D_f = observed internal diameter (mm) for a given intravascular pressure, and D_0 = initial diameter (mm) at 4 mmHg. Arterial stiffness can be determined by Young's elastic modulus (E =

stress/strain). However, since the stress-strain relationship is non-linear, a tangential or incremental elastic modulus (E_{inc}) was obtained by determining the slope of the stress-strain curve. An exponential curve was fitted to data from each animal using the equation: $Y = Y_0 \exp(k \times x)$, where Y = circumferential stress, Y_0 = circumferential stress at 4 mmHg, k = the rate constant, and x = circumferential strain. Deriving this equation, we find that $E_{inc} = kY$ and, therefore, for any given circumferential stress, E_{inc} is directly proportional to k, the rate constant. This means that any increase in the rate constant implies an increase in E_{inc} and, therefore, an increase in arterial stiffness. Conversely, any decrease in the rate constant implies an increase in arterial elasticity.

2.8. Induction of experimental thoracic aortic aneurysm by periadventitial treatment of porcine pancreatic elastase

TAA was induced in mice of each genotype by treating the descending thoracic aorta with porcine pancreatic elastase Type I (30 U/ml) for 5 minutes using a modified protocol (381). Briefly, 8-10 weeks old mice of either gender were anesthetized with intraperitoneal injection of ketamine/xylazine cocktail and intubated by direct visualization. Then the mice were carefully rotated to the right lateral decubitus position and were connected to a mouse ventilator (MiniVent Type 845, Harvard Apparatus) set at a respiratory rate of 160 breaths per minute with a tidal volume of 275 µl. A 1.0-cm lateral thoracotomy was made at the 7^{th} intercostal interspace. The parietal pleura was incised, and the lung was covered by a piece of sterile stretched parafilm to avoid contact with porcine pancreatic elastase solution. The pleura overlying the descending thoracic aorta was dissected with a pair of blunt fine tip forceps (Fine Science Tools, 11373-12), and the surrounding fluid was removed entirely using absorption spears and triangles (Fine Science Tools, 18105-01) before a piece of saline- or elastase-soaked sponge (5 mm × 1 mm × 1 mm) was applied directly to the surface of the exposed aorta. After 5 minutes of elastase exposure, the sponge was removed. The chest cavity was irrigated liberally with warm saline and the lungs were expanded by obstructing outflow on the rodent for two breaths. After all residual fluid in the chest cavity was removed, the ribs were closed with 6-0 silk sutures, and the muscle layers were closed followed by the skin closure with wound clips (Kent Scientific, INS750344). Hibitane (Zoetis, 00053201) was applied topically to the incision area to reduce potential infection. After surgery, the mice were extubated, given Meloxicam (2 mg/kg BW, *i.p.*, Metacam®) for pain relief, and allowed to recover on a heating pad until they were fully recovered from anesthesia. Sham mice underwent the same

procedure, expect elastase exposure to the descending thoracic aortas. All the mice were then maintained in animal facility for 3 days or 14 days post-TAA surgery.

The modification made in our procedure compared to the previously published report (381), rather than applying the concentrated stock porcine pancreatic elastase solution directly to the mouse aortas, we first performed a screening panel by treating descending thoracic aortas in WT mice with a serial dilutions of elastase solution ranging from 10 U/ml to 50 U/ml (data for 40 U/ml and 50 U/ml are not shown) to explore the minimal elastase concentration required for reproducible and consistent aneurysmal phenotype. We found that treating WT descending thoracic aortas with at least 30 U/ml of elastase solution for 5 minutes can induce advanced TAA (at day 14 post elastase treatment) with a diameter ~60% larger than that of controls.

2.9. Administration of an ADAM17-selective inhibitor

To study the therapeutic potential of ADAM17 inhibition in TAA, an ADAM17-selective inhibitor (PF-5480090/PF-548, *Pfizer*) was suspended in 2% Tween 80/0.5% methylcellulose. Since the half-life of this inhibitor is 1.5 hours (unpublished data), we dosed the animals with this inhibitor at a high concentration twice daily. Specifically, mice received PF-548 (100 mg/kg *b.i.d.*) or vehicle (2% Tween 80/0.5% methylcellulose) by oral gavage, starting prior to, or after induction of TAA to test the effects of PF-548 on TAA formation (disease onset) (**Figure 4.17A**) and small TAA growth (disease progression) (**Figure 4.17E**). The technicians from *Pfizer*, Inc. helped us determine the plasma concentrations of PF-548 in wildtype mice at 0.5 hour, 1 hour, 3 hours, and 24 hours after one dose (100 mg/kg) **(Figure 4.18A)**.

2.10. Aorta dissection and imaging

At indicated time points, mice of each genotype were anesthetized, and perfuse-fixed at 100 mmHg (calibrated using a saline bag hung at the height of 136 cm) with 10% buffered neutral formalin for 15 minutes. The entire aortas were excised and secured on a home-made black silicon plate (SYLGARD170, Dow Corning, 3097340-0116) using stainless steel minutien pins (Fine Science Tools, 26002-20) and imaged by a digital camera. A ruler was always aligned parallel to the aortas as a reference for the size of the aorta and to allow for cross-comparison between aortas harvested at different times.

2.11. Morphometric and immunofluorescent analyses of human and mouse aneurysmal aortas

After the whole mouse aorta was formalin-fixed (as described above), the thoracic aorta (where elastase was applied) were excised and embedded in OCT media, and sectioned at a thickness of 5 μm. The cross-sections were air-dried and fixed in 4% paraformaldehyde (PFA in 1×PBS, pH7.4) at room temperature for 20 minutes. The sections were washed in 1×PBS (pH7.4) 3 times for 5 minutes. To assess the severity of elastin fiber deterioration in the aneurysmal aortas of different groups, cross-sections were stained with an elastic fiber kit (termed as Verhoeff-Van Gieson staining) as per the manufacturer's instructions (Sigma-Aldrich). Images of full cross-sections were captured at a low magnification (×50), and the internal aortic diameters were calculated from the internal circumference of the cross-sections, with the assumption that the cross-sections were full circles (378). Collagen deposition and distribution in aneurysmal aortas were visualized by picrosirius red (PSR) staining as described before (378). For immunofluorescence staining, aortic sections were further permeabilized in 0.1% Triton-X100 in 1× TBS, pH 7.4 for 10 minutes. Next, sections were blocked with 1% BSA (prepared in 1× TBST, pH 7.4) for 1 hour, and then incubated with primary antibodies (diluted in 1% BSA in 1× TBST, pH 7.4) overnight at 4 °C followed by incubation with fluorophore-conjugated secondary antibodies (diluted in 1% BSA/1× TBST, pH 7.4) for 1 hour at room temperature. Primary antibodies targeting CD68 (macrophage), Ly6G (neutrophil) and Calponin (smooth muscle cell) were used. DeadEnd™ Fluorometric TUNEL kit (Promega) was used to detect apoptotic cells in 3-day aneurysmal samples of different groups as per the manufacturer's instructions.

Formalin-fixed human aortas were embedded in paraffin. After being deparaffinized and rehydrated, 5-μm-thick sections were subjected to antigen retrieval in sodium citrate buffer (10 mM sodium citrate, 0.05% Tween 20, pH 6.0) at 98 °C for 25 minutes in a microwave (1,100 W, 40% of power). Then the sections underwent 3 times of 1× PBS wash, non-specific antigen blocking, primary and secondary antibody incubation as described above. Rabbit anti-ADAM17 antibody (1:500, EMD Millipore) was used to detect the abundance and distribution of ADAM17 protein in control versus TAA aortic samples.

In all stainings, Prolong Gold Antifade Reagent with DAPI (Invitrogen, P36935) was used to stain the nuclei. Negative control for each fluorescent staining was performed by incubating a parallel set of sections with isotype-matched IgG antibodies for all immunostainings. Fluorescent

images were visualized and captured by an Olympus motorized inverted research microscope model IX81.

2.12. Primary mouse and human smooth muscle cell isolation and subculture

Primary mouse thoracic aortic smooth muscle cells (mSMCs) were isolated from 3-week-old male *Adam17*$^{f/f}$ and *Adam17*$^{f/f}$*/Sm22*$^{Cre/+}$ mice as described (508). Briefly, the descending aorta was excised and stripped off the surrounding adipose and connective tissue in ice-cold sterile PBS containing 100 U/ml penicillin, 100 μg/ml streptomycin and 250 ng/ml Fungizone. The cleaned aorta was incubated in digestion buffer (1× HBSS, 2 mg/ml BSA, 1 mg/ml collagenase type II, 0.774 U/ml elastase, and 1 mg/ml soybean trypsin inhibitor) at 37 °C for 10 minutes to dissociate the adventitial layer from the medial layer. Following removal of the adventitial layer, aortic tunica media was minced into small pieces (2 mm × 2 mm) and further incubated in the digestion buffer at 37°C for up to 2 hours. The digestion process was terminated by adding an equal volume of DMEM/F12 culture medium supplemented with 20% FBS (DF20). The cell pellet was collected by centrifugation (300 ×*g* for 5 min), washed once with DMEM/F12 culture medium before resuspension into a small volume of DF20 (+100 U/ml penicillin/100 μg/ml streptomycin). Cells were left undisturbed in a humidified incubator (37 °C/5% CO2 in air) for at least 48 hours to allow attaching and spreading. The purity of mSMC isolation using this technique is >95% purity as verified by staining for SMC-specific markers, SM22α, calponin and smooth muscle myosin heavy chain 11 (214). For all experiments, cells at passages 3-5 were used to minimize phenotypic switching which can occur with prolonged culture period and at later passages. Cells were serum-deprived for 24 hours prior to the start of indicated experimental protocols.

Primary human aortic SMCs (hSMCs) were isolated from the ascending aorta of non-failing hearts that were not used for transplant, through the HOPE program (from three donors: male, 29 years; male, 38 years; female, 21 years). A modified enzymatic dispersal method was used (509). Briefly, the aorta was washed 3 times with ice-cold 1×HBSS, cut open to expose the intima, endothelium was removed by gentle scraping with a Falcon® Cell Scraper (Corning, 353085). The medial layer of the aorta was cut into small pieces (2 mm × 2 mm), transferred to a sterile 50-ml conical tube containing enzymatic digestion buffer (500 U/ml collagenase type I and 1 U/ml elastase, prepared in 1×HBSS; 37 °C) to a final aortic tissue (g)-to-enzyme solution (ml) ratio of 1/5 (w/v). The conical tube was then incubated in a water bath with a shaking platform at 37°C for

up to 2.5 hours. The digestion process was terminated by adding an equal volume of DF10. The cell clumps were dissociated using a plugged wide-mouth pipet and passed through a 70-μm cell strainer (Corning, 352350) to remove tissue debris. Cells were collected by centrifugation (300×*g* for 5 minutes) and washed once with DMEM/F12 culture medium before resuspension into a small volume of DF20 supplemented with 100 U/ml penicillin and 100 μg/ml streptomycin. Human aortic SMCs were seeded at a density of 10^4 cells/cm^2 in 6-well plates and left undisturbed for 48 hours before changing the culture media. We used hSMCs at passages 3-5 in this study. Cells were serum-deprived for 24 hours prior to the start of indicated experimental protocols.

2.13. Endothelial cell culture

Primary human aortic endothelial cells (HAoECs, lot# 70001318, demographic information of the donor: male, Caucasian, 2 years of age) were purchased from ATCC (American Type Culture Collection) and cultured in vascular cell basal medium supplemented with endothelial cell growth kit-VEGF, 2% FBS, 100 U/ml penicillin and100 μg/ml streptomycin (endothelial cell growth medium). Cells were cultured at 37 °C in an atmosphere of 5% CO_2/95% air. The purity of cells was confirmed by the cobblestone morphology and the vWF immunocytochemical staining. HAoECs at passages 2-5 were used for experiments.

2.14. *ADAM17* siRNA transfection in human aortic SMCs and ECs

For siRNA transfection, hSMCs and HAoECs were plated at subconfluence (10^5 cells on each well of a 6-well plate) in DF10 and endothelial cell growth medium with no antibiotics (which could interfere with siRNA transfection efficiency). The next day, cells were transfected with Lipofectamine® RNAiMAX transfection reagent (Invitrogen, 13778-150) as per the manufacturer's protocol. We transfected hSMCs and HAoECs with two sets of *ADAM17* siRNAs (Ambion, s13718, siRNA#1 and s13720, siRNA#2, final concentration 30 pmol/l) for 24 hours, and protein lysates prepared 72 hours post-transfection were subjected to immunoblotting for ADAM17. We found that while both *ADAM17* siRNAs almost completely knocked down ADAM17 in hSMCs (**Figure 2.2A**), *ADAM17* siRNA #2 showed higher knockdown efficiency than siRNA #1 in HAoECs (**Figure 2.2B**). Therefore, we used *ADAM17* siRNA #2 for the all siRNA transfection experiments on both cell types in this study. Scrambled siRNA (Ambion, 4390844) was served as controls. After siRNA transfection, hSMCs were serum starved in DF0 for 24 hours prior to the start of

indicated experimental protocols, whereas HAoECs were serum starved in vascular cell basal medium supplemented with 1% FBS for 24 hours prior to the start of indicated molecular experiments. We did not starve HAoECs for *in vitro* permeability assay or for VE-cadherin staining, as we observed that serum starvation could cause non-negligible cell death and therefore would compromise the integrity of the monolayer even before elastase treatment. This would, in turn, result in pseudo-positive signals (increased permeability) even at baseline. All assays were performed 48 hours after siRNA transfection.

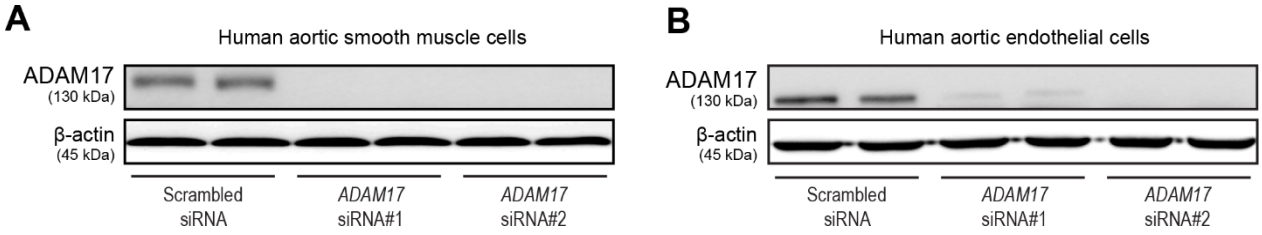

Figure 2.2 *ADAM17* knockdown efficiency in human aortic smooth muscle cells and endothelial cells after targeted siRNA transfection. (**A**) A representative immunoblot showing ADAM17 knockdown efficiency by two specific *ADAM17* siRNAs (#1 and #2) in human aortic SMCs. The data shown are representatives of three independent experiments. (**B**) A representative immunoblot showing ADAM17 knockdown efficiency in human aortic endothelial cells transfected with two *ADAM17* siRNAs. *ADAM17* siRNA #2 showed a more efficient *ADAM17* knockdown efficiency than *ADAM17* siRNA #1. Therefore, *ADAM17* siRNA #2 was used in this study to knockdown *ADAM17* in both human aortic smooth muscle cells and endothelial cells. The data shown are representative of three independent experiments.

2.15. BrdU incorporation assay

A total number of 5×10^4 mouse or human aortic SMCs were seeded into 4-well Nunc® Lab-Tek® II chamber slides (Nalge Nunc International, Naperville). To assess the effects of ADAM17 deletion on Ang II-induced cell proliferation, human aortic SMCs were transfected with scrambled siRNA or *ADAM17* siRNA before being seeded into the chamber slides, whereas mouse aortic VSMCs from both genotypes (*Adam17*$^{f/f}$ and *Adam17*$^{f/f}$*/Sm22*$^{Cre/+}$) were used. After 24 hours of serum deprivation, cells were incubated in serum-free DMEM/F12 culture medium containing 10 μM BrdU (5-bromo-2'-deoxyuridine, Abcam) in the presence or absence of Ang II (1 μM) for 24 hours. BrdU incorporation was terminated by washing the cells ice-cold PBS and fixing them with 4% PFA. SMC DNA was denatured by 2 mol/l HCl at 37 °C for 10 minutes, and Borate buffer (0.1 mol/l, pH 8.5) were used for neutralization. Cells were then stained with FITC-labelled anti-BrdU antibody. Rate of aortic SMC proliferation was quantified by counting BrdU-positive stained cells

and expressed as a percentage of total number of cells (stained by DAPI) in the same fields. The experiments were repeated from three independent isolations, and 60 random fields from each group were used for quantification.

2.16. Wound healing assay

SMC migration was assessed using an *in vitro* wound healing assay as described before (510). In brief, VSMC monolayers (5 $\times 10^5$ cells/ml) grown on 6-well plates were serum-deprived for 24 hours. Human VSMCs were treated with scrambled siRNA or *ADAM17* siRNA for 48 hours prior to serum starvation. A scratch wound was created manually in each well by gently scraping the cells with a sterile 200 µl pipette tip along a straight line (0 hour). VSMCs were maintained in DMEM/F12 culture medium containing 0.5% FBS (DF0.5) in the presence or absence of Ang II (1 µmol/l). By using direct microscopic visualization, cell migration into the scratch-wound surface was monitored after 24, 48 and 72 hours. The cell-free areas at each time points were measured by Image-Pro Plus (version 6.0, Media Cybernetics). For quantification purposes, the wound area generated at 0 hour was set as S_0, and the uncovered areas captured at 24 hr, 48 hr, and 72 hr were recorded as S_i (i=24, 48 or 72). The wound closure rate was then calculated by the following equation: wound closure rate (%)=$\frac{S_0-S_i}{S_0}\times 100$. The microscopic images of both human and mouse VSMCs were obtained from three independent experiments, and 20 fixed fields per group, per experiment were used.

2.17. Flow cytometric analysis of angiotensin II-induced vascular smooth muscle cell apoptosis

Human SMCs were transfected with scrambled siRNA or *ADAM17* siRNA for 24 hours. Confluent ADAM17-intact or -deficient human and mouse SMCs grown in 6-well plates were serum deprived and treated with Ang II (1 µmol/l) or saline for 24 hours. Experiments were repeated with three independent SMC isolations, and for each repeated experiment, each treatment was carried out in triplicate. Cell apoptosis was evaluated by using an Annexin VPE/7-AAD Staining Kit. Cells were rinsed with ice-cold PBS and incubated with Accutase® Cell Detachment Solution (EMD Millipore) at 37 °C for 5 minutes. The detached cells were collected by centrifugation at 300 ×g for 5 minutes. Cell were washed twice with ice-cold PBS and resuspended in 100 µl binding buffer (from the Annexin V-PE/7-AAD staining Kit). Annexin V-PE and 7-AAD

were added to the cells (5 µl of each) and incubated in the dark at room temperature for 15 minutes. After incubation, 400 µl binding buffer was added to each sample. Staurosporine (1 µmol/l) was used to induce cell death (apoptosis and necrosis) in SMCs and served as positive control and compensation control. Data acquisition was performed on a BD LSR Fortessa-SORP cytometer (BD Biosciences) and analyzed using the FlowJo software (version 10.0.7, TreeStar, Inc.).

2.18. *In vitro* acute exposure of elastase to primary cultured cells

To better understand the underlying cellular behaviors and signaling alternations in ADAM17-intact or -deficient SMCs (mouse and human, m/hSMCs) or HAoECs subjected to acute elastase exposure, we established an *in vitro* model by incubating serum-starved primary m/hSMCs or HAoECs in elastase solution (0.4 U/ml in basal medium) for 5 minutes to mimic our *in vivo* TAA model. After the elastase solution was removed, m/hSMCs or HAoECs were further cultured in freshly replenished serum-free DMEM/F12 medium (DF0) or vascular cell basal medium supplemented with endothelial cell growth kit-VEGF and 1% FBS respectively for the indicated period of time in each experimental setting.

2.19. Immunocytofluorescence of VE-cadherin on human aortic endothelial cell monolayers

Immunofluorescent visualization of VE-cadherin structural integrity in response to acute elastase exposure was performed on cultured primary HAoECs at passage 2. Briefly, HAoECs were transfected with scrambled or *ADAM17* siRNA in 6-well plates for 24 hours and were detached with Accutase® Cell Detachment Solution (EMD Millipore). A total number of 10^4 of transfected HAoECs were seeded on glass coverslips precoated with human plasma fibronectin (5 µg/ml). Cells were allowed to form an intact monolayer before elastase treatment. *ADAM17*-intact or -deficient HAoECs were subjected to vehicle (basal medium) or porcine pancreatic elastase type I (0.4 U/ml in basal medium, Sigma-Aldrich) treatment for 5 minutes, followed by freshly replenished vascular cell basal medium supplemented with endothelial cell growth kit-VEGF and 2% FBS. After 6 hours, HAoECs were briefly washed once with 1×PBS (pH 7.4), and then fixed in 4% PFA (prepared in 1×PBS, pH 7.4) at room temperature for 10 minutes, and permeabilized with 0.1% Triton-X100 (prepared in 1× TBS, pH 7.4) for 10 minutes at room temperature. HAoECs were blocked with 1% BSA (prepared in 1× TBST, pH 7.4) for 30 minutes, and incubated with rabbit anti-VE-cadherin (1: 400) overnight at 4 °C followed by incubation with goat anti-rabbit

Alexa Fluor Plus 555 secondary antibody (1:1, 000) and Alexa Fluor 488 Phalloidin (1:40) cocktail for 1 hour at room temperature. Finally, cell nuclei were stained by Prolong Gold Antifade Reagent with DAPI. VE-cadherin structural integrity and F-actin distribution patterns for each group were visualized and captured by an Olympus motorized inverted research microscope model IX81.

2.20. *In vitro* endothelial cell permeability assay

The effects of *ADAM17* knockdown on elastase-induced endothelial cell permeability was measured by an *in vitro* vascular permeability assay kit as per the manufacturer's instructions (EMD Millipore). Briefly, HAoECs were transfected with scrambled or *ADAM17* siRNA for 24 hours as described above. After trypsinization, a total number of 10^6 HAoECs at passage 3 were seeded on each porous cell culture insert provided in the kit. The cells were maintained for 72 hours to allow for monolayer formation. Following endothelial monolayer formation, growth medium was carefully removed from each insert and the receiver plate well and replaced with basal medium containing vehicle or porcine pancreatic elastase type I (0.4 U/ml) for 5 minutes. Next, 150 µl of culture medium containing FITC-dextran was added to each insert, and 500 µl of growth medium without FITC-dextran was added to each receiver plate well. The FITC-dextran was allowed to permeate through the monolayer, and levels of FITC-dextran was measured in the receiver chamber over 3 hours. Every 30 minutes, 100 µl of media was collected from the receiver well and was replaced with an equal volume of fresh medium. Permeability was quantified by fluorescent intensity (of FITC-dextran) on a plate reader (SpectraMax M5, Molecular Devices) via fluorescence at 485 nm excitation/535 nm emission wavelengths in a time-dependent fashion. The fluorescent intensity signal for each group was normalized to that of the scrambled siRNA-vehicle group at each time point. The experiment was run in triplicates, and data from two independent experiments were averaged.

2.21. *In vivo* Evans blue permeability assay

Evans blue dye binds to albumin in the blood, and its detection beyond the arterial lumen indicates impaired intimal layer and increased permeability of the endothelial cell barrier. Therefore, we took advantage of this technique to evaluate whether ADAM17 deficiency in endothelial cells would affect intimal layer permeability after acute elastase treatment of the thoracic aorta. At day 3 post-TAA surgery, eight male $Adam17^{f/f}$ and $Adam17^{f/f}/Tie2^{Cre/+}$ mice were

injected with 100 µl of a 1% Evans blue solution in 1× PBS through sub-retinal injection. All mice were euthanized after 1 hour of dye injection. Mice were perfused through the left ventricle with PBS to clear out the Evans Blue dye in the whole body. Then the whole aortas were carefully dissected, the surrounding adipose tissues were removed, and images of the whole aorta were captured using a digital camera. The aortic segments that underwent elastase treatment were embedded in OCT medium. Ten-micrometer-thick OCT sections were cut and fixed in 4% PFA. After 3 times wash with PBS, the cross-sections were mounted by Prolong Gold Antifade Reagent with DAPI and used for imaging. Due to the autofluorescence characteristic of Evans blue (excitation at 620 nm, emission at 680 nm), the amount of Evans blue that permeated into the aortic wall was visualized (red) using the fluorescent microscope as mentioned above.

2.22. RNA isolation and quantitative real-time PCR

Total RNA was extracted from the tunica media of *Adam17*$^{f/f}$*/Sm22*$^{Cre/+}$ mice and their littermate controls, *Adam17*$^{f/f}$ mice, before and 3 days post-TAA surgery using TRIzol reagent (Invitrogen, 15596026) according to the manufacturer's protocol. After acute elastase exposure, primary mouse aortic SMCs (*Adam17*$^{f/f}$ and *Adam17*$^{f/f}$*/Sm22*$^{Cre/+}$) and human aortic SMCs (scrambled siRNA *vs* *ADAM17* siRNA transfected) were harvested at indicated time points and underwent total RNA extraction using the same protocol above. One microgram of total RNA was used for cDNA synthesis (Invitrogen). Quantitative real time-PCR was carried out on a LightCycler 480 II system (Roche) using the LightCycler 480 Probes Master kit (Roche, 04887301001) and TaqMan primer-probe mix (**Table 2.5**) for each gene. mRNA extracted from wildtype mouse brain was used to generate cDNA and used as a standard curve by serial dilution. The reference gene *18S* or hypoxanthine-guanine phosphoribosyltransferase (*Hprt*) was used as an internal control.

Table 2.5 Mouse assay IDs for TaqMan real-time PCR

Gene name	Protein name	Assay ID
Adam9	A disintegrin and metalloproteinase 9	Mm01218460_m1
Adam10	A disintegrin and metalloproteinase 10	Mm00545742_m1
Adam12	A disintegrin and metalloproteinase 12	Mm00475719_m1
Adam15	A disintegrin and metalloproteinase 15	Mm00477328_m1
Adam17	A disintegrin and metalloproteinase 17	Mm00456428_m1
Adam19	A disintegrin and metalloproteinase 19	Mm00477337_m1
At1	Angiotensin II receptor type 1	Mm00558224_s1
At2	Angiotensin II receptor type 2	Mm00431727_g1
Col1a1	Collagen type I alpha 1 chain	Mm00801666_g1
Col3a1	Collagen type III alpha 1 chain	Mm00802300_m1
Eln	Elastin	Mm00514670_m1

2.23. Tissue and cell protein extraction and immunoblotting

Aortic tissues post indicated treatments were dissected and cleaned of surrounding adipose and connective tissues in ice-cold PBS. In order to extract protein from the aortic tunica media only from *Adam17*$^{f/f}$ and *Adam17*$^{f/f}$/*Sm22*$^{Cre/+}$ mice, tunica adventitia was mechanically removed and the aortic lumen was further cut open longitudinally to remove the intima by gentle scraping of the aorta using fine-tip curved forceps. Aorta with intact structure (three layers) or medial layer only were then snap frozen in liquid nitrogen and crushed into fine powder. Proteins were extracted from the homogenized aortic tissues and cultured human or mouse VSMCs using CelLytic™ M lysis buffer (C2978, Sigma-Aldrich) containing a protease and phosphatase inhibitor cocktail (Calbiochem). The amount of protein in each sample was quantified using DC™ Protein Assay Kit (Bio-Rad) according to the manufacturer's instructions.

For immunoblotting analyses, equal amounts (20 μg-35 μg) of total protein was separated by electrophoresis under denaturing conditions on a 4-20% SDS-polyacrylamide gel and transferred onto a piece of Immobilon-P PVDF membrane (EMD Millipore, IPV00010). Since gradient gel usually gives a better separation of proteins with a wide range of molecular weights, we aimed to blot 2-3 proteins from the same membrane by cutting the membrane into small pieces. The target proteins were ensured to fall into the middle of truncated membranes. In brief, membranes were pre-stained by Pierce™ reversible protein stain kit for PVDF Membranes and cut into 2-3 pieces based on the predicted molecular weights of target proteins by direct visualization, using a pre-

stained Spectra Multicolor Broad Range Protein Ladder (Thermo Fisher Scientific, 26623) as a reference. The PVDF membranes were blocked in 3% BSA (prepared in 1× TBST, pH 7.4, same as below) for 1 hour at room temperature, and incubated with primary antibodies with desired dilution ratio in 3% BSA/TBST overnight at 4 °C. The next day, the membranes were washed 3 times for 5 minutes with 1× TBST and incubated with species-relevant HRP-linked secondary antibodies (1:5, 000-10, 000) for 1 hour at room temperature. After TBST wash, membranes were incubated in Amersham ECL Prime Western Blotting Detection Reagent (GE Healthcare, RPN2232) or Clarity Max™ Western ECL Substrate (Bio-Rad, 1705062) as per the manufacturer's protocols, and target bands were detected by ImageQuant LAS 400 system (GE Healthcare). The intensity of bands was quantified using the inbuilt ImageQuant TL software (Version 7.0 GE Healthcare) and normalized to an α-tubulin or a β-actin control.

2.24. *In vitro* gelatin zymography

MMP2 and MMP9 activation in sham and 3 day-TAA samples of all genotypes were confirmed by *in vitro* gelatin zymography as described before (378). In brief, equal amounts (20 μg) of nonreduced aorta lysates were run on 8% SDS-PAGE gel containing 2 mg/ml gelatin. After electrophoresis, gels were renatured with 2.5% Triton X-100 buffer for 60 minutes at room temperature. The gels were then immersed in developing buffer (pH 7.5, composition in mmol/l, 50 Tris-Cl, pH 8.0, 5 $CaCl_2$, 150 NaCl) and incubated overnight at 37 °C. Then the gels were stained with 0.05% Coomassie Blue G-250, and grayscale images were scanned and inverted for densitometric quantification.

2.25. *In vitro* ADAM17 enzymatic activity assay

In vitro ADAM17 enzymatic activity was measured as described before (336). In brief, aortic protein was extracted by a lysis buffer with a high yield of membrane-bound proteins (Cacodylic acid 10mM, NaCl 150 nM, $ZnCl_2$ 1 μM, $CaCl_2$ 20 mM, NaN_3 1.5 mM, Triton X-100 1%, pH 5.0). Mca-Pro-Leu-Ala-Gln-Ala-Val-Dpa-Arg-Ser-Ser-Ser-Arg-NH_2 fluorogenic peptide substrate III (R & D Systems) was used as the substrate for ADAM17. Calibration standard Mca-Pro-Leu-OH (Bachem) was used to calculate conversion factor, and recombinant mouse ADAM17 (R & D Systems) was served as a positive control. The ADAM17 activity assay was carried out as per the protocol provided by R & D Systems. A total amount of 5 μg protein was used for ADAM17

enzymatic activity assay, and the assay was run as a kinetic assay mode for 24 hours. Each sample was run in triplicates, and the data represent the mean values of three independent experiments. The specific ADAM17 activity is expressed as pmol/min/μg tissue protein.

2.26. Beads-based multiplex assay

Cytokine and chemokine profiles in mouse sham, 3 day-TAA and 14 day-TAA samples were quantified using Mouse Cytokine Array / Chemokine Array 31-Plex Panel (Eve Technologies, MD31). The 31-plex Discovery assay is based on the Luminex technology and utilizes the MILLIPLEX® MAP Mouse Cytokine/ Chemokine Magnetic Bead Panel Assay (EMD Millipore, MCYTMAG70PMX32BK) that comprises of fluorescent color-coded beads pre-coated with capture antibodies targeting 31 specific cytokines. In brief, sham- and elastase-treated aorta segments at day 3 and day 14 post-TAA surgery were collected, and due to a limited amount of protein yield from an individual aorta, we pooled three aorta segments/genotype/treatment into one sample. Therefore, 18 aortas were used to get 6 samples for each genotype and each treatment. Proteins were extracted in RIPA lysis and extraction buffer, and total protein concentration was adjusted to 2 mg/ml in an equal volume of 120 μl for each sample. Protein samples were incubated with the beads before the addition of biotinylated detection antibodies followed by phycoerythrin-conjugated streptavidin. Bound cytokines and chemokines were identified and quantitated using the Bio-Rad BioPlex 200 bead analyzer consisting of a dual-laser system which activates the fluorescent beads to identify the specific cytokines; and excites the PE conjugate to determine the magnitude of fluorescence, which is in direct proportion to reflect the amount of bound cytokine/chemokine. Fluorescence intensity values were recorded as relative fluorescent units (RFU) and converted to protein concentration (pg/ml) based on a protein standard linear curve consisting of purified cytokines at known concentrations included in each batch run. The individual cytokine/chemokine concentrations were further converted to pg per mg aortic protein. All samples were run in duplicates.

2.27. ELISA quantification assay for soluble VE-cadherin in conditioned culture media

The cleaved form (soluble) of VE-cadherin released by HAoECs to the culture medium in response to acute elastase exposure was quantified by a Quantikine ELISA human VE-cadherin Immunoassay kit (R & D Systems). In brief, after HAoECs underwent siRNA transfection, serum

starvation and elastase treatment, 1 ml of fresh endothelial cell culture medium was added to each well of a 6-well plate, and conditioned medium was collected at 6 hours post elastase exposure. Conditioned media were centrifugated at 3,000 × *g* for 15 minutes to remove cell debris. Undiluted conditioned media were used to quantify soluble VE-cadherin levels according to the manufacturer's instructions. The concentration of soluble VE-cadherin is expressed as ng per ml of conditioned media. All samples were run in triplicates.

2.28. Statistics

Statistical analyses were performed by using IBM SPSS software (Version 21). Normality of data distribution was determined via the Kolmogorov–Smirnov test, and all data showed normal distribution. Comparisons between any two groups (human control and TAA, and vehicle- or ADAM17 inhibitor-treated mice) was performed with unpaired student's *t*-test. Comparison among multiple groups (>3) with one main factor was performed by one-way ANOVA followed by Bonferroni *post-hoc* test. Comparison among multiple groups (genotype × treatment) was performed by two-way ANOVA followed by Bonferroni *post-hoc* test. Averaged values are presented as mean ± SEM. All *in vitro* experiments were done in triplicate for each experimental group and performed in two to five independent experiments, and each *n* value corresponds to an independent experiment. For *in vivo* data, each *n* value corresponds to an individual mouse, and the number of mice used for each *in vivo* analysis is indicated in the figure legends. Statistical significance was recognized at $P < 0.05$.

CHAPTER 3

ROLE OF ADAM17 IN ANGIOTENSIN II-INDUCED HYPERTENSION AND END-ORGAN DAMAGE

LOSS OF SMOOTH MUSCLE CELL DISINTEGRIN AND METALLOPROTEINASE 17 TRANSIENTLY SUPPRESSES ANGIOTENSIN II-INDUCED HYPERTENSION AND END-ORGAN DAMAGE

Mengcheng Shen, MSc[1,3], Jude Morton, PhD[1,2, 4], Sandra T Davidge, PhD[1,2,3, 4], Zamaneh Kassiri, PhD[1,3]

[1]Department of Physiology, [2]Department of Obstetrics and Gynecology, Faculty of Medicine and Dentistry, [3]Cardiovascular Research Centre, Mazankowski Alberta Heart Institute, [4]Women and Children's Health Research Institute, University of Alberta, Edmonton, Alberta, Canada

Contributions:

MS: Conceived and designed experiments, performed all the *in vivo* and *in vitro* experiments, acquired data, analyzed data, prepared figures, and wrote the manuscript.

JM: Conducted *ex vivo* pressure myography experiments and helped with result interpretation.

STD: Provided *ex vivo* pressure myography experimental settings and provided critical review of this manuscript.

ZK: Corresponding author. Conceived hypothesis, analyzed data, wrote, and revised the manuscript.

A version of this chapter has been published. ***Shen M, Morton J, Davidge ST, and Kassiri Z. Loss of smooth muscle cell disintegrin and metalloproteinase 17 transiently suppresses angiotensin II-induced hypertension and end-organ damage. Journal of molecular and cellular cardiology. 2017;103:11-21.*** *This chapter has been modified from this article.*

3.1. Introduction

Hypertension is a significant health problem that continues to underlie the morbidity and mortality associated with cardiovascular diseases (511). Angiotensin II (Ang II) is the central product of the renin-angiotensin system, and is a key player in the etiology of hypertension and associated pathologies such as cardiovascular and renal diseases. Vascular remodeling, mainly hypertrophy and hyperplasia of vascular smooth muscle cells (VSMC), are hallmarks of hypertension. Ang II is a strong hypertensive agent that, in addition to triggering SMC contraction (512), promotes VSMC proliferation, hypertrophy and migration; thereby contributing to vascular remodeling (513). The main pathway identified for this function of Ang II has been reported to be through activation of the angiotensin II receptor type-1 (AT_1) and transactivation of epidermal growth factor receptor (EGFR) (514, 515). EGFR can be activated by a number of ligands including heparin-binding epidermal growth factor-like growth factor (HB-EGF), transforming growth factor-alpha (TGFα), amphiregulin, β-cellulin, epigen, and epiregulin (516). A disintegrin and metalloprotease 17 (ADAM17) is a membrane-bound enzyme that can proteolytically cleave and release a variety of membrane-bound growth factors and cytokines (517), and thereby it can regulate multiple cell functions. A role for ADAM17 has been reported in cultured VSMCs (317), and its loss was recently linked to short-term protection against Ang II-induced cardiac hypertrophy (311).

In this study, we aimed to determine the long-term impact of ADAM17 loss in smooth muscle cells in response to Ang II-induced hypertension and end-organ damage, and to identify the underlying mechanism. We used *in vitro* culture systems of mouse and human VSMCs, and mice with SMC-specific *Adam17* deletion ($Adam17^{f/f}/Sm22^{Cre/+}$) to demonstrate that loss of *Adam17* in SMCs results in a transient suppression of Ang II-induced hypertension along with reduced cardiac and renal hypertrophy and fibrosis, but this protective effect does not persist with prolonged Ang II infusion.

3.2. Materials and methods

The detailed Materials and methods information is available in **Chapter 2 Materials and Methods**.

3.2.1. Experimental Animals

Mice lacking *Adam17* in SMCs (*Adam17$^{flox/flox}$/Sm22αCre*, *Adam17$^{f/f}$/Sm22$^{Cre/+}$*) were generated by cross-breeding mice carrying floxed *Adam17* alleles (*Adam17$^{tm1.2Bbl}$/J, Adam17$^{f/f}$*) with mice expressing Cre-recombinase under the control of the smooth muscle cell promoter (*Sm22α-Tg(Tagln-cre)1Her/J*, *Sm22$^{Cre/+}$*). Litter-mate male *Adam17$^{f/f}$* and *Adam17$^{f/f}$/Sm22$^{Cre/+}$* mice were used in this study. All experiments were conducted in accordance with the guidelines of the University of Alberta Animal Care and Use Committee (ACUC) and the Canadian Council of Animal Care. All the mice are at a C57/Bl6 background.

3.2.2. Angiotensin II pump implantation

Alzet micro-osmotic pumps were implanted subcutaneously in 10 to 12 weeks old mice of either genotype as previously described (378).

3.2.3. Telemetric blood pressure measurement

The effect of SMC ADAM17 deletion on Ang II-induced blood pressure changes in conscious and active mice of either genotype was evaluated using telemetry as described (518). A pilot study was also conducted to investigate the effect of endothelial cell *Adam17* deletion on Ang II-induced blood pressure changes, and our preliminary data showing blunted blood pressure rise in EC-*Adam17*-deficient mice (*Adam17$^{f/f}$/Tie2$^{Cre/+}$*) in response to Ang II infusion offers us a promising direction for future studies on this particular genotype (details for EC-specific *Adam17*-deficient mice are described in **Chapter 2.4**).

3.2.4. Ex vivo pressure myography

After 2 weeks of saline or Ang II infusion, second-order mesenteric arteries from either genotype were used for *ex vivo* pressure myography assessment as previously described (507).

3.2.5. Primary mouse and human vascular smooth muscle cell isolation and culture

Primary human and mouse VSMCs were isolated using a modified enzyme dispersal method (508, 519). Human and mouse VSMCs were used at passages 3-5 for experiments to minimize phenotypic switching which can occur with prolonged culture period and at later passages. Cells were serum-deprived for 24 hours prior to the start of the experimental protocols.

3.2.6. Human ADAM17 siRNA transfection

ADAM17-knockdown in human VSMCs *in vitro* was achieved by *ADAM17*-siRNA oligonucleotide pairs as previously described (318).

3.2.7. BrdU incorporation assay

Human VSMCs transfected with scrambled siRNA or human *ADAM17*-siRNA pairs, and mouse VSMCs from $Adam17^{f/f}$ or $Adam17^{f/f}/Sm22^{Cre/+}$ were incubated with 10 μM BrdU (5-bromo-2'-deoxyuridine, Abcam)-containing serum-free culture medium in the presence or absence of Ang II (1 μmol/l) for 24 hours. After being stained with FITC-conjugated anti-BrdU antibody, the rate of VSMC proliferation was quantified by the number of BrdU-positive cells as a percentage of total number of cells (DAPI-positive) in the same field.

3.2.8. Wound healing assay

The effect of SMC *ADAM17* deletion on Ang II-induced human and mouse VSMC migration was assessed using an *in vitro* wound healing assay as described previously (510).

3.2.9. Flow cytometric analysis

Cell apoptosis was evaluated by using an Annexin V-PE/7-AAD staining Kit (BD Biosciences) and a BD LSR Fortessa-SORP cytometer (BD Biosciences). Data were analyzed using the FlowJo software (version 10.0.7, TreeStar, Inc.).

3.2.10. RNA expression analysis

Messenger RNA (mRNA) expression levels for *Adams-9, 10, 12, 15, 17, and 19*, Ang II receptor type 1 (*At1*), and Ang II receptor type 2 (*At2*) in mouse VSMCs after 24 hours of vehicle (saline)

or Ang II treatment were measured by TaqMan RT-PCR as previously described (318). Hypoxanthine-guanine phosphoribosyltransferase (HPRT) was used as an internal control.

3.2.11. Immunohistological analyses

Saline or Ang II-infused hearts and kidneys were paraffin-embedded and processed for Masson's trichrome and picrosirious red (PSR) staining as previously described (318, 520). Collagen content was quantified from PSR-stained sections using Image-Pro Plus software (version 6.0, Media Cybernetics). Briefly, 8 high power fields were randomly selected from each heart and kidney section (total n=80 images per group/genotype) for quantification. The collagen content in each examined filed was calculated as PSR positive-to-total tissue area ratio. The value for *Adam17*$^{f/f}$-saline group was set at 1.

3.2.12. Statistics

Averaged data are presented as mean ± SEM. For comparison of the main effects of 2 factors (*Adam17*-deficiency and Ang II treatment) 2-way ANOVA followed by Bonferroni's *post-hoc* tests were used. Statistics were carried out using the IBM SPSS statistics 21 software, and bar graphs were plotted using the OriginPro 2015 software. Statistical significance was recognized at $P< 0.05$.

3.3. Results

3.3.1. Loss of ADAM17 does not alter the general morphology of mouse or human VSMCs

The purity of vascular smooth muscle cell (VSMC) cultures was >95% (mouse and human) as indicated by immunofluorescent staining for SMC-specific proteins SM22α, SM-MHC11 (smooth muscle myosin heavy chain 11), and calponin (**Figure 3.1, A and B**). Loss of ADAM17 did not alter the appearance of the VSMCs (**Figure 3.1, A and B**), nor the expression levels of contractile proteins (**Figure 3.1, C and D**). In order to minimize phenotypic switching of SMCs with prolonged culture, all of the *in vitro* experiments in this study were performed at passages 3-5.

3.3.2. Loss of ADAM17 inhibits Ang II-induced EGFR transactivation in VSMCs

Ang II elevated ADAM17 protein levels in *Adam17*$^{f/f}$ VSMCs, while as expected, ADAM17 was not detectable in *Adam17*$^{f/f}$*/Sm22*$^{Cre/+}$ VSMCs (**Figure 3.2E**). In *Adam17*$^{f/f}$ cells, Ang II increased expression of the cleaved form of HB-EGF (23 kDa), whereas this increase was not detected in *Adam17*-deficient VSMCs (**Figure 3.2, A and B**). HB-EGF is a well-known ligand for EGFR, and consistent with the reduced levels of cleaved HB-EGF, we observed significantly lower EGFR activation in *Adam17*-deficient compared to *Adam17*-intact VSMCs following Ang II stimulation (**Figure 3.2, A and B**). Measurement of mRNA expression of other Adams showed that Ang II treatment increased *Adams 10*, *12*, *15*, *17*, and *19* in *Adam17*$^{f/f}$ VSMCs, but in *Adam17*$^{f/f}$*/Sm22*$^{Cre/+}$ VSMCs, the increase in *Adam 12* and *Adam 19* were significantly greater, whereas *Adam 10* and *Adam 17* did not increase (**Figure 3.2C**). Expression of all *Adams* was comparable at baseline between genotypes (**Figure 3.3**). Ang II treatment also increased the expression of its receptors, AT1 and AT2, however, the Ang II-mediated increase in *At1*, but not *At2*, was markedly suppressed in *Adam17*-deficient VSMCs (**Figure 3.2D**).

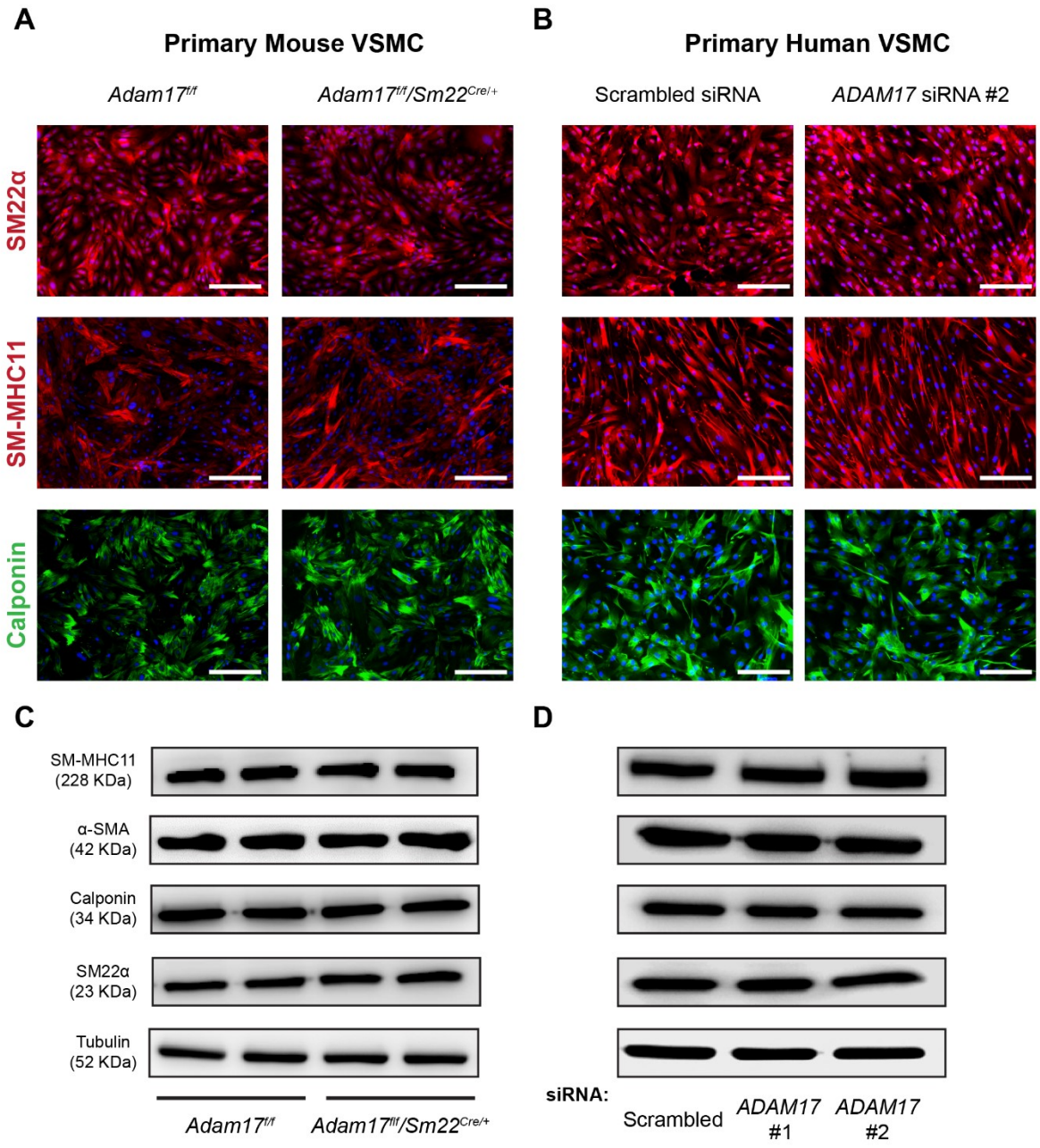

Figure 3.1 Loss of ADAM17 does not alter the morphology of mouse or human primary vascular smooth muscle cells (VSMCs). Representative immunofluorescence images for SMC markers (SM22α, SM-MHC1, and calponin) from mouse (**A**) and human (**B**) VSMCs showing similar morphology with and without ADAM17 expression. Positive SMC marker staining showed in the majority of mouse (**A**) and human (**B**) VSMCs (stained by DAPI) of the examined fields indicates a high SMC purity (>95%) achieved by the cell isolation protocols used in this study. Scale bars: 200 μm. Representative immunoblots showing unaltered contractile protein expression levels (SM22α, SM-MHC11, calponin, and α-SMA) in mouse (**C**) and human (**D**) VSMCs with and without ADAM17 expression. SM-MHC11, smooth muscle myosin heavy chain 11; α-SMA, α-smooth muscle actin; ADAM17, a disintegrin and metalloproteinase 17.

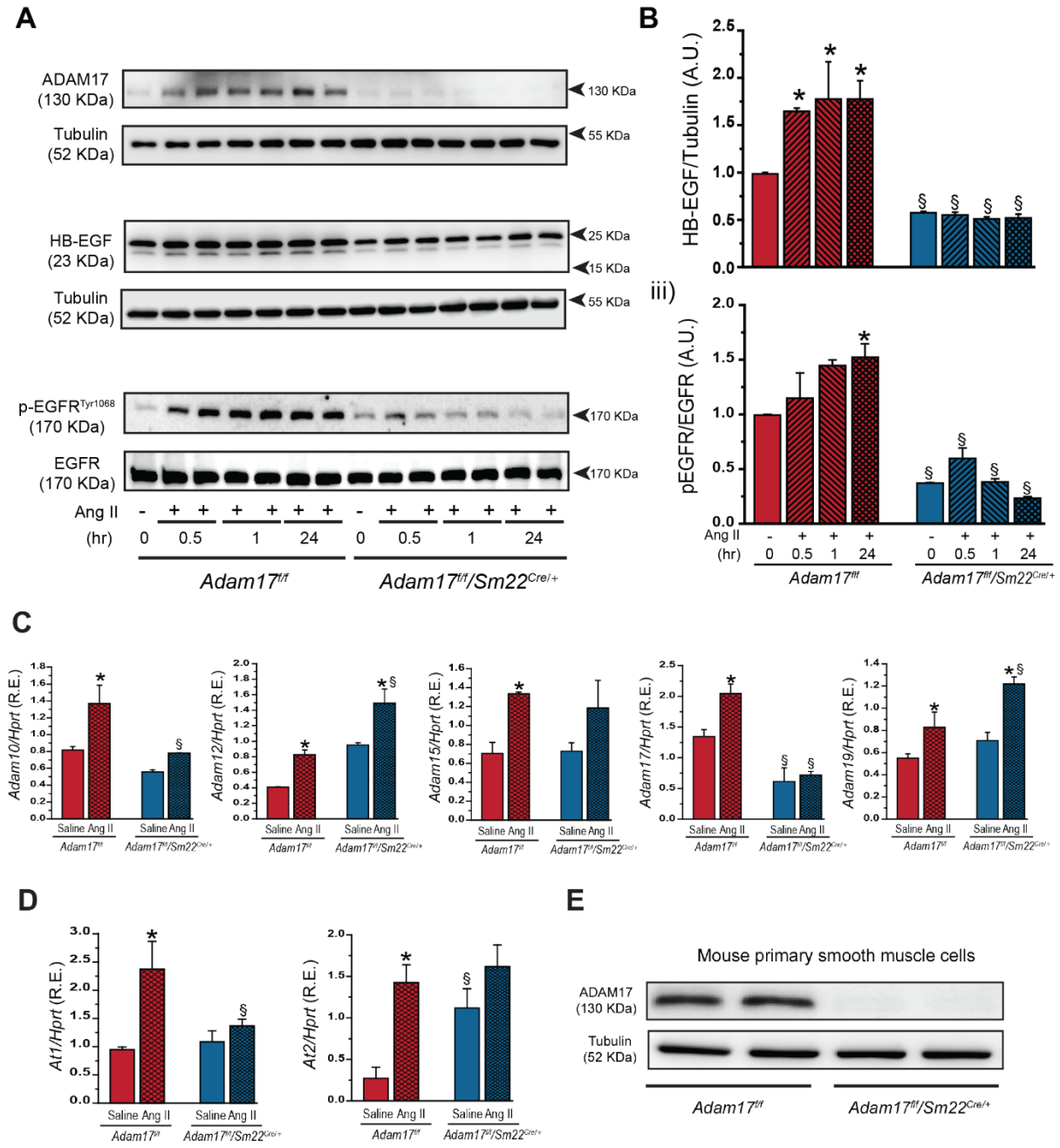

Figure 3.2 Loss of ADAM17 inhibits Ang II-induced EGFR transactivation in VSMCs. (**A**) Representative immunoblots for ADAM17, HB-EGF, phospho-EGFR^{Tyr1068}, and EGFR levels in *Adam17$^{f/f}$* and *Adam17$^{f/f}$/Sm22$^{Cre/+}$* VSMCs following different durations of exposure to Ang II (1 μmol/l). Alpha-tubulin was used as the loading control for ADAM17 blot. (**B**) Densitometric quantification of cleaved HB-EGF (23 kDa) and EGFR activation (phopho-to-total ratio) in indicated groups. Averaged mRNA expression for (**C**) Adams-10, -12, -15, -17 and -19, angiotensin receptors, (**D**) *At1* and *At2* receptor in indicated groups. **P*<0.05 versus corresponding saline group, §*P*<0.05 versus corresponding *Adam17$^{f/f}$* group using 2-way ANOVA followed by Bonferroni's *post-hoc* test. *n* = 6/group/genotype/isolation. Averaged values represent mean ± SEM. (**E**) A representative immunoblot for ADAM17 in *Adam17$^{f/f}$* and *Adam1$^{f/f}$/Sm22$^{Cre/+}$* VSMCs at baseline. EGFR, epidermal growth factor receptor; HB-EGF, heparin binding EGF-like growth factor; At1 & At2, angiotensin receptors type 1 & 2; ADAM17, a disintegrin and metalloproteinase 17; *Adam17$^{f/f}$*, *Adam17$^{flox/flox}$*; *Adam17$^{f/f}$/Sm22$^{Cre/+}$*, *Adam17$^{flox/flox}$/Sm22αCre*.

3.3.3. Adam17-deficiency diminishes Ang II-induced proliferation and migration but not apoptosis in VSMCs

Next, we assessed how the decreased Ang II-induced EGFR activation in *Adam17*-deficient VSMCs alters the cell function. Using a BrdU incorporation assay, we found that Ang II-induced cell proliferation (**Figure 3.3A**), and migration (**Figure 3.3B**) were significantly blocked in *Adam17*-deficient mouse VSMCs while the apoptotic response was not altered in these cells (**Figure 3.4**). Erk1/2 (extracellular signal-regulated kinase 1/2) and Akt signaling pathways are important in regulation of growth and migration of VSMCs, and are downstream of EGFR activation (521-523). Ang II caused a time-dependent rise in Erk1/2 activation in *Adam17*-intact cells, which was suppressed in *Adam17*-deficient cells (**Figure 3.3C**). Akt activation (phosphorylated-to-total ratio) was comparable between genotypes despite a significant rise at 1 hour in the *Adam17*-deficient cells (**Figure 3.3E**). Surprisingly, the basal Akt activation level was significantly higher in ADAM17-deficient VSMCs and remained unaltered post-Ang II stimulation (**Figure 3.3D**).

Adam17-deficiency in human VSMCs similarly reduced the rate of proliferation (BrdU incorporation) (**Figure 3.5A**) and migration (**Figure 3.5B**) without altering apoptosis (**Figure 3.6**) in response to Ang II. The greater reduction in ADAM17 proteins with siRNA #2 (compared to siRNA #1) (**Figure 3.1D**) was associated with a much slower growth rate in human VSMCs, suggesting the correlation between *Adam17*-deficiency and lower proliferation rate (**Figure 3.5, A and B**).

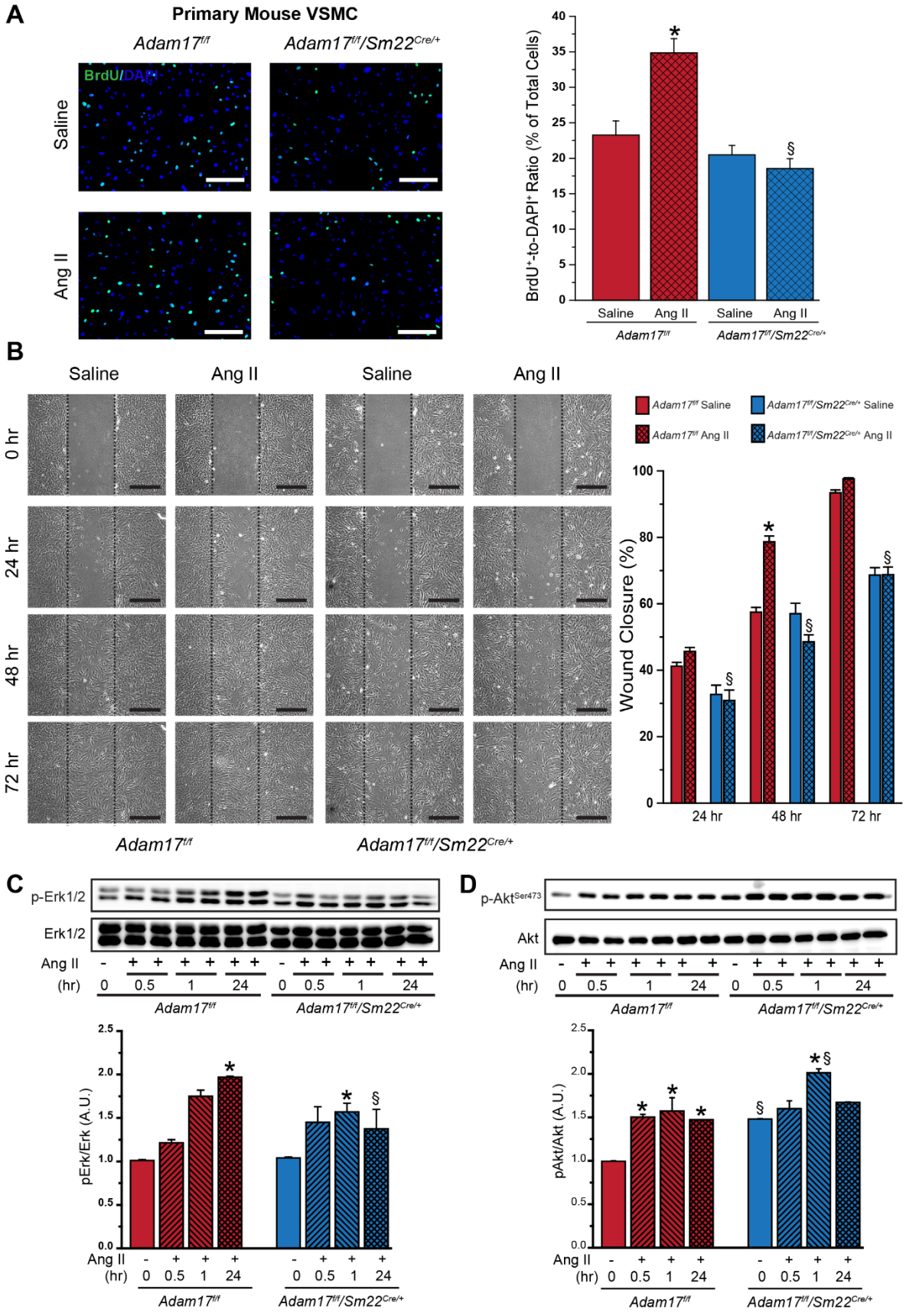
A
Primary Mouse VSMC
Adam17f/f
Adam17f/f/Sm22Cre/+
BrdU/DAPI
Saline
Ang II
BrdU+-to-DAPI+ Ratio (% of Total Cells)
Saline
Ang II
Saline
Ang II
Adam17f/f
Adam17f/f/Sm22Cre/+
B
Saline
Ang II
Saline
Ang II
0 hr
24 hr
48 hr
72 hr
Adam17f/f Saline
Adam17f/f/Sm22Cre/+ Saline
Adam17f/f Ang II
Adam17f/f/Sm22Cre/+ Ang II
Wound Closure (%)
24 hr
48 hr
72 hr
Adam17f/f
Adam17f/f/Sm22Cre/+
C
p-Erk1/2
Erk1/2
Ang II
(hr)
Adam17f/f
Adam17f/f/Sm22Cre/+
pErk/Erk (A.U.)
D
p-AktSer473
Akt
Ang II
(hr)
Adam17f/f
Adam17f/f/Sm22Cre/+
pAkt/Akt (A.U.)

Figure 3.3 Loss of ADAM17 diminishes proliferation and migration of mouse VSMCs in response to Ang II stimulation. (**A**) Representative immunofluorescence images showing BrdU incorporation (green) after 24 h of saline or Ang II (1 µmol/l) exposure, and averaged BrdU incorporation rate (cell proliferation rate) expressed as the percentage of $BrdU^+$ cells to total number of cells ($DAPI^+$ cells) for indicated groups (n = 60 random fields/group/genotype). Scale bars: 200 µm. (**B**) Representative microscopic images of scratch assay in confluent SMC monolayers of either genotype treated with saline or Ang II (1 µmol/l). Cell migration into the scratched area was monitored at the same area at indicated time points (0 h, 24 h, 48 h and 72 h), and cell migration rate was quantified as the closure rate at indicated time points (n = 20 random fields/group/genotype/isolation at indicated time points). Scale bars: 500 µm (**C**) Representative immunoblots and densitometric quantification showing total and phosphorylated Erk1/2, (**D**) and total and phosphorylated Akt in *Adam17*$^{f/f}$ and *Adam17*$^{f/f}$*/Sm22*$^{Cre/+}$ VSMCs. *P<0.05 compared to the corresponding saline group, $^{\S}P$<0.05 compared to corresponding $Adam17^{f/f}$ group using 2-way ANOVA followed by Bonferroni's *post-hoc* test. Averaged values present mean ± SEM. BrdU, 5-bromo-2'-deoxyuridine; ADAM17, a disintegrin and metalloproteinase 17; *Adam17*$^{f/f}$, *Adam17*$^{flox/flox}$; *Adam17*$^{f/f}$*/Sm22*$^{Cre/+}$, *Adam17*$^{flox/flox}$*/Sm22αCre*.

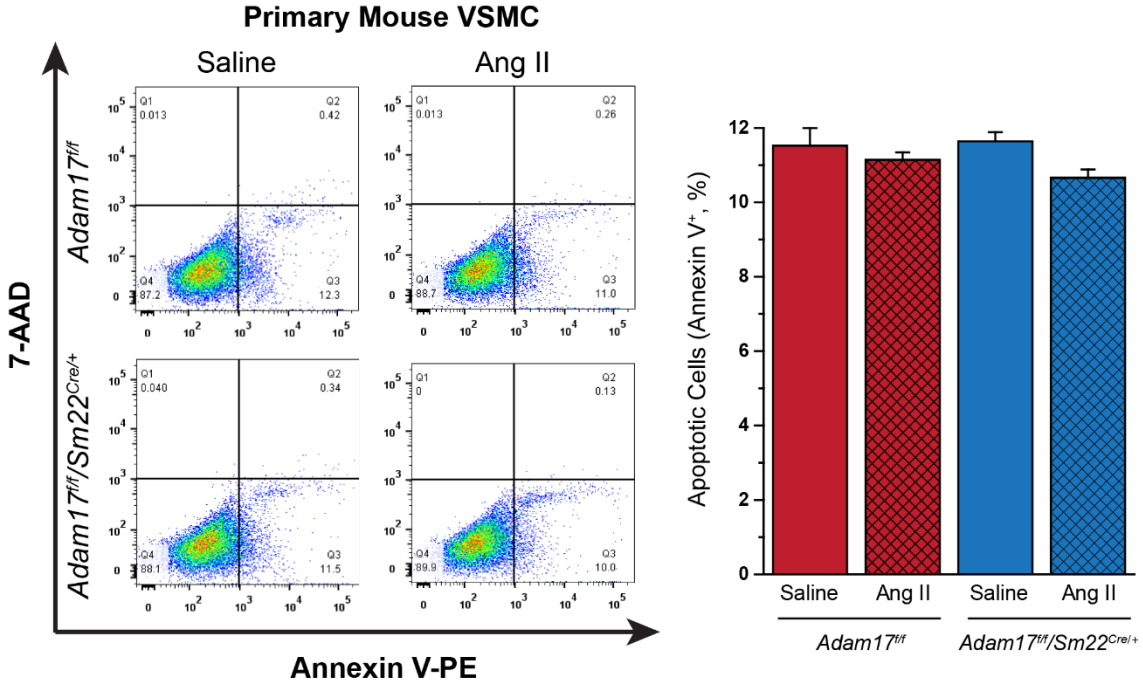

Figure 3.4 Neither Ang II treatment nor *ADAM17* deficiency affects apoptosis in mouse VSMCs. Confluent *Adam17*$^{f/f}$ and *Adam17*$^{f/f}$*/Sm22*$^{Cre/+}$ VSMCs were stained with Annexin V-PE and 7-AAD after treatment with saline or Ang II (1 µmol/l), and analyzed by flow cytometry. Early and late apoptotic cells were identified as Annexin $V\text{-}PE^+/7\text{-}AAD^-$ cells and Annexin $V\text{-}PE^+/7\text{-}AAD^+$cells, respectively. Cell apoptosis was quantified in indicated groups. Averaged values represent Mean ± SEM. Experiments were carried out in triplicates/group/condition and repeated with 3 independent isolations. ADAM17, a disintegrin and metalloproteinase 17; *Adam17*$^{f/f}$, *Adam17*$^{flox/flox}$; *Adam17*$^{f/f}$*/Sm22*$^{Cre/+}$, *Adam17*$^{flox/flox}$*/Sm22αCre*.

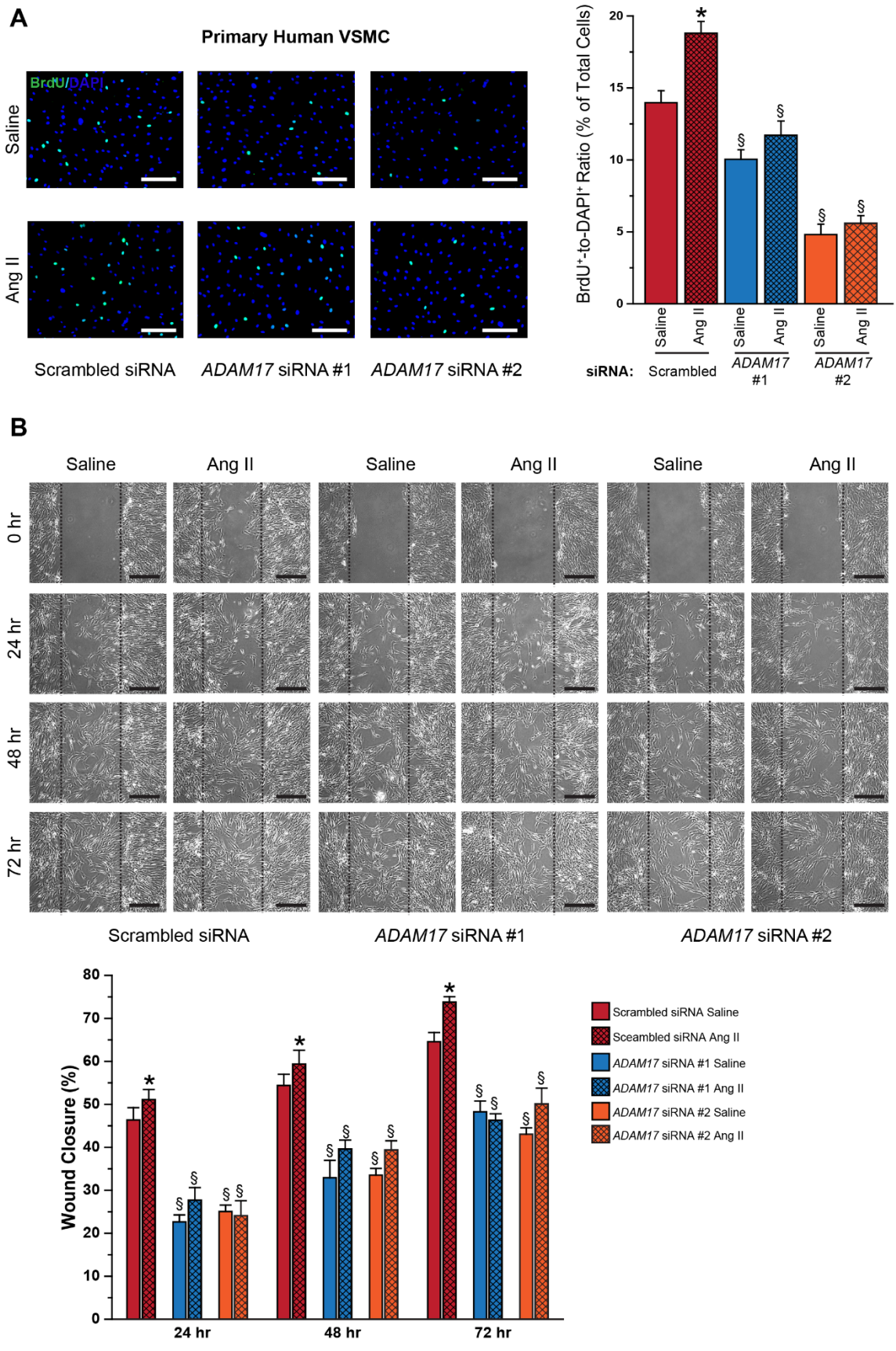
A
Primary Human VSMC
BrdU/DAPI
Saline
Ang II
Scrambled siRNA
ADAM17 siRNA #1
ADAM17 siRNA #2
BrdU+-to-DAPI+ Ratio (% of Total Cells)
siRNA:
Scrambled
ADAM17 #1
ADAM17 #2
B
0 hr
24 hr
48 hr
72 hr
Wound Closure (%)
24 hr
48 hr
72 hr
Scrambled siRNA Saline
Sceambled siRNA Ang II
ADAM17 siRNA #1 Saline
ADAM17 siRNA #1 Ang II
ADAM17 siRNA #2 Saline
ADAM17 siRNA #2 Ang II

Figure 3.5 *ADAM17*-deficiency in human VSMCs suppresses Ang II-induced cell proliferation and migration. (**A**) Representative immunofluorescence images showing BrdU incorporation (green) in human VSMCs transfected with scrambled or *ADAM17* siRNAs (#1 and #2, 10 nM for 48 hours) after 24 h of exposure to saline or Ang II (1 µmol/l), and averaged BrdU incorporation reflecting cell proliferation rate expressed as the percentage of $BrdU^+$ cells to total number of cells ($DAPI^+$ cells) for indicated groups (n = 60 random fields/group). Scale bars: 200 µm. (**B**) Representative microscopic images of scratch assay in confluent human VSMCs (± scrambled or ADAM17 siRNA transfection) treated with saline or Ang II (1 µmol/l). Cell migration into the scratch surface was monitored at the same spots at indicated time points, and the cell migration rate was quantified as scratch closure rate at indicated time points. Scale bars: 500 µm. *P<0.05 compared to corresponding saline group, $^{§}P$<0.05 compared to corresponding *Adam17*$^{f/f}$ group using 2-way ANOVA followed by Bonferroni's post-hoc test. Averaged values present mean ± SEM. BrdU, 5-bromo-2'-deoxyuridine; ADAM17, a disintegrin and metalloproteinase 17; *Adam17*$^{f/f}$, *Adam17*$^{flox/flox}$; *Adam17*$^{f/f}$/*Sm22*$^{Cre/+}$, *Adam17*$^{flox/flox}$/*Sm22αCre*.

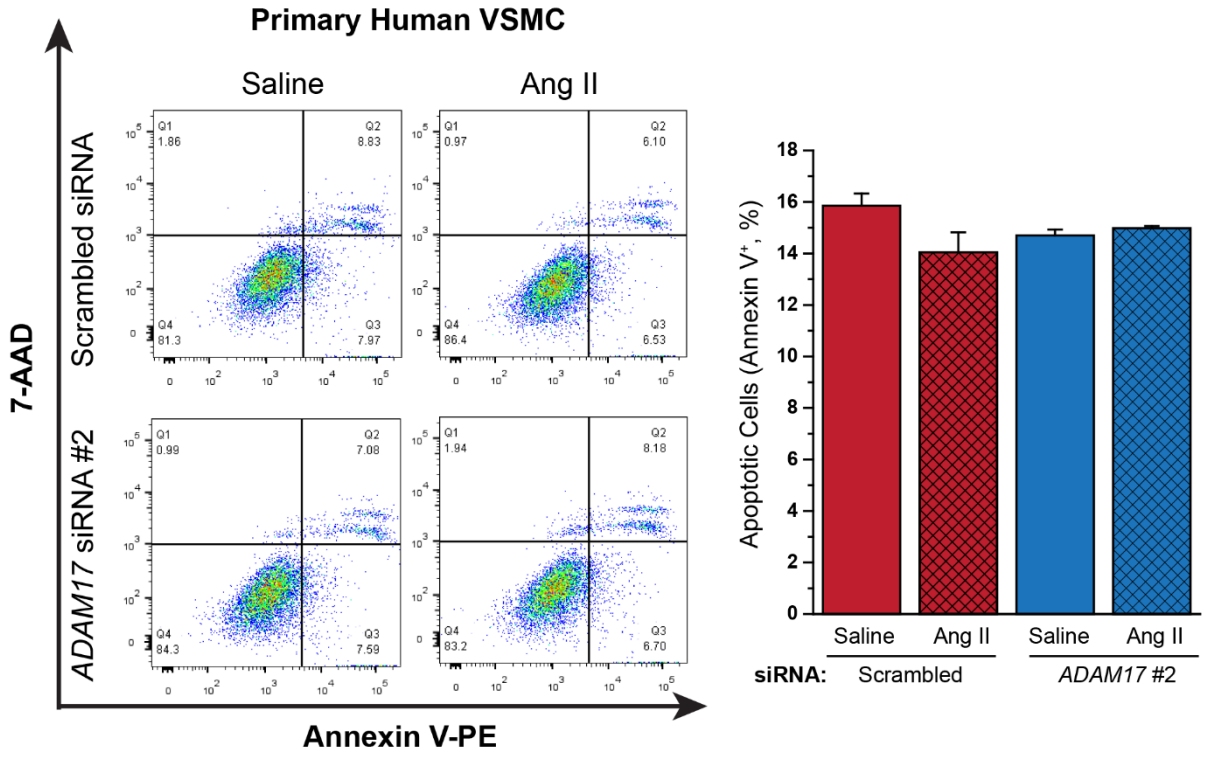

Figure 3.6 Neither Ang II treatment nor *ADAM17* deficiency affects apoptosis in human VSMCs. Confluent human VSMCs were transfected with scrambled or *ADAM17* siRNAs. After treatment with saline or Ang II (1 µmol/l), cells were stained with Annexin V-PE and 7-AAD analyzed by flow cytometry. Early and late apoptotic cells were identified as Annexin $V\text{-}PE^+/7\text{-}AAD^-$ cells and Annexin $V\text{-}PE^+/7\text{-}AAD^+$cells, respectively. Cell apoptosis was quantified in indicated groups. Averaged values represent Mean ± SEM. Experiments were carried out in triplicates/group/condition and repeated with 3 independent isolations. ADAM17, a disintegrin and metalloproteinase 17.

3.3.4. Loss of ADAM17 in VSMCs transiently lowers Ang II-induced hypertension

Based on our *in vitro* findings that *Adam17* knockdown suppresses VSMC proliferation and migration in response to Ang II, we hypothesized that Ang II-induced hypertension could be suppressed in *Adam17$^{f/f}$/Sm22$^{Cre/+}$* mice. Daily monitoring of blood pressure in conscious and freely-moving mice revealed that the Ang II-induced rise in systolic, diastolic and mean blood pressure was suppressed in *Adam17$^{f/f}$/Sm22$^{Cre/+}$* mice within the first week of Ang II infusion, particularly during the nighttime (**Figure 3.7, A and B**). However, after the first week, blood pressure in these mice gradually rose and converged with that in *Adam17$^{f/f}$* mice by the second week, and it plateaued for both groups for the remaining 2 weeks of Ang II infusion (**Figure 3.7, A and B**).

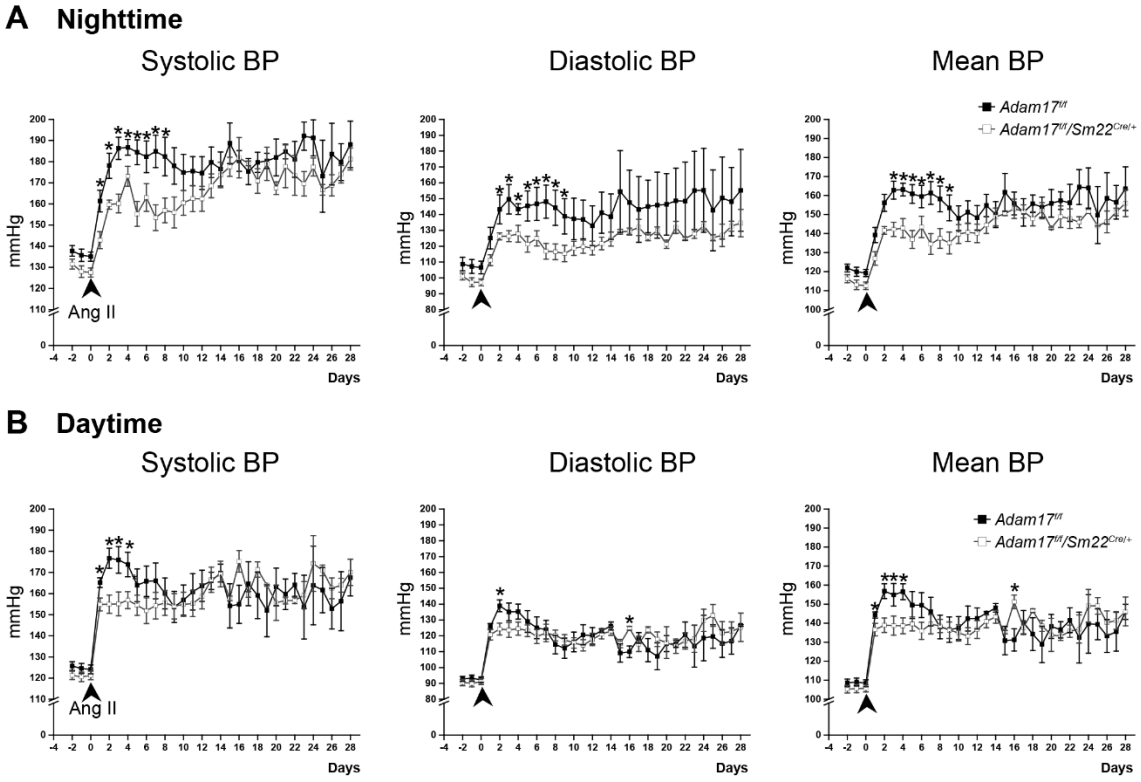

Figure 3.7 Loss of ADAM17 in VSMCs transiently lowers Ang II-induced hypertension. Averaged daily recordings of systolic, diastolic and mean blood pressure at baseline and over 4 weeks after Ang II infusion (1.5 mg/kg/d) in *Adam17$^{f/f}$* and *Adam17$^{f/f}$/Sm22$^{Cre/+}$* mice at (**A**) nighttime (10 pm-12 am) and (B) daytime (10 am-12 pm). **P*<0.05 *Adam17$^{f/f}$* versus *Adam17$^{f/f}$/Sm22$^{Cre/+}$* using unpaired Student's *t*-test. *n*= 12 mice/genotype. Averaged values represent mean ± SEM. Arrowhead denotes the day of Ang II pump implantation. ADAM17, a disintegrin and metalloproteinase 17; *Adam17$^{f/f}$*, *Adam17$^{flox/flox}$*; *Adam17$^{f/f}$/Sm22$^{Cre/+}$*, *Adam17$^{flox/flox}$/Sm22αCre*.

We assessed the mechanical property of mesenteric arteries, which are the main regulatory site for blood pressure, in both genotypes. *Ex vivo* pressure myography on mesenteric arteries from saline- or Ang II-infused mice (2 weeks) showed that the acute response to a vasoconstrictor (phenylephrine, PE) was increased similarly in Ang II-infused *Adam17*$^{f/f}$ and *Adam17*$^{f/f}$*/Sm22*$^{Cre/+}$ mice compared to parallel saline-infused mice (**Figure 3.8A**). Methacholine (MCh)-mediated vasodilation, however, was not altered with Ang II infusion and was similar among all groups (**Figure 3.8B**).

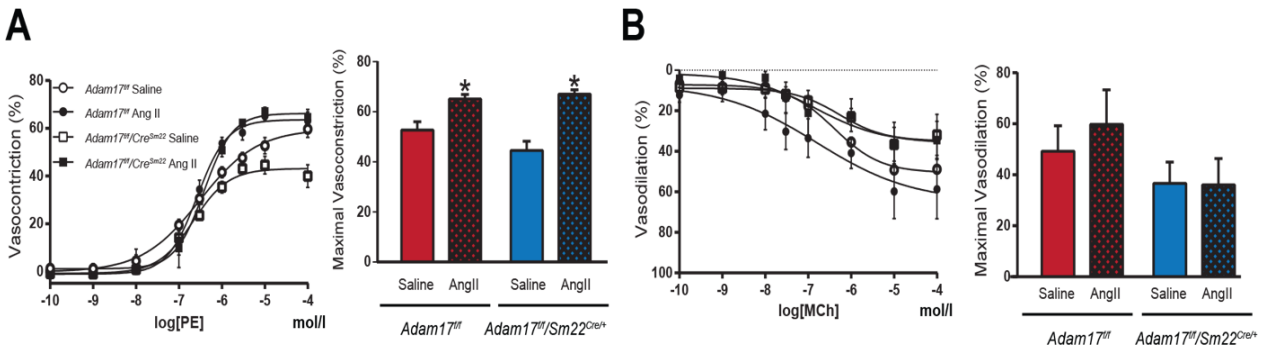

Figure 3.8 Chronic Ang II infusion shows similar acute vasoconstriction and vasodilation responses in the mesenteric arteries of SMC *ADAM17*-intact or -deficient mice. (**A**) Percent vasoconstriction (as compared to the initial vessel diameter) in response to increasing concentrations of phenylephrine (PE), and maximal vasoconstriction induced by PE (at 10^{-5} mol/l) in indicated groups. (**B**) Vasodilation responses to increasing doses of methacholine (MCh), and maximal vasodilation (at 10^{-5} mol/l of MCh) in indicated groups. **P*<0.05 compared to the corresponding control (saline) group using 2-way ANOVA followed by Bonferroni's *post-hoc* test. *n*=6 mice/group/genotype. Averaged values represent Mean ± SEM. ADAM17, a disintegrin and metalloproteinase 17; *Adam17*$^{f/f}$, *Adam17*$^{flox/flox}$; *Adam17*$^{f/f}$*/Sm22*$^{Cre/+}$, *Adam17*$^{flox/flox}$*/Sm22αCre.*

Next, we assessed passive changes in arterial diameter as a function of increasing pressure (0 mmHg to 140 mmHg) in Ca^{2+}-free solution. Mesenteric arteries from Ang II-infused mice of either genotype showed significantly decreased distensibility compared to parallel saline-infused mice, however, this response was not altered by *Adam17* loss in SMCs (**Figure 3.9A**). Ang II-induced arterial stiffness was also comparable between genotypes as reflected by a similar rate constant for the stress-strain relationship (k=12.3 ± 3.0 in *Adam17*$^{f/f}$-Ang II *vs.*13.2 ± 1.8 in *Adam17*$^{f/f}$*/Sm22*$^{Cre/+}$-Ang II) (**Figure 3.9B**). However, 2 weeks of Ang II infusion increased the mesenteric wall thickness in *Adam17*$^{f/f}$ which was not observed in *Adam17*$^{f/f}$*/Sm22*$^{Cre/+}$ mesenteric arteries (**Figure 3.9C**).

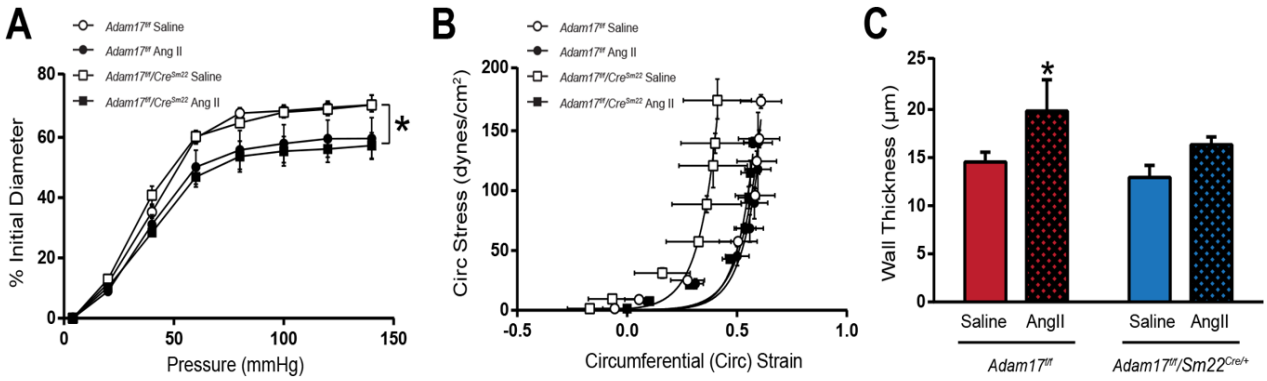

Figure 3.9 Loss of ADAM17 in VSMCs does not affect wall tension but blunts wall thickness of mesenteric arteries after 2 weeks of Ang II infusion. (**A**) *Ex vivo* passive pressure myography, (**B**) and calculated circumferential wall stress-strain relationships) in second-order mesenteric arteries in *Adam17*$^{f/f}$ (square) and *Adam17*$^{f/f}$*/Sm22*$^{Cre/+}$ mice (circle) after 2 weeks of saline (open symbol) or Ang II infusion (solid symbol). (**C**) Averaged wall thickness in mesenteric arteries from both genotypes after 2 weeks of saline or Ang II infusion. **P*<0.05 compared to corresponding control (saline) group using 2-way ANOVA followed by Bonferroni's *post-hoc* test. *n* = 6 mice/group/genotype. Averaged values represent Mean ± SEM. ADAM17, a disintegrin and metalloproteinase 17; *Adam17*$^{f/f}$, *Adam17*$^{flox/flox}$; *Adam17*$^{f/f}$*/Sm22*$^{Cre/+}$, *Adam17*$^{flox/flox}$*/Sm22αCre*.

3.3.5. Ang II-mediated activation of EGFR is suppressed in SMC-ADAM17 deficient mice.

To determine if ADAM17 deficiency affected the same signaling pathways in the mice as it did *in vitro*, we assessed HB-EGF and EGFR activity in the arteries from mice of either genotype after saline infusion, or after 2 or 4 weeks of Ang II -infusion. In protein extracts from the whole aorta (including the adventitia), HB-EGF (**Figure 3.10A**) or EGFR activation (phospho-to-total ratio) were not suppressed in *Adam17*$^{f/f}$*/Sm22*$^{Cre/+}$ following Ang II infusion (**Figure 3.10B**). However, when only the aortic tunica media (that is rich in SMCs) was assessed, a marked reduction in HB-EGF and EGFR activation (phospho-to-total ratio) were detected in *Adam17*$^{f/f}$*/Sm22*$^{Cre/+}$ mice after 2 weeks and 4 weeks of Ang II infusion (**Figure 3.10, A and B**).

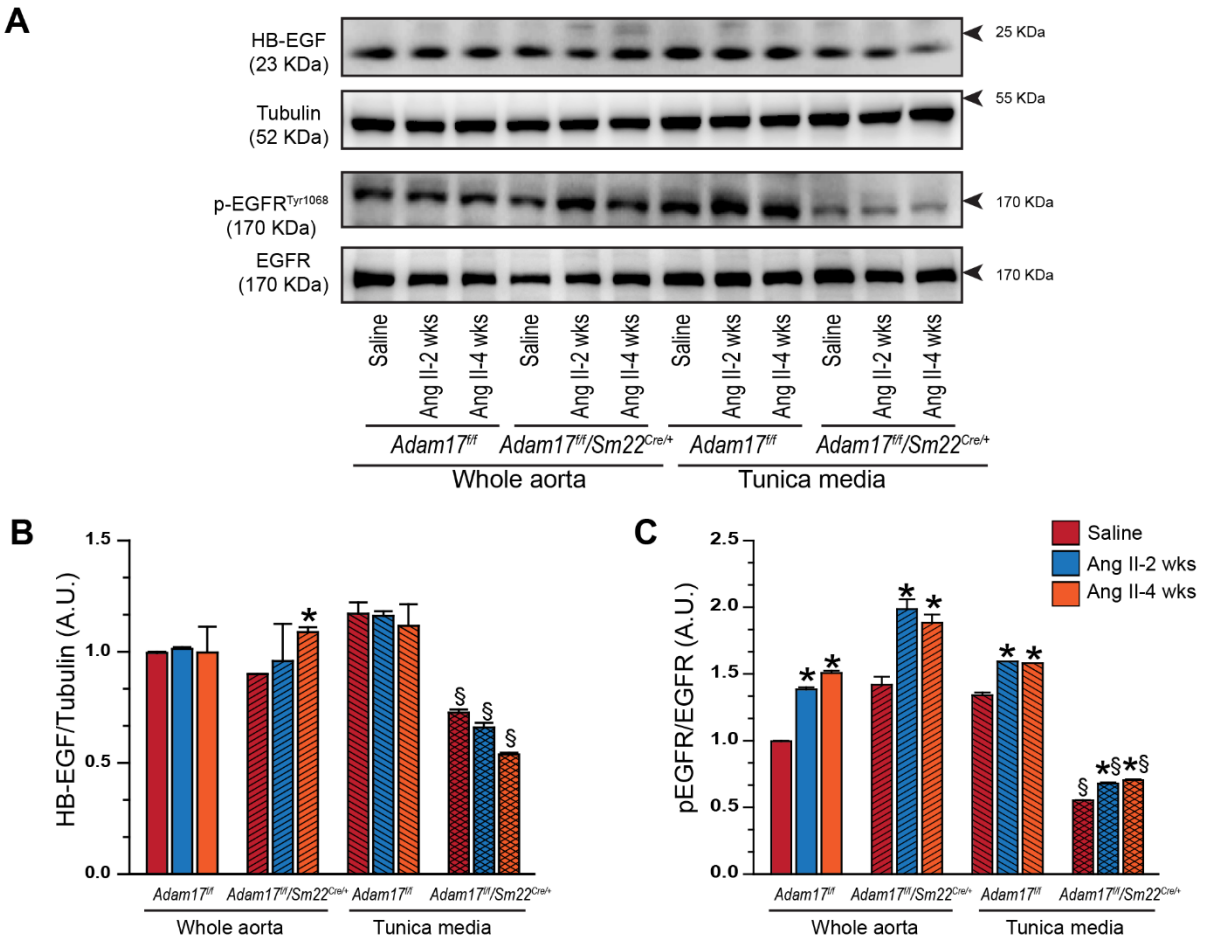

Figure 3.10 Ang II-mediated EGFR activation is suppressed in aortic tunica media due to the loss of ADAM17 in SMCs. Representative immunoblots (**A**) and densitometric quantification of averaged proteins levels for HB-EGF (**B**) and EGFR (phosphor-to-total) (**C**) protein extracts from the whole aorta or aortic tunica media in indicated groups after saline or Ang II infusion (2 or 4 weeks). **P*<0.05 compared to the corresponding saline group, §*P*<0.05 compared to corresponding *Adam17*$^{f/f}$ group using 2-way ANOVA followed by Bonferroni's *post-hoc* test. *n* = 4 aortas/group/genotype. Averaged values present mean ± SEM. EGFR, epidermal growth factor receptor; HB-EGF, heparin-binding EGF-like growth factor; ADAM17, a disintegrin and metalloproteinase 17; *Adam17*$^{f/f}$, *Adam17*$^{flox/flox}$; *Adam17*$^{f/f}$*/Sm22*$^{Cre/+}$, *Adam17*$^{flox/flox}$*/Sm22αCre*.

Measurement of mRNA expression of vascular ADAMs in mesenteric arteries showed that at baseline, *Adam10* levels were higher in *Adam17*$^{f/f}$*/Sm22*$^{Cre/+}$ mice while other ADAMs were comparable between genotypes (**Figure 3.11**). Following Ang II infusion, *Adam10* and *Adam15* levels increased similarity in both genotypes, whereas the rise in *Adam12* and *Adam19* was significantly greater in *Adam17*$^{f/f}$*/Sm22*$^{Cre/+}$ mice (**Figure 3.11**).

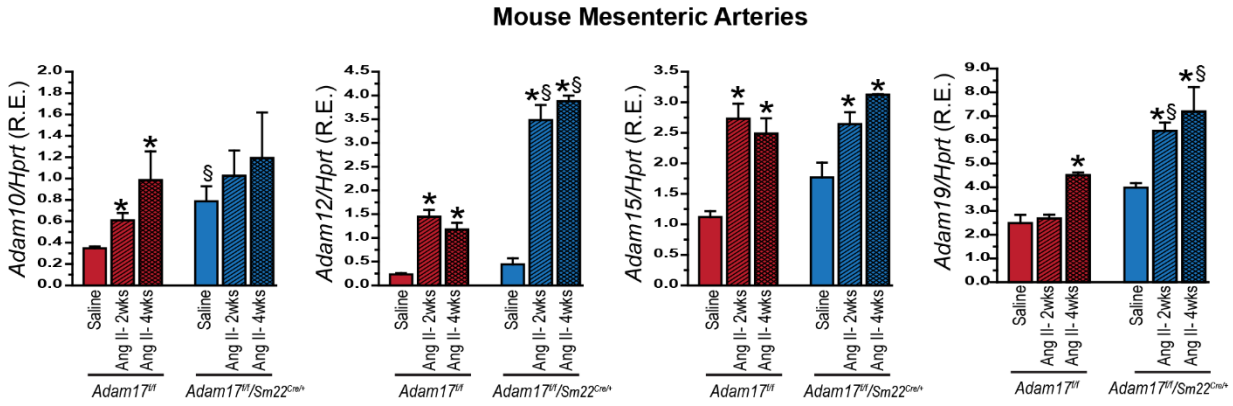

Figure 3.11 Other vascular ADAMs show different expression patterns in the mesenteric arteries of SMC *Adam17*-deficient mice compared to SMC *Adam17*-intact mice. Averaged mRNA expression levels of *Adams* 10, 12, 15, and 19. **P*<0.05 compared to the corresponding saline group, §*P*<0.05 compared to corresponding *Adam17*$^{f/f}$ group using 2-way ANOVA followed by Bonferroni's *post-hoc* test. *n* =10 mice/group/genotype. Averaged values present mean ± SEM. ADAM17, a disintegrin and metalloproteinase 17; *Adam17*$^{f/f}$, *Adam17*$^{flox/flox}$; *Adam17*$^{f/f}$*/Sm22*$^{Cre/+}$, *Adam17*$^{flox/flox}$*/Sm22αCre*.

3.3.6. Ang II infusion resulted in a biphasic end-organ damage in mice lacking SMC-ADAM17

Sustained high levels of circulating Ang II can result in a variety of pathological effects including progressive end-organ damage such as cardiac and renal hypertrophy and fibrosis. Since Ang II-induced hypertension was transiently suppressed in *Adam17*$^{f/f}$*/Sm22*$^{Cre/+}$ mice, we investigated the early and late impact of Ang II infusion on the heart and the kidneys in each genotype. Two weeks of Ang II infusion resulted in a less severe cardiac hypertrophy (heart weight-to-tibial length ratio, **Figure 3.12, A and C**) and fibrosis (fibrillar collagen content in PSR-stained sections, **Figure 3.12, B and D**), and less renal fibrosis (**Figure 3.12, F and H**) in *Adam17*$^{f/f}$*/Sm22*$^{Cre/+}$ mice. However, after 4 weeks of Ang II infusion, cardiac and renal hypertrophy and fibrosis in *Adam17*$^{f/f}$*/Sm22*$^{Cre/+}$ increased to similar levels as in *Adam17*$^{f/f}$ mice (**Figure 3.13**).

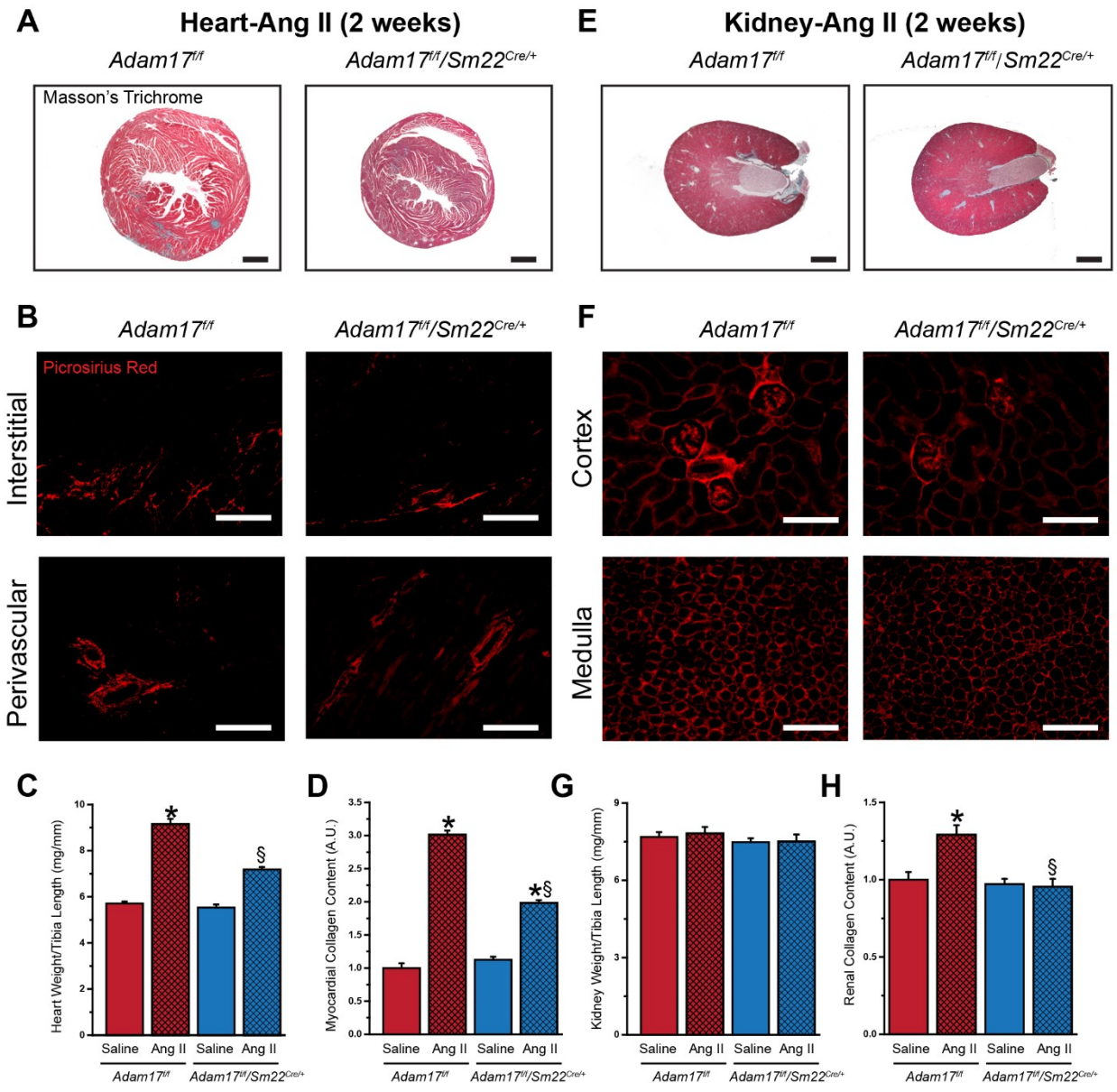

Figure 3.12 Loss of ADAM17 in SMCs reduces Ang II-induced end-organ damage at 2 weeks. Representative Masson's trichrome stained transverse cross-sections of heart (**A**) and kidney (**E**) from *Adam17$^{f/f}$* and *Adam17$^{f/f}$/Sm22$^{Cre/+}$* mice after 2 weeks of Ang II (1.5 mg/kg/d) infusion. Scale bar: 1 mm. Representative PSR-stained images showing Ang II-induced fibrosis in the heart (**B**) and kidneys (**F**) in mice of indicated genotype. Scale bar: 200 µm for heart sections and 100 µm for kidney sections. Averaged heart weight-to-tibial length ratio (**C**) and quantification of cardiac fibrosis (**D**) and averaged kidney weight-to-tibial length ratio (**G**) and quantification of renal fibrosis (**H**) in *Adam17$^{f/f}$* and *Adam17$^{f/f}$/Sm22$^{Cre/+}$* mice after 2 weeks of saline or Ang II infusion. **P*<0.05 compared to the corresponding saline group, §*P*<0.05 compared to corresponding *Adam17$^{f/f}$* group using 2-way ANOVA followed by Bonferroni's *post-hoc* test. *n* =10 mice/group/genotype. Averaged values present mean ± SEM. ADAM17, a disintegrin and metalloproteinase 17; *Adam17$^{f/f}$*, *Adam17$^{flox/flox}$*; *Adam17$^{f/f}$/Sm22$^{Cre/+}$*, *Adam17$^{flox/flox}$/Sm22αCre*.

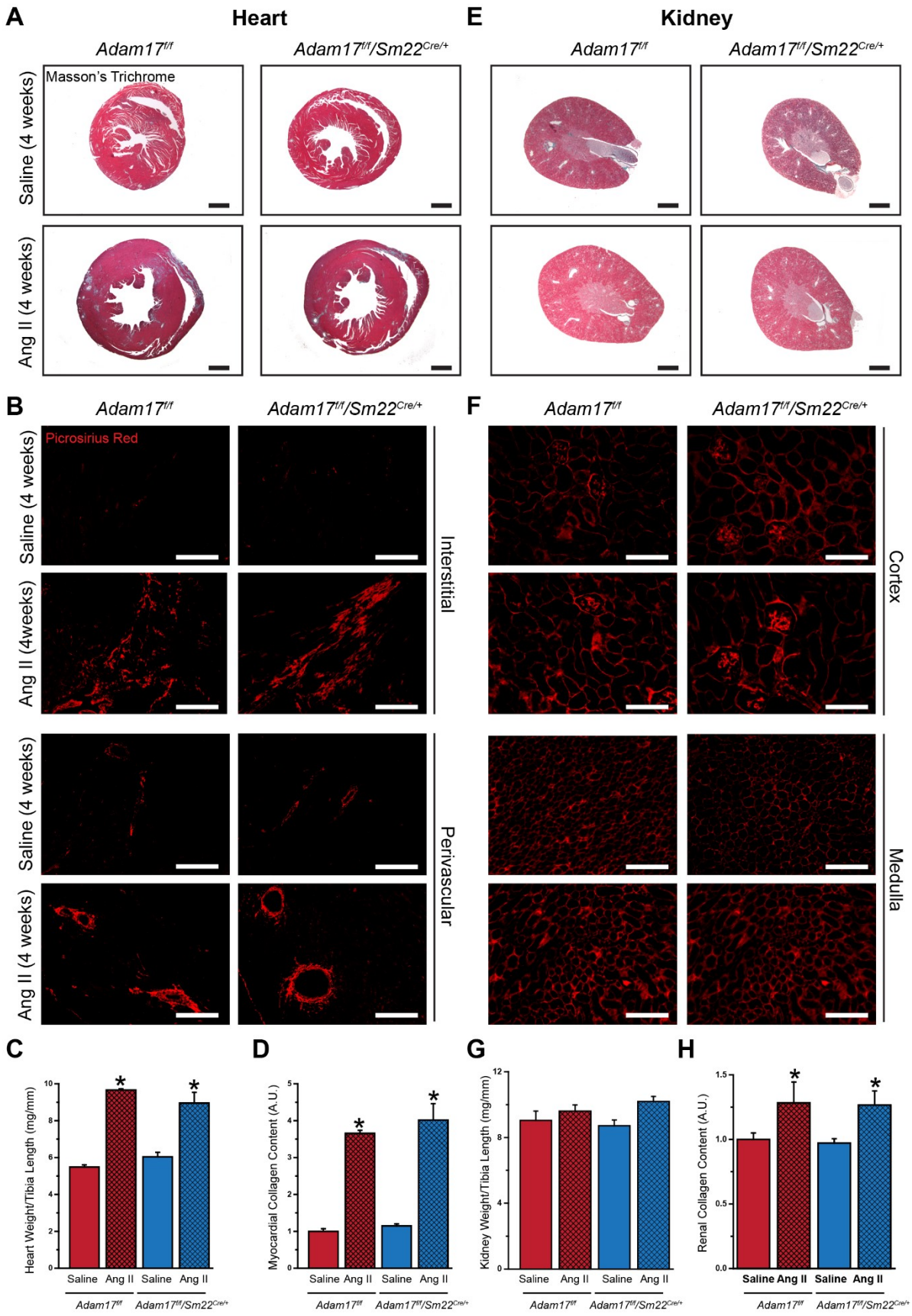
A
Heart
E
Kidney
Adam17f/f
Adam17f/f/Sm22Cre/+
Masson's Trichrome
Saline (4 weeks)
Ang II (4 weeks)
B
F
Picrosirius Red
Saline (4 weeks)
Ang II (4weeks)
Interstitial
Cortex
Perivascular
Medulla
C
D
G
H
Heart Weight/Tibia Length (mg/mm)
Myocardial Collagen Content (A.U.)
Kidney Weight/Tibia Length (mg/mm)
Renal Collagen Content (A.U.)
Saline
Ang II
Saline
Ang II
Adam17f/f
Adam17f/f/Sm22Cre/+

Figure 3.13 Prolonged Ang II infusion results in similar end-organ damage in mice lacking SMC-ADAM17. Representative Masson's trichrome stained transverse cross-sections of the heart (**A**) and the kidney (**E**) from *Adam17*$^{f/f}$ and *Adam17*$^{f/f}$/*Sm22*$^{Cre/+}$ mice after 4 weeks of Ang II (1.5 mg/kg/d) infusion. Scale bar: 1 mm. Representative PSR stained sections showing interstitial and perivascular fibrosis in the heart (**B**) and fibrosis in the kidney (cortex and medulla) (**F**) in either genotype after 4 weeks of saline or Ang II infusion. Scale bar: 200 μm for heart sections and 100 μm for kidney sections. Averaged heart weight-to-tibial length ratio (**C**) and quantification of cardiac fibrosis (**D**); and averaged single kidney weight-to-tibial length ratio (**G**) and quantification of renal fibrosis (H) in each genotype after infusion of saline or Ang II for 4 weeks. **P*<0.05 compared to corresponding saline group, §*P*<0.05 compared to corresponding *Adam17*$^{f/f}$ group using 2-way ANOVA followed by Bonferroni's *post-hoc* test. *n* =10 mice/group/genotype. Averaged values present mean ± SEM. ADAM17, a disintegrin and metalloproteinase 17; *Adam17*$^{f/f}$, *Adam17*$^{flox/flox}$; *Adam17*$^{f/f}$/*Sm22*$^{Cre/+}$, *Adam17*$^{flox/flox}$/*Sm22αCre*.

3.3.7. Loss of ADAM17 in endothelial cells persistently lowers Ang II-induced hypertension

Since we failed to detect long-term blood pressure lowering effects in SMC *Adam17*-deficiency mice during 4 weeks of Ang II infusion (**Figure 3.14**), we conducted a pilot study to explore the effects of endothelial cell (EC) *Adam17*-deficiency on Ang II-dependent blood pressure changes. Although only a small number of EC *Adam17*-deficient mice (*Adam17*$^{f/f}$/*Tie2*$^{Cre/+}$) and their control littermates (*Adam17*$^{f/f}$) were subjected to telemetric blood pressure recording for 4 weeks after Ang II infusion, we observed very promising blood pressure lowering effects due to the loss of ADAM17 in endothelial cells. Intriguingly, Ang II-induced rise in diastolic and mean blood pressure was significantly suppressed in *Adam17*$^{f/f}$/*Tie2*$^{Cre/+}$ mice starting at day 10 post-Ang II infusion until the end of recording during both nighttime (**Figure 3.14A**) and daytime (**Figure 3.14B**). Systolic blood pressure, however, was only found significantly lower in *Adam17*$^{f/f}$/*Tie2*$^{Cre/+}$ mice as compared to *Adam17*$^{f/f}$ mice during daytime (**Figure 3.14B**). The underlying mechanisms by which EC *Adam17*-deficiency suppresses Ang II-induced blood pressure increase require further studies. However, it is plausible that ADAM17 in ECs may be a key player in regulating nitric oxide signaling and oxidative stress in response to Ang II stimulation.

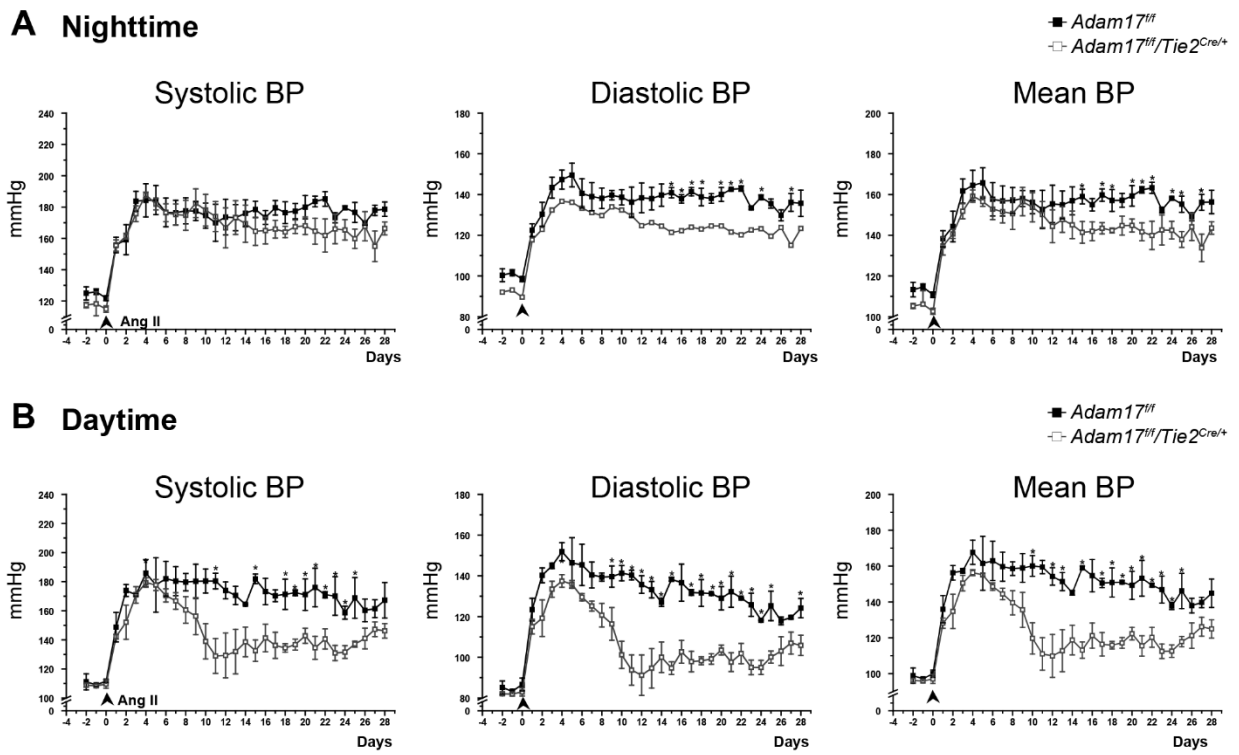

Figure 3.14 Loss of ADAM17 in ECs persistently lowers Ang II-induced hypertension. Averaged daily recordings of systolic, diastolic and mean blood pressure at baseline and over 4 weeks after Ang II infusion (1.5 mg/kg/d) in *Adam17*$^{f/f}$ and *Adam17*$^{f/f}$*/Tie2*$^{Cre/+}$ mice at (A) nighttime (10 pm-12 am) and (B) daytime (10 am-12 pm). **P*<0.05 *Adam17*$^{f/f}$ versus *Adam17*$^{f/f}$*/Tie2*$^{Cre/+}$ using unpaired Student's *t*-test. *n*= 3/genotype. Averaged values represent mean ± SEM. Arrowhead denotes the day of Ang II osmotic pump implantation. ADAM17, a disintegrin and metalloproteinase 17; *Adam17*$^{f/f}$, *Adam17*$^{flox/flox}$; *Adam17*$^{f/f}$*/Tie2*$^{Cre/+}$, *Adam17*$^{flox/flox}$*/Tie2MerCreMer*.

3.4. Discussion

Ang II is the major renin-angiotensin-aldosterone system effector, and is a critical player in hypertension and related end-organ-damage. In this study, we investigated the role of SMC ADAM17 in Ang II-mediated effects. We found that *Adam17*-deficiency reduced proliferation and migration of mouse and human VSMCs, which was accompanied by reduced HB-EGF processing, EGFR transactivation and *At1* expression. *In vivo*, *Adam17* downregulation transiently blunted the Ang II-induced hypertension and associated end-organ damage; however, the protective effects of *Adam17* downregulation was abolished with prolonged Ang II infusion. Consistently, *ex vivo* pressure myography revealed unaltered compliance and acute vasoconstrictive responses in *Adam17*$^{f/f}$*/Sm22*$^{Cre/+}$ compared to *Adam17*$^{f/f}$ mice.

It was recently reported that *Adam17*-deficiency in SMCs prevented myocardial hypertrophy and fibrosis by Ang II infusion (311). However, this study only examined the short-term effects of Ang II at 2 weeks of infusion (311). Here we report that the protective effect of SMC *Adam17*-deficiency is indeed a transient effect and is abolished with prolonged Ang II-infusion. In addition, the observed early reduction in cardiac and renal hypertrophy and fibrosis could be directly linked to the transient suppression of Ang II-induced hypertension in SMC *Adam17*-deficient mice.

Crosstalk between the AT1 receptor and EGFR has been implicated in regulating a variety of signaling pathways which are involved in the development and cardiovascular diseases (232). As such, the reduced *At1* levels in *Adam17*-deficient VSMCs could be responsible for the suppressed Ang II-mediated HB-EGF processing and EGFR activation in these cells. It is well recognized that proteolytic cleavage of precursor HB-EGF is required for EGFR transactivation through G-protein-coupled receptors (524). ADAM17 has been reported to be a dominant protease in proteolytic processing of HB-EGF in response to Ang II, through the AT1 receptor, leading to subsequent EGFR transactivation (317, 525, 526). *In vitro* studies have also reported that ADAM17 mediates Ang II-induced SMC hypertrophy (increased cell size) (317). Here we report that ADAM17 is required for Ang II-induced SMC proliferation and migration, concomitant with activation of Erk1/2, consistent with earlier reports that Erk signaling pathway is required for VSMC mitogenesis following Ang II-mediated EGFR transactivation (523). The reduced proliferation and migration in *Adam17*-deficient SMCs could underlie the reduced mesenteric wall thickness in Ang II-infused $Adam17^{f/f}/Sm22^{Cre/+}$ mice. We further demonstrate that *Adam17*-deficiency impacts proliferation and migration of mouse and human VSMCs similarly, thereby providing parallels in the function of ADAM17 in mouse and human smooth muscle cells.

The transient effects of SMC *Adam17*-deficiency on Ang II-induced hypertension could be due to a number of factors. For instance, other members in the ADAM family could compensate for the loss of ADAM17, as ADAM12 has been reported to cleave HB-EGF in cardiomyocytes (175), and ADAM19 cleaved HB-EGF in *Adam17*-knockdown fibroblasts (268). We found that Ang II triggered a greater increase in *Adam12* and *Adam19* in mesenteric arteries from $Adam17^{f/f}/Sm22^{Cre/+}$ mice. However, since EGFR activation remained suppressed throughout the 4 weeks of Ang II infusion in $Adam17^{f/f}/Sm22^{Cre/+}$ mice, this suggests that HB-EGF bio-availability was not increased through elevated ADAM12 or ADAM19 and therefore, the greater rise in

Adam12 or *Adam19* cannot explain the rebound in blood pressure in *Adam17*$^{f/f}$/*Sm22*$^{Cre/+}$ mice. It is plausible that Ang II-mediated activation of the neurohumoral pathways and/or oxidative stress-mediated endothelial and renal dysfunction could provide compensatory mechanisms to negate the initial suppression of Ang II-induced hypertension in the VSMC *Adam17*-deficient mice.

3.5. Conclusion

In summary, our findings demonstrate that SMC-specific deletion of *Adam17* can transiently suppress Ang II-induced hypertension and the resulting cardiac and renal hypertrophy and fibrosis. The transient nature of this protective effect suggests the involvement of a compensatory mechanism, and that SMC ADAM17 inhibition would not be sufficient for long-term protection against Ang II-induced hypertension and end-organ damage. In contrast, our preliminary data demonstrate that EC ADAM17 deletion exerts a sustained blood pressure lowering effects after Ang II infusion. It would be intriguing to investigate the role of EC *Adam17*-deficiency in Ang II-induced hypertension and end-organ damage in the future. Moreover, the differential protection effects of Ang II-induced hypertension due to the loss of ADAM17 in ECs versus SMCs also suggest cell type-specific functions of ADAM17 in the cardiovascular system.

CHAPTER 4

ROLE OF CELL-SPECIFIC FUNCTIONS OF ADAM17 IN THE PROGRESSION OF THORACIC AORTIC ANEURYSM

CELL-SPECIFIC FUNCTIONS OF ADAM17 REGULATE THE PROGRESSION OF THORACIC AORTIC ANEURYSM

Mengcheng Shen[1,3] MSc, Mei Hu[1,3] MSc, Paul W.M. Fedak[4] MD/PhD, Gavin Y. Oudit[2,3] MD/PhD, Zamaneh Kassiri[1,2] PhD

[1]Department of Physiology, [2]Department of Medicine, [3]Faculty of Medicine and Dentistry, Cardiovascular Research Centre, Mazankowski Alberta Heart Institute, University of Alberta, Edmonton, Alberta, Canada, [4] Section of Cardiac Surgery, Department of Cardiac Sciences, University of Calgary, Libin Cardiovascular Institute of Alberta, Calgary, Alberta

Contributions:

MS: Conceived and designed experiments, performed all experiments on human specimens, established the murine TAA model and primary mouse and human aortic smooth muscle cell culture techniques, performed all the cell culture work and related *in vitro* experiments, collected and analyzed the data, prepared figures, interpreted the results, and wrote the manuscript.

MH: Contributed to immunoblotting experiments.

PWMF: Provided human TAA specimens, contributed to data interpretation, and edited the manuscript.

GYO: Provided human non-diseased aortas, contributed to data interpretation, and edited the manuscript.

ZK: Corresponding author. Conceived hypothesis, interpreted the results, and wrote the manuscript.

A version of this chapter has been published. ***Shen M, Hu M, Fedak PWM, Oudit GY, and Kassiri Z. Cell-specific functions of ADAM17 regulate the progression of thoracic aortic aneurysm. Circulation Research. 2018. (doi: 10.1161/CIRCRESAHA.118.313181)*** *This chapter has been modified from this article.*

4.1. Introduction

Aortic aneurysm is the second most frequent disease affecting the aorta and globally accounts for an annual mortality rate of 2.6 cases per 100, 000 people (527). Aortic growth is often progressive and aortic aneurysm has no direct pharmacological therapy. Prophylactic surgical resection is used to prevent long-term complications such as rupture or dissection and is performed when the risk of important aortic events outweighs the risk of surgery. Surgical therapy is entertained when the aorta reaches a specific size threshold. Preventing further aortic growth with non-invasive medical therapy could decrease the burden of surgery and prevent acute aortic complications. The incidence of TAA has been reported to be increasing in the past decades (528, 529). TAA can occur at any age, in males or females, and in the absence of significant cardiovascular risk factors. The poor prognosis for TAA patients (64% 5-year survival post-surgical repair) (346, 530) further highlights the need for understanding the mechanisms responsible for pathogenesis and progression of TAA.

A disintegrin and metalloproteinase-17 (ADAM17) is a type I transmembrane sheddase that can proteolytically release more than 80 membrane-tethered molecules so far identified, including cytokines, chemokines, adhesion molecules, growth factors and/or their receptors (4, 531). While it has been implicated in a variety of pathologies and vascular diseases (328-330), no information is yet available on the function of ADAM17 in the pathogenesis of TAA. In this study, we found increased ADAM17 activity in aneurysmal human thoracic aorta, and we investigated the function of ADAM17 in endothelial cells (tunica intima) versus the vascular smooth muscle cells (tunica media) in TAA. Using an optimized periadventitial elastase-injury induced experimental *in vivo* model of TAA (381, 393). This model resembles the characteristics of the early onset (e.g., adventitial elastolysis) and the advanced form of aortic aneurysm in human patients (532). We found that ADAM17 deletion in SMCs prevents the contractile-to-synthetic phenotype switching in these cells, and therefore prevents the excess perivascular fibrosis, cell death, and inflammation. ADAM17 deficiency in ECs, on the other hand, preserves the adherens junction (VE-cadherin) and tight junctions (junctional adhesion molecule-A/JAM-A and claudin), suppressing inflammation and subsequent tissue damage, thereby hindering TAA-mediated dilation of the thoracic aorta. *In vitro* studies confirmed these functions of ADAM17 in primary human aortic SMCs and ECs. Moreover, pharmacological inhibition of ADAM17, before or after the onset of TAA, significantly

reduced ADAM17 activity and proved to be effective in markedly limiting the aortic dilation. These novel findings provide therapeutic targets for emerging pharmacological therapies to effectively limit the progression of aortic dilation in patients with TAA.

4.2. Materials and methods

The detailed Materials and methods information is available in **Chapter 2 Materials and Methods**.

4.2.1. Experimental Animals

Mice lacking *Adam17* in SMCs (*Adam17$^{flox/flox}$/Sm22αCre*, *Adam17$^{f/f}$/Sm22$^{Cre/+}$*) were generated by cross-breeding mice carrying floxed *Adam17* alleles (*Adam17$^{tm1.2Bbl}$/J, Adam17$^{f/f}$*) with mice expressing Cre-recombinase under the control of the smooth muscle cell promoter (*Sm22α-Tg(Tagln-cre)1Her/J*, *Sm22$^{Cre/+}$*). Mice lacking *Adam17* in ECs (*Adam17$^{flox/flox}$/Tie2-MerCreMer, Adam17$^{f/f}$/Tie2$^{Cre/+}$*) were generated by cross-breeding *Adam17$^{f/f}$* mice with *Tie2-CreER^{T2}*-expressing (*Tie2-MerCreMer*) mice with a tamoxifen-inducible *CreER^{T2}*-recombinase (503). Activation of the inducible *CreER^{T2}*-recombinase in *Adam17$^{f/f}$/Tie2$^{Cre/+}$* mice was achieved by tamoxifen treatment. Littermate *Adam17$^{f/f}$* mice were used as controls for both cell-specific ADAM17 deficient mice, but only those used as controls for *Adam17$^{f/f}$/Tie2$^{Cre/+}$* mice were treated with tamoxifen. Both genders were used in this study. All animal procedures were performed according to the ARRIVE (Animal Research: Reporting of *in vivo* Experiments) guidelines, and according to the guidelines of Animal Care and Use Committee (ACUC) at the University of Alberta and the Canadian Council of Animal Care (CCAC).

4.2.2. Human control (non-diseased) and aneurysmal thoracic aorta specimens

Human aneurysmal specimens were procured from the proximal ascending aorta of patients (*n*=5 for each sex) undergoing prophylactic resection as a consequence of bicuspid aortic valve (BAV) associated aortopathy. Control samples (*n*=5 for each sex) were non-aneurysmal healthy ascending aortas obtained from donors through the HOPE (Human Organ Procurement and Exchange) Program at the University of Alberta. The study protocols were approved by the Human Research Ethics Review Process (HERO) at the University of Alberta. Aortic samples were either

flash-frozen in liquid nitrogen and stored at -80°C for molecular studies or fixed in 10 % formalin for histological analyses.

4.2.3. Induction of experimental thoracic aortic aneurysm (TAA) by periadventitial treatment of porcine pancreatic elastase

TAA was induced in mice of each genotype by treating the descending thoracic aorta with porcine pancreatic elastase Type I (30 U/ml) for 5 minutes using a modified protocol (381). Sham mice underwent the same procedure, except elastase exposure to the descending thoracic aortas. All the mice were then maintained in animal facility for 3 days (small aortic aneurysm) or 14 days (advanced aortic aneurysm) post TAA surgery.

4.2.4. Administration of an ADAM17-selective inhibitor

An ADAM17-selective inhibitor (PF-5480090/PF-548, *Pfizer*) was suspended in 2% Tween 80/0.5% methylcellulose. Male wildtype mice received PF-548 or vehicle by oral gavage for indicated time of periods as illustrated in **Chapter 2.9**.

4.2.5. Aorta dissection and imaging

At indicated time points, mice of each genotype were anesthetized, perfuse-fixed, and excised to remove surrounding adipose tissue. Cleaned aortas were fixed on a black silicon plate for imaging to assess the gross morphology of TAA phenotype.

4.2.6. Morphometric and immunofluorescent analyses of human and mouse aneurysmal aortas

Formalin-fixed, elastase treated mouse aortic segments were excised and embedded into OCT media for cross-sections. Cryosections of each genotype, each gender and each time point were stained for elastic fiber (VVG), fibrillar collagen contents (PSR), smooth muscle cell density (calponin), cell apoptosis (TUNEL), inflammatory cells (i.e., macrophages/CD68 and neutrophils/Ly6G) by classical histological staining protocol or immunohistofluorescence. Human healthy and aneurysmal aortas were paraffin-embedded, and sections were used for ADAM17 staining after antigen retrieval.

4.2.7. Smooth muscle cell isolation and culture

Primary mouse thoracic aortic smooth muscle cells (mSMCs) were isolated from 3-week-old male *Adam17*$^{f/f}$ and *Adam17*$^{f/f}$/*Sm22*$^{Cre/+}$ mice as described (508). Primary human aortic SMCs (hSMCs) were isolated from the aorta of non-failing hearts that were not used for transplant, through the HOPE program. A modified enzymatic dispersal method was used (509). We used SMCs of both species at passages 3-5 in this study. Cells were serum-deprived for 24 hours prior to the start of indicated experimental protocols.

4.2.8. Human aortic endothelial cell culture

Primary human aortic endothelial cells (HAoECs) were purchased from ATCC (American Type Culture Collection) and cultured in vascular cell basal medium supplemented with endothelial cell growth kit-VEGF, 2% FBS, 100 U/ml penicillin and100 μg/ml streptomycin (endothelial cell growth medium). HAoECs at passages 2-5 were used for experiments.

4.2.9. ADAM17 siRNA transfection in human aortic SMCs and ECs

Human aortic SMCs and ECs were seeded at subconfluence and transfected with scrambled or *ADAM17* siRNA (Ambion, s13720) for 24 hours. After siRNA transfection, human aortic SMCs were starved in serum-free media for 24 hours prior to the start of indicated experimental protocols, whereas HAoECs were serum starved in vascular cell basal medium supplemented with 1% FBS for 24 hours prior to the start of indicated molecular experiments. HAoECs used for *in vitro* permeability assay and VE-cadherin staining were not subjected to serum starvation, since we observed that serum depletion could cause a small amount of cell death and result in pseudo-positive signals even at baseline.

4.2.10. In vitro acute exposure of elastase to primary cultured cells

To dissect the underlying cellular behaviors and signaling alternations in *Adam17*-intact or -deficient SMCs (mouse and human, m/hSMCs) or HAoECs subjected to acute elastase exposure, we established an *in vitro* model by incubating serum-starved primary m/hSMCs or HAoECs in elastase solution (0.4 U/ml in basal medium) for 5 minutes to mimic our *in vivo* TAA model. After elastase treatment, cells were further cultured in serum-deprived (for SMCs) or -reduced (for ECs)

media for different time of periods varying from 0.5 hour to 6 hours for different experiments as indicated.

4.2.11. Immunocytofluorescence of VE-cadherin in human aortic endothelial cell monolayers

Scrambled or *ADAM17* siRNA transfected HAoECs were seeded on human fibronectin pre-coated glass coverslips. Cells were treated with vehicle or elastase (0.4 U/ml) for 5 min after an intact monolayer was formed. Then the cells were replenished with full growth media and collected at 6 hours after elastase treatment for VE-cadherin immunocytofluorescence.

4.2.12. In vitro endothelial cell permeability assay

Scrambled or *ADAM17* siRNA transfected HAoECs were seeded on porous, collagen-coated inserts provided in the *in vitro* vascular permeability assay kit (EMD Millipore). Cells were treated with vehicle or elastase (0.4 U/ml) for 5 min after an intact monolayer was formed. Then FITC-dextran was added to each insert, and an equal volume of media from the receiving chamber was collected every 30 min in a 3-hour time course. Collected media were measured for fluorescent intensity. The fluorescent intensity signal for each group was normalized to that of the scrambled siRNA-vehicle group at each time point, and was plotted in a time-dependent fashion. Higher fluorescent intensity indicates higher permeability.

4.2.13. In vivo Evans blue permeability assay

At day 3 post-TAA surgery, eight male *Adam17*$^{f/f}$ and *Adam17*$^{f/f}$*/Tie2*$^{Cre/+}$mice were injected with 100 µl of a 1% Evans blue solution in 1× PBS through sub-retinal injection. All mice were euthanized after 1 hour of dye injection. Elastase treated segments of both genotypes were embedded in OCT media. Cryosections were used to visualize Evans blue dye (autofluorescence) distribution in different layers of the aorta.

4.2.14. RNA isolation and quantitative real-time PCR

Total RNA was extracted from the tunica media of *Adam17*$^{f/f}$*/Sm22*$^{Cre/+}$ mice and their littermate controls, *Adam17*$^{f/f}$ mice, before and 3 days post-TAA surgery using TRIzol reagent (Invitrogen, 15596026) according to the manufacturer's protocol. After acute elastase exposure, primary mouse

aortic SMCs (*Adam17*$^{f/f}$ and *Adam17*$^{f/f}$*/Sm22*$^{Cre/+}$) and human aortic SMCs (scrambled siRNA *vs* *ADAM17* siRNA transfected) were harvested at indicated time points and underwent total RNA extraction using the same protocol above. A list of TaqMan primer-probe mix for each targeted gene was shown in **Table 2.5**. The reference gene 18S was used as an internal control.

4.2.15. Immunoblotting

For immunoblotting analysis, equal amounts (20-35 μg) of total protein was fractionated by electrophoresis under denaturing conditions on a 4-20% SDS-polyacrylamide gel, and transferred onto a piece of Immobilon-P PVDF membrane (EMD Millipore). All the following procedure was described in detail in **Chapter 2.23**.

4.2.16. In vitro gelatin zymography

MMP2 and MMP9 activation in sham and 3 d-TAA samples of all genotypes were confirmed by *in vitro* gelatin zymography as described before (378), and is also described in detail in **Chapter 2.24**.

4.2.17. In vitro ADAM17 enzymatic activity assay

In vitro ADAM17 enzymatic activity in human healthy and aneurysmal aortic specimens and in mouse sham and TAA (3 days and 14 days) samples was measured as described before (336). A total amount of 5 μg protein was used for ADAM17 enzymatic activity assay, and the assay was run as a kinetic assay mode for 24 hours. Each sample was run in triplicates, and the data represent the mean values of three independent experiments. The specific ADAM17 activity is expressed as pmol/min/μg tissue protein.

4.2.18. Beads-based multiplex assay

Cytokine and chemokine profiles in mouse sham, 3d-TAA and 14d-TAA samples were quantified using Mouse Cytokine Array / Chemokine Array 31-Plex Panel (Eve Technologies, MD31). The individual cytokine/chemokine concentrations were expressed as pg per mg aortic protein. All samples were run in duplicates. The more detailed protocol is available in **Chapter 2.26**.

4.2.19. ELISA quantification assay for soluble VE-cadherin in conditioned culture media

The cleaved form (soluble) of VE-cadherin released by HAoECs to the culture medium in response to acute elastase exposure was quantified by a Quantikine ELISA human VE-cadherin Immunoassay kit (R & D Systems) as per the manufacturer's instructions.

4.2.20. Statistics

Statistical analyses were performed by using IBM SPSS software (Version 21). Normality of data distribution was determined via the Kolmogorov-Smirnov test, and all data showed normal distribution. Comparisons between any two groups (human control and TAA, and vehicle- or ADAM17 inhibitor-treated mice) was performed with unpaired student's *t*-test. Comparison among multiple groups (>3) with one main factor was performed by one-way ANOVA followed by Bonferroni *post-hoc* test. Comparison among multiple groups (genotype × treatment) was performed by two-way ANOVA followed by Bonferroni *post-hoc* test. Averaged values are presented as mean ± SEM. All *in vitro* experiments were done in triplicate for each experimental group and performed in two to five independent experiments, and each *n* value corresponds to an independent experiment. For *in vivo* data, each *n* value corresponds to an individual mouse, and the number of mice used for each *in vivo* analysis is indicated in the figure legends. Statistical significance was recognized at $P < 0.05$.

4.3. Results

4.3.1. ADAM17 is significantly increased in aneurysmal aorta from TAA patients

To determine the involvement of AFigDAM17 in the pathogenesis of TAA, we first examined the ADAM17 levels and activity in human aortic tissue from TAA patients and non-aneurysmal controls. As compared to controls, TAA specimens showed markedly higher ADAM17 levels in the intimal and the medial regions of the thoracic aorta (**Figure 4.1, A and B**) and in total aortic homogenate (**Figure 4.1C**), concomitant with a significantly higher ADAM17 enzymatic activity (**Figure 4.1D**).

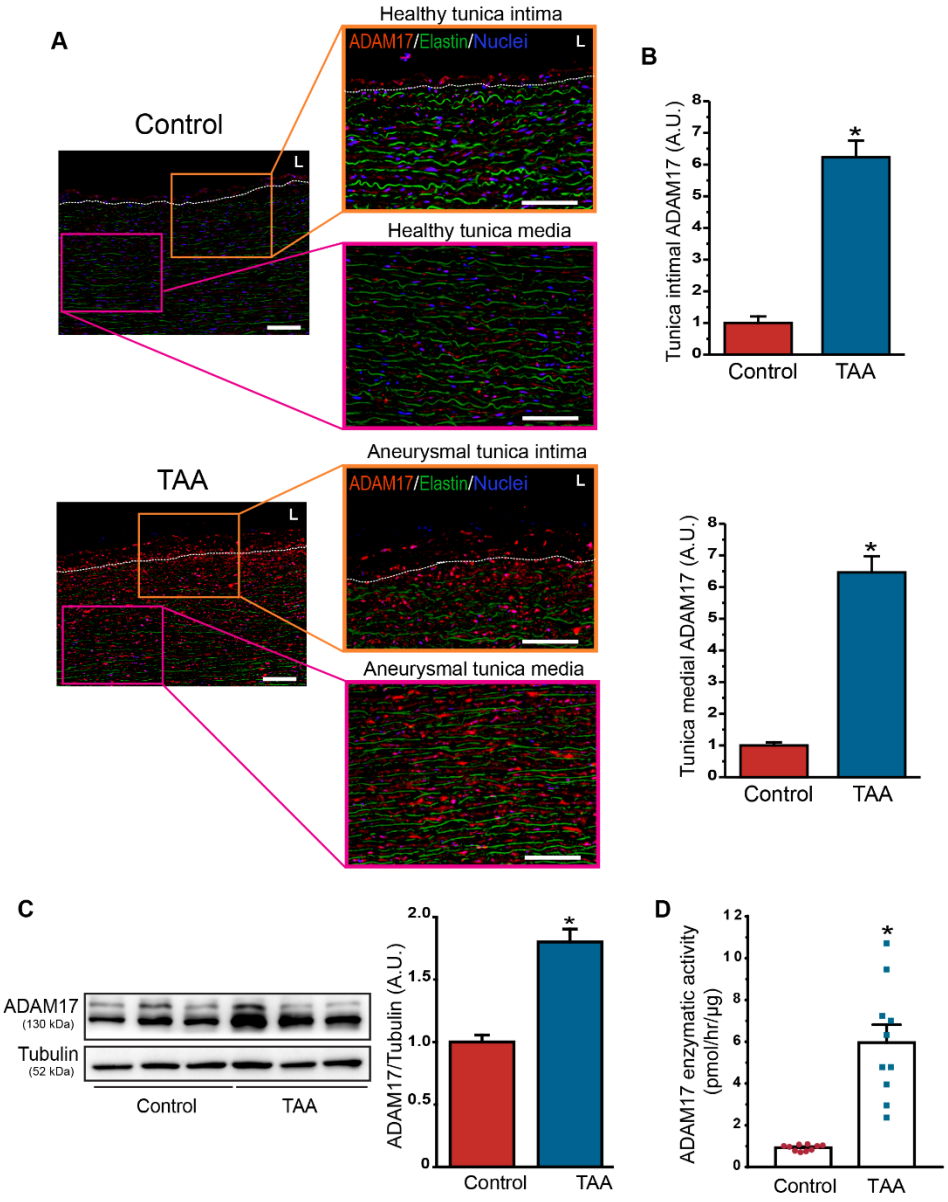

Figure 4.1 ADAM17 expression and activity are increased in the aneurysmal thoracic aorta (TAA) in humans. (**A**) Representative immunofluorescent staining showing ADAM17 levels and distribution patterns in control (non-diseased) and aneurysmal aortas (TAAs). (**B**) Quantitative analysis of fluorescent intensity revealed elevated ADAM17 levels in the tunica intima and media of TAA compared to control aortas. n=10 per group. Scale bars: 100 μm. (**C**) Representative immunoblot showing ADAM17 protein levels in human control (non-aneurysmal/non-diseased) aortas and TAAs. Densitometric quantification analysis confirmed higher ADAM17 protein levels in TAA aortas. The data shown are representative of three independent experiments. (**D**) *In vitro* enzymatic activity assay showed significantly increased ADAM17 activity in aneurysmal aortas (TAA) compared to control aortas. n=10 per group. *P<0.05 compared to the healthy control group using unpaired student's t-test. Values in all bar graphs represent mean ± SEM. While dotted line separates the tunica media from tunica intima in human aortic sections. L, aortic lumen; TAA, thoracic aortic aneurysm.

4.3.2. Genetic deletion of Adam17 in smooth muscle cells or endothelial cells suppresses TAA progression

Given the elevated ADAM17 levels observed in patients with TAA, we investigated if *Adam17*-deficiency could attenuate TAA formation. We optimized a previously published experimental model of *in vivo* TAA in mice (381, 393) to generate TAA with reproducible severity (dilation of >50%) first in wild-type control mice (**Figure 4.2**). This model recapitulates the key pathological and gross morphological features of human TAA, such as degradation of elastic lamellae, loss of smooth muscle cells and apoptosis (**Figure 4.3**).

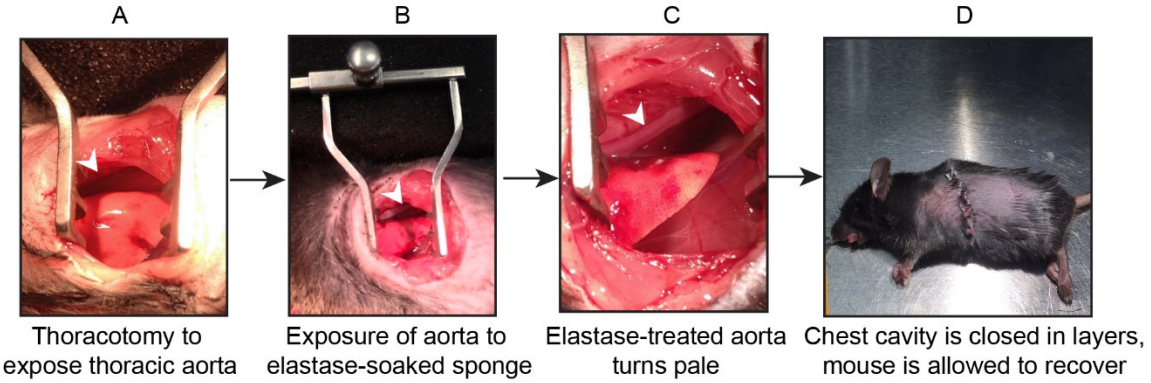

Figure 4.2 Surgical procedure for induction of experimental thoracic aortic aneurysm (TAA) by porcine pancreatic elastase exposure. The entire surgical procedure consists of (**A**) Exposure of the descending thoracic aorta through a left thoracotomy at the 7th intercostal interspace; (**B**) Application of a piece of sponge soaked in porcine pancreatic elastase to the exposed region of the thoracic aorta for 5 min; (**C**) Removal of the sponge (the treated aorta turned pale in color); (**D**) Closure of the incision after the thorax cavity was thoroughly rinsed with warm saline. Arrows indicate the region of the aorta treated with porcine pancreatic elastase.

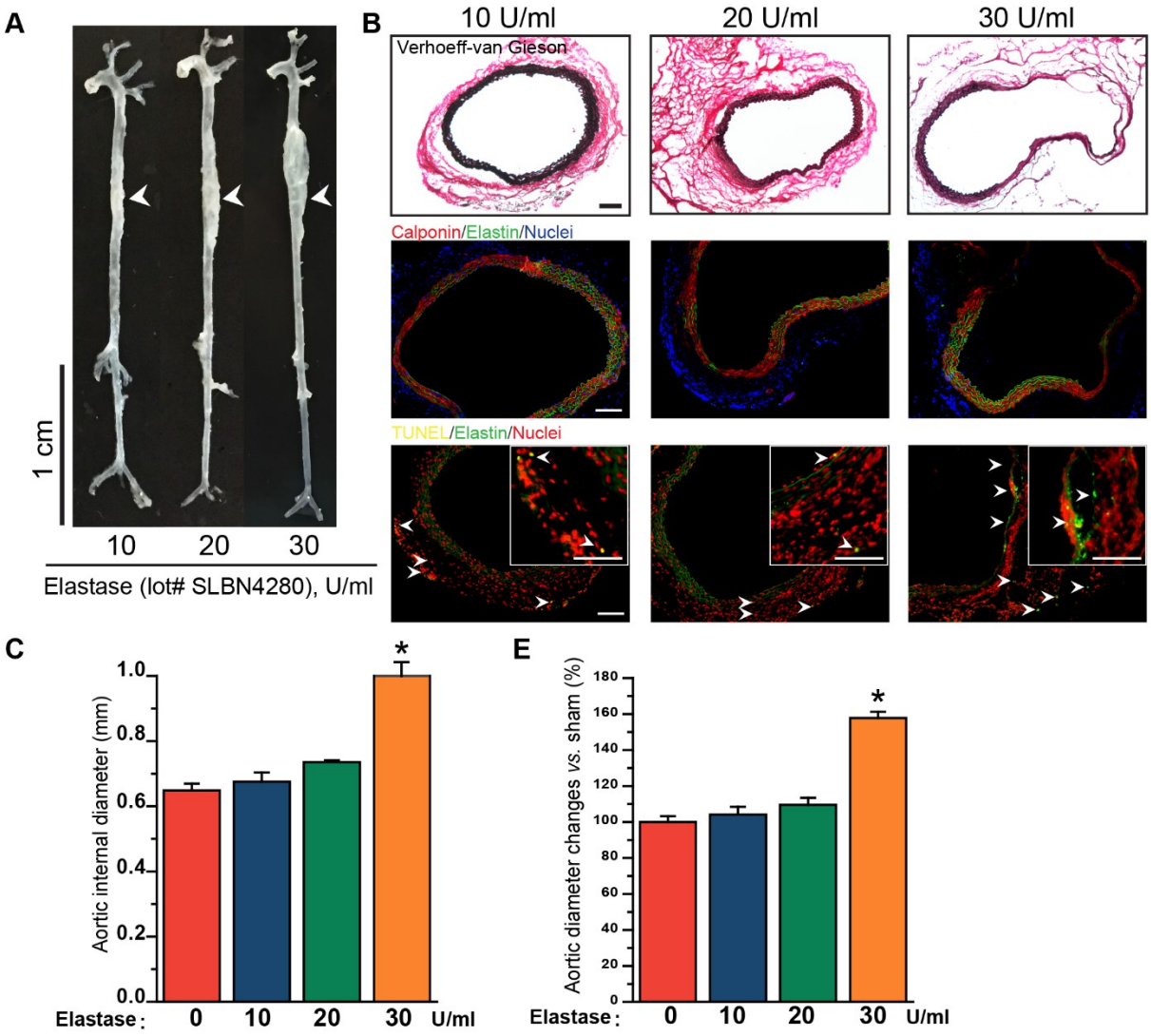

Figure 4.3 Screening of optimal concentration of porcine pancreatic elastase to induce reproducible experimental TAA phenotype that recapitulates the major pathological characteristic of human TAA. (**A**) A representative image showing the morphology of entire aortas of male wild-type mice 14 days after treatment with different concentrations of porcine pancreatic elastase (i.e., 10, 20 and 30 U/ml). Arrows indicate the site of elastase exposure. Scale bar: 1 cm. *n*=5 per group. (**B**) Representative histological and immunofluorescence staining showing the structural integrity of the elastin lamellae (Verhoeff-van Gieson, black lines), SMC density (Calponin^{+}, red) and apoptotic cells (TUNEL, yellow, arrows indicate apoptotic cells, inserts showing positive staining at higher magnification) in the thoracic aortic sections after 14 days of exposure to the indicated concentrations of elastase. Scale bars: 200 µm. *n*=5 per group. (**C**) The internal aortic diameter (thoracic region), and (**D**) the percent change in aortic diameter (compared to the age-matched sham group) shows that maximal aortic dilation was achieved by using 30 U/ml of porcine pancreatic elastase. Therefore, 30 U/ml elastase concentration was used in our study to induce TAA. *n*=5 per group. **P*<0.05 compared to the sham group using 1-way ANOVA followed by Bonferroni's *post-hoc* test. Bar graphs represent Mean ± SEM. TUNEL, Terminal deoxynucleotidyl transferase (TdT) dUTPNick-End Labeling.

Since somatic deletion of *Adam17* in mice is embryonically lethal (252), and as we observed elevated expression and activity of ADAM17 in the medial and intimal regions of TAA specimens, we generated mice lacking ADAM17 in the smooth muscle cell (*Adam17*$^{flox/flox}$/*Sm22*$^{Cre/+}$, *Adam17*$^{f/f}$/*Sm22*$^{Cre/+}$) or in the endothelial cell (*Adam17*$^{flox/flox}$/*Tie2*$^{Cre/+}$, *Adam17*$^{f/f}$/*Tie2*$^{Cre/+}$) to delineate the cell-specific function of ADAM17 in the pathogenesis of TAAs. Knockdown of *Adam17* in smooth muscle cells (SMCs) was confirmed by the reduced mRNA levels of *Adam17*, but not other vascular ADAMs, such as *Adams 9, 10,* and *15* (**Figure 4.4**), and the marked reduction in ADAM17 protein levels in the medial thoracic aorta in *Adam17*$^{f/f}$/*Sm22*$^{Cre/+}$ mice (**Figure 4.5A**). To generate endothelial deletion of *Adam17*, we used the inducible *Tie2MerCreMer*-recombinase (533) instead of the constitutively active Cre-recombinase. This approach avoids *Adam17* deletion in hematopoietic cells during embryonic development since *Tie2-Cre* is expressed in hematopoietic cells in addition to ECs (504, 505). Endothelial deletion of *Adam17* was induced in adult mice and confirmed by immunoblotting (**Figure 4.5B**).

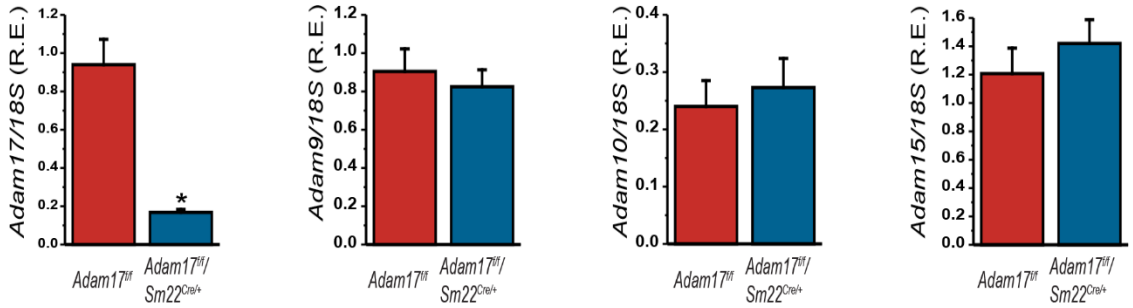

Figure 4.4 Smooth muscle cell loss of ADAM17 does not alter expression levels of other vascular ADAMs. mRNA levels for *ADAMs*-9, 10, 12, 15 and 17 were measured by quantitative TaqMan real-time PCR in the thoracic aortas from *Adam17*$^{f/f}$/*Sm22*$^{Cre/+}$ and *Adam17*$^{f/f}$ mice. *P<0.05 compared to the *Adam17*-intact group using unpaired student's t-test. Averaged values in all bar graphs are mean ± SEM. n=5/gender/genotype. ADAM17, a disintegrin and metalloproteinase 17; *Adam17*$^{f/f}$, *Adam17*$^{flox/flox}$; *Adam17*$^{f/f}$/*Sm22*$^{Cre/+}$, *Adam17*$^{flox/flox}$/*Sm22αCre*.

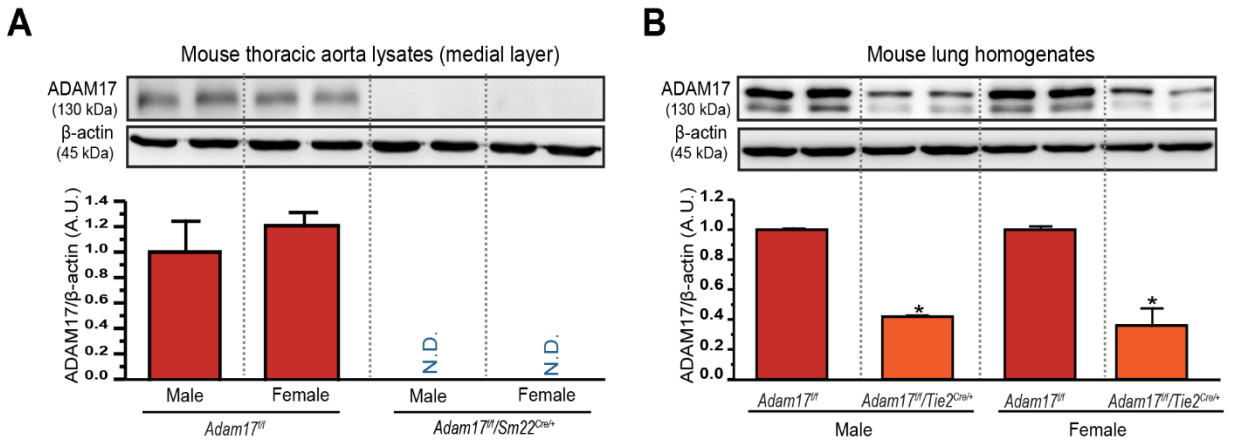

Figure 4.5 *Adam17* knockdown efficiency in smooth muscle cell- and endothelial cell-specific *Adam17* knockout mice. (**A**) Representative immunoblot showing absence of ADAM17 protein in thoracic aorta (tunica media) of male and female *Adam17*$^{f/f}$*Sm22*$^{Cre/+}$ mice, and the corresponding densitometric quantification. *n*=4/gender/genotype. (**B**) Representative immunoblot showing endothelial *Adam17*-knockdown efficiency (lung protein homogenate) in *Adam17*$^{f/f}$*/Tie2*$^{Cre/+}$ mice after 3 days of oral gavage of Tamoxifen (60 mg/kg/day) to induce activation of *Tie2-MerCreMer* recombinase; and the corresponding densitometric quantification. *n*=4/gender/genotype. **P*<0.05 compared to ADAM17-intact group using unpaired student's *t*-test. Values in all bar graphs are presented as mean ± SEM.

Using the optimized elastase-induced TAA model, we found that *Adam17*-deficiency in SMCs or ECs resulted in significant protection against TAA development as evident by the suppressed aortic dilation at 3 days and 14 days following TAA induction in male (**Figure 4.6**) and female mice (**Figure 4.7**). Mice expressing only the Cre-recombinase enzyme in smooth muscle cells (*Sm22*$^{Cre/+}$) or in endothelial cells (*Tie2*$^{Cre/+}$), with unaltered ADAM17 expression, developed TAA of similar severity as the control wildtype and *Adam17*$^{f/f}$ mice (**Figure 4.8**), demonstrating that the observed protection against TAA is related to *Adam17*-deficiency in each cell type. In *Adam17*-intact mice, TAA triggered a significant rise in ADAM17 activity which was markedly reduced in *Adam17*-deficient aortas (**Figure 4.9A**), along with a TAA-induced reduction in TIMP3, the only known endogenous inhibitor of ADAM17 (487, 534), which could contribute to the rise in ADAM17 activity (**Figure 4.9B**). Similarly, the TAA-induced increase in MMP2 and MMP9 levels, two proteases often involved in vascular diseases, were markedly lower in mice with *Adam17*-deficiency in the SMC or ECs (**Figure 4.9, C and D**).

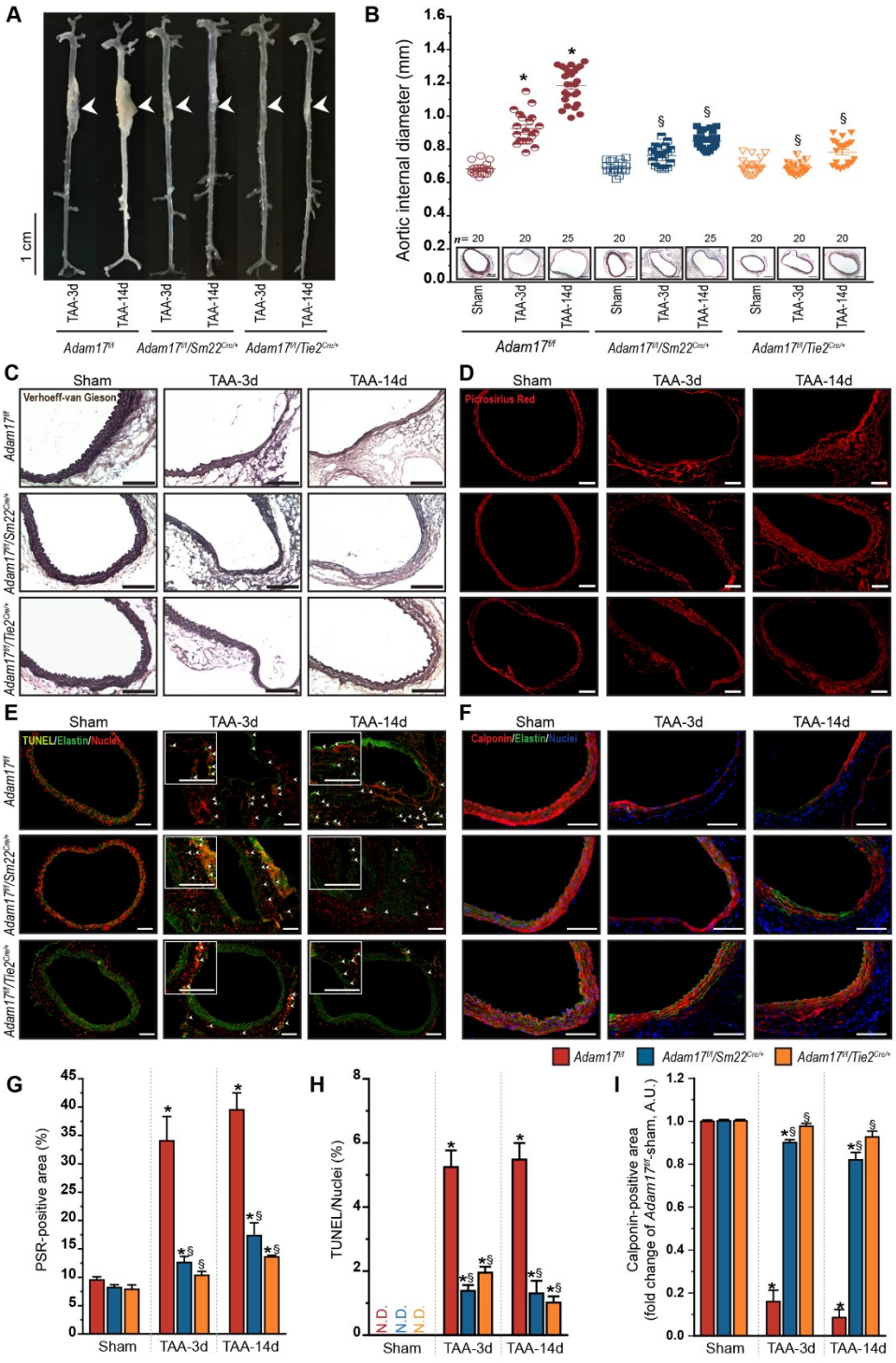

Figure 4.6 Lack of ADAM17 in smooth muscle cells (SMC) or endothelial cells (EC) attenuates elastase-induced TAA development in male mice. (**A**) Representative pictures of whole aorta in male mice with intact ADAM17 (*Adam17*$^{f/f}$), SMC *Adam17*-deficiency (*Adam17*$^{f/f}$/*Sm22*$^{Cre/+}$) and EC *Adam17*-deficiency (*Adam17*$^{f/f}$/*Tie2*$^{Cre/+}$) 3 days and 14 days post-elastase treatment (30 U/ml for 5 min). Arrows indicate the site where elastase was applied. Scale bar:1 cm. (**B**) Scatter plot shows the maximum aortic internal diameter for mice in each group. Representative full aortic cross-section (thoracic) from each group is embedded in the scatter plot (magnification ×50). Scale bars: 100 μm. The sample size for each group is indicated in the dot plot. *P<0.05 compared to the corresponding sham group; §P<0.05 compared to the corresponding A*dam17*$^{f/f}$ group using 2-way ANOVA followed by Bonferroni's *post-hoc* test.

The mean ± SEM for each group is also included in the dot plot. (**C**) Representative images of aortic sections in all groups showing elastin fiber structure (Verhoeff-van Gieson staining), and (**D**) fibrillar collagen deposition (picrosirius red staining). *n*=6 per group. Scale bars: 100 μm. (E) Representative immunofluorescence images of aortic sections of all groups show the apoptotic cells (TUNEL$^+$, yellow, indicated by arrows, inserts showing positive staining in higher magnification) and (**F**) SMC density (calponin$^+$, red) in the tunica media. Elastin autofluorescence appears in green in these images. *n*=6 per group. Scale bars:100 μm. **(G-I)** Quantification of PSR **(G)**, TUNEL **(H)**, and calponin **(I)** in all indicated groups. **P*<0.05 vs corresponding sham group; §*P*<0.05 *vs* corresponding *Adam17$^{f/f}$* group (two-way ANOVA, Bonferroni's *post-hoc* test). N.D., not detected. SMC, smooth muscle cell; EC, endothelial cell; TUNEL, Terminal deoxynucleotidyl transferase (TdT) dUTPNick-End Labeling; TAA, thoracic aortic aneurysm. ADAM17, a disintegrin and metalloproteinase 17; *Adam17$^{f/f}$*, *Adam17$^{flox/flox}$*; *Adam17$^{f/f}$/Sm22$^{Cre/+}$*, *Adam17$^{flox/flox}$/Sm22αCre*.

Medial elastin lamellae and interstitial collagens in the media and adventitia determine the structural integrity and biomechanical properties of the aortic wall. Fourteen days post-TAA, elastin fibers (visualized by VVG) were disrupted and reduced in *Adam17$^{f/f}$* mice. In contrast, elastin content and fiber architecture were markedly preserved in *Adam17$^{f/f}$/Sm22$^{Cre/+}$* and *Adam17$^{f/f}$/Tie2$^{Cre/+}$* male (**Figure 4.6C**) and female mice (**Figure 4.7C**). Adventitial fibrosis that contributes to stiffness resulting in outward remodeling of the aneurysmal aorta was detected at the TAA site in *Adam17$^{f/f}$* mice which worsened over the course of the disease (3 days to 14 days post-TAA). Adventitial fibrosis was markedly diminished in *Adam17$^{f/f}$/Sm22$^{Cre/+}$*-TAA and *Adam17$^{f/f}$/Tie2$^{Cre/+}$*-TAA male and female mice (**Figure 4.6, D and G and Figure 4.7, D and G**). In addition, a marked increase in cell death (detected by TUNEL staining, (**Figure 4.6, E and H**) and reduced number of viable SMCs (calponin$^+$ cells) were observed in the aneurysmal region of *Adam17$^{f/f}$*-TAA aortas (**Figure 4.6, F and I**), but significantly ameliorated in *Adam17$^{f/f}$/Sm22$^{Cre/+}$*-TAA and *Adam17$^{f/f}$/Tie2$^{Cre/+}$*-TAA mice (**Figure 4.6, E and H, F and I; Figure 4.7, E and H, F and I**). These data confirm that *Adam17*-deficiency in either EC or SMC is sufficient to deter a pathological process that would lead to the formation of TAA.

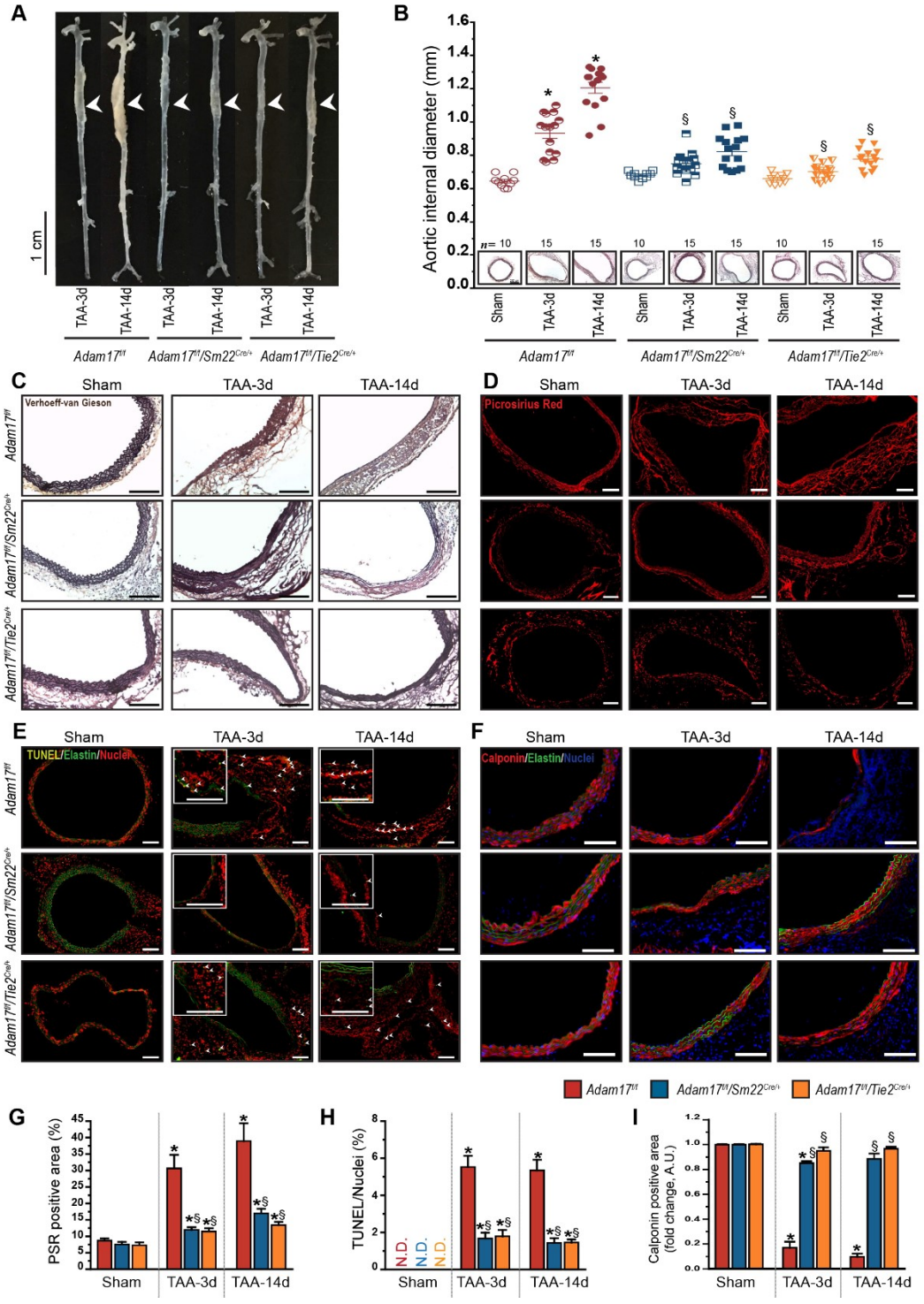

Figure 4.7 Lack of ADAM17 in smooth muscle cells (SMC) or endothelial cells (EC) attenuates elastase-induced TAA development in female mice. (A) Whole aorta images, **(B)** aortic internal diameter and representative aorta cross-section for indicated group/genotype. **(C-D)** Elastin staining (VVG) and PSR-staining of the thoracic aorta in indicated groups. E) TUNEL staining (yellow) superimposed with elastin autofluorescence (green). **(F)** Calponin staining (red) superimposed with elastin auto-fluorescence (green) and nuclear DAPI staining (blue). Additional details are similar to what is described in Figure 4.6 (except the sex of animals).

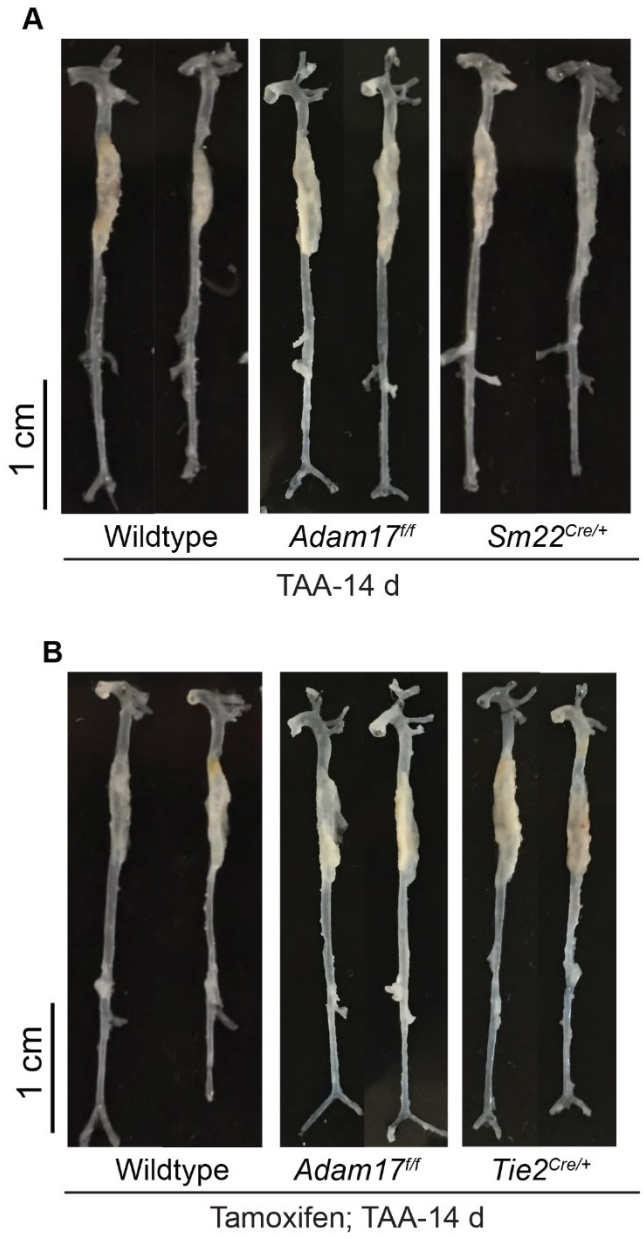

Figure 4.8 The genetic control groups for cell-specific *Adam17*-deficiency showing that Cre-recombinase expression alone did not alter the TAA response. (**A**) Representative images showing the morphology of the aortas from male WT, *Adam17*$^{f/f}$ (*Adam17* allele is floxed but not deleted), and *Sm22*$^{Cre/+}$ (SMC recombinase is expressed, but *Adam17* is not floxed, therefore not deleted) at 14 days after elastase treatment. All three genotypes express intact *Adam17* in SMCs and serve as controls for SMC *Adam17*-deficient (*Adam17*$^{f/f}$/*Sm22*$^{Cre/+}$) mice. *Adam17*$^{f/f}$ mice are littermates for *Adam17*$^{f/f}$/*Sm22*$^{Cre/+}$ mice. *n*=6/genotype. (**B**) Representative pictures of entire aortas of male wildtype, *Adam17*$^{f/f}$ (*Adam17* allele is floxed but not deleted), and *Tie2*$^{Cre/+}$ *mice* (*Tie2-MerCreMer* recombinase is expressed, but *Adam17* is not floxed, therefore not deleted) at day 14 post elastase treatment. These three genotypes received Tamoxifen (oral gavage) at 6 weeks of age, for three consecutive days, and underwent TAA surgery three weeks after Tamoxifen administration. The three genotypes served as controls for EC *Adam17*-deficient (*Adam17*$^{f/f}$/*Tie2*$^{Cre/+}$) mice. *Adam17*$^{f/f}$ mice are littermates for *Adam17*$^{f/f}$/*Tie2*$^{Cre/+}$ mice. *n*=6 for each genotype. Scale bar: 1 cm. TAA, thoracic aortic aneurysm. ADAM17, a disintegrin and metalloproteinase 17; *Adam17*$^{f/f}$, *Adam17*$^{flox/flox}$; *Adam17*$^{f/f}$/*Sm22*$^{Cre/+}$, *Adam17*$^{flox/flox}$/*Sm22αCre*.

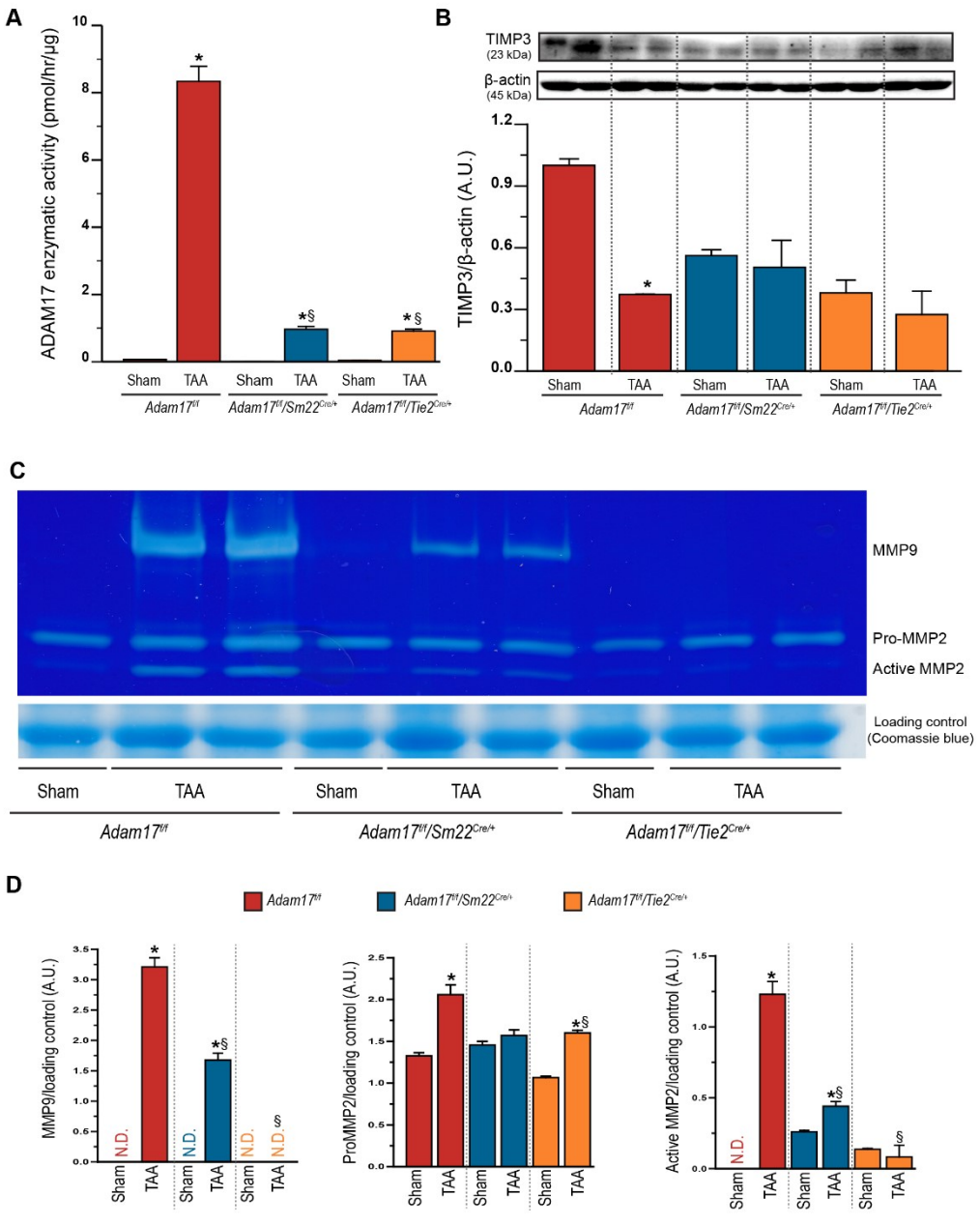

Figure 4.9 TAA-induced rise in proteolytic activities is markedly reduced with cell-specific *Adam17*-deficiency. (**A**) ADAM17 enzymatic activity significantly increased in the aneurysmal aortas in ADAM17-intact (*Adam17$^{f/f}$*) mice and was significantly lower in the aortas of SMC *Adam17*-deficient (*Adam17$^{f/f}$/Sm22$^{Cre/+}$*) mice and EC *Adam17*-deficient mice (*Adam17$^{f/f}$/Tie2$^{Cre/+}$*). *n*=6 per group. (**B**) Representative immunoblot and averaged quantification of TIMP3 protein levels in the indicated genotypes following sham or TAA. *n*=6 per group. **P*<0.05 compared to sham using 2-way ANOVA followed by Bonferroni's *post-hoc* test. (**C**) Representative in vitro gelatin zymography showing MMP9 and MMP2 levels in *Adam17*-intact (*Adam17$^{f/f}$*) and cell-specific *Adam17*-deficient aortas following sham or TAA. (**D**) The corresponding densitometric quantification of MMP9, pro-MMP2 and active MMP2 levels in each group. Coomassie blue-stained gel served as loading control. *n*=6 per group. The data shown are representative of three independent experiments. **P*<0.05 compared to sham; §*P*<0.05 compared to *Adam17$^{f/f}$*-TAA group using 2-way ANOVA followed by Bonferroni's *post-hoc* test. Averaged values are mean ± SEM. A.U., arbitrary units; N.D., not detected. TAA, thoracic aortic aneurysm. ADAM17, a disintegrin and metalloproteinase 17; *Adam17$^{f/f}$*, *Adam17$^{flox/flox}$*; *Adam17$^{f/f}$/Sm22$^{Cre/+}$*, *Adam17$^{flox/flox}$/Sm22αCre*.

4.3.3. TAA triggers an inflammatory response that is suppressed by Adam17-deficiency

One of the characteristics of TAA in humans is increased inflammation in the aortic wall (535). Immunofluorescent staining revealed marked accumulation of neutrophils (**Figure 4.10, A and C**) and macrophages (**Figure 4.10, B and D**) in *Adam17*$^{f/f}$-TAA aortas early post-TAA (3 days) that persisted up to 14 days post-TAA. *Adam17*-deficiency in SMCs or ECs markedly suppressed the inflammation in the aortic wall of male mice (**Figure 4.10, A through D**). Similar transmural inflammatory phenotypes, and comparable ameliorations with *Adam17* deletion were observed in female mice of corresponding genotypes (**Figure 4.11**). The extent of inflammation was quantified by measuring the protein levels of cytokines and chemokines in the thoracic aorta. Consistent with our observations with immunofluorescent staining, pro-inflammatory cytokines (interferon-gamma/IFNγ, tumor necrosis factor-alpha/TNFα, interleukins-1alpha/IL1α, IL6, and IL12) (**Figure 4.10E**), and chemokines (CXCL9, CXCL10, and CCL2) (**Figure 4.10F**) were elevated in the aneurysmal aorta of *Adam17*$^{f/f}$ mice but markedly suppressed in *Adam17*$^{f/f}$*/Sm22*$^{Cre/+}$ and *Adam17*$^{f/f}$*/Tie2*$^{Cre/+}$ mice at 3 days and 14 days post-TAA. Majority of the inflammatory cytokines peaked at 3 days post-TAA and declined by day 14. Anti-inflammatory cytokines, ILs 4, 10, and 13, were similarly altered among genotypes. IL4 was transiently elevated in all three genotypes at 3 days post-TAA, but returned to baseline levels by day 14 post-TAA (**Figure 4.10E**); IL10 was not altered in response to TAA in any genotype (**Figure 4.10E**); and IL13 was not detectable in any group (data not shown).

Colony-stimulating factors, such as granulocyte colony-stimulating factor (G-CSF) (398), granulocyte macrophage colony-stimulating factor (GM-CSF) (536), and macrophage colony-stimulating factor (M-CSF) (537), play an essential role in triggering an inflammatory response in aortopathies. Notably, at 3 days post-TAA, the rise in G-CSF, GM-CSF and M-CSF levels were significantly greater in *Adam17*$^{f/f}$ mice (by >2 fold), which persisted until 14 days post-TAA, compared to *Adam17*$^{f/f}$*/Sm22*$^{Cre/+}$and *Adam17*$^{f/f}$*/Tie2*$^{Cre/+}$ mice (**Figure 4.10G**), further supporting the less severe TAA-induced inflammatory response in *Adam17*-deficient mice.

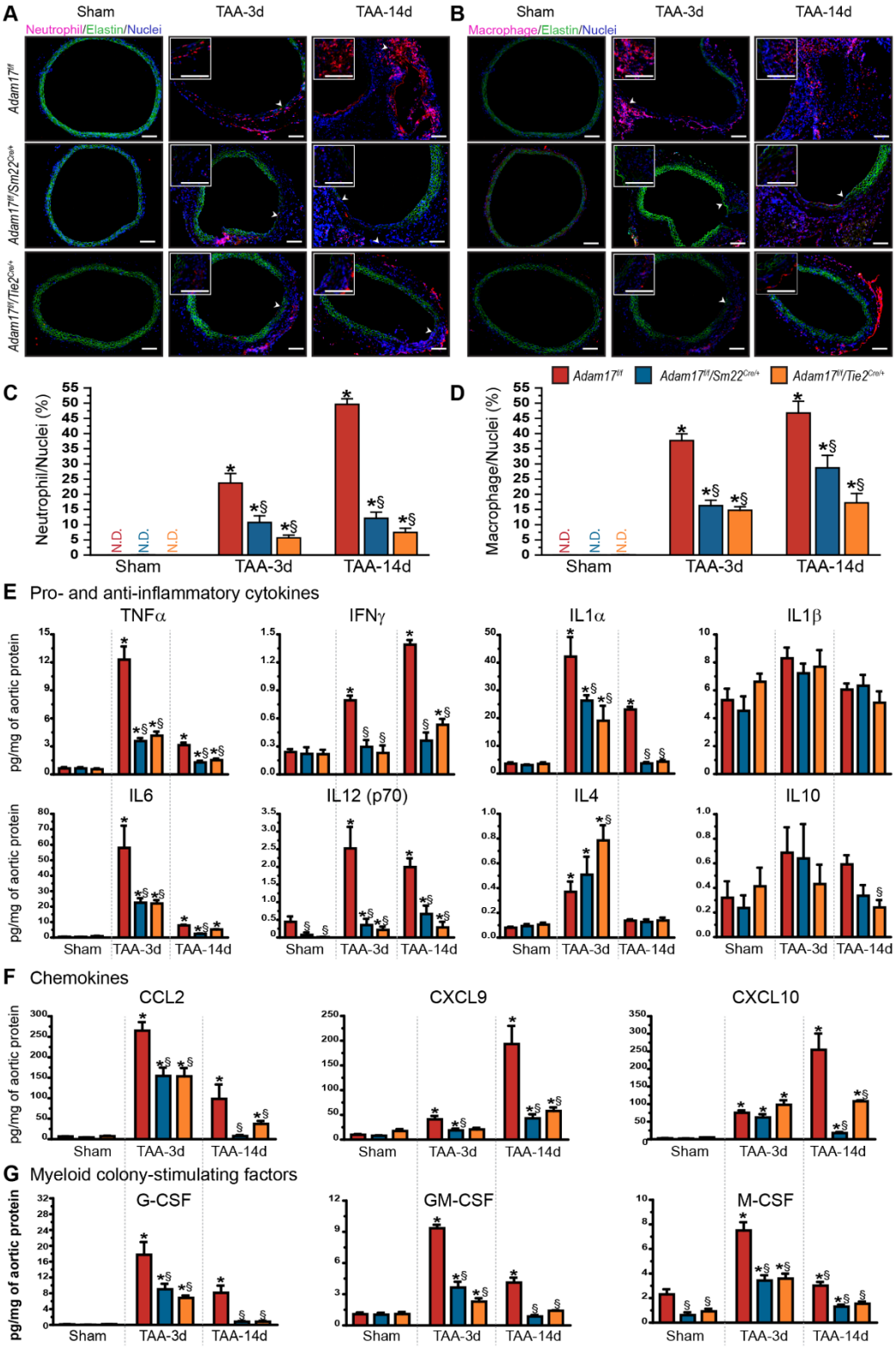

Figure 4.10 Loss of ADAM17 in smooth muscle cells (SMC) or endothelial cells (EC) suppresses the inflammatory response in TAA. Representative immunofluorescent staining and quantification showing increased neutrophil (Ly6G, red) (**A and C**) and macrophage (CD68, red) (**B and D**)infiltration into the tunica media of *Adam17*-

intact (*Adam17*$^{f/f}$) aortas compared to SMC *Adam17*-deficient (*Adam17*$^{f/f}$/*Sm22*$^{Cre/+}$) or EC *Adam17*-deficient (*Adam17*$^{f/f}$/*Tie2*$^{Cre/+}$) aortas at day 3 and day14 post-TAA induction in male mice. Arrows in the full aortic cross-sections indicate the area that is shown at higher magnification in the insets. *n*=6 per group. Scale bars:100 µm. (**E-G**) Bead-based multiplex assays were used to measure protein levels of inflammatory and anti-inflammatory cytokines (**E**), chemokines (**F**), and myeloid colony-stimulating factors (**G**) associated with vascular inflammation in thoracic aorta from *Adam17*-intact (red column), SMC *Adam17*-deficient (blue column) and EC *Adam17*-deficient mice (orange column) in sham-operated mice, and at 3 days or 14 days post-TAA. *n*=18 per group. **P*<0.05 compared to the corresponding sham group; §*P*<0.05 compared to the corresponding *Adam17*$^{f/f}$ group using 2-way ANOVA followed by Bonferroni's *post-hoc* test. Averaged values present mean ± SEM. TAA, thoracic aortic aneurysm. ADAM17, a disintegrin and metalloproteinase 17; *Adam17*$^{f/f}$, *Adam17*$^{flox/flox}$; *Adam17*$^{f/f}$/*Sm22*$^{Cre/+}$, *Adam17*$^{flox/flox}$/*Sm22αCre*.

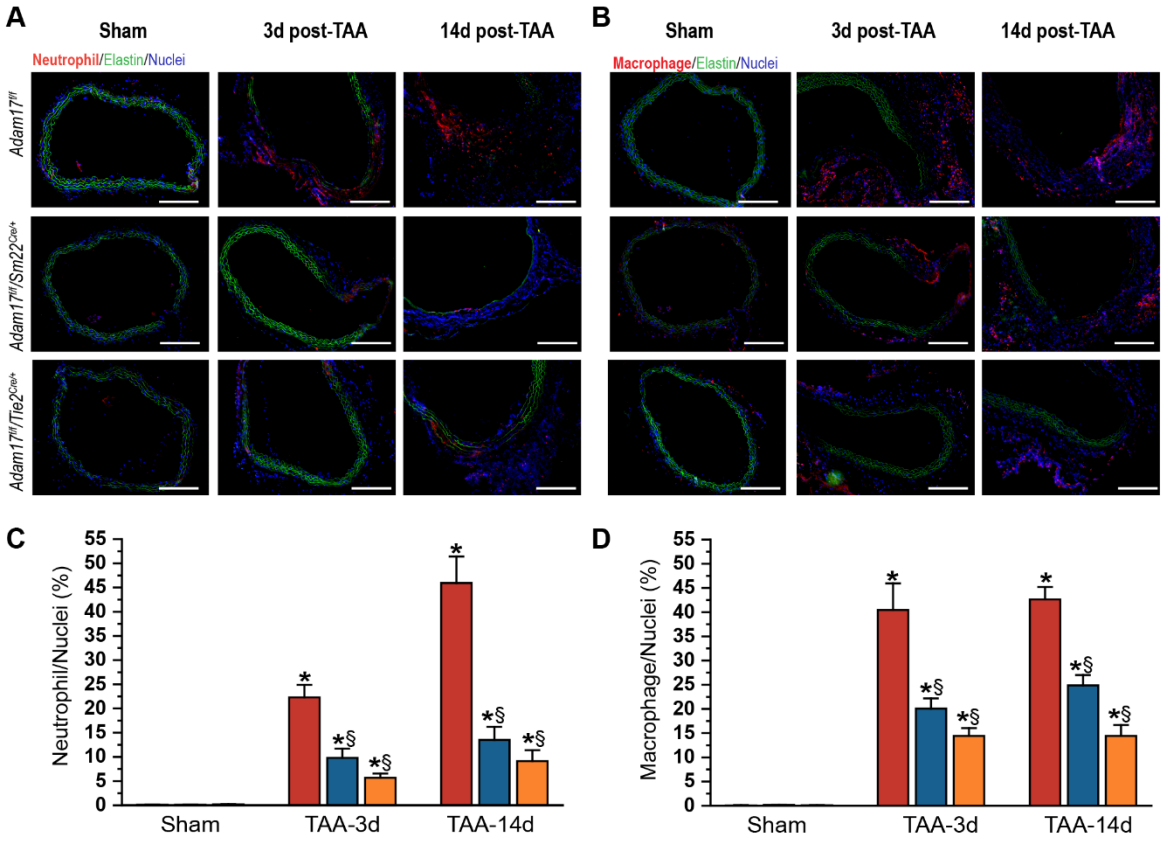

Figure 4.11 Loss of ADAM17 in smooth muscle cells (SMC) or endothelial cells (EC) suppresses post-TAA inflammatory response in female mouse aortas. Representative immunofluorescent staining and quantification showing increased neutrophil (Ly6G, red) **(A and C)** and macrophage (CD68, red/magenta) (**B and D**) infiltration into the tunica media of *Adam17*-intact (*Adam17*$^{f/f}$) aortas, but to a much lesser extent in SMC *Adam17*-deficient (*Adam17*$^{f/f}$/*Sm22*$^{Cre/+}$) or EC *Adam17*-deficient (*Adam17*$^{f/f}$/*Tie2*$^{Cre/+}$) aortas at day 3 and day 14 following TAA induction. Elastin autofluorescence appears as green. *n*=6 per group. Scale bars: 200 µm. **P*<0.05 *vs* corresponding sham group; §*P*<0.05 vs corresponding *Adam17*$^{f/f}$ group (two-way ANOVA, Bonferroni's *post-hoc* test). Scale bars: 200 µm. TAA, thoracic aortic aneurysm. ADAM17, a disintegrin and metalloproteinase 17; *Adam17*$^{f/f}$, *Adam17*$^{flox/flox}$; *Adam17*$^{f/f}$/*Sm22*$^{Cre/+}$, *Adam17*$^{flox/flox}$/*Sm22αCre*.

4.3.4. ADAM17 is responsible for injury-induced contractile-to-synthetic phenotype transition in SMCs

Next, we investigated the specific function of ADAM17 in each cell type in response to aneurysmal injury. In aortic disease, SMCs can switch from a contractile state (healthy) to synthetic state (diseased) triggering excessive ECM production, aortic stiffness, and pro-inflammatory signals (538-540). We measured the changes in known markers of SMC contractile phenotype, smooth muscle myosin heavy chain-11 (SM-MHC11), smoothelin, Sm22α and calponin, in the medial layer of thoracic aorta from male and female *Adam17*$^{f/f}$ and *Adam17*$^{f/f}$/*Sm22*$^{Cre/+}$ mice, at 3 days post-TAA or sham. *Adam17*-deficiency alone did not significantly alter the levels of these proteins in the sham groups. However, following TAA induction, Sm22α levels were decreased in *Adam17*-intact mice, but increased in aortas of SMC *Adam17*-deficient male and female mice; similarly smoothelin and calponin protein levels were higher in *Adam17*$^{f/f}$/*Sm22*$^{Cre/+}$-TAA group (**Figure 4.12, A and B**). To determine if this effect of ADAM17 on SMC function also applies to human SMCs, *Adam17* was knocked down in primary human aortic SMCs (isolated from non-diseased human thoracic aorta) by specific *ADAM17* siRNA (**Figure 4.13A**), and treated with elastase to simulate the *in vivo* TAA model. Similar to the *in vivo* TAA and *in vitro* murine aortic SMCs findings, elastase treatment in the face of *ADAM17*-deficiency in human thoracic SMCs resulted in increased expression of smoothelin, SM22α and calponin, markers of SMC contractile phenotype (**Figure 4.12, C and D**). Consistent with the notion of phenotype switching in SMCs, elastase treatment increased the protein levels of collagen type I and type III in control mouse or human SMCs (confirming their synthetic properties), but suppressed them in *ADAM17*-deficient cells (**Figure 4.12, E-G**). We further found that mRNA expression of collagen type I and type III (*Col1a1* and *Col3a1*) and elastin (*Eln)*, the main structural proteins in vascular matrix were significantly increased with elastase treatment in *Adam17*-intact mouse aorta and SMCs, but significantly suppressed in *Adam17*-deficient groups (**Figure 4.14, A and B**). These data indicate that *Adam17*-deficiency prevents the SMCs from acquiring synthetic characteristics in response to injury, and therefore prevents excess perivascular fibrosis and the associated inflammatory and proteolytic alterations in the aortic wall.

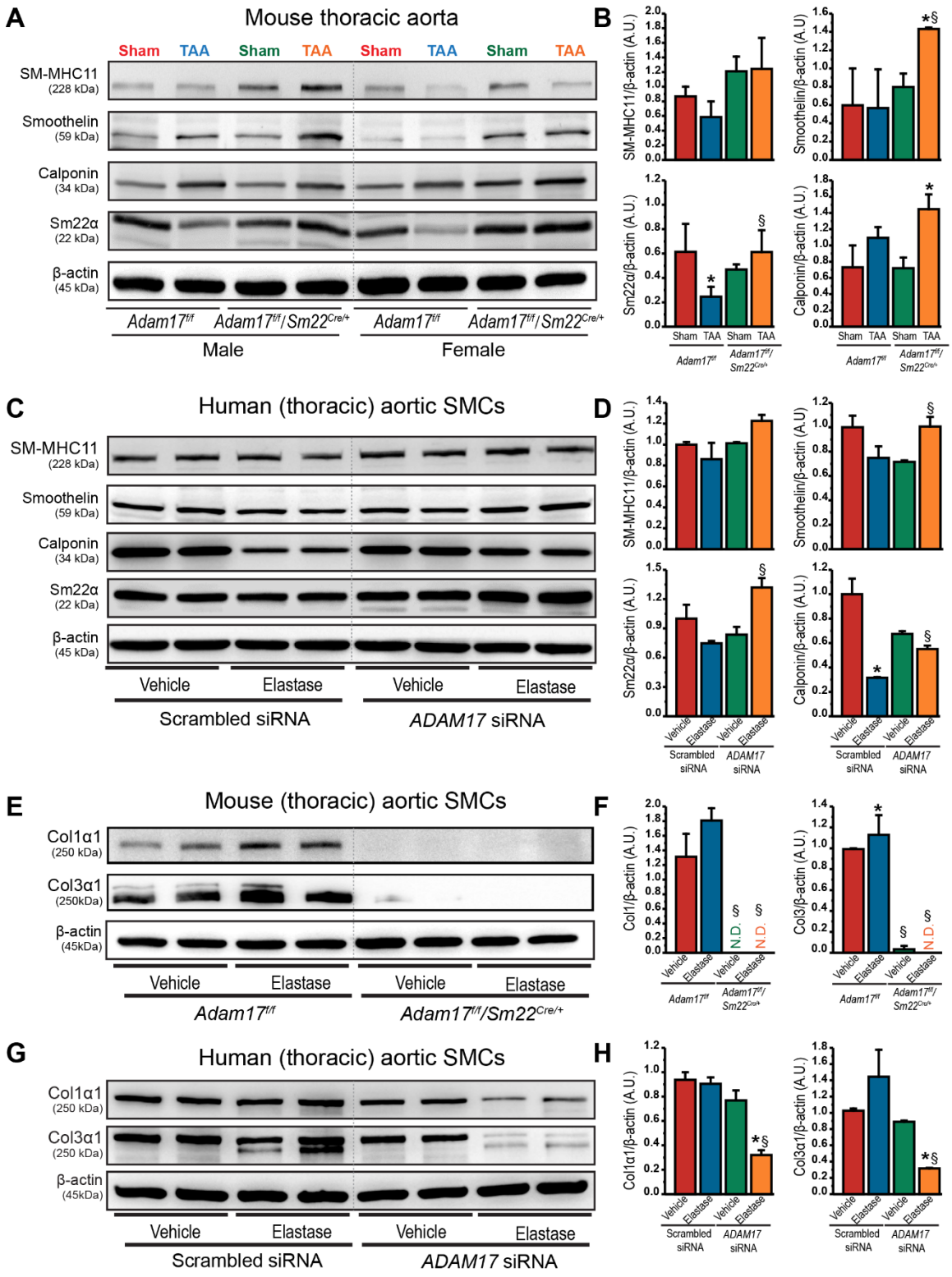

Figure 4.12 ADAM17 loss abolishes disease-induced contractile-to-synthetic phenotype switching in smooth muscle cells (SMCs). (**A**) Representative immunoblots for contractile proteins SM-MHC11, smoothelin, calponin and Sm22α in thoracic aorta from *Adam17*-intact (*Adam17*$^{f/f}$) and SMC *Adam17*-deficient (*Adam17*$^{f/f}$/*Sm22*$^{Cre/+}$) mice (male and female), following sham or 3 days post-TAA. (**B**) Densitometric quantification for each group (both sexes)

is shown. (**C**) Human thoracic aorta SMCs were transfected with scrambled or *ADAM17* siRNA and subjected to vehicle or elastase treatment (0.4 U/ml, 5 min). Representative immunoblots (**C**) and averaged quantification (**D**) for contractile proteins SM-MHC11, smoothelin, calponin and sm22α are shown. Mouse thoracic aorta SMCs from *Adam17*-intact and -deficient mice (**E-F**), and human thoracic SMCs transfected with scrambled or *ADAM17* siRNA (**G-H**), show a significant reduction in collagen type I and type III levels with ADAM17 loss. Bar graphs in panels (**F**) and (**H**) show densitometric quantification of the corresponding protein bands. All the immunoblots were repeated for 3-5 times, and the quantitative values in each experiment were normalized to that of *Adam17*-intact vehicle control within each set of experiments. **P*<0.05 compared to corresponding vehicle group; §*P*<0.05 compared to the corresponding *Adam17*-intact group; using 2-way ANOVA followed by Bonferroni's *post-hoc* test. Averaged values are presented as Mean ± SEM. A.U., arbitrary units. SM-MHC11, smooth muscle myosin heavy chain 11; TAA, thoracic aortic aneurysm. ADAM17, a disintegrin and metalloproteinase 17; *Adam17*$^{f/f}$, *Adam17*$^{flox/flox}$; *Adam17*$^{f/f}$*/Sm22*$^{Cre/+}$, *Adam17*$^{flox/flox}$*/Sm22αCre*.

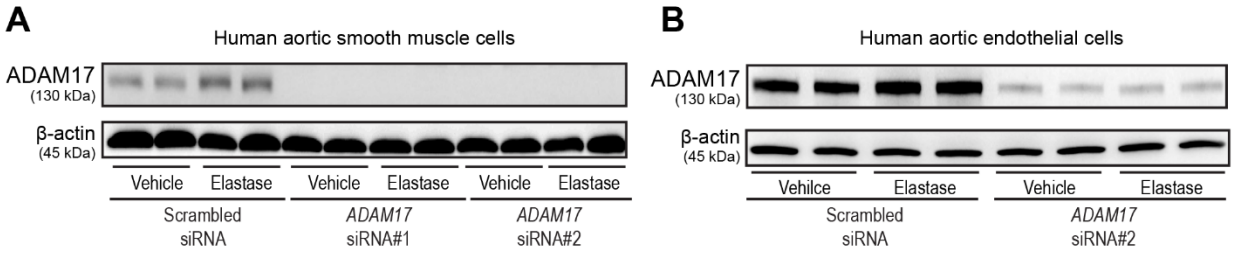

Figure 4.13 *ADAM17* siRNAs sufficiently knockdown ADAM17 in both human aortic smooth muscle cells (SMC) and endothelial cells (EC). (**A**) A representative immunoblot showing ADAM17 knockdown efficiency by two specific *ADAM17* siRNAs (#1 and #2) in human aortic SMCs. (**B**) A representative immunoblot showing ADAM17 knockdown efficiency in human aortic ECs transfected with *ADAM17* siRNA #2. Elastase-treated human aortic SMCs and ECs (+scrambled siRNA) showed increased ADAM17 expression levels. For both cell types, the data shown are representatives of three independent experiments. ADAM17, a disintegrin and metalloproteinase 17.

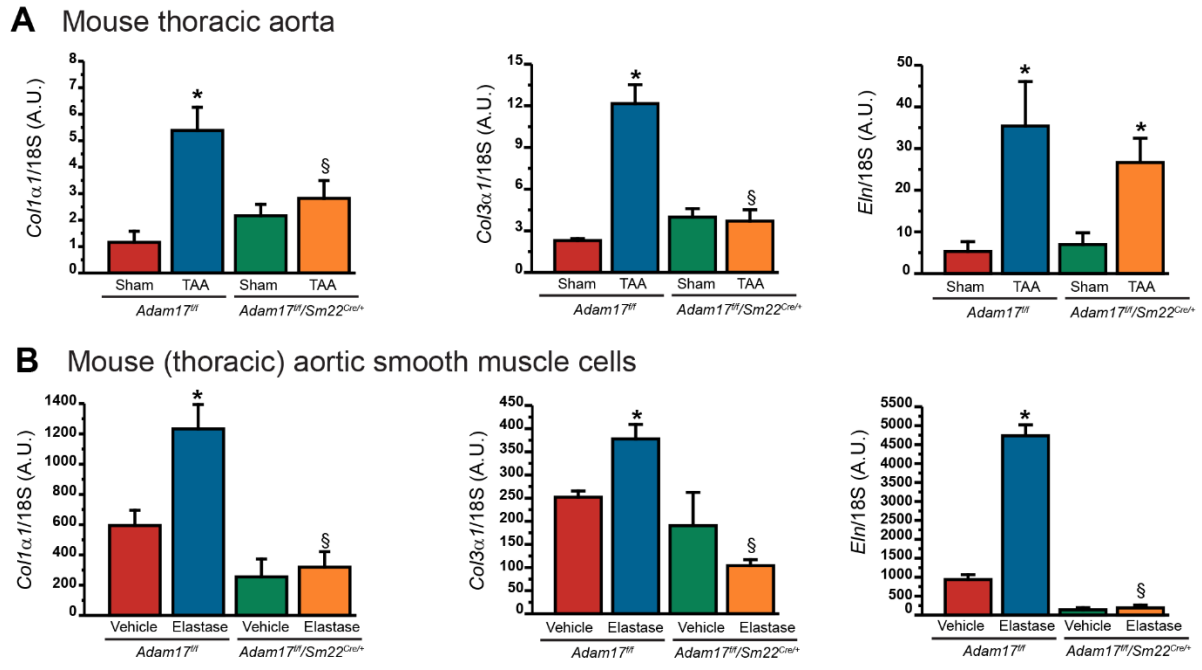

Figure 4.14 *Adam17*-deficiency blunts elastase-triggered upregulation of extracellular matrix protein in aortas and SMCs. (**A**) TaqMan mRNA expression of Col1a1, Col3a1, and Eln in thoracic aortic (tunica media) of *Adam17*-intact (*Adam17*$^{f/f}$) and SMC *Adam17*-deficient (*Adam17*$^{f/f}$*/Sm22*$^{Cre/+}$) mice at baseline (sham) and 3 days post-TAA. *n*=12 per group (male and female). (**B**) Taqman mRNA expression of *Col1a1*, *Col3a1*, and *Eln* mRNA expression

levels in cultured SMCs isolated from the thoracic aorta of *Adam17*-intact (*Adam17$^{f/f}$*) and SMC *Adam17*-deficient (*Adam17$^{f/f}$/Sm22$^{Cre/+}$*) mice, treated with vehicle or elastase (0.4 U/ml, 5min). The data shown are from three independent sets of SMC isolations, and for each experiment, each group was run in triplicates. **P*<0.05 compared to the corresponding sham group; §*P*<0.05 compared to corresponding *Adam17$^{f/f}$* group using 2-way ANOVA followed by Bonferroni's *post-hoc* test. Averaged values are Mean ± SEM. Eln, Elastin; *Col1a1*, collagen type I alpha 1 chain; *Col3a1*, collagen type 3 alpha 1 chain; 18S, ribosomal RNA and internal control for mRNA expression; A.U., arbitrary unit. TAA, thoracic aortic aneurysm. ADAM17, a disintegrin and metalloproteinase 17; *Adam17$^{f/f}$*, *Adam17$^{flox/flox}$*; *Adam17$^{f/f}$/Sm22$^{Cre/+}$*, *Adam17$^{flox/flox}$/Sm22αCre*.

4.3.5. Endothelial ADAM17 is a key regulator of intercellular endothelial adhesion by proteolytic processing of adherens junction and tight junctions

To investigate the mechanism underlying the protective effects of endothelial *Adam17*-deficiency in TAA, we first examined if the aortic intimal layer was damaged following TAA injury *in vivo*. Using an established *in vivo* Evans blue permeability assay (541), the permeability of the aortic intima was assessed at 3 days post-TAA in *Adam17$^{f/f}$* and *Adam17$^{f/f}$/Tie2$^{Cre/+}$* mice. Whole aorta pictures clearly showed a strong presence of Evans Blue dye (blue color) in the thoracic region of the aorta from *Adam17$^{f/f}$* mice, but not in *Adam17$^{f/f}$/Tie2$^{Cre/+}$* mice (**Figure 4.15A**). Permeation of Evans blue dye through the aortic wall was confirmed in cross-section images of the thoracic aorta showing a stronger autofluorescence signal of Evans Blue (red) in *Adam17$^{f/f}$* compared to *Adam17$^{f/f}$/Tie2$^{Cre/+}$* mice, while elastin autofluorescence appears green (**Figure 4.15A-insets**).

To directly examine the function of ADAM17 in permeability of ECs, we used an *in vitro* permeability assay where monolayers of human aortic endothelial cells (HAoEC) were transfected with scrambled siRNA (control) or with *ADAM17* siRNA to knock down *ADAM17* (**Figure 4.13B**). Elastase treatment increased the permeability of *ADAM17*-intact cells, but to a significantly lower extent in *ADAM17*-deficient HAoECs (**Figure 4.15B**). Vehicle-treated cells from both groups served as controls and showed no increase in permeability over the 3-hour course of the experiment confirming intact monolayers (**Figure 4.15B**). VE-cadherin is a key adhesion molecule responsible for the intercellular connection of neighboring ECs (542, 543). In *ADAM17*-intact ECs, elastase treatment triggered VE-cadherin shedding as evident by the increased levels of soluble VE-cadherin in the conditioned media, whereas *ADAM17*-deficient HAoECs showed a minimal rise in levels of soluble (shed) VE-cadherin in the conditioned media (**Figure 4.15C**). Immunofluorescence co-staining for VE-cadherin and F-actin in HAoECs revealed diminished

presence of VE-cadherin (red), and formation of stress fibers (F-actin, green), following elastase treatment in *ADAM17*-intact HAoECs (**Figure 4.15D**). In *ADAM17*-deficient HAoECs, however, presence and arrangement of VE-cadherin were significantly preserved, and formation of stress fibers was not evident following elastase treatment (**Figure 4.15D**). Merged images of VE-cadherin and F-actin provide further evidence that *ADAM17* knockdown protected the endothelial cells against elastase-induced disruption of cell-cell adhesion and preserved the integrity of the endothelial monolayer (**Figure 4.15D**). Immunoblotting on protein extracts from these cells further demonstrated reduced membrane-bound VE-cadherin levels in elastase-treated *ADAM17*-intact, but not in *ADAM17*-deficient HAoECs (**Figure 4.15, E and F**). Moreover, junctional adhesion molecule-A (JAM-A) and claudin-5, two major tight junction proteins important for endothelial barrier integrity (542, 544), reported as substrates for ADAM17 (106, 115, 492), were present at higher levels in *ADAM17*-deficient HAoECs following elastase exposure (**Figure 4.15, E and F**). Vinculin, a mechanosensory protein that is upregulated to repair the impaired EC barrier, was markedly elevated in elastase-treated *ADAM17*-intact compared to *ADAM17*-deficient cells (**Figure 4.15, E and F**). In our analysis of other adhesion molecules involved in endothelial cell adhesion, we found that neither catenin molecules (alpha, beta, or gamma), nor their phosphorylation, were altered by elastase treatment or *ADAM17* knockdown in HAoECs (**Figure 4.16A**). Similarly, total and phosphorylated levels of paxillin (member of focal adhesion complex) was comparable among all groups, while phosphorylated focal adhesion kinase (pFAK) was reduced in elastase-treated *ADAM17*-deficient HAoECs consistent with less stress fiber formation in these cells (**Figure 4.16B**). These *in vivo* and *in vitro* data collectively demonstrate that ADAM17 is a key regulator of EC permeability through proteolytic processing of adherens junction and tight junctions.

4.3.6. Pharmacological inhibition of ADAM17 suppressed the onset of TAA formation as well as the growth of small TAA

To explore the therapeutic application of ADAM17 inhibition in TAA, we used a pharmacological ADAM17-selective inhibitor (PF-548) to determine if ADAM17 inhibition can prevent TAA formation (**Figure 4.17, A-D**), and/or can prevent further growth of a small aneurysm after it has formed (**Figure 4.17, E-H**). Administration of PF-548 *prior* to TAA induction (**Figure 4.17A**) significantly suppressed the severity of TAA dilation and aortic wall damage in wildtype

mice as evident in macroscopic images of the whole aorta (**Figure 4.17B**), the markedly preserved elastin lamellae structure in VVG-stained aortic cross-sections (**Figure 4.17C**), and the smaller thoracic aortic diameter in mice receiving PF-548 (**Figure 4.17D**). More intriguingly, administration of PF-548 three days *after* TAA induction (**Figure 4.17E**) effectively prevented further progression of aortic dilation and formation of thoracic aneurysm (**Figure 4.17F**), elastin fiber degradation (**Figure 4.17G**), and the significantly smaller aortic diameters (**Figure 4.17H**). Consistent with these beneficial outcomes, PF-548 was elevated in plasma (**Figure 4.18A**) and markedly reduced TAA-induced rise in ADAM17 activity (**Figure 4.18B**). In addition, pre- or post-TAA treatment with PF-548 significantly hindered vascular inflammation (**Figure 4.18, C and G, D and H**), diminished adventitial collagen deposition and fibrosis (**Figure 4.18, E and I**), and preserved SMC density (**Figure 4.18, D and J**) in the thoracic aortic wall. Therefore, pharmacological inhibition of ADAM17 that inhibits this enzyme in both SMCs and ECs, effectively protects against the TAA-induced maladaptive remodeling and disease progression.

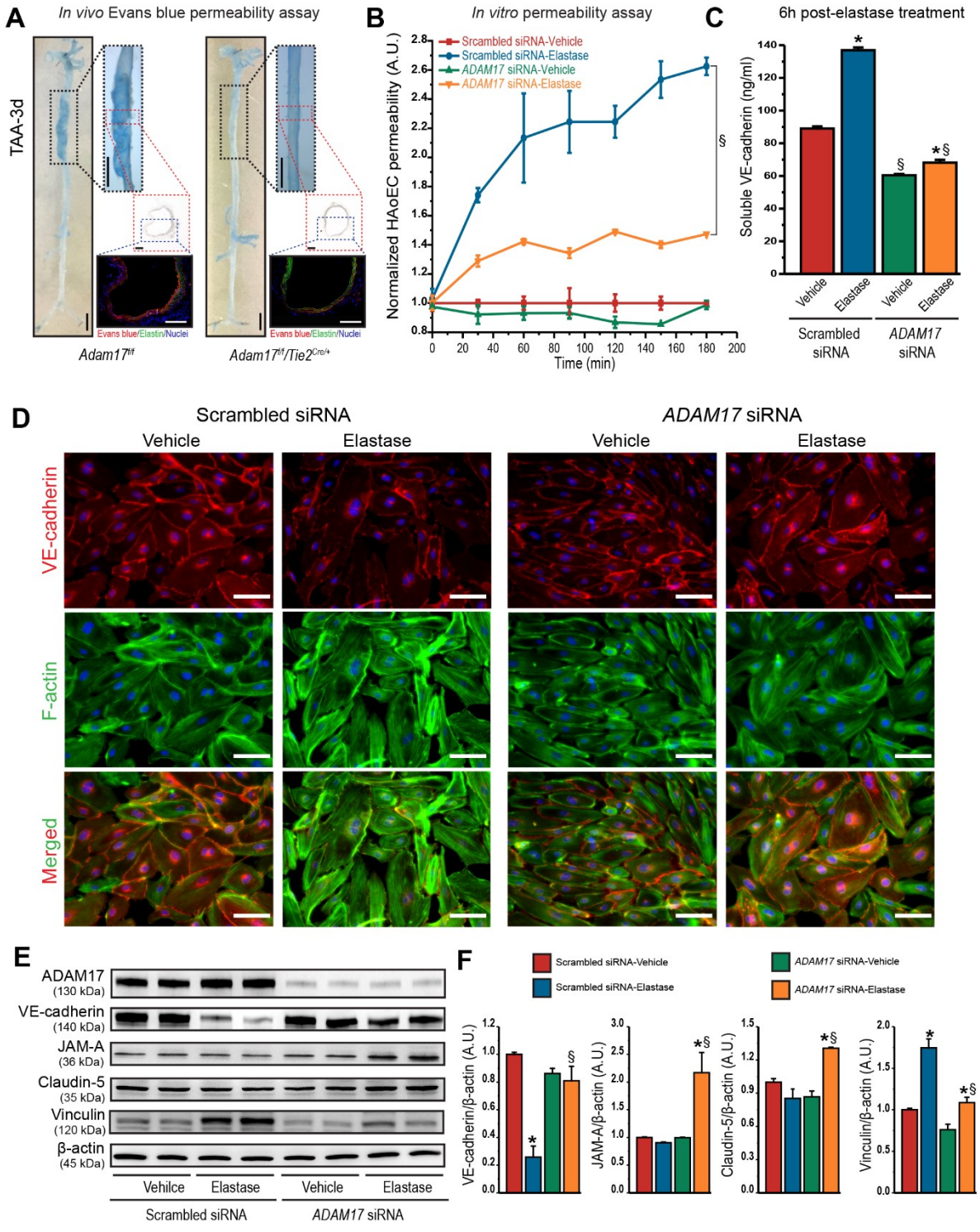

Figure 4.15 Deletion of ADAM17 in ECs attenuates elastase-induced permeability *in vivo* and *in vitro*. (**A**) Male *Adam17*-intact (*Adam17*$^{f/f}$) and EC *Adam17*-deficient (*Adam17*$^{f/f}$/*Tie2*$^{Cre/+}$) mice received Evans blue dye (1% w/v in PBS, sub-retinal injection) at 3 days post-TAA, aortas were collected and cryopreserved. Representative whole aorta and cross-section images show more Evans blue dye (red autofluorescence) in the aortic wall of *Adam17*-intact mice compared to EC *Adam17*-deficient mice (green, elastin fiber autofluorescence). *n*=8 per genotype. Scale bars: 200 µm. (**B**) Human aortic ECs (HAoECs) were transfected with scrambled or *ADAM17* siRNA, seeded in collagen-coated

porous cell culture inserts, allowed for monolayer formation, treated with vehicle or elastase (0.4 U/ml, 5min), followed by fresh media containing FITC-Dextran. Permeation of FITC-Dextran through the EC monolayer to the receiving chamber was measured over 3 hrs. (**C**) HAoECs transfected with scrambled or *ADAM17* siRNA, and treated with vehicle/elastase as above. After 6 hrs, significantly lower levels of soluble (shed) VE-cadherin was detected in the conditioned media of *ADAM17*-deficient ECs (ELISA). (**D**) Cultured HAoECs transfected with siRNA and treated with elastase as above. After 6 hrs, cells were fixed and stained for VE-cadherin (red) and stress fibers (Alexa Fluor 488-Phalloidin, green). Representative images show disrupted VE-cadherin integrity and increased the presence of stress fibers after elastase treatment in control, but not in *ADAM17*-deficient HAoECs. Scale bars: 100 μm. Representative immunoblots (**E**) and quantification (**F**) of protein levels for ADAM17, VE-cadherin (adherens junction), JAM-A and claudin-5 (tight junctions), and vinculin (a marker of impaired EC adhesion) in HAoECs in the indicated groups. All *in vitro* data are from three independent experiments, and samples were run in triplicates each time. **P*<0.05 compared to corresponding vehicle group; $^{\S}P$<0.05 compared to the corresponding *ADAM17*-intact group, using 2-way ANOVA followed by Bonferroni's *post-hoc* test. Average values are mean ± SEM. A.U., arbitrary units; VE-cadherin, vascular endothelial cadherin; JAM-A, junctional adhesion molecule-A. TAA, thoracic aortic aneurysm. ADAM17, a disintegrin and metalloproteinase 17; *Adam17*$^{f/f}$, *Adam17*$^{flox/flox}$; *Adam17*$^{f/f}$*/Sm22*$^{Cre/+}$, *Adam17*$^{flox/flox}$*/Sm22αCre*.

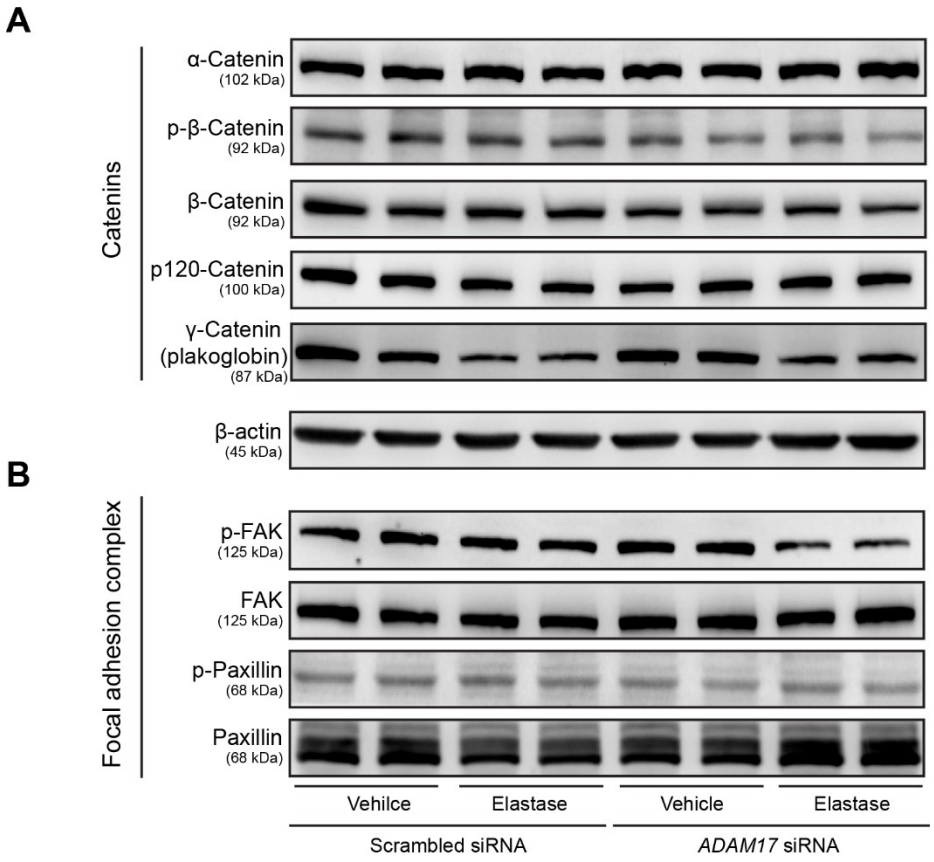

Figure 4.16 Protein levels of adhesion complex molecules were not altered by elastase treatment nor by *ADAM17*-deficiency in human aortic endothelial cells (HAoECs). (**A**) Representative immunoblots for α-catenin, phospho- and total-β-catenin, p120-Catenin, and γ-catenin (or plakoglobin) in primary HAoECs with intact *ADAM17* (scrambled siRNA) or *ADAM17*-knockdown (*ADAM17* siRNA) following elastase treatment. (**B**) Representative immunoblots for phosphorylated- and total focal adhesion kinase (FAK) and paxillin, components of the focal adhesion complex in the indicated groups.

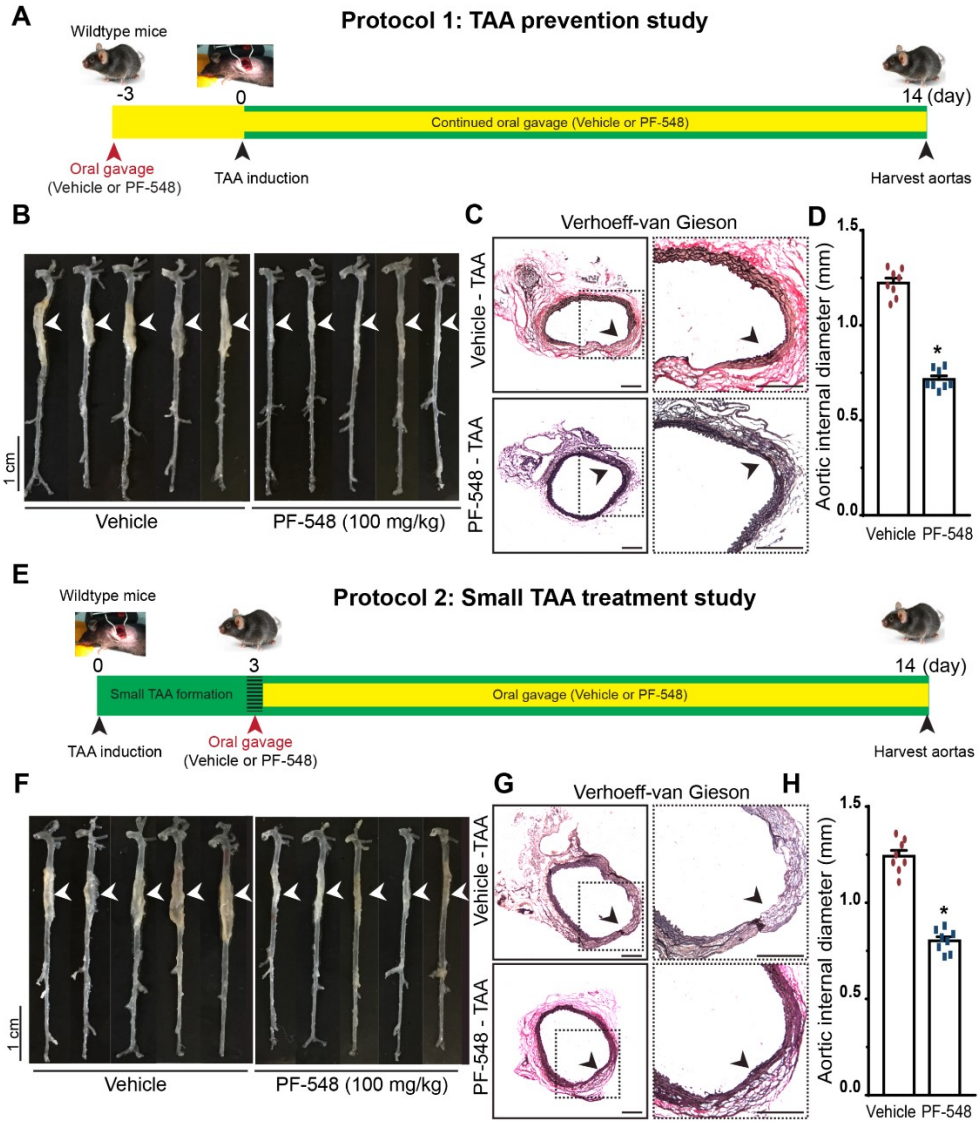

Figure 4.17 Administration of a selective pharmacological ADAM17 inhibitor (PF-548) suppresses elastase-induced TAA formation (Protocol 1), and growth of small aneurysms (Protocol 2). (**A-D**) Protocol 1: (**A**) WT male mice were randomly divided into two groups to receive vehicle or a selective ADAM17 inhibitor PF-5480090 (PF-548) (oral gavage) starting 3 days PRIOR to TAA induction and for 14 days. (**B**) Representative pictures of whole aortas harvest at day 14 post-TAA in each group. *n*=8 per group. Arrows indicate the site where elastase solution was applied. Scale bar:1 cm. (**C**) Representative images of thoracic aorta cross-sections showing the elastic fiber structure (Verhoeff-van Gieson staining). The image on the right is a higher magnification of the area within the dotted-line frame. Arrows point to the site of elastase application highlighting the partially preserved elastin lamellae in the group that received PF-548. Scale bars: 200 µm. (**D**) Average internal diameter of thoracic aorta. *n*=8 per group. (**E-H**) Protocol 2: (**E**) WT male mice underwent TAA induction, on day 3 post-TAA when small aneurysms were formed, mice were randomly divided into two groups to receive vehicle or PF-548 (oral gavage) for the remaining duration of the experimental protocol. (**F**) Representative pictures of whole aortas harvested at day 14 post-TAA in each group. Arrows indicate the site where elastase solution was applied. Scale bar:1 cm. (**G**) Representative images (low and high magnifications) of thoracic aorta cross-sections showing the elastic fiber structure (Verhoeff-van Gieson staining). Arrows point to the site of elastase application and the partially preserved elastin lamellae in the PF-548 group. Scale bars: 200 µm. (**H**) Averaged internal aortic diameter in mice with established small TAAs, receiving vehicle or PF-548. *n*=8 per group. **P*<0.05 compared to vehicle group, 1-way ANOVA followed by Bonferroni's *post-hoc* test. Averaged values in bar graphs are mean ± SEM. TAA, thoracic aortic aneurysm.

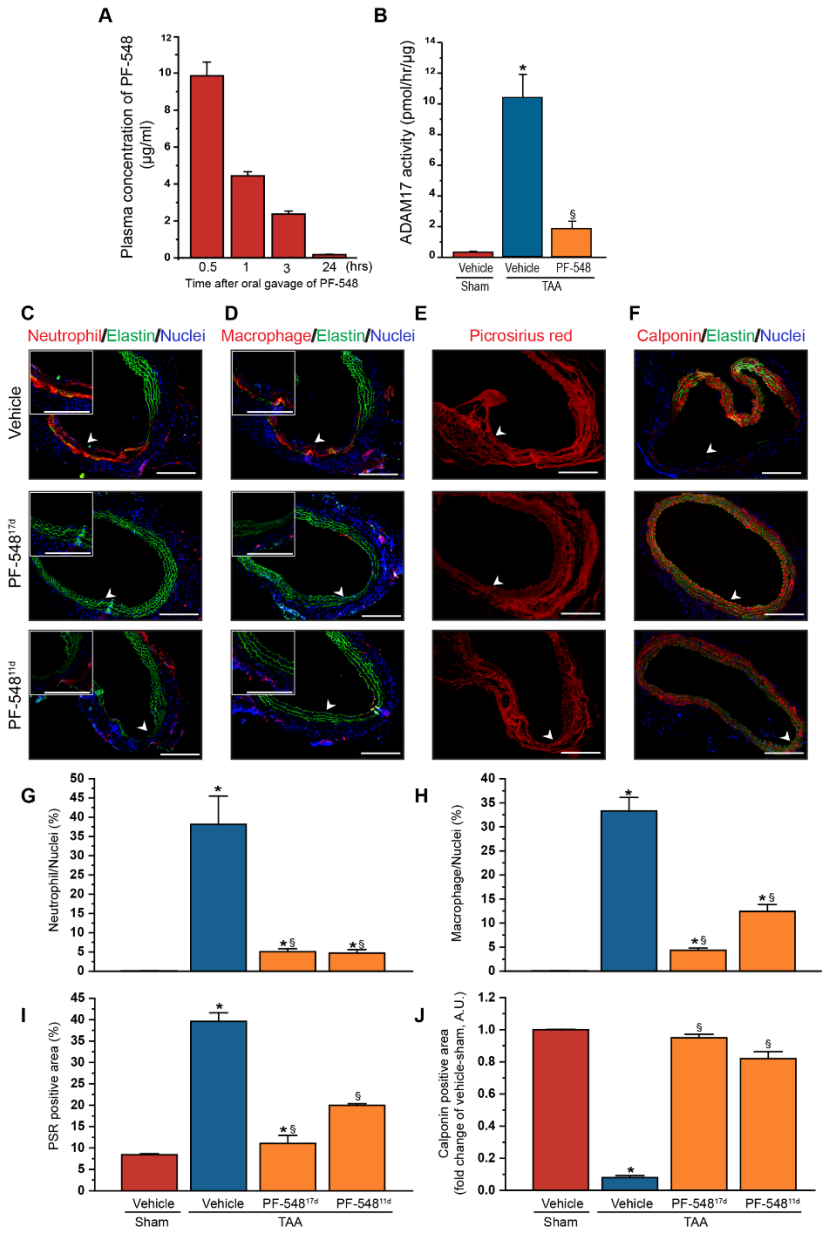

Figure 4.18 Pharmacological ADAM17 inhibition (by PF-548) efficiently inhibited ADAM17 activity and abolished elastase-induced inflammatory cell infiltration, collagen deposition, and SMC loss in the aortas. (**A**) Plasma concentrations of PF-548 at indicated times after one-time oral gavage (100 mg/kg). (**B**) ADAM17 enzymatic activity was significantly increased in the aneurysmal aortas of vehicle-treated WT mice, and was significantly lower in the aortas of WT mice receiving PF-548 treatment. n=5 per group. *P<0.05 compared to sham; $^{\S}P$<0.05 compared to vehicle-TAA group using 1-way ANOVA followed by Bonferroni's *post-hoc* test. Values in all bar graphs are presented as mean ± SEM. Representative immunofluorescent staining images and quantification show decreased neutrophil (Ly6G, red) (**C and G**), macrophage (CD68, red) (**D and H**) infiltration into the aortic walls of WT mice receiving PF-548 prior to (PF548^{17d}), or after (PF548^{11d}) TAA induction, compared to vehicle. Scale bars: 200 μm. n=8 per group. Representative fluorescent images and quantification showing less collagen deposition (Picrosirius red staining) (**E and I**), and more preserved SMCs (calponin^{+}, red) **(F and J)** in the aortic media of WT mice receiving PF-548 prior to, or after TAA induction compared to vehicle. Scale bars: 200 μm. n=8 per group. *P<0.05 vs sham-vehicle; $^{\S}P$<0.05 *vs* vehicle-TAA group (one-way ANOVA, Bonferroni's *post-hoc* test). Values represent mean±SEM. Arrows in all images indicate the site where elastase solution was initially applied. PF-548, an ADAM17-selective inhibitor.

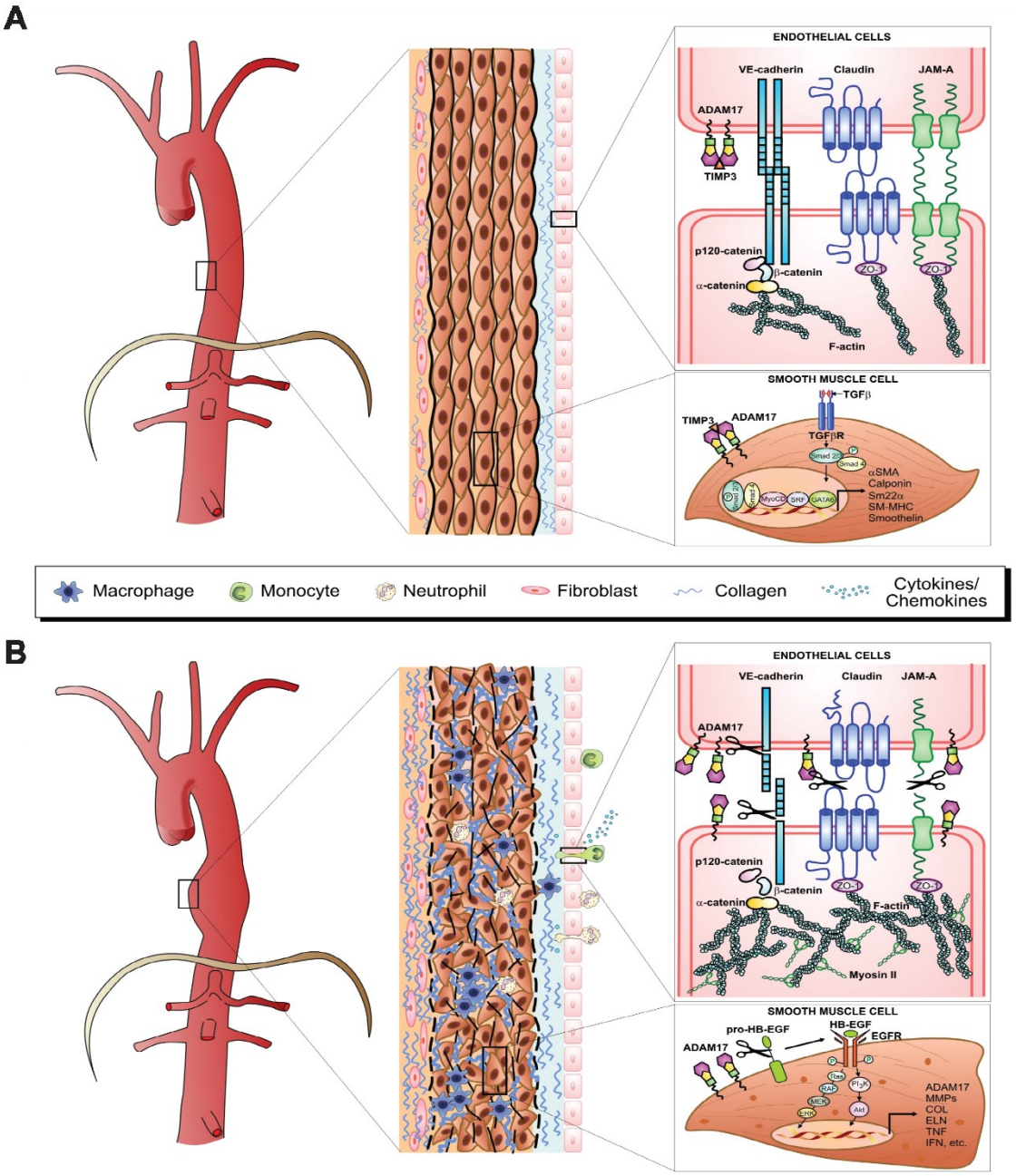

Figure 4.19 Illustration of how the injury-induced increase in ADAM17 levels increases the permeability of endothelial cells (EC), and triggers the phenotype switch in smooth muscle cells (SMC) in TAA. (**A**) Healthy aorta with intact intimal barrier (intact EC-EC adhesion), healthy medial layer with intermittent SMCs and elastin fiber arrangements. (**B**) Aortic wall after TAA. ADAM17 levels are increased in both ECs and SMCs. In ECs, it mediated proteolysis of junction molecules disrupted the EC-EC adhesion and compromised the intimal barrier allowing for infiltration of inflammatory cells. In SMCs, ADAM17 causes transformation to the synthetic phenotype, expressing excess matrix proteins, proteases (MMPs), and cytokines. In the medial layer, the lamellar units are disrupted because of SMC death, collagen deposition, fragmented elastin (that acts chemoattractants), as well as adventitial fibrosis.

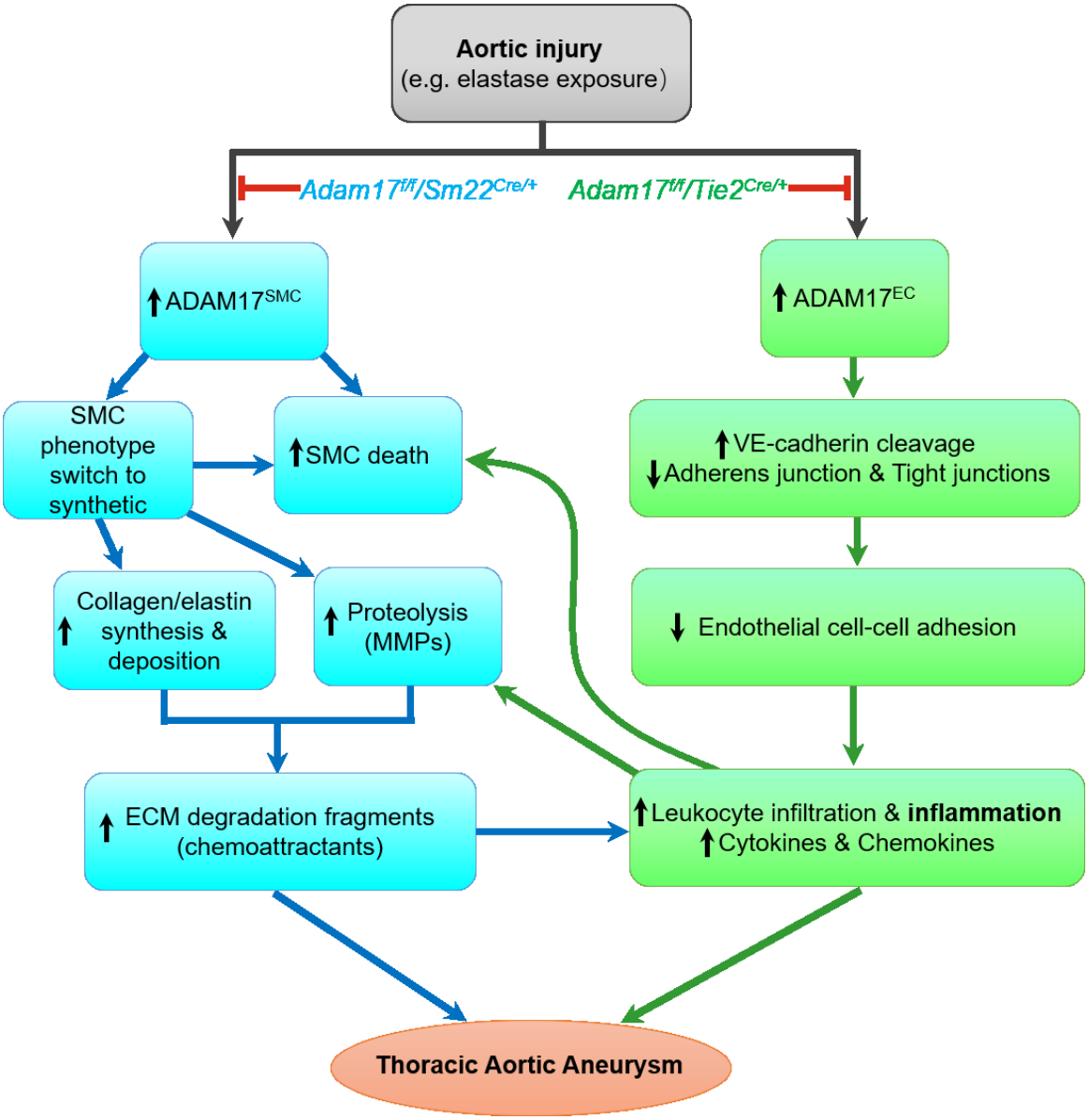

Figure 4.20 A schematic demonstration of the cellular events following injury that leads to the formation of thoracic aortic aneurysm. The rise in ADAM17 levels in smooth muscle cells (SMC) and endothelial cells (EC) initiates an orchestrated series of events that collectively lead to the formation of thoracic aortic aneurysm (TAA). Loss of ADAM17 in either cell type (SMC or EC) is sufficient to prevent the formation of TAA.

4.4. Discussion

Despite the rising prevalence and the adverse prognosis associated with TAA in both men and women, TAA has remained a less explored type of aortic aneurysm. In this study we report that in TAA, the increased ADAM17 activity in the aortic intimal and medial layers orchestrates cellular and molecular responses that lead to SMC phenotypic switching (to a synthetic phenotype) and to compromised endothelial barrier integrity, leading to excess matrix synthesis and deposition, cell death, inflammation, overall adverse structural remodeling, and aneurysm formation in the injured aorta (**Figure 4.19**). We demonstrate that ADAM17 mediates different molecular events in SMCs versus the ECs based on our findings in cell-specific *Adam17*-deficient mice, *in vivo* model of TAA, and *in vitro* primary culture of murine and human aortic SMCs and ECs. The protective effects of genetic deletion of *Adam17* were recapitulated by a pharmacological ADAM17-selective inhibitor, PF-548, that was effective when administered prior to, or early after induction of TAA.

We used an adventitial elastase-exposure model of TAA which shares the characteristics of aortic aneurysm in patients since adventitial elastolysis has been reported to be an early event in AAA patients (532),and adventitial damage and inflammation have been reported as common features of aortic aneurysm (545). Our *in vivo* and *in vitro* experiments reveal that *Adam17* knockdown in SMCs preserves the contractile properties of these cells and hinders their conversion to the synthetic phenotype. A phenotypic switch of SMCs in the aorta, from contractile to synthetic phenotype, is often associated with aortic diseases (546). During this phenotypic transition, SMCs exhibit decreased contractile protein content, decreased contractility, increased secretion of proinflammatory cytokines, adhesion molecules and matrix metalloproteins, giving rise to a pro-inflammatory and highly proteolytic environment that promotes adverse remodeling of the aorta (396). We previously reported that SMC proliferation and migration induced by angiotensin II, a hormone commonly elevated in cardiovascular diseases, was blunted in *Adam17*-deficient SMCs (214), due to the reduced ADAM17-dependent shedding of heparin-binding EGF-like growth factor (HB-EGF), a ligand for epidermal growth factor receptor (EGFR) (214). *Adam17*-knockdown in SMCs attenuated abdominal aortic aneurysm (AAA) induced by combined administration of angiotensin II and a lysyl oxidase inhibitor (BAPN), mainly through inhibition of EGFR activation (414). Activation of EGFR has also been linked to the SMC phenotypic switching which can explain the role of ADAM17 in this transformation. Notably, mutations in

genes coding for vascular SMC contractile apparatus, such as α-smooth muscle actin, SM-MHC11, and myosin light chain kinase have been identified as the underlying etiologies for a group of familial TAAs in humans (360). A genome-wide copy number variant analysis also suggested that disrupted SMC contractile apparatus is involved in the pathogenesis of sporadic TAAs (547, 548). Our current study demonstrates for the first time that ADAM17-deficiency, indeed preserves the contractile properties of the SMCs and prevents them from transforming to a pathological state.

ADAM17 can mediate proteolytic shedding of various transmembrane proteins (517). Here, we identified members of the adherens junction (VE-cadherin) and tight junctions (JAM-A and Claudin) as the target substrates for ADAM17 in TAA. We used a tamoxifen-inducible *Tie2-MerCreMer* to generate endothelial *Adam17*-deficiency in adult mice ($Adam17^{f/f}/Tie2^{Cre/+}$) rather than the constitutively active *Tie2-Cre* recombinase mice. Tie2 is also expressed in hematopoietic cells during embryonic development and in early weeks after birth, and ADAM17knockdown in hematopoietic cells could adversely impact the physiological development of the animals (504, 505), as well the inflammatory response that is a key characteristic of post-TAA events. The inducible expression of *Tie2-MerCreMer* recombinase has been demonstrated to only target ECs (503, 533). Endothelial *Adam17*-deficiency markedly suppressed the presence of TAA-induced inflammatory cytokines, chemoattractants and CSFs in the aorta. Tissue-resident CSFs are involved in tissue inflammation in response to injury, and have distinct receptors that are expressed on monocytes, macrophages, neutrophils, and eosinophils. G-CSF, GM-CSF and M-CSF target monocytes, macrophages and neutrophils to increase their population in the injured tissue. M-CSF is often present at very low levels but are elevated with inflammatory stimuli and macrophage accumulation (536). G-CSF is a major factor in neutrophil recruitment and activation (398). Consistent with our finding that reduced IFNγ post-TAA was concomitant with reductions in CXCL9 and CXCL10 in *Adam17*-deficient mice, IFNγ has been reported to induce the expression of CXCL9 and CXCL10 (549).

Overall, the suppressed inflammatory response in $Adam17^{f/f}/Sm22^{Cre/+}$ and $Adam17^{f/f}/Tie2^{Cre/+}$ mice was accompanied by a marked reduction in aortic dilation and TAA formation. The mechanism underlying the reduced inflammatory response, however, is different in each case. In $Adam17^{f/f}/Tie2^{Cre/+}$ mice, *Adam17*-deficiency in ECs preserved the inter-endothelial adhesion by preserving the structural integrity of cell-cell adhesions and intimal barrier, and thereby hindered

infiltration of inflammatory cells into the injured aortic wall. In *Adam17*$^{f/f}$/*Sm22*$^{Cre/+}$ mice, on the other hand, the reduced inflammation was secondary to the lower rate of SMC loss, reduced SMC phenotypic switching to a synthetic form, and reduced deposition of matrix proteins whose degradation products serve as chemoattractants for inflammatory cells (550). This interaction between the functions of SMCs and ECs explains why *Adam17*-deficiency in either cell type exerted protection against TAA injuries (**Figure 4.20**).

Although aortic inflammation is often attributed to infiltration of inflammatory cells through the intimal barrier, the vasa vasorum that provides perfusion to the adventitia has also been shown to contribute to inflammation of the aortic wall. This could occur through vasa vasorum neovascularization that would create a conduit for inflammatory cell transport into the arterial wall promoting inflammation. Alternatively, the injury-induced rise in ADAM17 in ECs that leads to endothelial defects resulting in impaired intimal barrier in the aortic lumen can also affect the endothelial cells present in the vasa vasorum, enhancing infiltration of inflammatory cells into the arterial wall (551). It has also been shown that ADAM17 is involved in angiogenesis (335, 336), and newly formed vessels may represent an alternative venue where inflammatory cells can infiltrate into the vascular wall. Therefore, endothelial *Adam17*-deficiency could preserve intimal integrity in the aortic lumen as well as in the vasa vasorum, thereby exerting a 2-fold protective effect in reducing inflammation in the aortic wall.

4.5. Conclusion

Collectively, our data provide strong evidence that ADAM17 plays distinct cell-specific functions that are central to the development of TAA. The cellular and molecular mechanisms underlying TAA are poorly understood, and clinical corrections require invasive surgical approaches. ADAM17 activity in the vascular smooth muscle cells and endothelial cells within the aortic wall may regulate aortic growth in aortopathies. These observations provide novel insights into molecular mechanisms of human aortic disease and the potential to discover effective therapeutic targets to prevent disease progression.

CHAPTER 5

DISCUSSION

5.1. Important findings

5.1.1. Deletion of SMC-specific Adam17 shows mild and transient protection against Ang II-induced hypertension and end-organ damage

Deletion of *Adam17* in SMCs only transiently suppressed Ang II-induced hypertension during the first week of Ang II infusion, and the protective effect was abolished with prolonged Ang II infusion. Consistent with the biphasic blood pressure changes, the early reduction in cardiac and renal hypertrophy and fibrosis in SMC *Adam17*-deficient mice eventually bounced up to the comparable level observed in control mice. Mechanistic studies showed that a drastic increase in EGFR signaling in the adventitial layer of SMC *Adam17*-deficient mice might compensate for the defective signal in the medial layer through a paracrine manner. Therefore, the biphasic response was attributed to a net increase in EGFR signaling in the whole aorta.

Interestingly, a pilot study (n=3 for control and knockout mice) demonstrated that EC *Adam17*-deficient mice persistently showed much lower blood pressure compared to control mice during 4 weeks of Ang II infusion. Numerous studies have confirmed that Ang II infusion can increase vascular and renal inflammatory cell infiltration (552-554), whereas mice lacking monocytes, macrophage, or lymphocytes are resistant to hypertension induced by Ang II (555-557). Therefore, the suppressed blood pressure observed in Ang II-infused EC *Adam17*-deficient mice could be attributed to preserved endothelial barrier integrity and the subsequent attenuation of inflammation and oxidative stress. Importantly, the observation also suggests a cell type-dependent (i.e., SMCs versus ECs) function of ADAM17 in hypertension.

5.1.2. Vascular ADAM17 plays cell-dependent roles in the pathogenesis of TAA

Although *Adam17*-deficiency in either SMCs or ECs attenuated the formation and progression of TAA-induced by periadventitial elastase treatment, the protective mechanisms are cell type-dependent. While loss of ADAM17 in SMCs prevented a contractile-to-synthetic switch in these cells, and thereby suppressed perivascular fibrosis, inflammation, and adverse aortic remodeling, loss of ADAM17 ECs protected vascular integrity by preserving junction proteins such as VE-cadherin, JAM-A, and claudin-5, and thereby limited infiltration of inflammatory cells into the aorta and the subsequent inflammatory response. Interestingly, an ADAM17-selective inhibitor

tested in this study not only inhibited TAA formation but also prevented further expansion of small aneurysm, highlighting a therapeutic value of ADAM17 inhibition to treat established TAA.

5.1.3. ADAM17 plays a crucial role in modulating SMC phenotypic switching

As compared to *Adam17*-intact SMCs, deletion of *Adam17* did not change either the morphology or expression levels of contractile proteins such as SMA, calponin, SM-MHC, SM22α, and smoothelin in SMCs at baseline. However, it suppressed Ang II-induced cell proliferation and migration as a result of blunted EGFR-dependent signaling. Moreover, the expression levels of SMC-specific contractile proteins and ECM proteins (e.g., collagen I, collagen III, and elastin) were drastically downregulated and upregulated in *Adam17*-intact SMCs, respectively, after they were exposed to elastase, a trigger could cause cell injury. In comparison, ADAM17-deficient SMCs showed opposite phenotypes in response to acute exposure of elastase. Since the remarkable plasticity of SMCs has been implicated in a number of cardiovascular diseases, preserving the contractile phenotype of SMCs by inhibiting excessive ADAM17 activity may render beneficial effects on various vascular diseases other than aortic aneurysm, such as atherosclerosis and restenosis.

5.1.4. Periadventitial elastase-injury induced TAA model represents an ideal currently available disease model for TAAs

The TAA model I optimized in this study was originally developed by Johnston, *et al.* (381). However, since undiluted porcine pancreatic elastase solution was used in their study, the TAA phenotype they generated may not be reproducible by other groups or even by the same group if another batch of elastase was used. It is because the commercial available porcine pancreatic elastase usually shows a batch-to-batch variation in terms of its enzymatic activity. Moreover, there is also a possibility that the genetic impact on the pathogenesis of aneurysm would be plateaued if elastase-induced vascular injury is too severe. Therefore, in this study I conducted a screening panel to test for the optimal elastase concentration by diluting stock elastase to generate a serial of elastase working solutions ranging from 10 U/ml to 50 U/ml. All the elastase working solutions were used to treat the descending thoracic aortas of wildtype male mice of the same age identically, and the aortas were harvested after 14 days post-operation to evaluate the TAA phenotypes. Based on the assessment of general macroscopic morphology (i.e., aortic dilation) and main features of

TAA (e.g., elastic fiber fragmentation, SMC apoptosis, inflammatory cell infiltration, and perivascular fibrosis), I found that 30 U/ml is the optimal concentration for the TAA model. Since I observed that the reproducible TAA phenotype is dosage-dependent and elastase batch-independent, this TAA model might be suitable for interlaboratory and intralabortory comparison. More importantly, this TAA model resembles the characteristics of the early onset (e.g., adventitial elastolysis) and the advanced stage (e.g., cystic necrosis, inflammation, and ECM disruption) of human TAA. The optimized TAA model also showed a Th1-predominant inflammatory response, which has been well-documented in human TAA specimens (440). Overall, the TAA model I optimized in this study is reproducible and can recapitulate main features of human TAA, and therefore, can be used to explore the underlying mechanism for a pathological cue of interest that can contribute to the pathogenesis of sporadic TAAs.

5.2. SMC plasticity contributes to vascular remodeling

The vascular SMCs are a highly specialized cell type whose principal functions are contraction and blood pressure regulation. Under the basal state, SMCs within adult blood vessels show extremely low proliferation and synthetic activity, and express a unique repertoire of contractile proteins, ion channels, and signaling molecules for their contraction function (459). However, the nature of phenotypic plasticity makes the SMCs drastically increase their rate of proliferation, migration, and synthetic capacity in response to any stimuli that can cause vascular injury. Although this reversible phenotypic switching nature of SMCs plays a critical role in vascular repair, substantial changes in SMC morphology and functions have been proved to contribute to a number of major diseases in humans, including hypertension, atherosclerosis, and aortic aneurysm.

Although the etiology is extremely complex, a common feature of hypertension is an increase in peripheral resistance as a result of increased vascular tone (net outcome of SMC contractility) and vascular remodeling. It has been well-recognized that Ang II, the most important endocrine ligand in the renin-angiotensin system, contributes to hypertension and various cardiovascular complications via activation of protein kinases, generation of ROS, and induction of remodeling and inflammation. It has been shown that Ang II activates Erk1/2 via AT1 receptor-mediated EGFR transactivation in SMCs (515). Moreover, EGFR transactivation is also involved the activation of other downstream kinases, such as Akt, p70 S6 kinase, and p38, which collectively contribute to

hypertrophic response in SMCs (558, 559). *In vitro*, SMC *Adam17*-inactivation suppressed Ang II-induced SMC hypertrophy as a net outcome of EGFR suppression (317). In the current study, I observed that SMC *Adam17*-deficiency abolished Ang II-mediated cell proliferation and migration. *In vivo*, *Adam17*-deficiency in SMCs was first reported to protect against Ang II-induced vascular fibrosis and cardiac hypertrophy after a short term of infusion (311). However, our study revealed that this protective effect was transient, and it was abolished with prolonged Ang II infusion. I further demonstrated that the transient protective effect against Ang II-induced cardiac and renal hypertrophy occurred in parallel to the less severe Ang II-induced hypertension in SMC *Adam17*-deficiency mice. Although suppressed SMC hypertrophy may contribute to the delayed blood pressure increase in SMC *Adam17*-deficiency mice during the first week of Ang II infusion, ADAM17-mediated biological signaling other than the EGFR pathway seems to be more important to regulate Ang II-mediated hypertension. Indeed, systemic inhibition of EGFR only rescued Ang II-induced cardiac hypertrophy but not hypertension (560). TNFα inhibition attenuated Ang II-induced hypertension and cardiac hypertrophy (561). ADAM17 has been shown to cleave another substrate angiotensin-converting enzyme 2 (ACE2) in response to Ang II infusion, which subsequently contributed to cardiac hypertrophy as result of decreased generation of Ang (1-7) and increased retention of Ang II (562). Further studies showed that ACE2 is capable of cleaving the antihypertensive peptide, apelin (563), and *Apln*-deficiency is protective against Ang II-induced hypertension (unpublished data). Moreover, deletion of *Adam17* in ECs rather than in SMCs has been shown to be more effective to blunt Ang II-induced hypertension in this study. Taken together, inhibition of SMC hypertrophic response alone may not be an ideal strategy to mitigate Ang II-induced hypertension and end-organ damage.

SMC phenotypic switching has now been widely accepted to play an important role in atherosclerosis. Accumulating evidence shows that the role of SMCs varies depending on the stage of the disease. Genetic lineage tracing studies showed that >80% of SMCs underwent phenotypic switching and resulted in an increased population of macrophage-like SMCs that contribute to the progression of atherosclerosis, and a transcriptional factor, Krüppel-like factor-4 (KLF4), seems to play an important role in modulating the phenotype of SMCs (508). Reduced expression of SMC-specific contractile proteins, and increased production of proinflammatory cytokines, ECM components, and various proteases are the typical characteristics of these phenotypic-switched SMCs. However, the SMCs migrated into the fibrous cap are thought to play a beneficial role in

stabilizing plaques before activation of proteases that may contribute to plaque rupture, and the migratory property of SMCs might be directed by Octamer-binding transcriptional factor-4 (OCT4) (564). It has been shown that increased ADAM17 is predominantly found in macrophage maker-positive regions of human atheroma (326). Interestingly, a recent study showed that myeloid *Adam17*-deficiency resulted in more stable atherosclerotic plaques with a significant increase in SMC density and collagen deposition, suggesting myeloid ADAM17 may play an important role in inflammation and proteolysis during atherogenesis (330). A similar phenotype was observed in mice lacking myeloid *Adam10* (565). Since it has been proved that most SMCs undergo phenotypic switching under an inflammatory environment (508), the more preserved SMC density in myeloid *Adam17*-deficient plaques indicates that inflammation is an important factor that regulates phenotypic switching in SMCs. Therefore, it is plausible to predict that deletion of *Adam17* in SMCs may also be atheroprotective.

Accumulating evidence shows that an effective way to suppress the pathogenesis of vascular diseases is to maintain the contractile phenotype under pathological conditions such as chronic inflammation. While Doring, et al. (541) showed that *Cxcr4*-deficient SMCs were more susceptible to phenotypic switching, and therefore, contributed to the development of atherosclerosis, Liu, *et al*. (396) reported a protective effect of *Arhgap18*-deficiency on Ang II-induced TAA through suppressing the synthetic, proteolytic, and proinflammatory phenotype of SMCs. In our study, we observed that deletion of *Adam17* is protective against elastase-induced TAA formation, mainly due to preserved contractile phenotype of SMCs.

It has been proposed that the phenotypic switching of SMCs might be regulated by G/C repressor elements in response to environmental cues. The G/C repressor elements are found between CArG elements of many SMC marker gene promoters. When the vessel is injured, the expression levels of G/G repressor element binding factor Sp1 are increased, disrupting the interaction between SMC marker gene promoters and thereby inhibiting SMC marker gene expression (459). However, it remains to be determined how ADAM17 could regulate the transcription levels of these SMC marker genes under pathological conditions. Since ADAM17 has been shown to cleave a group of substrates that undergo the RIP process, it is possible that ADAM17-dependent RIP pathway may regulate the activities of some of the transcriptional factors that are required for the expression of SMC marker genes.

5.3. Adventitial-medial interactions in vascular pathologies

Based on the *in vitro* studies by Elliott, *et al.* (172) and ours (214), ADAM17 plays a critical role in Ang II-induced hypertrophy, proliferation, and migration, mainly through transactivation of the EGFR signaling. Since SMC hypertrophy and hyperplasia have been implicated in hypertension, we subjected SMC *Adam17*-deficient mice to chronic Ang II infusion and hypothesized that Ang II-induced hypertension and end-organ damage should be attenuated in these knockout mice as compared to control mice. Surprisingly, SMC *Adam17*-deletion only showed a transient protective effect on Ang II-induced hypertension and hypertrophy, which was abolished with prolonged Ang II infusion. Our mechanistic study suggested that fibroblast-ADAM17 in the adventitia may exert a paracrine effect on their adjacent *Adam17*-deficient SMCs, and thereby compensate for the loss of ADAM17 activity and EGFR signaling in SMCs. Note that the AT1 receptor is indispensable for Ang II-mediated EGFR transactivation and the downstream signaling (566). Therefore, an indirect piece of evidence further corroborated the critical role of adventitial fibroblasts in Ang II-mediated cardiovascular remodeling, as deletion of *At1* in fibroblasts but not in SMCs, ECs/hematopoietic cells, or neurons protected against Ang II-induced vascular hypertrophy (567). In addition, blockade of *At1* in none of these cell types was found to suppress Ang II-induced hypertension (567), which again supports the hypothesis that the attenuated Ang II-induced hypertension in EC *Adam17*-deficient mice but not in SMC *Adam17*-deficient mice might be independent of the EGFR signaling.

Accumulating evidence supports that aortic adventitial fibroblasts play an important role in vascular wall inflammation and vascular remodeling through an ‘outside-in’ mechanism (reviewed in (551)). Hallmarks of the ‘outside-in’ theory include inflammatory cell accumulation in the adventitia, the phenotypic switching of adventitial fibroblasts to migratory myofibroblasts, ECM deposition, and increased vasa vasorum neovascularization. Ang II-treated adventitial fibroblasts have been shown to constitutively secrete numerous cytokines, such as CCL2 and IL6. Mover, fibroblast-derived CCL2 is a potent chemoattractant which could trigger inflammatory cells extravasation *in vitro* (568). In aneurysmal tissues, the adventitial layer is the main spot where inflammatory cells accumulated, and it has been shown that elastolysis is the primary event in AAA formation before the overt loss of adventitial structural integrity occurs (532). Actually, these concepts and findings are the fundamental mechanisms supporting the notion that periadventitial

elastase-induced TAA model may be the most pathological model that mimics the actual onset of aortic aneurysm in humans. As such, it is not surprising that our experimental TAA model can recapitulate the main characteristics of human TAA.

Therefore, it would be intriguing to test the role of adventitial ADAM17 in Ang II-induced hypertension and end-organ damage using fibroblast *Adam17*-deficient mice. Alternatively, the paracrine effects of ADAM17 activity between adventitial fibroblasts and medial SMCs can be tested in a co-culture system.

5.4. Disrupted intimal integrity contributes to vascular remodeling through enhanced inflammatory responses

The endothelial barrier function is mediated by a junction protein complex including adherens junctions, tight junctions, and gap junctions, which are connected to the actin cytoskeleton via different adaptor molecules (569). In addition to maintaining adhesion between ECs, the junction proteins actively mediate vascular permeability and leukocyte infiltration via a complex balance between multiple signaling molecules (569). Adherens junctions are composed of VE-cadherin and a group of adaptor proteins including α-, β-, γ- and p120-catenin, vinculin, and α-actin, which are important for stability and dynamic permeability of the junctions. Tight junctions are composed of occludins, claudins, and JAMs. Claudins are the principal barrier-forming proteins, and claudin-5 is critical for endothelial permeability. JAMs are important in regulating leukocyte transendothelial migration (570). It has now been increasingly recognized that vascular intimal barrier hyperpermeability is associated with disruption of endothelial junction protein complex, and is implicated in diseases such as cancer, atherosclerosis, aortic aneurysm, hypertension, and inflammation.

Numerous studies have demonstrated that pro-inflammatory mediators contribute to increased endothelial permeability. Among a variety of regulatory mechanisms, the effects of kinase-mediated phosphorylation and internalization of VE-cadherin (571), and small GTPase-mediated cytoskeletal rearrangement and stress fiber formation (572) on increased endothelial permeability have been extensively elucidated.

In addition, ADAM17 was reported to cleave junction proteins such as claudin-5 (106) and JAM-A (115), whereas ADAM10 was shown to cleave VE-cadherin (324). Indeed, in our study we observed a significantly lower permeability to circulating Evans blue dye in EC *Adam17*-deficient TAA samples. *In vitro*, the *Adam17*-deficient EC monolayer showed a significantly decreased permeability in response to elastase treatment. Moreover, immunofluorescent staining showed that elastase-induced structural disruption of VE-cadherin in EC monolayers was preserved with *Adam17* deletion. While immunoblotting showed a drastic reduction of membrane-bound VE-cadherin in elastase-treated *Adam17*-intact ECs, soluble VE-cadherin in the corresponding conditioned media was significantly increased. These data suggest that VE-cadherin may be a potential substrate for ADAM17, and increased ADAM17 activity contribute to increased endothelial permeability by directly shedding the extracellular domains of VE-cadherin, JAM-A, and claudin-5. As expected, we observed less inflammatory cell infiltration into the aorta wall of EC *Adam17*-deficient mice after elastase exposure. In addition to the compromised endothelial barrier function as a result of enhanced shedding of membrane-bound VE-cadherin, soluble VE-cadherin has been shown to promote further breakdown of endothelial junction complex in an inflammatory environment, which further corroborates the crucial role of ADAM17-mediated endothelial barrier integrity and subsequent inflammation in the pathogenesis of TAA.

5.5. TAA and AAA are distinct vascular diseases

TAA has remained the less explored type of aortic aneurysm mainly due to its much lower prevalence than that of AAA in human populations. In addition, the risk factors for TAA are less well-defined (other than the genetic predispositions) as it can occur independent of age, sex and environmental factors, and prognosis for TAA is much less promising than AAA (346, 573), whereas the risk factors for AAA are better defined to include age, male sex, hypertension, hyperlipidemia, and tobacco use (352, 574). It has become increasingly evident that the regional structural heterogeneity of the aorta (thoracic versus abdominal) is highly specialized to meet the corresponding functional demands. Thoracic aorta has a greater number of lamellar units and higher elastin-to-collagen content to receive a large volume of blood pumped by the heart during systole, compared to the abdominal aorta that is primarily responsible for blood distribution to major lower body arteries (higher collagen-to-elastin content).

As such, it is now recognized that TAA and AAA are different vascular diseases with distinct underlying mechanisms (349, 530), mainly due to the different regional structures, embryonic origins of SMCs, elastin-to-collagen ratios, and hemodynamics of thoracic versus abdominal aorta (reviewed in **Chapter 1.11.6.1**). Consistently, opposite functions of specific proteases on AAA versus TAA have been demonstrated (378, 453). ADAM17 and its polymorphism have been linked to AAA in patients (476, 478) and in animal models (414, 480), however, information on the function of ADAM17 in TAA is severely lacking.

In studies included in this dissertation, we showed that the increased ADAM17 activity in the intimal and medial layers in TAA orchestrates cellular and molecular responses that lead to SMC phenotypic switching and to compromised endothelial barrier integrity, collectively leading to excess matrix synthesis and deposition, cell death, inflammation, and overall adverse structural remodeling of the injured aorta. Using cell-specific *Adam17*-deficient mice, an *in vivo* model of TAA, and *in vitro* primary culture of aortic SMCs and ECs, we demonstrated that ADAM17 can mediate diverse molecular events in SMCs versus the ECs.

5.6. ADAM17 exhibits cell type-specific biological functions

As shown in **Table 1.4**, cell type-specific ADAM17 plays distinct functions by shedding a diverse array of membrane-tethered substrates. Accumulating evidence shows that the function of ADAM17 is both cell type-specific and disease condition-specific. Systemic *Adam17*-deficiency promoted atherosclerosis mainly through preserving p75 TNR level on the cell membrane which consequently contributed to aberrant proliferation and reduced apoptosis of macrophages and SMCs (329). However, myeloid and EC ADAM17 showed cell type-specific and counteractive effects in atherosclerosis development, with the former playing an atheroprotective effect and the latter an atheroprogression effect (329). Cardiomyocyte *Adam17*-deficiency preserved the heart function post-MI, but exacerbated pressure overload-induced cardiac hypertrophy (318, 336). In our study, although both SMC and EC *Adam17*-deficiency protected against elastase-induced TAA due to attenuated inflammation, the way that ADAM17 in the two cell types mediating inflammatory response was distinct. In response to elastase-induced aortic injury, ADAM17 in ECs was activated to cleave junction protein complex to let more inflammatory cells get into the subendothelial space of the aorta; ADAM17 in SMCs was activated in response to inflammation

and underwent contractile-to-synthetic phenotypic switching, and presented as proinflammatory and proteolytic SMCs which further augmented inflammatory responses in the aortic wall.

5.7. Perspectives of developing ADAM17 inhibitors as potential therapeutic strategies for aortic aneurysm

Currently, no validated therapeutic drugs are available to treat aortic aneurysm, and elective surgery is the only option when the aneurysmal diameter reaches threshold diameter. However, during the waiting frame, the aneurysm bears the risk of rupture, which could lead to significant mortality and morbidity. The ideal drugs for aortic aneurysm is to suppress or stop the expansion of aneurysmal aorta, and if possible, to reverse the aneurysm phenotype. Nowadays, general inhibition of ADAM17 has been tested in clinical trials to treat inflammatory diseases and cancer. Considering the cell type-specific function of ADAM17, it is important to develop cell type- or substrate-specific targeting strategies of ADAM17 to improve drug specificity and efficacy on the one hand, and to minimize the disturbance of physiological functions of ADAM17 on the other hand.

Moreover, since ADAM17 (and also some other physiological indispensable ADAMs) plays an important role in regulating various important cellular functions, a temporal administration of ADAM inhibitors might also be required. In our study, we administered an ADAM17-selective inhibitor to wildtype mice prior to, or early after induction of TAA and confirmed the beneficial effects of ADAM17 inhibition on the pathogenesis of TAA. Since in our study, systemic inhibition of ADAM17 was sustained for only a short period of time, it is not known whether prolonged treatment of ADAM17 inhibitor in mice would trigger any side-effects such as organ toxicity. A better understanding of the role of ADAM17 in other cell types (e.g., leukocytes and fibroblasts) may help us decide which regimen should be used to achieve ADAM17 inhibition to maximize the suppression effects on the progression of aortic aneurysm and to ensure normal physiological activity of ADAM17 in the whole body.

CHAPTER 6

LIMITATIONS AND FUTURE DIRECTIONS

6.1. Limitations

6.1.1. SMC Adam17-deficient mouse

The genetically modified mice serve as very useful tools to address specific scientific questions, however, they are not flawless. ADAM17 deletion in SMCs was achieved by crossing *Adam17$^{f/f}$* mice and *Sm22α-Cre* mice. Although Sm22α is specifically expressed in adult SMCs, genetic lineage tracing experiments showed that this gene is also transiently expressed in the cardiac cells (between E8.0 and E12.5) and skeletal muscle cells (between E9.5 and E12.5) during embryogenesis (575, 576). However, Sm22α promoter has been widely used for constitutive deletion of target genes in SMCs (541, 577, 578) or for SMC-lineage tracing experiments.(579-581) In addition, a recent study by Doring *et al.*(541) showed that deletion of CXCR4 in SMCs using inducible *SM-MHC-C*re (*SmmhcCreER^{T2}*) or constitutive *Sm22α-Cre* resulted in a similar increase in atherosclerotic lesions, suggesting *Sm22α-Cre* is as effective and specific as *SmmhcCreER^{T2}* for gene knockdown in vascular SMCs.

6.1.2. Role of adventitial fibroblast ADAM17 in Ang II-induced hypertension and end-organ damage

As discussed in **Chapter 5.3**, adventitial inflammation is critical for cardiovascular remodeling and fibroblasts may represent an important cell type in Ang II-induced end-organ damage (and probably hypertension). Although we proposed that Ang II-induced activation of EGFR in the adventitial fibroblasts could compensate for the loss of ADAM17 in the SMCs through a paracrine effect, direct evidence is still lacking. Further studies are required to investigate the communication between adventitial fibroblasts and medial SMCs by a co-culture system. Moreover, the role of fibroblast ADAM17 in cardiovascular remodeling can be further investigated using fibroblast-specific *Adam17*-deficiency mice.

6.1.3. Experimental TAA model

Although the TAA model used in the current study may represent the most 'pathological' model that resembles the characteristics of the onset as well as the advanced forms of human TAA, there still some limitations. Firstly, the model is an acute TAA model, which only takes 2 weeks to develop advanced TAA. In contrast, it usually takes decades to develop TAA in humans. Therefore,

this animal model may not able to recapitulate the pathological changes during chronic inflammation observed in human TAA. Secondly, the experimental TAA model does not show thrombus, calcification, and rupture, which are normally found in humans. Thirdly, this TAA model used in the current study has been reported to start to self-heal after 2 weeks of elastase exposure (381), which phenomenon is usually absent in humans. A recent study conducted by Lu, *et al.* (382) showed that administration of BAPN through drinking water together with periadventitial elastase treatment could induce a chronic, advanced-stage AAA with characteristics of persistent aneurysm growth, thrombus formation, and spontaneous rupture. More importantly, since this model demonstrates all stages of aneurysm formation in more detail in terms of changes in aortic structure, cytokine profiles, and inflammatory cell profiles, it represents a better AAA model for aneurysm studies and will provide a much clearer picture of the cellular and molecular changes from the initiation stage to the advanced stage during the progression of aortic aneurysm. Technically, this novel model may be adapted to induce chronic advanced-stage TAA with modifications.

6.1.4. The role of immunity in the pathogenesis of TAA

As briefly discussed in **Chapter 1.11.6.3**, the role of autoimmunity in aneurysm formation has been increasingly recognized (reviewed in (447, 448)). In the current study, we reported suppressed inflammation accounts for the mitigated TAA phenotypes in mice lacking ADAM17 in SMCs and ECs. However, we only explored a subpopulation of inflammatory cells in the TAA, namely macrophages and neutrophils. The contribution of T lymphocytes-specific ADAM17 to the pathogenesis of TAA in both cell type-specific knockout mice may provide more mechanistic insights of the functional role of ADAM17 in the regulation of inflammation during TAA development.

6.1.5. The underlying mechanism for ADAM17-mediated SMC phenotypic switching

Although in the current study, we provided strong evidence *in vitro* and *in vivo* that ADAM17 plays a crucial role in modulating the phenotypic switching of SMC under pathological conditions, the precise mechanisms are still lacking. Further studies are required to identify which transcriptional factors are affected to downregulate the transcription levels of SMC contractile proteins.

6.1.6. The potential cell and organ toxicity of PF-548

Due to the short half-life of PF-548, we gavaged mice with this drug twice at a relatively high concentration. Although it has been shown that this inhibitor selectively suppresses the activity of ADAM17 but not other MMPs or ADAMs, such a high dose may disturb physiological functions of other proteases and contribute to cell and organ toxicity. Future studies are warranted to evaluate the potential side-effects and toxicity of this inhibitor in mice.

6.2. Future directions

6.2.1. To uncover the underlying mechanisms by which EC Adam17-deficiency suppresses Ang II-induced hypertension

During my Ph.D. studies, I found that deletion of *Adam17* in ECs persistently suppressed Ang II-induced hypertension, unlike the transient impact of SMC *Adam17*-deficiency. However, the underlying mechanisms for the profound protective effect are yet to be investigated. Further studies can focus on how Ang II affects (I) endothelial dysfunction (e.g., eNOS); (II) oxidative stress; and (III) endothelial barrier disruption and inflammatory cell patterns (e.g., leukocytes and regulatory T cells (582)).

6.2.2. To target transcriptional factors downstream of ADAM17 that are involved in modulating SMC phenotypic switching

Although a number of transcriptional factors (e.g., KLF4, E26 ETS-like transcription factor-1/ELK1, and HES-related repressor protein-1/HERP1) have been suggested to suppress SMC marker gene expression (546), whether ADAM17-mediated ectodomain shedding or RIP process may regulate these transcriptional factors need to be investigated.

6.2.3. To identify complete ADAM profiles in different types of TAAs and AAAs

Since a number of ADAM-associated biological functions are involved in the pathogenesis of aortic aneurysm, it is necessary to identify the ADAM expression and activity profiles in different types of TAAs and AAAs before we can better understand their roles in the pathogenesis of aortic aneurysms and explore therapeutic targets for the two types of devastating vascular diseases. Although current studies (although quite limited) showed marked heterogeneity in ADAM

expression profiles between different TAA and AAA etiologies, possibly suggesting different mechanistic pathways. Nevertheless, a lack of uniformity between study protocols can substantially affect the results and hinder the translational values of these findings. Therefore, in order to obtain reliable ADAM expression profiles, the following parameters need to be standardized: (I) aorta harvesting sites; (II) aortic diameter at the time of harvest; (III) using ADAM expression levels instead of ADAM activities (which can be used as another parameter); and (IV) be aware of regional variations in ADAM expression along the circumference (average ADAM expression value is preferred).

REFERENCES

1. Huovila AP, Turner AJ, Pelto-Huikko M, Karkkainen I, and Ortiz RM. Shedding light on ADAM metalloproteinases. *Trends Biochem Sci.* 2005;30(7):413-422.
2. Arribas J, and Esselens C. ADAM17 as a therapeutic target in multiple diseases. *Curr Pharm Des.* 2009;15(20):2319-2335.
3. Gooz M. ADAM-17: the enzyme that does it all. *Critical Reviews in Biochemistry and Molecular Biology.* 2010;45(2):146-169.
4. Scheller J, Chalaris A, Garbers C, and Rose-John S. ADAM17: a molecular switch to control inflammation and tissue regeneration. *Trends Immunol.* 2011;32(8):380-387.
5. Rose-John S. ADAM17, shedding, TACE as therapeutic targets. *Pharmacol Res.* 2013;71:19-22.
6. Xu J, Mukerjee S, Silva-Alves CR, Carvalho-Galvao A, Cruz JC, Balarini CM, et al. A Disintegrin and Metalloprotease 17 in the Cardiovascular and Central Nervous Systems. *Front Physiol.* 2016;7:469.
7. Kjeldsen SE. Hypertension and cardiovascular risk: General aspects. *Pharmacol Res.* 2018;129:95-99.
8. Zunke F, and Rose-John S. The shedding protease ADAM17: Physiology and pathophysiology. *Biochim Biophys Acta.* 2017;1864(11 Pt B):2059-2070.
9. Perez-Silva JG, Espanol Y, Velasco G, and Quesada V. The Degradome database: expanding roles of mammalian proteases in life and disease. *Nucleic Acids Res.* 2016;44(D1):D351-355.
10. Lopez-Otin C, and Overall CM. Protease degradomics: a new challenge for proteomics. *Nature reviews Molecular cell biology.* 2002;3(7):509-519.
11. Hooper N. *Proteases in biology and medicine.* Portland Press; 2002.
12. Puente XS, and Lopez-Otin C. A genomic analysis of rat proteases and protease inhibitors. *Genome research.* 2004;14(4):609-622.
13. Puente XS, Sanchez LM, Overall CM, and Lopez-Otin C. Human and mouse proteases: a comparative genomic approach. *Nature Reviews Genetics.* 2003;4(7):544-558.
14. Iyer RP, de Castro Bras LE, Jin YF, and Lindsey ML. Translating Koch's postulates to identify matrix metalloproteinase roles in postmyocardial infarction remodeling: cardiac metalloproteinase actions (CarMA) postulates. *Circ Res.* 2014;114(5):860-871.
15. Takawale A, Sakamuri SS, and Kassiri Z. Extracellular matrix communication and turnover in cardiac physiology and pathology. *Compr Physiol.* 2015;5(2):687-719.
16. Amar S, Smith L, and Fields GB. Matrix metalloproteinase collagenolysis in health and disease. *Biochim Biophys Acta.* 2017;1864(11 Pt A):1940-1951.
17. Iyer RP, Jung M, and Lindsey ML. MMP-9 signaling in the left ventricle following myocardial infarction. *American journal of physiology Heart and circulatory physiology.* 2016;311(1):H190-198.
18. DeLeon-Pennell KY, Meschiari CA, Jung M, and Lindsey ML. Matrix Metalloproteinases in Myocardial Infarction and Heart Failure. *Progress in molecular biology and translational science.* 2017;147:75-100.
19. Blobel CP, Wolfsberg TG, Turck CW, Myles DG, Primakoff P, and White JM. A potential fusion peptide and an integrin ligand domain in a protein active in sperm-egg fusion. *Nature.* 1992;356(6366):248-252.
20. Wolfsberg TG, Bazan JF, Blobel CP, Myles DG, Primakoff P, and White JM. The precursor region of a protein active in sperm-egg fusion contains a metalloprotease and a disintegrin domain: structural, functional, and evolutionary implications. *Proceedings of the National Academy of Sciences of the United States of America.* 1993;90(22):10783-10787.
21. Wolfsberg TG, Straight PD, Gerena RL, Huovila AP, Primakoff P, Myles DG, et al. ADAM, a widely distributed and developmentally regulated gene family encoding membrane proteins with a disintegrin and metalloprotease domain. *Developmental biology.* 1995;169(1):378-383.
22. Edwards DR, Handsley MM, and Pennington CJ. The ADAM metalloproteinases. *Mol Aspects Med.* 2008;29(5):258-289.
23. White JM. ADAMs: modulators of cell-cell and cell-matrix interactions. *Current opinion in cell biology.* 2003;15(5):598-606.
24. Wei S, Whittaker CA, Xu G, Bridges LC, Shah A, White JM, et al. Conservation and divergence of ADAM family proteins in the Xenopus genome. *BMC evolutionary biology.* 2010;10:211.
25. Cho C. In: Hooper NM, and Lendeckel U eds. *The ADAM Family of Proteases*. Dordrecht: Springer; 2005:239-259.
26. Sagane K, Yamazaki K, Mizui Y, and Tanaka I. Cloning and chromosomal mapping of mouse ADAM11, ADAM22 and ADAM23. *Gene.* 1999;236(1):79-86.
27. Sagane K, Ishihama Y, and Sugimoto H. LGI1 and LGI4 bind to ADAM22, ADAM23 and ADAM11. *Int J Biol Sci.* 2008;4(6):387-396.

28. Blobel CP. Metalloprotease-disintegrins: links to cell adhesion and cleavage of TNF alpha and Notch. *Cell.* 1997;90(4):589-592.
29. Stocker W, Grams F, Baumann U, Reinemer P, Gomis-Ruth FX, McKay DB, et al. The metzincins--topological and sequential relations between the astacins, adamalysins, serralysins, and matrixins (collagenases) define a superfamily of zinc-peptidases. *Protein science: a publication of the Protein Society.* 1995;4(5):823-840.
30. Anders A, Gilbert S, Garten W, Postina R, and Fahrenholz F. Regulation of the alpha-secretase ADAM10 by its prodomain and proprotein convertases. *FASEB journal: official publication of the Federation of American Societies for Experimental Biology.* 2001;15(10):1837-1839.
31. Seals DF, and Courtneidge SA. The ADAMs family of metalloproteases: multidomain proteins with multiple functions. *Genes Dev.* 2003;17(1):7-30.
32. Gonzales PE, Solomon A, Miller AB, Leesnitzer MA, Sagi I, and Milla ME. Inhibition of the tumor necrosis factor-alpha-converting enzyme by its pro domain. *The Journal of biological chemistry.* 2004;279(30):31638-31645.
33. Milla ME, Gonzales PE, and Leonard JD. The TACE zymogen: re-examining the role of the cysteine switch. *Cell biochemistry and biophysics.* 2006;44(3):342-348.
34. Leonard JD, Lin F, and Milla ME. Chaperone-like properties of the prodomain of TNFalpha-converting enzyme (TACE) and the functional role of its cysteine switch. *Biochem J.* 2005;387(Pt 3):797-805.
35. Moss ML, Bomar M, Liu Q, Sage H, Dempsey P, Lenhart PM, et al. The ADAM10 prodomain is a specific inhibitor of ADAM10 proteolytic activity and inhibits cellular shedding events. *Journal of Biological Chemistry.* 2007;282(49):35712-35721.
36. Esselens CW, Malapeira J, Colome N, Moss M, Canals F, and Arribas J. Metastasis-associated C4.4A, a GPI-anchored protein cleaved by ADAM10 and ADAM17. *Biological chemistry.* 2008;389(8):1075-1084.
37. Zhou A, Webb G, Zhu X, and Steiner DF. Proteolytic processing in the secretory pathway. *The Journal of biological chemistry.* 1999;274(30):20745-20748.
38. Schlomann U, Wildeboer D, Webster A, Antropova O, Zeuschner D, Knight CG, et al. The metalloprotease disintegrin ADAM8. Processing by autocatalysis is required for proteolytic activity and cell adhesion. *The Journal of biological chemistry.* 2002;277(50):48210-48219.
39. Howard L, Maciewicz RA, and Blobel CP. Cloning and characterization of ADAM28: evidence for autocatalytic pro-domain removal and for cell surface localization of mature ADAM28. *Biochem J.* 2000;348 Pt 1:21-27.
40. Takeda S. ADAM and ADAMTS Family Proteins and Snake Venom Metalloproteinases: A Structural Overview. *Toxins.* 2016;8(5).
41. Sahin U, Weskamp G, Kelly K, Zhou HM, Higashiyama S, Peschon J, et al. Distinct roles for ADAM10 and ADAM17 in ectodomain shedding of six EGFR ligands. *The Journal of cell biology.* 2004;164(5):769-779.
42. Shi Z, Xu W, Loechel F, Wewer UM, and Murphy LJ. ADAM 12, a disintegrin metalloprotease, interacts with insulin-like growth factor-binding protein-3. *The Journal of biological chemistry.* 2000;275(24):18574-18580.
43. Roy R, Wewer UM, Zurakowski D, Pories SE, and Moses MA. ADAM 12 cleaves extracellular matrix proteins and correlates with cancer status and stage. *The Journal of biological chemistry.* 2004;279(49):51323-51330.
44. Becherer JD, and Blobel CP. Biochemical properties and functions of membrane-anchored metalloprotease-disintegrin proteins (ADAMs). *Current topics in developmental biology.* 2003;54:101-123.
45. Dreymueller D, Pruessmeyer J, Groth E, and Ludwig A. The role of ADAM-mediated shedding in vascular biology. *European journal of cell biology.* 2012;91(6-7):472-485.
46. Kleino I. *Variable expressions of ADAM family genes in tissues and cancer cells.* Finland: University of Tampere; 2007.
47. Yacoub D, Benslimane N, Al-Zoobi L, Hassan G, Nadiri A, and Mourad W. CD154 is released from T-cells by a disintegrin and metalloproteinase domain-containing protein 10 (ADAM10) and ADAM17 in a CD40 protein-dependent manner. *The Journal of biological chemistry.* 2013;288(50):36083-36093.
48. Lemjabbar H, Li D, Gallup M, Sidhu S, Drori E, and Basbaum C. Tobacco smoke-induced lung cell proliferation mediated by tumor necrosis factor alpha-converting enzyme and amphiregulin. *The Journal of biological chemistry.* 2003;278(28):26202-26207.
49. Vahdat AM, Reiners KS, Simhadri VL, Eichenauer DA, Boll B, Chalaris A, et al. TNF-alpha-converting enzyme (TACE/ADAM17)-dependent loss of CD30 induced by proteasome inhibition through reactive oxygen species. *Leukemia.* 2010;24(1):51-57.
50. Leksa V, Loewe R, Binder B, Schiller HB, Eckerstorfer P, Forster F, et al. Soluble M6P/IGF2R released by TACE controls angiogenesis via blocking plasminogen activation. *Circ Res.* 2011;108(6):676-685.
51. Garton KJ, Gough PJ, Blobel CP, Murphy G, Greaves DR, Dempsey PJ, et al. Tumor necrosis factor-alpha-converting enzyme (ADAM17) mediates the cleavage and shedding of fractalkine (CX3CL1). *The Journal of biological chemistry.* 2001;276(41):37993-38001.

52. Contin C, Pitard V, Itai T, Nagata S, Moreau JF, and Dechanet-Merville J. Membrane-anchored CD40 is processed by the tumor necrosis factor-alpha-converting enzyme. Implications for CD40 signaling. *The Journal of biological chemistry.* 2003;278(35):32801-32809.
53. Guo L, Eisenman JR, Mahimkar RM, Peschon JJ, Paxton RJ, Black RA, et al. A proteomic approach for the identification of cell-surface proteins shed by metalloproteases. *Molecular & cellular proteomics: MCP.* 2002;1(1):30-36.
54. Schramme A, Abdel-Bakky MS, Kampfer-Kolb N, Pfeilschifter J, and Gutwein P. The role of CXCL16 and its processing metalloproteinases ADAM10 and ADAM17 in the proliferation and migration of human mesangial cells. *Biochem Biophys Res Commun.* 2008;370(2):311-316.
55. Horiuchi K, Miyamoto T, Takaishi H, Hakozaki A, Kosaki N, Miyauchi Y, et al. Cell surface colony-stimulating factor 1 can be cleaved by TNF-alpha converting enzyme or endocytosed in a clathrin-dependent manner. *Journal of immunology (Baltimore, Md : 1950).* 2007;179(10):6715-6724.
56. Bech-Serra JJ, Santiago-Josefat B, Esselens C, Saftig P, Baselga J, Arribas J, et al. Proteomic identification of desmoglein 2 and activated leukocyte cell adhesion molecule as substrates of ADAM17 and ADAM10 by difference gel electrophoresis. *Mol Cell Biol.* 2006;26(13):5086-5095.
57. Cho RW, Park JM, Wolff SB, Xu D, Hopf C, Kim JA, et al. mGluR1/5-dependent long-term depression requires the regulated ectodomain cleavage of neuronal pentraxin NPR by TACE. *Neuron.* 2008;57(6):858-871.
58. Kawaguchi N, Horiuchi K, Becherer JD, Toyama Y, Besmer P, and Blobel CP. Different ADAMs have distinct influences on Kit ligand processing: phorbol-ester-stimulated ectodomain shedding of Kitl1 by ADAM17 is reduced by ADAM19. *J Cell Sci.* 2007;120(Pt 6):943-952.
59. Dyczynska E, Sun D, Yi H, Sehara-Fujisawa A, Blobel CP, and Zolkiewska A. Proteolytic processing of delta-like 1 by ADAM proteases. *The Journal of biological chemistry.* 2007;282(1):436-444.
60. Peng M, Guo S, Yin N, Xue J, Shen L, Zhao Q, et al. Ectodomain shedding of Fcalpha receptor is mediated by ADAM10 and ADAM17. *Immunology.* 2010;130(1):83-91.
61. Bozkulak EC, and Weinmaster G. Selective use of ADAM10 and ADAM17 in activation of Notch1 signaling. *Mol Cell Biol.* 2009;29(21):5679-5695.
62. Chitadze G, Lettau M, Bhat J, Wesch D, Steinle A, Furst D, et al. Shedding of endogenous MHC class I-related chain molecules A and B from different human tumor entities: heterogeneous involvement of the "a disintegrin and metalloproteases" 10 and 17. *Int J Cancer.* 2013;133(7):1557-1566.
63. Etzerodt A, Maniecki MB, Moller K, Moller HJ, and Moestrup SK. Tumor necrosis factor alpha-converting enzyme (TACE/ADAM17) mediates ectodomain shedding of the scavenger receptor CD163. *J Leukoc Biol.* 2010;88(6):1201-1205.
64. Okamura Y, Kohmura E, and Yamashita T. TACE cleaves neogenin to desensitize cortical neurons to the repulsive guidance molecule. *Neuroscience research.* 2011;71(1):63-70.
65. Coglievina M, Guarnaccia C, Zlatev V, Pongor S, and Pintar A. Jagged-1 juxtamembrane region: biochemical characterization and cleavage by ADAM17 (TACE) catalytic domain. *Biochem Biophys Res Commun.* 2013;432(4):666-671.
66. Sahin U, and Blobel CP. Ectodomain shedding of the EGF-receptor ligand epigen is mediated by ADAM17. *FEBS Lett.* 2007;581(1):41-44.
67. Li N, Wang Y, Forbes K, Vignali KM, Heale BS, Saftig P, et al. Metalloproteases regulate T-cell proliferation and effector function via LAG-3. *EMBO J.* 2007;26(2):494-504.
68. Ahmed Z, Suggate EL, Brown ER, Dent RG, Armstrong SJ, Barrett LB, et al. Schwann cell-derived factor-induced modulation of the NgR/p75NTR/EGFR axis disinhibits axon growth through CNS myelin in vivo and in vitro. *Brain: a journal of neurology.* 2006;129(Pt 6):1517-1533.
69. Zheng Y, Saftig P, Hartmann D, and Blobel C. Evaluation of the contribution of different ADAMs to tumor necrosis factor alpha (TNFalpha) shedding and of the function of the TNFalpha ectodomain in ensuring selective stimulated shedding by the TNFalpha convertase (TACE/ADAM17). *The Journal of biological chemistry.* 2004;279(41):42898-42906.
70. Cruz AC, Frank BT, Edwards ST, Dazin PF, Peschon JJ, and Fang KC. Tumor necrosis factor-alpha-converting enzyme controls surface expression of c-Kit and survival of embryonic stem cell-derived mast cells. *The Journal of biological chemistry.* 2004;279(7):5612-5620.
71. Weskamp G, Schlondorff J, Lum L, Becherer JD, Kim TW, Saftig P, et al. Evidence for a critical role of the tumor necrosis factor alpha convertase (TACE) in ectodomain shedding of the p75 neurotrophin receptor (p75NTR). *The Journal of biological chemistry.* 2004;279(6):4241-4249.
72. Young J, Yu X, Wolslegel K, Nguyen A, Kung C, Chiang E, et al. Lymphotoxin-alphabeta heterotrimers are cleaved by metalloproteinases and contribute to synovitis in rheumatoid arthritis. *Cytokine.* 2010;51(1):78-86.

73. Horiuchi K, Morioka H, Takaishi H, Akiyama H, Blobel CP, and Toyama Y. Ectodomain shedding of FLT3 ligand is mediated by TNF-alpha converting enzyme. *Journal of immunology (Baltimore, Md : 1950).* 2009;182(12):7408-7414.
74. Yang Y, Wang Y, Zeng X, Ma XJ, Zhao Y, Qiao J, et al. Self-control of HGF regulation on human trophoblast cell invasion via enhancing c-Met receptor shedding by ADAM10 and ADAM17. *The Journal of clinical endocrinology and metabolism.* 2012;97(8):E1390-1401.
75. Bell JH, Herrera AH, Li Y, and Walcheck B. Role of ADAM17 in the ectodomain shedding of TNF-alpha and its receptors by neutrophils and macrophages. *J Leukoc Biol.* 2007;82(1):173-176.
76. Gawel-Beben K, Ali N, Ellis V, Velasco G, Poghosyan Z, Ager A, et al. TMEFF2 shedding is regulated by oxidative stress and mediated by ADAMs and transmembrane serine proteases implicated in prostate cancer. *Cell Biol Int.* 2018;42(3):273-280.
77. Qu D, Wang Y, Esmon NL, and Esmon CT. Regulated endothelial protein C receptor shedding is mediated by tumor necrosis factor-alpha converting enzyme/ADAM17. *Journal of thrombosis and haemostasis : JTH.* 2007;5(2):395-402.
78. Lum L, Wong BR, Josien R, Becherer JD, Erdjument-Bromage H, Schlondorff J, et al. Evidence for a role of a tumor necrosis factor-alpha (TNF-alpha)-converting enzyme-like protease in shedding of TRANCE, a TNF family member involved in osteoclastogenesis and dendritic cell survival. *The Journal of biological chemistry.* 1999;274(19):13613-13618.
79. Fleck D, van Bebber F, Colombo A, Galante C, Schwenk BM, Rabe L, et al. Dual cleavage of neuregulin 1 type III by BACE1 and ADAM17 liberates its EGF-like domain and allows paracrine signaling. *J Neurosci.* 2013;33(18):7856-7869.
80. Rio C, Buxbaum JD, Peschon JJ, and Corfas G. Tumor necrosis factor-alpha-converting enzyme is required for cleavage of erbB4/HER4. *The Journal of biological chemistry.* 2000;275(14):10379-10387.
81. Ludeman MJ, Zheng YW, Ishii K, and Coughlin SR. Regulated shedding of PAR1 N-terminal exodomain from endothelial cells. *The Journal of biological chemistry.* 2004;279(18):18592-18599.
82. Wang Y, and Sul HS. Ectodomain shedding of preadipocyte factor 1 (Pref-1) by tumor necrosis factor-alpha converting enzyme (TACE) and inhibition of adipocyte differentiation. *Mol Cell Biol.* 2006;26(14):5421-5435.
83. Zhang Y, Jiang J, Black RA, Baumann G, and Frank SJ. Tumor necrosis factor-alpha converting enzyme (TACE) is a growth hormone binding protein (GHBP) sheddase: the metalloprotease TACE/ADAM-17 is critical for (PMA-induced) GH receptor proteolysis and GHBP generation. *Endocrinology.* 2000;141(12):4342-4348.
84. Ruhe JE, Streit S, Hart S, and Ullrich A. EGFR signaling leads to downregulation of PTP-LAR via TACE-mediated proteolytic processing. *Cellular Signalling.* 2006;18(9):1515-1527.
85. Zhu L, Bergmeier W, Wu J, Jiang H, Stalker TJ, Cieslak M, et al. Regulated surface expression and shedding support a dual role for semaphorin 4D in platelet responses to vascular injury. *Proceedings of the National Academy of Sciences of the United States of America.* 2007;104(5):1621-1626.
86. Bergmeier W, Piffath CL, Cheng G, Dole VS, Zhang Y, von Andrian UH, et al. Tumor necrosis factor-alpha-converting enzyme (ADAM17) mediates GPIbalpha shedding from platelets in vitro and in vivo. *Circ Res.* 2004;95(7):677-683.
87. Chow JP, Fujikawa A, Shimizu H, Suzuki R, and Noda M. Metalloproteinase- and gamma-secretase-mediated cleavage of protein-tyrosine phosphatase receptor type Z. *The Journal of biological chemistry.* 2008;283(45):30879-30889.
88. Stoeck A, Keller S, Riedle S, Sanderson MP, Runz S, Le Naour F, et al. A role for exosomes in the constitutive and stimulus-induced ectodomain cleavage of L1 and CD44. *Biochem J.* 2006;393(Pt 3):609-618.
89. Gardiner EE, Karunakaran D, Shen Y, Arthur JF, Andrews RK, and Berndt MC. Controlled shedding of platelet glycoprotein (GP)VI and GPIb-IX-V by ADAM family metalloproteinases. *Journal of thrombosis and haemostasis : JTH.* 2007;5(7):1530-1537.
90. Kapp K, Siemens J, Haring HU, and Lammers R. Proteolytic processing of the protein tyrosine phosphatase alpha extracellular domain is mediated by ADAM17/TACE. *European journal of cell biology.* 2012;91(9):687-693.
91. Tsakadze NL, Sithu SD, Sen U, English WR, Murphy G, and D'Souza SE. Tumor necrosis factor-alpha-converting enzyme (TACE/ADAM-17) mediates the ectodomain cleavage of intercellular adhesion molecule-1 (ICAM-1). *The Journal of biological chemistry.* 2006;281(6):3157-3164.
92. Bender M, Hofmann S, Stegner D, Chalaris A, Bosl M, Braun A, et al. Differentially regulated GPVI ectodomain shedding by multiple platelet-expressed proteinases. *Blood.* 2010;116(17):3347-3355.
93. Moller-Hackbarth K, Dewitz C, Schweigert O, Trad A, Garbers C, Rose-John S, et al. A disintegrin and metalloprotease (ADAM) 10 and ADAM17 are major sheddases of T cell immunoglobulin and mucin domain 3 (Tim-3). *The Journal of biological chemistry.* 2013;288(48):34529-34544.

94. Li Y, Brazzell J, Herrera A, and Walcheck B. ADAM17 deficiency by mature neutrophils has differential effects on L-selectin shedding. *Blood.* 2006;108(7):2275-2279.
95. Yang WS, Kim JJ, Lee MJ, Lee EK, and Park SK. ADAM17-Mediated Ectodomain Shedding of Toll-Like Receptor 4 as a Negative Feedback Regulation in Lipopolysaccharide-Activated Aortic Endothelial Cells. *Cell Physiol Biochem.* 2018;45(5):1851-1862.
96. Langjahr P, Diaz-Jimenez D, De la Fuente M, Rubio E, Golenbock D, Bronfman FC, et al. Metalloproteinase-dependent TLR2 ectodomain shedding is involved in soluble toll-like receptor 2 (sTLR2) production. *PLoS One.* 2014;9(12):e104624.
97. Nielsen MA, Andersen T, Etzerodt A, Kragstrup TW, Rasmussen TK, Stengaard-Pedersen K, et al. A disintegrin and metalloprotease-17 and galectin-9 are important regulators of local 4-1BB activity and disease outcome in rheumatoid arthritis. *Rheumatology (Oxford).* 2016;55(10):1871-1879.
98. Kawahara R, Granato DC, Yokoo S, Domingues RR, Trindade DM, and Paes Leme AF. Mass spectrometry-based proteomics revealed Glypican-1 as a novel ADAM17 substrate. *Journal of proteomics.* 2017;151:53-65.
99. Reddy P, Slack JL, Davis R, Cerretti DP, Kozlosky CJ, Blanton RA, et al. Functional analysis of the domain structure of tumor necrosis factor-alpha converting enzyme. *The Journal of biological chemistry.* 2000;275(19):14608-14614.
100. Lorenzen I, Lokau J, Dusterhoft S, Trad A, Garbers C, Scheller J, et al. The membrane-proximal domain of A Disintegrin and Metalloprotease 17 (ADAM17) is responsible for recognition of the interleukin-6 receptor and interleukin-1 receptor II. *FEBS Lett.* 2012;586(8):1093-1100.
101. Diaz-Rodriguez E, Cabrera N, Esparis-Ogando A, Montero JC, and Pandiella A. Cleavage of the TrkA neurotrophin receptor by multiple metalloproteases generates signalling-competent truncated forms. *The European journal of neuroscience.* 1999;11(4):1421-1430.
102. Thathiah A, Blobel CP, and Carson DD. Tumor necrosis factor-alpha converting enzyme/ADAM 17 mediates MUC1 shedding. *The Journal of biological chemistry.* 2003;278(5):3386-3394.
103. Pruessmeyer J, Martin C, Hess FM, Schwarz N, Schmidt S, Kogel T, et al. A disintegrin and metalloproteinase 17 (ADAM17) mediates inflammation-induced shedding of syndecan-1 and -4 by lung epithelial cells. *The Journal of biological chemistry.* 2010;285(1):555-564.
104. Althoff K, Reddy P, Voltz N, Rose-John S, and Mullberg J. Shedding of interleukin-6 receptor and tumor necrosis factor alpha. Contribution of the stalk sequence to the cleavage pattern of transmembrane proteins. *European journal of biochemistry / FEBS.* 2000;267(9):2624-2631.
105. Feuerbach D, Schindler P, Barske C, Joller S, Beng-Louka E, Worringer KA, et al. ADAM17 is the main sheddase for the generation of human triggering receptor expressed in myeloid cells (hTREM2) ectodomain and cleaves TREM2 after Histidine 157. *Neuroscience letters.* 2017;660:109-114.
106. Cui D, Arima M, Takubo K, Kimura T, Horiuchi K, Minagawa T, et al. ADAM12 and ADAM17 are essential molecules for hypoxia-induced impairment of neural vascular barrier function. *Sci Rep.* 2015;5:12796.
107. Franke M, Schroder J, Monhasery N, Ackfeld T, Hummel TM, Rabe B, et al. Human and Murine Interleukin 23 Receptors Are Novel Substrates for A Disintegrin and Metalloproteases ADAM10 and ADAM17. *The Journal of biological chemistry.* 2016;291(20):10551-10561.
108. Franzke CW, Tasanen K, Schacke H, Zhou Z, Tryggvason K, Mauch C, et al. Transmembrane collagen XVII, an epithelial adhesion protein, is shed from the cell surface by ADAMs. *EMBO J.* 2002;21(19):5026-5035.
109. Budagian V, Bulanova E, Orinska Z, Ludwig A, Rose-John S, Saftig P, et al. Natural soluble interleukin-15Ralpha is generated by cleavage that involves the tumor necrosis factor-alpha-converting enzyme (TACE/ADAM17). *The Journal of biological chemistry.* 2004;279(39):40368-40375.
110. Raikwar NS, Liu KZ, and Thomas CP. N-terminal cleavage and release of the ectodomain of Flt1 is mediated via ADAM10 and ADAM 17 and regulated by VEGFR2 and the Flt1 intracellular domain. *PLoS One.* 2014;9(11):e112794.
111. Gerlach JC, Foka HG, Thompson RL, Gridelli B, and Schmelzer E. Epithelial cell adhesion molecule fragments and signaling in primary human liver cells. *Journal of cellular physiology.* 2018;233(6):4841-4851.
112. Lambert DW, Yarski M, Warner FJ, Thornhill P, Parkin ET, Smith AI, et al. Tumor necrosis factor-alpha convertase (ADAM17) mediates regulated ectodomain shedding of the severe-acute respiratory syndrome-coronavirus (SARS-CoV) receptor, angiotensin-converting enzyme-2 (ACE2). *The Journal of biological chemistry.* 2005;280(34):30113-30119.
113. Liu Q, Zhang J, Tran H, Verbeek MM, Reiss K, Estus S, et al. LRP1 shedding in human brain: roles of ADAM10 and ADAM17. *Molecular neurodegeneration.* 2009;4:17.
114. Swendeman S, Mendelson K, Weskamp G, Horiuchi K, Deutsch U, Scherle P, et al. VEGF-A stimulates ADAM17-dependent shedding of VEGFR2 and crosstalk between VEGFR2 and ERK signaling. *Circ Res.* 2008;103(9):916-918.

115. Koenen RR, Pruessmeyer J, Soehnlein O, Fraemohs L, Zernecke A, Schwarz N, et al. Regulated release and functional modulation of junctional adhesion molecule A by disintegrin metalloproteinases. *Blood.* 2009;113(19):4799-4809.
116. Zatovicova M, Sedlakova O, Svastova E, Ohradanova A, Ciampor F, Arribas J, et al. Ectodomain shedding of the hypoxia-induced carbonic anhydrase IX is a metalloprotease-dependent process regulated by TACE/ADAM17. *Br J Cancer.* 2005;93(11):1267-1276.
117. Maretzky T, Schulte M, Ludwig A, Rose-John S, Blobel C, Hartmann D, et al. L1 is sequentially processed by two differently activated metalloproteases and presenilin/gamma-secretase and regulates neural cell adhesion, cell migration, and neurite outgrowth. *Mol Cell Biol.* 2005;25(20):9040-9053.
118. Thorp E, Vaisar T, Subramanian M, Mautner L, Blobel C, and Tabas I. Shedding of the Mer tyrosine kinase receptor is mediated by ADAM17 protein through a pathway involving reactive oxygen species, protein kinase Cdelta, and p38 mitogen-activated protein kinase (MAPK). *The Journal of biological chemistry.* 2011;286(38):33335-33344.
119. Endres K, Postina R, Schroeder A, Mueller U, and Fahrenholz F. Shedding of the amyloid precursor protein-like protein APLP2 by disintegrin-metalloproteinases. *The FEBS journal.* 2005;272(22):5808-5820.
120. Vincent B, Paitel E, Saftig P, Frobert Y, Hartmann D, De Strooper B, et al. The disintegrins ADAM10 and TACE contribute to the constitutive and phorbol ester-regulated normal cleavage of the cellular prion protein. *The Journal of biological chemistry.* 2001;276(41):37743-37746.
121. Fabre-Lafay S, Garrido-Urbani S, Reymond N, Goncalves A, Dubreuil P, and Lopez M. Nectin-4, a new serological breast cancer marker, is a substrate for tumor necrosis factor-alpha-converting enzyme (TACE)/ADAM-17. *The Journal of biological chemistry.* 2005;280(20):19543-19550.
122. Buxbaum JD, Liu KN, Luo Y, Slack JL, Stocking KL, Peschon JJ, et al. Evidence that tumor necrosis factor alpha converting enzyme is involved in regulated alpha-secretase cleavage of the Alzheimer amyloid protein precursor. *The Journal of biological chemistry.* 1998;273(43):27765-27767.
123. Kummer MP, Maruyama H, Huelsmann C, Baches S, Weggen S, and Koo EH. Formation of Pmel17 amyloid is regulated by juxtamembrane metalloproteinase cleavage, and the resulting C-terminal fragment is a substrate for gamma-secretase. *The Journal of biological chemistry.* 2009;284(4):2296-2306.
124. Wu J, Tao N, Tian Y, Xing G, Lv H, Han J, et al. Proteolytic maturation of Drosophila Neuroligin 3 by tumor necrosis factor alpha-converting enzyme in the nervous system. *Biochim Biophys Acta.* 2018;1862(3):440-450.
125. Wanger TM, Dewitt S, Collins A, Maitland NJ, Poghosyan Z, and Knauper V. Differential regulation of TROP2 release by PKC isoforms through vesicles and ADAM17. *Cellular signalling.* 2015;27(7):1325-1335.
126. Kalus I, Bormann U, Mzoughi M, Schachner M, and Kleene R. Proteolytic cleavage of the neural cell adhesion molecule by ADAM17/TACE is involved in neurite outgrowth. *J Neurochem.* 2006;98(1):78-88.
127. Dolnik O, Volchkova V, Garten W, Carbonnelle C, Becker S, Kahnt J, et al. Ectodomain shedding of the glycoprotein GP of Ebola virus. *EMBO J.* 2004;23(10):2175-2184.
128. Malapeira J, Esselens C, Bech-Serra JJ, Canals F, and Arribas J. ADAM17 (TACE) regulates TGFbeta signaling through the cleavage of vasorin. *Oncogene.* 2011;30(16):1912-1922.
129. Garton KJ, Gough PJ, Philalay J, Wille PT, Blobel CP, Whitehead RH, et al. Stimulated shedding of vascular cell adhesion molecule 1 (VCAM-1) is mediated by tumor necrosis factor-alpha-converting enzyme (ADAM 17). *The Journal of biological chemistry.* 2003;278(39):37459-37464.
130. Romee R, Foley B, Lenvik T, Wang Y, Zhang B, Ankarlo D, et al. NK cell CD16 surface expression and function is regulated by a disintegrin and metalloprotease-17 (ADAM17). *Blood.* 2013;121(18):3599-3608.
131. Chen CD, Podvin S, Gillespie E, Leeman SE, and Abraham CR. Insulin stimulates the cleavage and release of the extracellular domain of Klotho by ADAM10 and ADAM17. *Proceedings of the National Academy of Sciences of the United States of America.* 2007;104(50):19796-19801.
132. Valeva A, Walev I, Weis S, Boukhallouk F, Wassenaar TM, Endres K, et al. A cellular metalloproteinase activates Vibrio cholerae pro-cytolysin. *The Journal of biological chemistry.* 2004;279(24):25143-25148.
133. Huang TF, Holt JC, Lukasiewicz H, and Niewiarowski S. Trigramin. A low molecular weight peptide inhibiting fibrinogen interaction with platelet receptors expressed on glycoprotein IIb-IIIa complex. *The Journal of biological chemistry.* 1987;262(33):16157-16163.
134. Huang J, Bridges LC, and White JM. Selective modulation of integrin-mediated cell migration by distinct ADAM family members. *Molecular biology of the cell.* 2005;16(10):4982-4991.
135. Eto K, Huet C, Tarui T, Kupriyanov S, Liu HZ, Puzon-McLaughlin W, et al. Functional classification of ADAMs based on a conserved motif for binding to integrin alpha 9beta 1: implications for sperm-egg binding and other cell interactions. *The Journal of biological chemistry.* 2002;277(20):17804-17810.
136. Tomczuk M, Takahashi Y, Huang J, Murase S, Mistretta M, Klaffky E, et al. Role of multiple beta1 integrins in cell adhesion to the disintegrin domains of ADAMs 2 and 3. *Experimental cell research.* 2003;290(1):68-81.

137. Bridges LC, Sheppard D, and Bowditch RD. ADAM disintegrin-like domain recognition by the lymphocyte integrins alpha4beta1 and alpha4beta7. *Biochem J.* 2005;387(Pt 1):101-108.
138. Ridley AJ, Schwartz MA, Burridge K, Firtel RA, Ginsberg MH, Borisy G, et al. Cell migration: integrating signals from front to back. *Science (New York, NY).* 2003;302(5651):1704-1709.
139. Luo BH, and Springer TA. Integrin structures and conformational signaling. *Current opinion in cell biology.* 2006;18(5):579-586.
140. Takeda S. Three-dimensional domain architecture of the ADAM family proteinases. *Seminars in cell & developmental biology.* 2009;20(2):146-152.
141. Takeda S, Igarashi T, Mori H, and Araki S. Crystal structures of VAP1 reveal ADAMs' MDC domain architecture and its unique C-shaped scaffold. *EMBO J.* 2006;25(11):2388-2396.
142. Iba K, Albrechtsen R, Gilpin B, Fröhlich C, Loechel F, Zolkiewska A, et al. The cysteine-rich domain of human ADAM 12 supports cell adhesion through syndecans and triggers signaling events that lead to β1 integrin–dependent cell spreading. *The Journal of cell biology.* 2000;149(5):1143-1156.
143. Thodeti CK, Albrechtsen R, Grauslund M, Asmar M, Larsson C, Takada Y, et al. ADAM12/syndecan-4 signaling promotes beta 1 integrin-dependent cell spreading through protein kinase Calpha and RhoA. *The Journal of biological chemistry.* 2003;278(11):9576-9584.
144. Iba K, Albrechtsen R, Gilpin BJ, Loechel F, and Wewer UM. Cysteine-rich domain of human ADAM 12 (meltrin alpha) supports tumor cell adhesion. *The American journal of pathology.* 1999;154(5):1489-1501.
145. Lee MH, Dodds P, Verma V, Maskos K, Knauper V, and Murphy G. Tailoring tissue inhibitor of metalloproteinases-3 to overcome the weakening effects of the cysteine-rich domains of tumour necrosis factor-alpha converting enzyme. *Biochem J.* 2003;371(Pt 2):369-376.
146. Janes PW, Saha N, Barton WA, Kolev MV, Wimmer-Kleikamp SH, Nievergall E, et al. Adam meets Eph: an ADAM substrate recognition module acts as a molecular switch for ephrin cleavage in trans. *Cell.* 2005;123(2):291-304.
147. White J, Bridges L, DeSimone D, Tomczuk M, and Wolfsberg T. *The ADAM Family of Proteases*. Springer; 2005:1-28.
148. Fan H, Turck CW, and Derynck R. Characterization of growth factor-induced serine phosphorylation of tumor necrosis factor-alpha converting enzyme and of an alternatively translated polypeptide. *The Journal of biological chemistry.* 2003;278(20):18617-18627.
149. Le Gall SM, Maretzky T, Issuree PD, Niu XD, Reiss K, Saftig P, et al. ADAM17 is regulated by a rapid and reversible mechanism that controls access to its catalytic site. *J Cell Sci.* 2010;123(Pt 22):3913-3922.
150. Arribas J, and Ruiz-Paz S. *The ADAM family of proteases*. Springer; 2005:171-197.
151. Murphy G. *Seminars in cell & developmental biology*. Elsevier; 2009:138-145.
152. Gutwein P, Mechtersheimer S, Riedle S, Stoeck A, Gast D, Joumaa S, et al. ADAM10-mediated cleavage of L1 adhesion molecule at the cell surface and in released membrane vesicles. *FASEB journal : official publication of the Federation of American Societies for Experimental Biology.* 2003;17(2):292-294.
153. Schlondorff J, Becherer JD, and Blobel CP. Intracellular maturation and localization of the tumour necrosis factor alpha convertase (TACE). *Biochem J.* 2000;347 Pt 1:131-138.
154. Prox J, Willenbrock M, Weber S, Lehmann T, Schmidt-Arras D, Schwanbeck R, et al. Tetraspanin15 regulates cellular trafficking and activity of the ectodomain sheddase ADAM10. *Cellular and molecular life sciences : CMLS.* 2012;69(17):2919-2932.
155. Adrain C, Zettl M, Christova Y, Taylor N, and Freeman M. Tumor necrosis factor signaling requires iRhom2 to promote trafficking and activation of TACE. *Science (New York, NY).* 2012;335(6065):225-228.
156. Allinson TM, Parkin ET, Turner AJ, and Hooper NM. ADAMs family members as amyloid precursor protein alpha-secretases. *Journal of neuroscience research.* 2003;74(3):342-352.
157. Hundhausen C, Misztela D, Berkhout TA, Broadway N, Saftig P, Reiss K, et al. The disintegrin-like metalloproteinase ADAM10 is involved in constitutive cleavage of CX3CL1 (fractalkine) and regulates CX3CL1-mediated cell-cell adhesion. *Blood.* 2003;102(4):1186-1195.
158. Matthews V, Schuster B, Schutze S, Bussmeyer I, Ludwig A, Hundhausen C, et al. Cellular cholesterol depletion triggers shedding of the human interleukin-6 receptor by ADAM10 and ADAM17 (TACE). *The Journal of biological chemistry.* 2003;278(40):38829-38839.
159. Argast GM, Campbell JS, Brooling JT, and Fausto N. Epidermal growth factor receptor transactivation mediates tumor necrosis factor-induced hepatocyte replication. *The Journal of biological chemistry.* 2004;279(33):34530-34536.
160. McGeehan GM, Becherer JD, Bast RC, Jr., Boyer CM, Champion B, Connolly KM, et al. Regulation of tumour necrosis factor-alpha processing by a metalloproteinase inhibitor. *Nature.* 1994;370(6490):558-561.

161. Zhang Z, Oliver P, Lancaster JR, Jr., Schwarzenberger PO, Joshi MS, Cork J, et al. Reactive oxygen species mediate tumor necrosis factor alpha-converting, enzyme-dependent ectodomain shedding induced by phorbol myristate acetate. *FASEB J.* 2001;15(2):303-305.
162. Massague J, and Pandiella A. Membrane-anchored growth factors. *Annu Rev Biochem.* 1993;62(1):515-541.
163. Arribas J, and Merlos-Suarez A. Shedding of plasma membrane proteins. *Curr Top Dev Biol.* 2003;54:125-144.
164. Black RA, Rauch CT, Kozlosky CJ, Peschon JJ, Slack JL, Wolfson MF, et al. A metalloproteinase disintegrin that releases tumour-necrosis factor-alpha from cells. *Nature.* 1997;385(6618):729-733.
165. Doedens JR, and Black RA. Stimulation-induced down-regulation of tumor necrosis factor-alpha converting enzyme. *The Journal of biological chemistry.* 2000;275(19):14598-14607.
166. Doedens JR, Mahimkar RM, and Black RA. TACE/ADAM-17 enzymatic activity is increased in response to cellular stimulation. *Biochem Biophys Res Commun.* 2003;308(2):331-338.
167. Fischer OM, Hart S, Gschwind A, and Ullrich A. EGFR signal transactivation in cancer cells. *Biochem Soc Trans.* 2003;31(Pt 6):1203-1208.
168. Schafer B, Marg B, Gschwind A, and Ullrich A. Distinct ADAM metalloproteinases regulate G protein-coupled receptor-induced cell proliferation and survival. *The Journal of biological chemistry.* 2004;279(46):47929-47938.
169. Schafer B, Gschwind A, and Ullrich A. Multiple G-protein-coupled receptor signals converge on the epidermal growth factor receptor to promote migration and invasion. *Oncogene.* 2004;23(4):991-999.
170. Ohtsu H, Dempsey PJ, and Eguchi S. ADAMs as mediators of EGF receptor transactivation by G protein-coupled receptors. *American journal of physiology Cell physiology.* 2006;291(1):C1-10.
171. Xu P, and Derynck R. Direct activation of TACE-mediated ectodomain shedding by p38 MAP kinase regulates EGF receptor-dependent cell proliferation. *Molecular cell.* 2010;37(4):551-566.
172. Elliott KJ, Bourne AM, Takayanagi T, Takaguri A, Kobayashi T, Eguchi K, et al. ADAM17 silencing by adenovirus encoding miRNA-embedded siRNA revealed essential signal transduction by angiotensin II in vascular smooth muscle cells. *Journal of molecular and cellular cardiology.* 2013;62:1-7.
173. Lemjabbar H, and Basbaum C. Platelet-activating factor receptor and ADAM10 mediate responses to Staphylococcus aureus in epithelial cells. *Nat Med.* 2002;8(1):41-46.
174. Yan Y, Shirakabe K, and Werb Z. The metalloprotease Kuzbanian (ADAM10) mediates the transactivation of EGF receptor by G protein-coupled receptors. *The Journal of cell biology.* 2002;158(2):221-226.
175. Asakura M, Kitakaze M, Takashima S, Liao Y, Ishikura F, Yoshinaka T, et al. Cardiac hypertrophy is inhibited by antagonism of ADAM12 processing of HB-EGF: metalloproteinase inhibitors as a new therapy. *Nat Med.* 2002;8(1):35-40.
176. Wakatsuki S, Kurisaki T, and Sehara-Fujisawa A. Lipid rafts identified as locations of ectodomain shedding mediated by Meltrin beta/ADAM19. *J Neurochem.* 2004;89(1):119-123.
177. Amour A, Slocombe PM, Webster A, Butler M, Knight CG, Smith BJ, et al. TNF-alpha converting enzyme (TACE) is inhibited by TIMP-3. *FEBS Lett.* 1998;435(1):39-44.
178. Xu P, Liu J, Sakaki-Yumoto M, and Derynck R. TACE activation by MAPK-mediated regulation of cell surface dimerization and TIMP3 association. *Science signaling.* 2012;5(222):ra34.
179. Amour A, Knight CG, Webster A, Slocombe PM, Stephens PE, Knauper V, et al. The in vitro activity of ADAM-10 is inhibited by TIMP-1 and TIMP-3. *FEBS Lett.* 2000;473(3):275-279.
180. Amour A, Knight CG, English WR, Webster A, Slocombe PM, Knauper V, et al. The enzymatic activity of ADAM8 and ADAM9 is not regulated by TIMPs. *FEBS Lett.* 2002;524(1-3):154-158.
181. Muraguchi T, Takegami Y, Ohtsuka T, Kitajima S, Chandana EP, Omura A, et al. RECK modulates Notch signaling during cortical neurogenesis by regulating ADAM10 activity. *Nature neuroscience.* 2007;10(7):838-845.
182. Moss ML, Bomar M, Liu Q, Sage H, Dempsey P, Lenhart PM, et al. The ADAM10 prodomain is a specific inhibitor of ADAM10 proteolytic activity and inhibits cellular shedding events. *J Biol Chem.* 2007;282(49):35712-35721.
183. Kefaloyianni E, Muthu ML, Kaeppler J, Sun X, Sabbisetti V, Chalaris A, et al. ADAM17 substrate release in proximal tubule drives kidney fibrosis. *JCI Insight.* 2016;1(13).
184. Wong E, Cohen T, Romi E, Levin M, Peleg Y, Arad U, et al. Harnessing the natural inhibitory domain to control TNFalpha Converting Enzyme (TACE) activity in vivo. *Sci Rep.* 2016;6:35598.
185. Sagi I, Wong E, and Afik R. Variants of TACE pro-domain as TNF-A inhibitor and their medical use. U.S. Patent 9,764,008.; 2017.
186. Kenny PA. Tackling EGFR signaling with TACE antagonists: a rational target for metalloprotease inhibitors in cancer. *Expert Opin Ther Targets.* 2007;11(10):1287-1298.
187. Moss ML, Sklair-Tavron L, and Nudelman R. Drug insight: tumor necrosis factor-converting enzyme as a pharmaceutical target for rheumatoid arthritis. *Nat Clin Pract Rheumatol.* 2008;4(6):300-309.

188. Moss ML, and Minond D. Recent Advances in ADAM17 Research: A Promising Target for Cancer and Inflammation. *Mediators Inflamm.* 2017;2017:9673537.
189. Tellier E, Canault M, Rebsomen L, Bonardo B, Juhan-Vague I, Nalbone G, et al. The shedding activity of ADAM17 is sequestered in lipid rafts. *Exp Cell Res.* 2006;312(20):3969-3980.
190. von Tresckow B, Kallen KJ, von Strandmann EP, Borchmann P, Lange H, Engert A, et al. Depletion of cellular cholesterol and lipid rafts increases shedding of CD30. *J Immunol.* 2004;172(7):4324-4331.
191. Srinivasan S, Romagnoli M, Bohm A, and Sonenshein GE. N-glycosylation regulates ADAM8 processing and activation. *J Biol Chem.* 2014;289(48):33676-33688.
192. Fry JL, and Toker A. Secreted and membrane-bound isoforms of protease ADAM9 have opposing effects on breast cancer cell migration. *Cancer Res.* 2010;70(20):8187-8198.
193. Kodama T, Ikeda E, Okada A, Ohtsuka T, Shimoda M, Shiomi T, et al. ADAM12 is selectively overexpressed in human glioblastomas and is associated with glioblastoma cell proliferation and shedding of heparin-binding epidermal growth factor. *Am J Pathol.* 2004;165(5):1743-1753.
194. Howard L, Nelson KK, Maciewicz RA, and Blobel CP. Interaction of the metalloprotease disintegrins MDC9 and MDC15 with two SH3 domain-containing proteins, endophilin I and SH3PX1. *J Biol Chem.* 1999;274(44):31693-31699.
195. Chavaroche A, Cudic M, Giulianotti M, Houghten RA, Fields GB, and Minond D. Glycosylation of a disintegrin and metalloprotease 17 affects its activity and inhibition. *Anal Biochem.* 2014;449:68-75.
196. Minond D, Cudic M, Bionda N, Giulianotti M, Maida L, Houghten RA, et al. Discovery of novel inhibitors of a disintegrin and metalloprotease 17 (ADAM17) using glycosylated and non-glycosylated substrates. *J Biol Chem.* 2012;287(43):36473-36487.
197. Ehrnsperger A, Rehli M, Thu-Hang P, and Kreutz M. Epigenetic regulation of the dendritic cell-marker gene ADAM19. *Biochem Biophys Res Commun.* 2005;332(2):456-464.
198. Chan MW, Huang YW, Hartman-Frey C, Kuo CT, Deatherage D, Qin H, et al. Aberrant transforming growth factor beta1 signaling and SMAD4 nuclear translocation confer epigenetic repression of ADAM19 in ovarian cancer. *Neoplasia (New York, NY).* 2008;10(9):908-919.
199. Yang Y, Haitchi HM, Cakebread J, Sammut D, Harvey A, Powell RM, et al. Epigenetic mechanisms silence a disintegrin and metalloprotease 33 expression in bronchial epithelial cells. *The Journal of allergy and clinical immunology.* 2008;121(6):1393-1399, 1399 e1391-1314.
200. Ray BK, Dhar S, Henry C, Rich A, and Ray A. Epigenetic regulation by Z-DNA silencer function controls cancer-associated ADAM-12 expression in breast cancer: cross-talk between MeCP2 and NF1 transcription factor family. *Cancer research.* 2013;73(2):736-744.
201. Nakao K, Miyaaki H, and Ichikawa T. Antitumor function of microRNA-122 against hepatocellular carcinoma. *Journal of gastroenterology.* 2014;49(4):589-593.
202. Albrechtsen R, Kveiborg M, Stautz D, Vikesa J, Noer JB, Kotzsh A, et al. ADAM12 redistributes and activates MMP-14, resulting in gelatin degradation, reduced apoptosis and increased tumor growth. *Journal of cell science.* 2013;126(Pt 20):4707-4720.
203. Mochizuki S, Shimoda M, Shiomi T, Fujii Y, and Okada Y. ADAM28 is activated by MMP-7 (matrilysin-1) and cleaves insulin-like growth factor binding protein-3. *Biochem Biophys Res Commun.* 2004;315(1):79-84.
204. Chan KM, Wong HL, Jin G, Liu B, Cao R, Cao Y, et al. MT1-MMP inactivates ADAM9 to regulate FGFR2 signaling and calvarial osteogenesis. *Dev Cell.* 2012;22(6):1176-1190.
205. Wang X, Chow FL, Oka T, Hao L, Lopez-Campistrous A, Kelly S, et al. Matrix metalloproteinase-7 and ADAM-12 (a disintegrin and metalloproteinase-12) define a signaling axis in agonist-induced hypertension and cardiac hypertrophy. *Circulation.* 2009;119(18):2480-2489.
206. Odenbach J, Wang X, Cooper S, Chow FL, Oka T, Lopaschuk G, et al. MMP-2 mediates angiotensin II-induced hypertension under the transcriptional control of MMP-7 and TACE. *Hypertension.* 2011;57(1):123-130.
207. Xiao LJ, Lin P, Lin F, Liu X, Qin W, Zou HF, et al. ADAM17 targets MMP-2 and MMP-9 via EGFR-MEK-ERK pathway activation to promote prostate cancer cell invasion. *Int J Oncol.* 2012;40(5):1714-1724.
208. Li YQ, Yan JP, Xu WL, Wang H, Xia YJ, Wang HJ, et al. ADAM17 mediates MMP9 expression in lung epithelial cells. *PloS one.* 2013;8(1):e51701.
209. Moss ML, Jin SL, Milla ME, Bickett DM, Burkhart W, Carter HL, et al. Cloning of a disintegrin metalloproteinase that processes precursor tumour-necrosis factor-alpha. *Nature.* 1997;385(6618):733-736.
210. Black RA. Tumor necrosis factor-alpha converting enzyme. *Int J Biochem Cell Biol.* 2002;34(1):1-5.
211. Driscoll WS, Vaisar T, Tang J, Wilson CL, and Raines EW. Macrophage ADAM17 deficiency augments CD36-dependent apoptotic cell uptake and the linked anti-inflammatory phenotype. *Circ Res.* 2013;113(1):52-61.

212. McMahan RS, Riehle KJ, Fausto N, and Campbell JS. A disintegrin and metalloproteinase 17 regulates TNF and TNFR1 levels in inflammation and liver regeneration in mice. *Am J Physiol Gastrointest Liver Physiol.* 2013;305(1):G25-34.
213. Kawahara R, Lima RN, Domingues RR, Pauletti BA, Meirelles GV, Assis M, et al. Deciphering the role of the ADAM17-dependent secretome in cell signaling. *J Proteome Res.* 2014;13(4):2080-2093.
214. Shen M, Morton J, Davidge ST, and Kassiri Z. Loss of smooth muscle cell disintegrin and metalloproteinase 17 transiently suppresses angiotensin II-induced hypertension and end-organ damage. *Journal of molecular and cellular cardiology.* 2017;103:11-21.
215. Brakebusch C, Varfolomeev EE, Batkin M, and Wallach D. Structural requirements for inducible shedding of the p55 tumor necrosis factor receptor. *The Journal of biological chemistry.* 1994;269(51):32488-32496.
216. Migaki GI, Kahn J, and Kishimoto TK. Mutational analysis of the membrane-proximal cleavage site of L-selectin: relaxed sequence specificity surrounding the cleavage site. *The Journal of experimental medicine.* 1995;182(2):549-557.
217. Mullberg J, Althoff K, Jostock T, and Rose-John S. The importance of shedding of membrane proteins for cytokine biology. *Eur Cytokine Netw.* 2000;11(1):27-38.
218. Arribas J, Lopez-Casillas F, and Massague J. Role of the juxtamembrane domains of the transforming growth factor-alpha precursor and the beta-amyloid precursor protein in regulated ectodomain shedding. *The Journal of biological chemistry.* 1997;272(27):17160-17165.
219. Tang P, Hung MC, and Klostergaard J. Length of the linking domain of human pro-tumor necrosis factor determines the cleavage processing. *Biochemistry.* 1996;35(25):8226-8233.
220. Caescu CI, Jeschke GR, and Turk BE. Active-site determinants of substrate recognition by the metalloproteinases TACE and ADAM10. *Biochem J.* 2009;424(1):79-88.
221. Black RA, Doedens JR, Mahimkar R, Johnson R, Guo L, Wallace A, et al. Substrate specificity and inducibility of TACE (tumour necrosis factor α-converting enzyme) revisited: the Ala-Val preference, and induced intrinsic activity. *Biochemical Society Symposia.* 2003;70:39-52.
222. Althoff K, Mullberg J, Aasland D, Voltz N, Kallen K, Grotzinger J, et al. Recognition sequences and structural elements contribute to shedding susceptibility of membrane proteins. *Biochem J.* 2001;353(Pt 3):663-672.
223. Franzke CW, Tasanen K, Borradori L, Huotari V, and Bruckner-Tuderman L. Shedding of collagen XVII/BP180: structural motifs influence cleavage from cell surface. *The Journal of biological chemistry.* 2004;279(23):24521-24529.
224. Schantl JA, Roza M, Van Kerkhof P, and Strous GJ. The growth hormone receptor interacts with its sheddase, the tumour necrosis factor-alpha-converting enzyme (TACE). *Biochem J.* 2004;377(Pt 2):379-384.
225. Itai T, Tanaka M, and Nagata S. Processing of tumor necrosis factor by the membrane-bound TNF-alpha-converting enzyme, but not its truncated soluble form. *European journal of biochemistry / FEBS.* 2001;268(7):2074-2082.
226. Luetteke NC, Qiu TH, Peiffer RL, Oliver P, Smithies O, and Lee DC. TGF alpha deficiency results in hair follicle and eye abnormalities in targeted and waved-1 mice. *Cell.* 1993;73(2):263-278.
227. Mann GB, Fowler KJ, Gabriel A, Nice EC, Williams RL, and Dunn AR. Mice with a null mutation of the TGF alpha gene have abnormal skin architecture, wavy hair, and curly whiskers and often develop corneal inflammation. *Cell.* 1993;73(2):249-261.
228. Iwamoto R, Yamazaki S, Asakura M, Takashima S, Hasuwa H, Miyado K, et al. Heparin-binding EGF-like growth factor and ErbB signaling is essential for heart function. *Proceedings of the National Academy of Sciences of the United States of America.* 2003;100(6):3221-3226.
229. Jackson LF, Qiu TH, Sunnarborg SW, Chang A, Zhang C, Patterson C, et al. Defective valvulogenesis in HB-EGF and TACE-null mice is associated with aberrant BMP signaling. *EMBO J.* 2003;22(11):2704-2716.
230. Miettinen PJ, Berger JE, Meneses J, Phung Y, Pedersen RA, Werb Z, et al. Epithelial immaturity and multiorgan failure in mice lacking epidermal growth factor receptor. *Nature.* 1995;376(6538):337-341.
231. Sibilia M, and Wagner EF. Strain-dependent epithelial defects in mice lacking the EGF receptor. *Science (New York, NY).* 1995;269(5221):234-238.
232. Blobel CP. ADAMs: key components in EGFR signalling and development. *Nature reviews Molecular cell biology.* 2005;6(1):32-43.
233. Hartmann D, de Strooper B, Serneels L, Craessaerts K, Herreman A, Annaert W, et al. The disintegrin/metalloprotease ADAM 10 is essential for Notch signalling but not for alpha-secretase activity in fibroblasts. *Human molecular genetics.* 2002;11(21):2615-2624.
234. Weskamp G, Cai H, Brodie TA, Higashyama S, Manova K, Ludwig T, et al. Mice lacking the metalloprotease-disintegrin MDC9 (ADAM9) have no evident major abnormalities during development or adult life. *Mol Cell Biol.* 2002;22(5):1537-1544.

235. Horiuchi K, Weskamp G, Lum L, Hammes HP, Cai H, Brodie TA, et al. Potential role for ADAM15 in pathological neovascularization in mice. *Mol Cell Biol.* 2003;23(16):5614-5624.
236. Kurisaki T, Masuda A, Sudo K, Sakagami J, Higashiyama S, Matsuda Y, et al. Phenotypic analysis of Meltrin alpha (ADAM12)-deficient mice: involvement of Meltrin alpha in adipogenesis and myogenesis. *Mol Cell Biol.* 2003;23(1):55-61.
237. Maretzky T, McIlwain DR, Issuree PD, Li X, Malapeira J, Amin S, et al. iRhom2 controls the substrate selectivity of stimulated ADAM17-dependent ectodomain shedding. *Proceedings of the National Academy of Sciences of the United States of America.* 2013;110(28):11433-11438.
238. Li X, Maretzky T, Weskamp G, Monette S, Qing X, Issuree PD, et al. iRhoms 1 and 2 are essential upstream regulators of ADAM17-dependent EGFR signaling. *Proceedings of the National Academy of Sciences of the United States of America.* 2015;112(19):6080-6085.
239. Chen G, and Goeddel DV. TNF-R1 signaling: a beautiful pathway. *Science (New York, NY).* 2002;296(5573):1634-1635.
240. Wajant H. The Fas signaling pathway: more than a paradigm. *Science (New York, NY).* 2002;296(5573):1635-1636.
241. Luo D, Luo Y, He Y, Zhang H, Zhang R, Li X, et al. Differential functions of tumor necrosis factor receptor 1 and 2 signaling in ischemia-mediated arteriogenesis and angiogenesis. *The American journal of pathology.* 2006;169(5):1886-1898.
242. Bzowska M, Jura N, Lassak A, Black RA, and Bereta J. Tumour necrosis factor-alpha stimulates expression of TNF-alpha converting enzyme in endothelial cells. *European journal of biochemistry / FEBS.* 2004;271(13):2808-2820.
243. Smalley DM, and Ley K. L-selectin: mechanisms and physiological significance of ectodomain cleavage. *J Cell Mol Med.* 2005;9(2):255-266.
244. Garton KJ, Gough PJ, and Raines EW. Emerging roles for ectodomain shedding in the regulation of inflammatory responses. *J Leukoc Biol.* 2006;79(6):1105-1116.
245. Pruessmeyer J, and Ludwig A. The good, the bad and the ugly substrates for ADAM10 and ADAM17 in brain pathology, inflammation and cancer. *Seminars in cell & developmental biology.* 2009;20(2):164-174.
246. Imhof BA, and Aurrand-Lions M. Adhesion mechanisms regulating the migration of monocytes. *Nat Rev Immunol.* 2004;4(6):432-444.
247. Dreymueller D, Theodorou K, Donners M, and Ludwig A. Fine Tuning Cell Migration by a Disintegrin and Metalloproteinases. *Mediators Inflamm.* 2017;2017:9621724.
248. Fambrough D, Pan D, Rubin GM, and Goodman CS. The cell surface metalloprotease/disintegrin Kuzbanian is required for axonal extension in Drosophila. *Proceedings of the National Academy of Sciences of the United States of America.* 1996;93(23):13233-13238.
249. Pruessmeyer J, Hess FM, Alert H, Groth E, Pasqualon T, Schwarz N, et al. Leukocytes require ADAM10 but not ADAM17 for their migration and inflammatory recruitment into the alveolar space. *Blood.* 2014;123(26):4077-4088.
250. Tang J, Zarbock A, Gomez I, Wilson CL, Lefort CT, Stadtmann A, et al. Adam17-dependent shedding limits early neutrophil influx but does not alter early monocyte recruitment to inflammatory sites. *Blood.* 2011;118(3):786-794.
251. Tsubota Y, Frey JM, Tai PW, Welikson RE, and Raines EW. Monocyte ADAM17 promotes diapedesis during transendothelial migration: identification of steps and substrates targeted by metalloproteinases. *Journal of immunology (Baltimore, Md : 1950).* 2013;190(8):4236-4244.
252. Peschon JJ, Slack JL, Reddy P, Stocking KL, Sunnarborg SW, Lee DC, et al. An essential role for ectodomain shedding in mammalian development. *Science (New York, NY).* 1998;282(5392):1281-1284.
253. Hooper NM, Karran EH, and Turner AJ. Membrane protein secretases. *Biochem J.* 1997;321 (Pt 2)(Pt 2):265-279.
254. Brown MS, Ye J, Rawson RB, and Goldstein JL. Regulated intramembrane proteolysis: a control mechanism conserved from bacteria to humans. *Cell.* 2000;100(4):391-398.
255. McCarthy AJ, Coleman-Vaughan C, and McCarthy JV. Regulated intramembrane proteolysis: emergent role in cell signalling pathways. *Biochem Soc Trans.* 2017;45(6):1185-1202.
256. Nanba D, Mammoto A, Hashimoto K, and Higashiyama S. Proteolytic release of the carboxy-terminal fragment of proHB-EGF causes nuclear export of PLZF. *The Journal of cell biology.* 2003;163(3):489-502.
257. Bao J, Wolpowitz D, Role LW, and Talmage DA. Back signaling by the Nrg-1 intracellular domain. *The Journal of cell biology.* 2003;161(6):1133-1141.
258. Postina R, Schroeder A, Dewachter I, Bohl J, Schmitt U, Kojro E, et al. A disintegrin-metalloproteinase prevents amyloid plaque formation and hippocampal defects in an Alzheimer disease mouse model. *J Clin Invest.* 2004;113(10):1456-1464.
259. Zhou HM, Weskamp G, Chesneau V, Sahin U, Vortkamp A, Horiuchi K, et al. Essential role for ADAM19 in cardiovascular morphogenesis. *Mol Cell Biol.* 2004;24(1):96-104.

260. Komatsu K, Wakatsuki S, Yamada S, Yamamura K, Miyazaki J, and Sehara-Fujisawa A. Meltrin beta expressed in cardiac neural crest cells is required for ventricular septum formation of the heart. *Developmental biology.* 2007;303(1):82-92.
261. Hoiruchi K, and Blobel CP. *The ADAM Family of Proteases*. Springer; 2005:29-64.
262. Kelly K, Hutchinson G, Nebenius-Oosthuizen D, Smith AJ, Bartsch JW, Horiuchi K, et al. Metalloprotease-disintegrin ADAM8: expression analysis and targeted deletion in mice. *Developmental dynamics : an official publication of the American Association of Anatomists.* 2005;232(1):221-231.
263. Vuohelainen V, Raitoharju E, Levula M, Lehtimaki T, Pelto-Huikko M, Honkanen T, et al. Myocardial infarction induces early increased remote ADAM8 expression of rat hearts after cardiac arrest. *Scandinavian journal of clinical and laboratory investigation.* 2011;71(7):553-562.
264. Wildeboer D, Naus S, Amy Sang QX, Bartsch JW, and Pagenstecher A. Metalloproteinase disintegrins ADAM8 and ADAM19 are highly regulated in human primary brain tumors and their expression levels and activities are associated with invasiveness. *Journal of neuropathology and experimental neurology.* 2006;65(5):516-527.
265. Chiba Y, Onoda S, Hattori Y, Maitani Y, Sakai H, and Misawa M. Upregulation of ADAM8 in the airways of mice with allergic bronchial asthma. *Lung.* 2009;187(3):179-185.
266. Guaiquil VH, Swendeman S, Zhou W, Guaiquil P, Weskamp G, Bartsch JW, et al. ADAM8 is a negative regulator of retinal neovascularization and of the growth of heterotopically injected tumor cells in mice. *Journal of molecular medicine.* 2010;88(5):497-505.
267. Mahoney ET, Benton RL, Maddie MA, Whittemore SR, and Hagg T. ADAM8 is selectively up-regulated in endothelial cells and is associated with angiogenesis after spinal cord injury in adult mice. *The Journal of comparative neurology.* 2009;512(2):243-255.
268. Horiuchi K, Zhou HM, Kelly K, Manova K, and Blobel CP. Evaluation of the contributions of ADAMs 9, 12, 15, 17, and 19 to heart development and ectodomain shedding of neuregulins beta1 and beta2. *Developmental biology.* 2005;283(2):459-471.
269. Bakken AM, Protack CD, Roztocil E, Nicholl SM, and Davies MG. Cell migration in response to the amino-terminal fragment of urokinase requires epidermal growth factor receptor activation through an ADAM-mediated mechanism. *Journal of vascular surgery.* 2009;49(5):1296-1303.
270. Guaiquil V, Swendeman S, Yoshida T, Chavala S, Campochiaro PA, and Blobel CP. ADAM9 is involved in pathological retinal neovascularization. *Mol Cell Biol.* 2009;29(10):2694-2703.
271. Zhang C, Tian L, Chi C, Wu X, Yang X, Han M, et al. Adam10 is essential for early embryonic cardiovascular development. *Developmental dynamics : an official publication of the American Association of Anatomists.* 2010;239(10):2594-2602.
272. Kurisaki T, Masuda A, Osumi N, Nabeshima Y, and Fujisawa-Sehara A. Spatially- and temporally-restricted expression of meltrin alpha (ADAM12) and beta (ADAM19) in mouse embryo. *Mechanisms of development.* 1998;73(2):211-215.
273. Yagami-Hiromasa T, Sato T, Kurisaki T, Kamijo K, Nabeshima Y, and Fujisawa-Sehara A. A metalloprotease-disintegrin participating in myoblast fusion. *Nature.* 1995;377(6550):652-656.
274. Frohlich C, Klitgaard M, Noer JB, Kotzsch A, Nehammer C, Kronqvist P, et al. ADAM12 is expressed in the tumour vasculature and mediates ectodomain shedding of several membrane-anchored endothelial proteins. *Biochem J.* 2013;452(1):97-109.
275. Naus S, Reipschlager S, Wildeboer D, Lichtenthaler SF, Mitterreiter S, Guan Z, et al. Identification of candidate substrates for ectodomain shedding by the metalloprotease-disintegrin ADAM8. *Biological chemistry.* 2006;387(3):337-346.
276. Gossens K, Naus S, Hollander GA, and Ziltener HJ. Deficiency of the metalloproteinase-disintegrin ADAM8 is associated with thymic hyper-cellularity. *PLoS One.* 2010;5(9):e12766.
277. Mauch C, Zamek J, Abety AN, Grimberg G, Fox JW, and Zigrino P. Accelerated wound repair in ADAM-9 knockout animals. *J Invest Dermatol.* 2010;130(8):2120-2130.
278. Harsha A, Stojadinovic O, Brem H, Sehara-Fujisawa A, Wewer U, Loomis CA, et al. ADAM12: a potential target for the treatment of chronic wounds. *Journal of molecular medicine.* 2008;86(8):961-969.
279. Moghadaszadeh B, Albrechtsen R, Guo LT, Zaik M, Kawaguchi N, Borup RH, et al. Compensation for dystrophin-deficiency: ADAM12 overexpression in skeletal muscle results in increased alpha 7 integrin, utrophin and associated glycoproteins. *Human molecular genetics.* 2003;12(19):2467-2479.
280. Bohm BB, Aigner T, Roy B, Brodie TA, Blobel CP, and Burkhardt H. Homeostatic effects of the metalloproteinase disintegrin ADAM15 in degenerative cartilage remodeling. *Arthritis Rheum.* 2005;52(4):1100-1109.

281. Zhao J, Chen H, Peschon JJ, Shi W, Zhang Y, Frank SJ, et al. Pulmonary hypoplasia in mice lacking tumor necrosis factor-alpha converting enzyme indicates an indispensable role for cell surface protein shedding during embryonic lung branching morphogenesis. *Developmental biology.* 2001;232(1):204-218.
282. Shi W, Chen H, Sun J, Buckley S, Zhao J, Anderson KD, et al. TACE is required for fetal murine cardiac development and modeling. *Developmental biology.* 2003;261(2):371-380.
283. Horiuchi K, Kimura T, Miyamoto T, Takaishi H, Okada Y, Toyama Y, et al. Cutting Edge: TNF- -Converting Enzyme (TACE/ADAM17) Inactivation in Mouse Myeloid Cells Prevents Lethality from Endotoxin Shock. *The Journal of Immunology.* 2007;179(5):2686-2689.
284. Canault M, Certel K, Schatzberg D, Wagner DD, and Hynes RO. The lack of ADAM17 activity during embryonic development causes hemorrhage and impairs vessel formation. *PLoS One.* 2010;5(10):e13433.
285. Chen C, Huang X, and Sheppard D. ADAM33 is not essential for growth and development and does not modulate allergic asthma in mice. *Mol Cell Biol.* 2006;26(18):6950-6956.
286. Puxeddu I, Pang YY, Harvey A, Haitchi HM, Nicholas B, Yoshisue H, et al. The soluble form of a disintegrin and metalloprotease 33 promotes angiogenesis: implications for airway remodeling in asthma. *The Journal of allergy and clinical immunology.* 2008;121(6):1400-1406, 1406 e1401-1404.
287. Al-Fakhri N, Wilhelm J, Hahn M, Heidt M, Hehrlein FW, Endisch AM, et al. Increased expression of disintegrin-metalloproteinases ADAM-15 and ADAM-9 following upregulation of integrins alpha5beta1 and alphavbeta3 in atherosclerosis. *Journal of cellular biochemistry.* 2003;89(4):808-823.
288. Maretzky T, Blobel CP, and Guaiquil V. Characterization of oxygen-induced retinopathy in mice carrying an inactivating point mutation in the catalytic site of ADAM15. *Investigative ophthalmology & visual science.* 2014;55(10):6774-6782.
289. Xie B, Shen J, Dong A, Swaim M, Hackett SF, Wyder L, et al. An Adam15 amplification loop promotes vascular endothelial growth factor-induced ocular neovascularization. *FASEB journal : official publication of the Federation of American Societies for Experimental Biology.* 2008;22(8):2775-2783.
290. Lu D, Xie S, Sukkar MB, Lu X, Scully MF, and Chung KF. Inhibition of airway smooth muscle adhesion and migration by the disintegrin domain of ADAM-15. *American journal of respiratory cell and molecular biology.* 2007;37(4):494-500.
291. Sahul ZH, Mukherjee R, Song J, McAteer J, Stroud RE, Dione DP, et al. Targeted imaging of the spatial and temporal variation of matrix metalloproteinase activity in a porcine model of postinfarct remodeling: relationship to myocardial dysfunction. *Circulation Cardiovascular imaging.* 2011;4(4):381-391.
292. Lee DC, Sunnarborg SW, Hinkle CL, Myers TJ, Stevenson M, Russell WE, et al. TACE/ADAM17 processing of EGFR ligands indicates a role as a physiological convertase. *Tissue Remodeling.* 2003;995:22-38.
293. Mendelson K, Swendeman S, Saftig P, and Blobel CP. Stimulation of the PDGFRβ activates ADAM17 and promotes metalloproteinase-dependent crosstalk between the PDGFRβ and EGFR signaling pathways. *Journal of Biological Chemistry.* 2010:jbc. M110. 102566.
294. Nuttall RK, Sampieri CL, Pennington CJ, Gill SE, Schultz GA, and Edwards DR. Expression analysis of the entire MMP and TIMP gene families during mouse tissue development. *FEBS Lett.* 2004;563(1-3):129-134.
295. Kurohara K, Komatsu K, Kurisaki T, Masuda A, Irie N, Asano M, et al. Essential roles of Meltrin beta (ADAM19) in heart development. *Developmental biology.* 2004;267(1):14-28.
296. Kalinowski A, Plowes NJ, Huang Q, Berdejo-Izquierdo C, Russell RR, and Russell KS. Metalloproteinase-dependent cleavage of neuregulin and autocrine stimulation of vascular endothelial cells. *FASEB journal : official publication of the Federation of American Societies for Experimental Biology.* 2010;24(7):2567-2575.
297. Zhou HM, Weskamp G, Chesneau V, Sahin U, Vortkamp A, Horiuchi K, et al. Essential Role for ADAM19 in Cardiovascular Morphogenesis. *Molecular and Cellular Biology.* 2003;24(1):96-104.
298. Van Eerdewegh P, Little RD, Dupuis J, Del Mastro RG, Falls K, Simon J, et al. Association of the ADAM33 gene with asthma and bronchial hyperresponsiveness. *Nature.* 2002;418(6896):426-430.
299. Holloway JW, Laxton RC, Rose-Zerilli MJ, Holloway JA, Andrews AL, Riaz Z, et al. ADAM33 expression in atherosclerotic lesions and relationship of ADAM33 gene variation with atherosclerosis. *Atherosclerosis.* 2010;211(1):224-230.
300. Lautrette A, Li S, Alili R, Sunnarborg SW, Burtin M, Lee DC, et al. Angiotensin II and EGF receptor cross-talk in chronic kidney diseases: a new therapeutic approach. *Nat Med.* 2005;11(8):867-874.
301. Deuss M, Reiss K, and Hartmann D. Part-time alpha-secretases: the functional biology of ADAM 9, 10 and 17. *Curr Alzheimer Res.* 2008;5(2):187-201.
302. Lichtenthaler SF. alpha-secretase in Alzheimer's disease: molecular identity, regulation and therapeutic potential. *J Neurochem.* 2011;116(1):10-21.

303. Lopez-Otin C, and Matrisian LM. Emerging roles of proteases in tumour suppression. *Nature reviews Cancer.* 2007;7(10):800-808.
304. Murphy G. The ADAMs: signalling scissors in the tumour microenvironment. *Nature reviews Cancer.* 2008;8(12):929-941.
305. Duffy MJ, McKiernan E, O'Donovan N, and McGowan PM. Role of ADAMs in cancer formation and progression. *Clinical cancer research : an official journal of the American Association for Cancer Research.* 2009;15(4):1140-1144.
306. van der Vorst EP, Keijbeck AA, de Winther MP, and Donners MM. A disintegrin and metalloproteases: molecular scissors in angiogenesis, inflammation and atherosclerosis. *Atherosclerosis.* 2012;224(2):302-308.
307. Dreymueller D, and Ludwig A. Considerations on inhibition approaches for proinflammatory functions of ADAM proteases. *Platelets.* 2017;28(4):354-361.
308. Messerli FH, Rimoldi SF, and Bangalore S. The Transition From Hypertension to Heart Failure: Contemporary Update. *JACC Heart failure.* 2017;5(8):543-551.
309. Rosario RF, and Wesson DE. Primary hypertension and nephropathy. *Current opinion in nephrology and hypertension.* 2006;15(2):130-134.
310. Wang X, Oka T, Chow FL, Cooper SB, Odenbach J, Lopaschuk GD, et al. Tumor necrosis factor-alpha-converting enzyme is a key regulator of agonist-induced cardiac hypertrophy and fibrosis. *Hypertension.* 2009;54(3):575-582.
311. Takayanagi T, Forrester SJ, Kawai T, Obama T, Tsuji T, Elliott KJ, et al. Vascular ADAM17 as a Novel Therapeutic Target in Mediating Cardiovascular Hypertrophy and Perivascular Fibrosis Induced by Angiotensin II. *Hypertension.* 2016;68(4):949-955.
312. Frey N, and Olson EN. Cardiac hypertrophy: the good, the bad, and the ugly. *Annu Rev Physiol.* 2003;65:45-79.
313. Rohini A, Agrawal N, Koyani CN, and Singh R. Molecular targets and regulators of cardiac hypertrophy. *Pharmacol Res.* 2010;61(4):269-280.
314. Fedak PW, Moravec CS, McCarthy PM, Altamentova SM, Wong AP, Skrtic M, et al. Altered expression of disintegrin metalloproteinases and their inhibitor in human dilated cardiomyopathy. *Circulation.* 2006;113(2):238-245.
315. Zeng SY, Chen X, Chen SR, Li Q, Wang YH, Zou J, et al. Upregulation of Nox4 promotes angiotensin II-induced epidermal growth factor receptor activation and subsequent cardiac hypertrophy by increasing ADAM17 expression. *Can J Cardiol.* 2013;29(10):1310-1319.
316. Geisterfer AA, Peach MJ, and Owens GK. Angiotensin II induces hypertrophy, not hyperplasia, of cultured rat aortic smooth muscle cells. *Circ Res.* 1988;62(4):749-756.
317. Ohtsu H, Dempsey PJ, Frank GD, Brailoiu E, Higuchi S, Suzuki H, et al. ADAM17 mediates epidermal growth factor receptor transactivation and vascular smooth muscle cell hypertrophy induced by angiotensin II. *Arterioscler Thromb Vasc Biol.* 2006;26(9):e133-137.
318. Fan D, Takawale A, Shen M, Samokhvalov V, Basu R, Patel V, et al. A Disintegrin and Metalloprotease-17 Regulates Pressure Overload-Induced Myocardial Hypertrophy and Dysfunction Through Proteolytic Processing of Integrin beta1. *Hypertension.* 2016;68(4):937-948.
319. Ross RS, Pham C, Shai SY, Goldhaber JI, Fenczik C, Glembotski CC, et al. Beta1 integrins participate in the hypertrophic response of rat ventricular myocytes. *Circ Res.* 1998;82(11):1160-1172.
320. Scheiermann C, Frenette PS, and Hidalgo A. Regulation of leucocyte homeostasis in the circulation. *Cardiovascular research.* 2015;107(3):340-351.
321. McEver RP. Selectins: initiators of leucocyte adhesion and signalling at the vascular wall. *Cardiovascular research.* 2015;107(3):331-339.
322. Gerhardt T, and Ley K. Monocyte trafficking across the vessel wall. *Cardiovascular research.* 2015;107(3):321-330.
323. Min JK, Kim YM, Kim SW, Kwon MC, Kong YY, Hwang IK, et al. TNF-related activation-induced cytokine enhances leukocyte adhesiveness: induction of ICAM-1 and VCAM-1 via TNF receptor-associated factor and protein kinase C-dependent NF-kappaB activation in endothelial cells. *Journal of immunology (Baltimore, Md : 1950).* 2005;175(1):531-540.
324. Schulz B, Pruessmeyer J, Maretzky T, Ludwig A, Blobel CP, Saftig P, et al. ADAM10 regulates endothelial permeability and T-Cell transmigration by proteolysis of vascular endothelial cadherin. *Circ Res.* 2008;102(10):1192-1201.
325. Satoh M, Ishikawa Y, Itoh T, Minami Y, Takahashi Y, and Nakamura M. The expression of TNF-alpha converting enzyme at the site of ruptured plaques in patients with acute myocardial infarction. *Eur J Clin Invest.* 2008;38(2):97-105.

326. Oksala N, Levula M, Airla N, Pelto-Huikko M, Ortiz RM, Jarvinen O, et al. ADAM-9, ADAM-15, and ADAM-17 are upregulated in macrophages in advanced human atherosclerotic plaques in aorta and carotid and femoral arteries--Tampere vascular study. *Ann Med.* 2009;41(4):279-290.
327. Akatsu T, Nakamura M, Satoh M, and Hiramori K. Increased mRNA expression of tumour necrosis factor-alpha and its converting enzyme in circulating leucocytes of patients with acute myocardial infarction. *Clinical science (London, England : 1979).* 2003;105(1):39-44.
328. Canault M, Peiretti F, Kopp F, Bonardo B, Bonzi MF, Coudeyre JC, et al. The TNF alpha converting enzyme (TACE/ADAM17) is expressed in the atherosclerotic lesions of apolipoprotein E-deficient mice: possible contribution to elevated plasma levels of soluble TNF alpha receptors. *Atherosclerosis.* 2006;187(1):82-91.
329. Nicolaou A, Zhao Z, Northoff BH, Sass K, Herbst A, Kohlmaier A, et al. Adam17 Deficiency Promotes Atherosclerosis by Enhanced TNFR2 Signaling in Mice. *Arterioscler Thromb Vasc Biol.* 2017;37(2):247-257.
330. van der Vorst EP, Zhao Z, Rami M, Holdt LM, Teupser D, Steffens S, et al. Contrasting effects of myeloid and endothelial ADAM17 on atherosclerosis development. *Thromb Haemost.* 2017;117(3):644-646.
331. Gooz P, Gooz M, Baldys A, and Hoffman S. ADAM-17 regulates endothelial cell morphology, proliferation, and in vitro angiogenesis. *Biochem Biophys Res Commun.* 2009;380(1):33-38.
332. Kwak HI, Mendoza EA, and Bayless KJ. ADAM17 co-purifies with TIMP-3 and modulates endothelial invasion responses in three-dimensional collagen matrices. *Matrix Biol.* 2009;28(8):470-479.
333. Libby P. Inflammation and Atherosclerosis. *Circulation.* 2002;105(9):1135-1143.
334. Silvestre-Roig C, de Winther MP, Weber C, Daemen MJ, Lutgens E, and Soehnlein O. Atherosclerotic plaque destabilization: mechanisms, models, and therapeutic strategies. *Circ Res.* 2014;114(1):214-226.
335. Weskamp G, Mendelson K, Swendeman S, Le Gall S, Ma Y, Lyman S, et al. Pathological neovascularization is reduced by inactivation of ADAM17 in endothelial cells but not in pericytes. *Circ Res.* 2010;106(5):932-940.
336. Fan D, Takawale A, Shen M, Wang W, Wang X, Basu R, et al. Cardiomyocyte A Disintegrin And Metalloproteinase 17 (ADAM17) Is Essential in Post-Myocardial Infarction Repair by Regulating Angiogenesis. *Circ Heart Fail.* 2015;8(5):970-979.
337. Caolo V, Swennen G, Chalaris A, Wagenaar A, Verbruggen S, Rose-John S, et al. ADAM10 and ADAM17 have opposite roles during sprouting angiogenesis. *Angiogenesis.* 2015;18(1):13-22.
338. Kessler T, Zhang L, Liu Z, Yin X, Huang Y, Wang Y, et al. ADAMTS-7 inhibits re-endothelialization of injured arteries and promotes vascular remodeling through cleavage of thrombospondin-1. *Circulation.* 2015;131(13):1191-1201.
339. Chau KH, and Elefteriades JA. Natural history of thoracic aortic aneurysms: size matters, plus moving beyond size. *Progress in cardiovascular diseases.* 2013;56(1):74-80.
340. Chaer RA, Vasoncelos R, Marone LK, Al-Khoury G, Rhee RY, Cho JS, et al. Synchronous and metachronous thoracic aneurysms in patients with abdominal aortic aneurysms. *Journal of vascular surgery.* 2012;56(5):1261-1265.
341. Itani Y, Watanabe S, Masuda Y, Hanamura K, Asakura K, Sone S, et al. Measurement of aortic diameters and detection of asymptomatic aortic aneurysms in a mass screening program using a mobile helical computed tomography unit. *Heart and vessels.* 2002;16(2):42-45.
342. Kalsch H, Lehmann N, Mohlenkamp S, Becker A, Moebus S, Schmermund A, et al. Body-surface adjusted aortic reference diameters for improved identification of patients with thoracic aortic aneurysms: results from the population-based Heinz Nixdorf Recall study. *Int J Cardiol.* 2013;163(1):72-78.
343. Norman PE, Jamrozik K, Lawrence-Brown MM, Le MT, Spencer CA, Tuohy RJ, et al. Population based randomised controlled trial on impact of screening on mortality from abdominal aortic aneurysm. *BMJ (Clinical research ed).* 2004;329(7477):1259.
344. Cosford PA, and Leng GC. Screening for abdominal aortic aneurysm. *Cochrane Database Syst Rev.* 2007(2):CD002945.
345. Svensjo S, Bjorck M, Gurtelschmid M, Djavani Gidlund K, Hellberg A, and Wanhainen A. Low prevalence of abdominal aortic aneurysm among 65-year-old Swedish men indicates a change in the epidemiology of the disease. *Circulation.* 2011;124(10):1118-1123.
346. Hiratzka LF, Bakris GL, Beckman JA, Bersin RM, Carr VF, Casey DE, Jr., et al. 2010 ACCF/AHA/AATS/ACR/ASA/SCA/SCAI/SIR/STS/SVM guidelines for the diagnosis and management of patients with Thoracic Aortic Disease: a report of the American College of Cardiology Foundation/American Heart Association Task Force on Practice Guidelines, American Association for Thoracic Surgery, American College of Radiology, American Stroke Association, Society of Cardiovascular Anesthesiologists, Society for Cardiovascular Angiography and Interventions, Society of Interventional Radiology, Society of Thoracic Surgeons, and Society for Vascular Medicine. *Circulation.* 2010;121(13):e266-369.

347. Freiberg MS, Arnold AM, Newman AB, Edwards MS, Kraemer KL, and Kuller LH. Abdominal aortic aneurysms, increasing infrarenal aortic diameter, and risk of total mortality and incident cardiovascular disease events: 10-year follow-up data from the Cardiovascular Health Study. *Circulation.* 2008;117(8):1010-1017.
348. Karthikesalingam A, Bahia SS, Patterson BO, Peach G, Vidal-Diez A, Ray KK, et al. The shortfall in long-term survival of patients with repaired thoracic or abdominal aortic aneurysms: retrospective case-control analysis of hospital episode statistics. *European journal of vascular and endovascular surgery : the official journal of the European Society for Vascular Surgery.* 2013;46(5):533-541.
349. Ruddy JM, Jones JA, and Ikonomidis JS. Pathophysiology of thoracic aortic aneurysm (TAA): is it not one uniform aorta? Role of embryologic origin. *Progress in cardiovascular diseases.* 2013;56(1):68-73.
350. Lederle FA, Johnson GR, Wilson SE, Gordon IL, Chute EP, Littooy FN, et al. Relationship of age, gender, race, and body size to infrarenal aortic diameter. The Aneurysm Detection and Management (ADAM) Veterans Affairs Cooperative Study Investigators. *Journal of vascular surgery.* 1997;26(4):595-601.
351. Guo DC, Papke CL, He R, and Milewicz DM. Pathogenesis of thoracic and abdominal aortic aneurysms. *Annals of the New York Academy of Sciences.* 2006;1085:339-352.
352. Golledge J, Muller J, Daugherty A, and Norman P. Abdominal aortic aneurysm: pathogenesis and implications for management. *Arterioscler Thromb Vasc Biol.* 2006;26(12):2605-2613.
353. Hellenthal FA, Buurman WA, Wodzig WK, and Schurink GW. Biomarkers of AAA progression. Part 1: extracellular matrix degeneration. *Nature reviews Cardiology.* 2009;6(7):464-474.
354. Hellenthal FA, Buurman WA, Wodzig WK, and Schurink GW. Biomarkers of abdominal aortic aneurysm progression. Part 2: inflammation. *Nature reviews Cardiology.* 2009;6(8):543-552.
355. Davis FM, Rateri DL, and Daugherty A. Mechanisms of aortic aneurysm formation: translating preclinical studies into clinical therapies. *Heart.* 2014;100(19):1498-1505.
356. Lindsay ME, and Dietz HC. The genetic basis of aortic aneurysm. *Cold Spring Harbor perspectives in medicine.* 2014;4(9):a015909.
357. Coady MA, Davies RR, Roberts M, Goldstein LJ, Rogalski MJ, Rizzo JA, et al. Familial patterns of thoracic aortic aneurysms. *Archives of surgery (Chicago, Ill : 1960).* 1999;134(4):361-367.
358. Albornoz G, Coady MA, Roberts M, Davies RR, Tranquilli M, Rizzo JA, et al. Familial thoracic aortic aneurysms and dissections—incidence, modes of inheritance, and phenotypic patterns. *The Annals of thoracic surgery.* 2006;82(4):1400-1405.
359. Albornoz G, Coady MA, Roberts M, Davies RR, Tranquilli M, Rizzo JA, et al. Familial thoracic aortic aneurysms and dissections--incidence, modes of inheritance, and phenotypic patterns. *Ann Thorac Surg.* 2006;82(4):1400-1405.
360. Luyckx I, Loeys BL, Curriculum topic: Disease of the a, trauma to the a, and heart. The genetic architecture of non-syndromic thoracic aortic aneurysm. *Heart.* 2015;101(20):1678-1684.
361. Fedak PW, Verma S, David TE, Leask RL, Weisel RD, and Butany J. Clinical and pathophysiological implications of a bicuspid aortic valve. *Circulation.* 2002;106(8):900-904.
362. Siu SC, and Silversides CK. Bicuspid aortic valve disease. *J Am Coll Cardiol.* 2010;55(25):2789-2800.
363. Cury M, Zeidan F, and Lobato AC. Aortic disease in the young: genetic aneurysm syndromes, connective tissue disorders, and familial aortic aneurysms and dissections. *International journal of vascular medicine.* 2013;2013:267215.
364. Garg V, Muth AN, Ransom JF, Schluterman MK, Barnes R, King IN, et al. Mutations in NOTCH1 cause aortic valve disease. *Nature.* 2005;437(7056):270-274.
365. Lee J, Shen M, Parajuli N, Oudit GY, McMurtry MS, and Kassiri Z. Gender-dependent aortic remodelling in patients with bicuspid aortic valve-associated thoracic aortic aneurysm. *Journal of molecular medicine.* 2014;92(9):939-949.
366. Saratzis A, and Bown MJ. The genetic basis for aortic aneurysmal disease. *Heart.* 2014;100(12):916-922.
367. Brownstein AJ, Ziganshin BA, Kuivaniemi H, Body SC, Bale AE, and Elefteriades JA. Genes Associated with Thoracic Aortic Aneurysm and Dissection: An Update and Clinical Implications. *Aorta (Stamford, Conn).* 2017;5(1):11-20.
368. Longo GM, Buda SJ, Fiotta N, Xiong W, Griener T, Shapiro S, et al. MMP-12 has a role in abdominal aortic aneurysms in mice. *Surgery.* 2005;137(4):457-462.
369. Pyo R, Lee JK, Shipley JM, Curci JA, Mao D, Ziporin SJ, et al. Targeted gene disruption of matrix metalloproteinase-9 (gelatinase B) suppresses development of experimental abdominal aortic aneurysms. *J Clin Invest.* 2000;105(11):1641-1649.
370. Lysgaard Poulsen J, Stubbe J, and Lindholt JS. Animal Models Used to Explore Abdominal Aortic Aneurysms: A Systematic Review. *European journal of vascular and endovascular surgery : the official journal of the European Society for Vascular Surgery.* 2016;52(4):487-499.

371. Senemaud J, Caligiuri G, Etienne H, Delbosc S, Michel JB, and Coscas R. Translational Relevance and Recent Advances of Animal Models of Abdominal Aortic Aneurysm. *Arterioscler Thromb Vasc Biol.* 2017;37(3):401-410.
372. Gertz SD, Kurgan A, and Eisenberg D. Aneurysm of the rabbit common carotid artery induced by periarterial application of calcium chloride in vivo. *J Clin Invest.* 1988;81(3):649-656.
373. Chiou AC, Chiu B, and Pearce WH. Murine aortic aneurysm produced by periarterial application of calcium chloride. *The Journal of surgical research.* 2001;99(2):371-376.
374. Wang Y, Krishna S, and Golledge J. The calcium chloride-induced rodent model of abdominal aortic aneurysm. *Atherosclerosis.* 2013;226(1):29-39.
375. Yamanouchi D, Morgan S, Stair C, Seedial S, Lengfeld J, Kent KC, et al. Accelerated aneurysmal dilation associated with apoptosis and inflammation in a newly developed calcium phosphate rodent abdominal aortic aneurysm model. *Journal of vascular surgery.* 2012;56(2):455-461.
376. Ikonomidis JS, Gibson WC, Gardner J, Sweterlitsch S, Thompson RP, Mukherjee R, et al. A murine model of thoracic aortic aneurysms. *The Journal of surgical research.* 2003;115(1):157-163.
377. Jones JA, Beck C, Barbour JR, Zavadzkas JA, Mukherjee R, Spinale FG, et al. Alterations in aortic cellular constituents during thoracic aortic aneurysm development: myofibroblast-mediated vascular remodeling. *The American journal of pathology.* 2009;175(4):1746-1756.
378. Shen M, Lee J, Basu R, Sakamuri SS, Wang X, Fan D, et al. Divergent roles of matrix metalloproteinase 2 in pathogenesis of thoracic aortic aneurysm. *Arterioscler Thromb Vasc Biol.* 2015;35(4):888-898.
379. Azuma J, Asagami T, Dalman R, and Tsao PS. Creation of murine experimental abdominal aortic aneurysms with elastase. *J Vis Exp.* 2009(29).
380. Bhamidipati CM, Mehta GS, Lu G, Moehle CW, Barbery C, DiMusto PD, et al. Development of a novel murine model of aortic aneurysms using peri-adventitial elastase. *Surgery.* 2012;152(2):238-246.
381. Johnston WF, Salmon M, Pope NH, Meher A, Su G, Stone ML, et al. Inhibition of interleukin-1beta decreases aneurysm formation and progression in a novel model of thoracic aortic aneurysms. *Circulation.* 2014;130(11 Suppl 1):S51-59.
382. Lu G, Su G, Davis JP, Schaheen B, Downs E, Roy RJ, et al. A novel chronic advanced stage abdominal aortic aneurysm murine model. *Journal of vascular surgery.* 2017;66(1):232-242 e234.
383. Ailawadi G, Eliason JL, Roelofs KJ, Sinha I, Hannawa KK, Kaldjian EP, et al. Gender differences in experimental aortic aneurysm formation. *Arterioscler Thromb Vasc Biol.* 2004;24(11):2116-2122.
384. Brophy CM, Tilson JE, Braverman IM, and Tilson MD. Age of onset, pattern of distribution, and histology of aneurysm development in a genetically predisposed mouse model. *Journal of vascular surgery.* 1988;8(1):45-48.
385. Pereira L, Lee SY, Gayraud B, Andrikopoulos K, Shapiro SD, Bunton T, et al. Pathogenetic sequence for aneurysm revealed in mice underexpressing fibrillin-1. *Proceedings of the National Academy of Sciences of the United States of America.* 1999;96(7):3819-3823.
386. Judge DP, Biery NJ, Keene DR, Geubtner J, Myers L, Huso DL, et al. Evidence for a critical contribution of haploinsufficiency in the complex pathogenesis of Marfan syndrome. *J Clin Invest.* 2004;114(2):172-181.
387. Gallo EM, Loch DC, Habashi JP, Calderon JF, Chen Y, Bedja D, et al. Angiotensin II-dependent TGF-beta signaling contributes to Loeys-Dietz syndrome vascular pathogenesis. *J Clin Invest.* 2014;124(1):448-460.
388. Ye P, Chen W, Wu J, Huang X, Li J, Wang S, et al. GM-CSF contributes to aortic aneurysms resulting from SMAD3 deficiency. *J Clin Invest.* 2013;123(5):2317-2331.
389. Zhang P, Hou S, Chen J, Zhang J, Lin F, Ju R, et al. Smad4 Deficiency in Smooth Muscle Cells Initiates the Formation of Aortic Aneurysm. *Circ Res.* 2016;118(3):388-399.
390. Gillis E, Kumar AA, Luyckx I, Preuss C, Cannaerts E, van de Beek G, et al. Candidate gene resequencing in a large bicuspid aortic valve-associated thoracic aortic aneurysm cohort: SMAD6 as an important contributor. *Frontiers in physiology.* 2017;8:400.
391. Ikonomidis JS, Barbour JR, Amani Z, Stroud RE, Herron AR, McClister DM, Jr., et al. Effects of deletion of the matrix metalloproteinase 9 gene on development of murine thoracic aortic aneurysms. *Circulation.* 2005;112(9 Suppl):I242-248.
392. Ikonomidis JS, Gibson WC, Butler JE, McClister DM, Sweterlitsch SE, Thompson RP, et al. Effects of deletion of the tissue inhibitor of matrix metalloproteinases-1 gene on the progression of murine thoracic aortic aneurysms. *Circulation.* 2004;110(11 Suppl 1):II268-273.
393. Pope NH, Salmon M, Johnston WF, Lu G, Lau CL, Upchurch GR, Jr., et al. Interleukin-6 Receptor Inhibition Prevents Descending Thoracic Aortic Aneurysm Formation. *Ann Thorac Surg.* 2015;100(5):1620-1626.
394. Liu S, Xie Z, Daugherty A, Cassis LA, Pearson KJ, Gong MC, et al. Mineralocorticoid receptor agonists induce mouse aortic aneurysm formation and rupture in the presence of high salt. *Arterioscler Thromb Vasc Biol.* 2013;33(7):1568-1579.

395. Daugherty A, Rateri DL, Charo IF, Owens AP, Howatt DA, and Cassis LA. Angiotensin II infusion promotes ascending aortic aneurysms: attenuation by CCR2 deficiency in apoE-/- mice. *Clinical science (London, England : 1979).* 2010;118(11):681-689.
396. Liu R, Lo L, Lay AJ, Zhao Y, Ting KK, Robertson EN, et al. ARHGAP18 Protects Against Thoracic Aortic Aneurysm Formation by Mitigating the Synthetic and Proinflammatory Smooth Muscle Cell Phenotype. *Circ Res.* 2017;121(5):512-524.
397. Martin-Alonso M, Garcia-Redondo AB, Guo D, Camafeita E, Martinez F, Alfranca A, et al. Deficiency of MMP17/MT4-MMP proteolytic activity predisposes to aortic aneurysm in mice. *Circ Res.* 2015;117(2):e13-26.
398. Anzai A, Shimoda M, Endo J, Kohno T, Katsumata Y, Matsuhashi T, et al. Adventitial CXCL1/G-CSF expression in response to acute aortic dissection triggers local neutrophil recruitment and activation leading to aortic rupture. *Circ Res.* 2015;116(4):612-623.
399. Maki JM, Rasanen J, Tikkanen H, Sormunen R, Makikallio K, Kivirikko KI, et al. Inactivation of the lysyl oxidase gene Lox leads to aortic aneurysms, cardiovascular dysfunction, and perinatal death in mice. *Circulation.* 2002;106(19):2503-2509.
400. Ishibashi S, Goldstein JL, Brown MS, Herz J, and Burns DK. Massive xanthomatosis and atherosclerosis in cholesterol-fed low density lipoprotein receptor-negative mice. *J Clin Invest.* 1994;93(5):1885-1893.
401. Nishijo N, Sugiyama F, Kimoto K, Taniguchi K, Murakami K, Suzuki S, et al. Salt-sensitive aortic aneurysm and rupture in hypertensive transgenic mice that overproduce angiotensin II. *Laboratory investigation; a journal of technical methods and pathology.* 1998;78(9):1059-1066.
402. Manning MW, Cassis LA, and Daugherty A. Differential effects of doxycycline, a broad-spectrum matrix metalloproteinase inhibitor, on angiotensin II-induced atherosclerosis and abdominal aortic aneurysms. *Arterioscler Thromb Vasc Biol.* 2003;23(3):483-488.
403. Cassis LA, Gupte M, Thayer S, Zhang X, Charnigo R, Howatt DA, et al. ANG II infusion promotes abdominal aortic aneurysms independent of increased blood pressure in hypercholesterolemic mice. *American journal of physiology Heart and circulatory physiology.* 2009;296(5):H1660-1665.
404. Satoh K, Nigro P, Matoba T, O'Dell MR, Cui Z, Shi X, et al. Cyclophilin A enhances vascular oxidative stress and the development of angiotensin II-induced aortic aneurysms. *Nat Med.* 2009;15(6):649-656.
405. Findeisen HM, Gizard F, Zhao Y, Cohn D, Heywood EB, Jones KL, et al. Telomerase deficiency in bone marrow-derived cells attenuates angiotensin II-induced abdominal aortic aneurysm formation. *Arterioscler Thromb Vasc Biol.* 2011;31(2):253-260.
406. Chen HZ, Wang F, Gao P, Pei JF, Liu Y, Xu TT, et al. Age-Associated Sirtuin 1 Reduction in Vascular Smooth Muscle Links Vascular Senescence and Inflammation to Abdominal Aortic Aneurysm. *Circ Res.* 2016;119(10):1076-1088.
407. Wang Y, Ait-Oufella H, Herbin O, Bonnin P, Ramkhelawon B, Taleb S, et al. TGF-beta activity protects against inflammatory aortic aneurysm progression and complications in angiotensin II-infused mice. *J Clin Invest.* 2010;120(2):422-432.
408. Basu R, Fan D, Kandalam V, Lee J, Das SK, Wang X, et al. Loss of Timp3 gene leads to abdominal aortic aneurysm formation in response to angiotensin II. *The Journal of biological chemistry.* 2012;287(53):44083-44096.
409. Ait-Oufella H, Wang Y, Herbin O, Bourcier S, Potteaux S, Joffre J, et al. Natural regulatory T cells limit angiotensin II-induced aneurysm formation and rupture in mice. *Arterioscler Thromb Vasc Biol.* 2013;33(10):2374-2379.
410. Takayanagi T, Crawford KJ, Kobayashi T, Obama T, Tsuji T, Elliott KJ, et al. Caveolin 1 is critical for abdominal aortic aneurysm formation induced by angiotensin II and inhibition of lysyl oxidase. *Clinical science (London, England : 1979).* 2014;126(11):785-794.
411. Liu Z, Morgan S, Ren J, Wang Q, Annis DS, Mosher DF, et al. Thrombospondin-1 (TSP1) contributes to the development of vascular inflammation by regulating monocytic cell motility in mouse models of abdominal aortic aneurysm. *Circ Res.* 2015;117(2):129-141.
412. Yodoi K, Yamashita T, Sasaki N, Kasahara K, Emoto T, Matsumoto T, et al. Foxp3+ regulatory T cells play a protective role in angiotensin II-induced aortic aneurysm formation in mice. *Hypertension.* 2015;65(4):889-895.
413. Zhang C, van der Voort D, Shi H, Zhang R, Qing Y, Hiraoka S, et al. Matricellular protein CCN3 mitigates abdominal aortic aneurysm. *J Clin Invest.* 2016;126(4):1282-1299.
414. Kawai T, Takayanagi T, Forrester SJ, Preston KJ, Obama T, Tsuji T, et al. Vascular ADAM17 (a Disintegrin and Metalloproteinase Domain 17) Is Required for Angiotensin II/beta-Aminopropionitrile-Induced Abdominal Aortic Aneurysm. *Hypertension.* 2017;70(5):959-963.
415. Deng GG, Martin-McNulty B, Sukovich DA, Freay A, Halks-Miller M, Thinnes T, et al. Urokinase-type plasminogen activator plays a critical role in angiotensin II–induced abdominal aortic aneurysm. *Circulation research.* 2003;92(5):510-517.

416. Zhang X, Thatcher S, Wu C, Daugherty A, and Cassis LA. Castration of male mice prevents the progression of established angiotensin II-induced abdominal aortic aneurysms. *Journal of vascular surgery.* 2015;61(3):767-776.
417. Kim HW, and Stansfield BK. Genetic and Epigenetic Regulation of Aortic Aneurysms. *BioMed research international.* 2017;2017:7268521.
418. Meijer CA, Stijnen T, Wasser MN, Hamming JF, van Bockel JH, Lindeman JH, et al. Doxycycline for stabilization of abdominal aortic aneurysms: a randomized trial. *Annals of internal medicine.* 2013;159(12):815-823.
419. Cassis LA, Rateri DL, Lu H, and Daugherty A. Bone marrow transplantation reveals that recipient AT1a receptors are required to initiate angiotensin II–induced atherosclerosis and aneurysms. *Arteriosclerosis, thrombosis, and vascular biology.* 2007;27(2):380-386.
420. Rateri DL, Moorleghen JJ, Knight V, Balakrishnan A, Howatt DA, Cassis LA, et al. Depletion of endothelial or smooth muscle cell-specific angiotensin II type 1a receptors does not influence aortic aneurysms or atherosclerosis in LDL receptor deficient mice. *PloS one.* 2012;7(12):e51483.
421. Kaschina E, Schrader F, Sommerfeld M, Kemnitz UR, Grzesiak A, Krikov M, et al. Telmisartan prevents aneurysm progression in the rat by inhibiting proteolysis, apoptosis and inflammation. *Journal of hypertension.* 2008;26(12):2361-2373.
422. Fujiwara Y, Shiraya S, Miyake T, Yamakawa S, Aoki M, Makino H, et al. Inhibition of experimental abdominal aortic aneurysm in a rat model by the angiotensin receptor blocker valsartan. *Int J Mol Med.* 2008;22(6):703-708.
423. Chen X, Lu H, Rateri DL, Cassis LA, and Daugherty A. Conundrum of angiotensin II and TGF-beta interactions in aortic aneurysms. *Current opinion in pharmacology.* 2013;13(2):180-185.
424. Habashi JP, Judge DP, Holm TM, Cohn RD, Loeys BL, Cooper TK, et al. Losartan, an AT1 antagonist, prevents aortic aneurysm in a mouse model of Marfan syndrome. *Science (New York, NY).* 2006;312(5770):117-121.
425. Moltzer E, te Riet L, Swagemakers SM, van Heijningen PM, Vermeij M, van Veghel R, et al. Impaired vascular contractility and aortic wall degeneration in fibulin-4 deficient mice: effect of angiotensin II type 1 (AT1) receptor blockade. *PLoS One.* 2011;6(8):e23411.
426. Habashi JP, Doyle JJ, Holm TM, Aziz H, Schoenhoff F, Bedja D, et al. Angiotensin II type 2 receptor signaling attenuates aortic aneurysm in mice through ERK antagonism. *Science (New York, NY).* 2011;332(6027):361-365.
427. Rateri DL, Moorleghen JJ, Balakrishnan A, Owens AP, Howatt DA, Subramanian V, et al. Endothelial Cell–Specific Deficiency of Ang II Type 1a Receptors Attenuates Ang II–Induced Ascending Aortic Aneurysms in LDL Receptor−/− MiceNovelty and Significance. *Circulation research.* 2011;108(5):574-581.
428. Rateri DL, Davis FM, Balakrishnan A, Howatt DA, Moorleghen JJ, O'Connor WN, et al. Angiotensin II induces region-specific medial disruption during evolution of ascending aortic aneurysms. *The American journal of pathology.* 2014;184(9):2586-2595.
429. El-Hamamsy I, and Yacoub MH. Cellular and molecular mechanisms of thoracic aortic aneurysms. *Nature reviews Cardiology.* 2009;6(12):771-786.
430. Kuzmik GA, Sang AX, and Elefteriades JA. Natural history of thoracic aortic aneurysms. *Journal of vascular surgery.* 2012;56(2):565-571.
431. Lu H, Rateri DL, Bruemmer D, Cassis LA, and Daugherty A. Involvement of the renin-angiotensin system in abdominal and thoracic aortic aneurysms. *Clinical science (London, England : 1979).* 2012;123(9):531-543.
432. He R, Guo DC, Sun W, Papke CL, Duraisamy S, Estrera AL, et al. Characterization of the inflammatory cells in ascending thoracic aortic aneurysms in patients with Marfan syndrome, familial thoracic aortic aneurysms, and sporadic aneurysms. *J Thorac Cardiovasc Surg.* 2008;136(4):922-929, 929 e921.
433. Dale MA, Ruhlman MK, and Baxter BT. Inflammatory cell phenotypes in AAAs: their role and potential as targets for therapy. *Arterioscler Thromb Vasc Biol.* 2015;35(8):1746-1755.
434. Curci JA, and Thompson RW. Adaptive cellular immunity in aortic aneurysms: cause, consequence, or context? *J Clin Invest.* 2004;114(2):168-171.
435. Kuivaniemi H, Platsoucas CD, and Tilson MD, 3rd. Aortic aneurysms: an immune disease with a strong genetic component. *Circulation.* 2008;117(2):242-252.
436. Szekanecz Z, Shah MR, Pearce WH, and Koch AE. Human atherosclerotic abdominal aortic aneurysms produce interleukin (IL)-6 and interferon-gamma but not IL-2 and IL-4: the possible role for IL-6 and interferon-gamma in vascular inflammation. *Agents and actions.* 1994;42(3-4):159-162.
437. Juvonen J, Surcel HM, Satta J, Teppo AM, Bloigu A, Syrjala H, et al. Elevated circulating levels of inflammatory cytokines in patients with abdominal aortic aneurysm. *Arterioscler Thromb Vasc Biol.* 1997;17(11):2843-2847.
438. Davis VA, Persidskaia RN, Baca-Regen LM, Fiotti N, Halloran BG, and Baxter BT. Cytokine pattern in aneurysmal and occlusive disease of the aorta. *The Journal of surgical research.* 2001;101(2):152-156.
439. Lacraz S, Nicod LP, Chicheportiche R, Welgus HG, and Dayer JM. IL-10 inhibits metalloproteinase and stimulates TIMP-1 production in human mononuclear phagocytes. *J Clin Invest.* 1995;96(5):2304-2310.

440. Tang PC, Yakimov AO, Teesdale MA, Coady MA, Dardik A, Elefteriades JA, et al. Transmural inflammation by interferon-gamma-producing T cells correlates with outward vascular remodeling and intimal expansion of ascending thoracic aortic aneurysms. *FASEB journal : official publication of the Federation of American Societies for Experimental Biology.* 2005;19(11):1528-1530.
441. Hannawa KK, Eliason JL, Woodrum DT, Pearce CG, Roelofs KJ, Grigoryants V, et al. L-Selectin–Mediated Neutrophil Recruitment in Experimental Rodent Aneurysm Formation. *Circulation.* 2005;112(2):241-247.
442. Tsuruda T, Kato J, Hatakeyama K, Kojima K, Yano M, Yano Y, et al. Adventitial mast cells contribute to pathogenesis in the progression of abdominal aortic aneurysm. *Circ Res.* 2008;102(11):1368-1377.
443. Sun J, Sukhova GK, Yang M, Wolters PJ, MacFarlane LA, Libby P, et al. Mast cells modulate the pathogenesis of elastase-induced abdominal aortic aneurysms in mice. *J Clin Invest.* 2007;117(11):3359-3368.
444. Ejiri J, Inoue N, Tsukube T, Munezane T, Hino Y, Kobayashi S, et al. Oxidative stress in the pathogenesis of thoracic aortic aneurysm: protective role of statin and angiotensin II type 1 receptor blocker. *Cardiovascular research.* 2003;59(4):988-996.
445. Branchetti E, Poggio P, Sainger R, Shang E, Grau JB, Jackson BM, et al. Oxidative stress modulates vascular smooth muscle cell phenotype via CTGF in thoracic aortic aneurysm. *Cardiovascular research.* 2013;100(2):316-324.
446. Dubick MA, Keen CL, DiSilvestro RA, Eskelson CD, Ireton J, and Hunter GC. Antioxidant enzyme activity in human abdominal aortic aneurysmal and occlusive disease. *Proceedings of the Society for Experimental Biology and Medicine Society for Experimental Biology and Medicine (New York, NY).* 1999;220(1):39-45.
447. Zhang J, Schmidt J, Ryschich E, Mueller-Schilling M, Schumacher H, and Allenberg JR. Inducible nitric oxide synthase is present in human abdominal aortic aneurysm and promotes oxidative vascular injury. *Journal of vascular surgery.* 2003;38(2):360-367.
448. McCormick ML, Gavrila D, and Weintraub NL. Role of oxidative stress in the pathogenesis of abdominal aortic aneurysms. *Arterioscler Thromb Vasc Biol.* 2007;27(3):461-469.
449. Emeto TI, Moxon JV, Au M, and Golledge J. Oxidative stress and abdominal aortic aneurysm: potential treatment targets. *Clinical science (London, England : 1979).* 2016;130(5):301-315.
450. Chen Q, Wang Q, Zhu J, Xiao Q, and Zhang L. Reactive oxygen species: key regulators in vascular health and diseases. *British journal of pharmacology.* 2018;175(8):1279-1292.
451. Tornwall ME, Virtamo J, Haukka JK, Albanes D, and Huttunen JK. Alpha-tocopherol (vitamin E) and beta-carotene supplementation does not affect the risk for large abdominal aortic aneurysm in a controlled trial. *Atherosclerosis.* 2001;157(1):167-173.
452. Rabkin SW. The Role Matrix Metalloproteinases in the Production of Aortic Aneurysm. *Progress in molecular biology and translational science.* 2017;147:239-265.
453. Longo GM, Xiong W, Greiner TC, Zhao Y, Fiotti N, and Baxter BT. Matrix metalloproteinases 2 and 9 work in concert to produce aortic aneurysms. *J Clin Invest.* 2002;110(5):625-632.
454. Vijungco J, Eskandari M, Flores A, Shively V, Pearce W, and Chisholm R. Enhanced abdominal aortic aneurysm (AAA) formation in timp-1-deficient (timp-1-/-) mice after local elastase perfusion. *Journal of Surgical Research.* 2003;114(2):248.
455. Xiong W, Knispel R, Mactaggart J, and Baxter BT. Effects of tissue inhibitor of metalloproteinase 2 deficiency on aneurysm formation. *Journal of vascular surgery.* 2006;44(5):1061-1066.
456. Dalton ML, Gadson PF, Jr., Wrenn RW, and Rosenquist TH. Homocysteine signal cascade: production of phospholipids, activation of protein kinase C, and the induction of c-fos and c-myb in smooth muscle cells. *FASEB journal : official publication of the Federation of American Societies for Experimental Biology.* 1997;11(8):703-711.
457. Gadson PF, Jr., Dalton ML, Patterson E, Svoboda DD, Hutchinson L, Schram D, et al. Differential response of mesoderm- and neural crest-derived smooth muscle to TGF-beta1: regulation of c-myb and alpha1 (I) procollagen genes. *Exp Cell Res.* 1997;230(2):169-180.
458. Iwasaki H, Eguchi S, Ueno H, Marumo F, and Hirata Y. Mechanical stretch stimulates growth of vascular smooth muscle cells via epidermal growth factor receptor. *American journal of physiology Heart and circulatory physiology.* 2000;278(2):H521-529.
459. Owens GK, Kumar MS, and Wamhoff BR. Molecular regulation of vascular smooth muscle cell differentiation in development and disease. *Physiol Rev.* 2004;84(3):767-801.
460. Beamish JA, He P, Kottke-Marchant K, and Marchant RE. Molecular regulation of contractile smooth muscle cell phenotype: implications for vascular tissue engineering. *Tissue Eng Part B Rev.* 2010;16(5):467-491.
461. Sachdeva J, Mahajan A, Cheng J, Baeten JT, Lilly B, Kuivaniemi H, et al. Smooth muscle cell-specific Notch1 haploinsufficiency restricts the progression of abdominal aortic aneurysm by modulating CTGF expression. *PLoS One.* 2017;12(5):e0178538.

462. Liang ES, Cheng W, Yang RX, Bai WW, Liu X, and Zhao YX. Peptidyl-prolyl isomerase Pin1 deficiency attenuates angiotensin II-induced abdominal aortic aneurysm formation in ApoE(-/-) mice. *Journal of molecular and cellular cardiology.* 2018;114:334-344.
463. Chiu JJ, and Chien S. Effects of disturbed flow on vascular endothelium: pathophysiological basis and clinical perspectives. *Physiol Rev.* 2011;91(1):327-387.
464. Baeyens N, Bandyopadhyay C, Coon BG, Yun S, and Schwartz MA. Endothelial fluid shear stress sensing in vascular health and disease. *J Clin Invest.* 2016;126(3):821-828.
465. Tsai MC, Chen L, Zhou J, Tang Z, Hsu TF, Wang Y, et al. Shear stress induces synthetic-to-contractile phenotypic modulation in smooth muscle cells via peroxisome proliferator-activated receptor alpha/delta activations by prostacyclin released by sheared endothelial cells. *Circ Res.* 2009;105(5):471-480.
466. Cai H, and Harrison DG. Endothelial dysfunction in cardiovascular diseases: the role of oxidant stress. *Circ Res.* 2000;87(10):840-844.
467. Gao L, Siu KL, Chalupsky K, Nguyen A, Chen P, Weintraub NL, et al. Role of uncoupled endothelial nitric oxide synthase in abdominal aortic aneurysm formation: treatment with folic acid. *Hypertension.* 2012;59(1):158-166.
468. Fan LM, Douglas G, Bendall JK, McNeill E, Crabtree MJ, Hale AB, et al. Endothelial cell-specific reactive oxygen species production increases susceptibility to aortic dissection. *Circulation.* 2014;129(25):2661-2672.
469. Goumans MJ, and Ten Dijke P. TGF-beta Signaling in Control of Cardiovascular Function. *Cold Spring Harbor perspectives in biology.* 2018;10(2).
470. Brown DJ, Rzucidlo EM, Merenick BL, Wagner RJ, Martin KA, and Powell RJ. Endothelial cell activation of the smooth muscle cell phosphoinositide 3-kinase/Akt pathway promotes differentiation. *Journal of vascular surgery.* 2005;41(3):509-516.
471. Behrendt D, and Ganz P. Endothelial function. From vascular biology to clinical applications. *Am J Cardiol.* 2002;90(10C):40L-48L.
472. Gonzalez MA, and Selwyn AP. Endothelial function, inflammation, and prognosis in cardiovascular disease. *Am J Med.* 2003;115 Suppl 8A:99S-106S.
473. Davignon J, and Ganz P. Role of endothelial dysfunction in atherosclerosis. *Circulation.* 2004;109(23 Suppl 1):III27-32.
474. Endemann DH, and Schiffrin EL. Endothelial dysfunction. *Journal of the American Society of Nephrology : JASN.* 2004;15(8):1983-1992.
475. Choke E, Cockerill GW, Dawson J, Wilson RW, Jones A, Loftus IM, et al. Increased angiogenesis at the site of abdominal aortic aneurysm rupture. *Annals of the New York Academy of Sciences.* 2006;1085:315-319.
476. Satoh H, Nakamura M, Satoh M, Nakajima T, Izumoto H, Maesawa C, et al. Expression and localization of tumour necrosis factor-alpha and its converting enzyme in human abdominal aortic aneurysm. *Clinical science (London, England : 1979).* 2004;106(3):301-306.
477. Folkesson M, Li C, Frebelius S, Swedenborg J, Wagsater D, Williams KJ, et al. Proteolytically active ADAM10 and ADAM17 carried on membrane microvesicles in human abdominal aortic aneurysms. *Thromb Haemost.* 2015;114(6):1165-1174.
478. Li Y, Yang C, Ma G, Cui L, Gu X, Chen Y, et al. Analysis of ADAM17 polymorphisms and susceptibility to sporadic abdominal aortic aneurysm. *Cell Physiol Biochem.* 2014;33(5):1426-1438.
479. Geng L, Wang W, Chen Y, Cao J, Lu L, Chen Q, et al. Elevation of ADAM10, ADAM17, MMP-2 and MMP-9 expression with media degeneration features CaCl2-induced thoracic aortic aneurysm in a rat model. *Experimental and molecular pathology.* 2010;89(1):72-81.
480. Kaneko H, Anzai T, Horiuchi K, Kohno T, Nagai T, Anzai A, et al. Tumor necrosis factor-alpha converting enzyme is a key mediator of abdominal aortic aneurysm development. *Atherosclerosis.* 2011;218(2):470-478.
481. Lederle FA. Vascular disease: is AAA screening worth the cost? *Nature reviews Cardiology.* 2009;6(10):616-618.
482. Fleming C, Whitlock EP, Beil TL, and Lederle FA. Screening for abdominal aortic aneurysm: a best-evidence systematic review for the U.S. Preventive Services Task Force. *Annals of internal medicine.* 2005;142(3):203-211.
483. Kent KC, Zwolak RM, Jaff MR, Hollenbeck ST, Thompson RW, Schermerhorn ML, et al. Screening for abdominal aortic aneurysm: a consensus statement. *Journal of vascular surgery.* 2004;39(1):267-269.
484. van Bogerijen GH, Tolenaar JL, Grassi V, Lomazzi C, Segreti S, Rampoldi V, et al. Biomarkers in TAA-the Holy Grail. *Progress in cardiovascular diseases.* 2013;56(1):109-115.
485. Gabel G, Northoff BH, Weinzierl I, Ludwig S, Hinterseher I, Wilfert W, et al. Molecular Fingerprint for Terminal Abdominal Aortic Aneurysm Disease. *Journal of the American Heart Association.* 2017;6(12).
486. Kuivaniemi H, Ryer EJ, Elmore JR, and Tromp G. Understanding the pathogenesis of abdominal aortic aneurysms. *Expert review of cardiovascular therapy.* 2015;13(9):975-987.

487. Zhang P, Shen M, Fernandez-Patron C, and Kassiri Z. ADAMs family and relatives in cardiovascular physiology and pathology. *Journal of molecular and cellular cardiology.* 2016;93:186-199.
488. Shimoda M, Horiuchi K, Sasaki A, Tsukamoto T, Okabayashi K, Hasegawa H, et al. Epithelial Cell-Derived a Disintegrin and Metalloproteinase-17 Confers Resistance to Colonic Inflammation Through EGFR Activation. *EBioMedicine.* 2016;5:114-124.
489. Di Gregoli K, Mohamad Anuar NN, Bianco R, White SJ, Newby AC, George SJ, et al. MicroRNA-181b Controls Atherosclerosis and Aneurysms Through Regulation of TIMP-3 and Elastin. *Circ Res.* 2017;120(1):49-65.
490. Horiuchi K, Kimura T, Miyamoto T, Miyamoto K, Akiyama H, Takaishi H, et al. Conditional inactivation of TACE by a Sox9 promoter leads to osteoporosis and increased granulopoiesis via dysregulation of IL-17 and G-CSF. *Journal of immunology (Baltimore, Md : 1950).* 2009;182(4):2093-2101.
491. Long C, Wang Y, Herrera AH, Horiuchi K, and Walcheck B. In vivo role of leukocyte ADAM17 in the inflammatory and host responses during E. coli-mediated peritonitis. *J Leukoc Biol.* 2010;87(6):1097-1101.
492. Dreymueller D, Martin C, Kogel T, Pruessmeyer J, Hess FM, Horiuchi K, et al. Lung endothelial ADAM17 regulates the acute inflammatory response to lipopolysaccharide. *EMBO Mol Med.* 2012;4(5):412-423.
493. Murthy A, Defamie V, Smookler DS, Di Grappa MA, Horiuchi K, Federici M, et al. Ectodomain shedding of EGFR ligands and TNFR1 dictates hepatocyte apoptosis during fulminant hepatitis in mice. *J Clin Invest.* 2010;120(8):2731-2744.
494. La Marca R, Cerri F, Horiuchi K, Bachi A, Feltri ML, Wrabetz L, et al. TACE (ADAM17) inhibits Schwann cell myelination. *Nature neuroscience.* 2011;14(7):857-865.
495. Murthy A, Shao YW, Narala SR, Molyneux SD, Zuniga-Pflucker JC, and Khokha R. Notch activation by the metalloproteinase ADAM17 regulates myeloproliferation and atopic barrier immunity by suppressing epithelial cytokine synthesis. *Immunity.* 2012;36(1):105-119.
496. Franzke CW, Cobzaru C, Triantafyllopoulou A, Loffek S, Horiuchi K, Threadgill DW, et al. Epidermal ADAM17 maintains the skin barrier by regulating EGFR ligand-dependent terminal keratinocyte differentiation. *The Journal of experimental medicine.* 2012;209(6):1105-1119.
497. Yan F, Liu L, Dempsey PJ, Tsai YH, Raines EW, Wilson CL, et al. A Lactobacillus rhamnosus GG-derived soluble protein, p40, stimulates ligand release from intestinal epithelial cells to transactivate epidermal growth factor receptor. *The Journal of biological chemistry.* 2013;288(42):30742-30751.
498. Ardito CM, Gruner BM, Takeuchi KK, Lubeseder-Martellato C, Teichmann N, Mazur PK, et al. EGF receptor is required for KRAS-induced pancreatic tumorigenesis. *Cancer cell.* 2012;22(3):304-317.
499. Xu W, Liu C, Kaartinen V, Chen H, Lu CH, Zhang W, et al. TACE in perinatal mouse lung epithelial cells promotes lung saccular formation. *Am J Physiol Lung Cell Mol Physiol.* 2013;305(12):L953-963.
500. Gravano DM, McLelland BT, Horiuchi K, and Manilay JO. ADAM17 deletion in thymic epithelial cells alters aire expression without affecting T cell developmental progression. *PLoS One.* 2010;5(10):e13528.
501. Kwok HF, Botkjaer KA, Tape CJ, Huang Y, McCafferty J, and Murphy G. Development of a 'mouse and human cross-reactive' affinity-matured exosite inhibitory human antibody specific to TACE (ADAM17) for cancer immunotherapy. *Protein Eng Des Sel.* 2014;27(6):179-190.
502. Caiazza F, McGowan PM, Mullooly M, Murray A, Synnott N, O'Donovan N, et al. Targeting ADAM-17 with an inhibitory monoclonal antibody has antitumour effects in triple-negative breast cancer cells. *Br J Cancer.* 2015;112(12):1895-1903.
503. Haddad G, Zhabyeyev P, Farhan M, Zhu LF, Kassiri Z, Rayner DC, et al. Phosphoinositide 3-kinase beta mediates microvascular endothelial repair of thrombotic microangiopathy. *Blood.* 2014;124(13):2142-2149.
504. Joseph C, Quach JM, Walkley CR, Lane SW, Lo Celso C, and Purton LE. Deciphering Hematopoietic Stem Cells in Their Niches: A Critical Appraisal of Genetic Models, Lineage Tracing, and Imaging Strategies. *Cell stem cell.* 2013;13(5):520-533.
505. Tang YF, Harrington A, Yang XH, Friesel RE, and Liaw L. The Contribution of the Tie2(+) Lineage to Primitive and Definitive Hematopoietic Cells. *Genesis.* 2010;48(9):563-567.
506. Van Vliet BN, Chafe LL, Antic V, Schnyder-Candrian S, and Montani JP. Direct and indirect methods used to study arterial blood pressure. *Journal of pharmacological and toxicological methods.* 2000;44(2):361-373.
507. Basu R, Lee J, Morton JS, Takawale A, Fan D, Kandalam V, et al. TIMP3 is the primary TIMP to regulate agonist-induced vascular remodelling and hypertension. *Cardiovascular research.* 2013;98(3):360-371.
508. Shankman LS, Gomez D, Cherepanova OA, Salmon M, Alencar GF, Haskins RM, et al. KLF4-dependent phenotypic modulation of smooth muscle cells has a key role in atherosclerotic plaque pathogenesis. *Nat Med.* 2015;21(6):628-637.
509. Kirschenlohr HL, Metcalfe JC, and Grainger DJ. Cultures of proliferating vascular smooth muscle cells from adult human aorta. *Methods Mol Med.* 1996;2:319-334.

510. Liang CC, Park AY, and Guan JL. In vitro scratch assay: a convenient and inexpensive method for analysis of cell migration in vitro. *Nature protocols.* 2007;2(2):329-333.
511. Egan BM, Li J, Hutchison FN, and Ferdinand KC. Hypertension in the United States, 1999 to 2012: progress toward Healthy People 2020 goals. *Circulation.* 2014;130(19):1692-1699.
512. Kanaide H, Ichiki T, Nishimura J, and Hirano K. Cellular mechanism of vasoconstriction induced by angiotensin II: it remains to be determined. *Circ Res.* 2003;93(11):1015-1017.
513. Touyz RM, and Schiffrin EL. Signal transduction mechanisms mediating the physiological and pathophysiological actions of angiotensin II in vascular smooth muscle cells. *Pharmacol Rev.* 2000;52(4):639-672.
514. Ushio-Fukai M, Zuo L, Ikeda S, Tojo T, Patrushev NA, and Alexander RW. cAbl tyrosine kinase mediates reactive oxygen species- and caveolin-dependent AT1 receptor signaling in vascular smooth muscle: role in vascular hypertrophy. *Circ Res.* 2005;97(8):829-836.
515. Eguchi S, Numaguchi K, Iwasaki H, Matsumoto T, Yamakawa T, Utsunomiya H, et al. Calcium-dependent epidermal growth factor receptor transactivation mediates the angiotensin II-induced mitogen-activated protein kinase activation in vascular smooth muscle cells. *The Journal of biological chemistry.* 1998;273(15):8890-8896.
516. Harris RC, Chung E, and Coffey RJ. EGF receptor ligands. *Experimental cell research.* 2003;284(1):2-13.
517. Gooz M. ADAM-17: the enzyme that does it all. *Critical reviews in biochemistry and molecular biology.* 2010;45(2):146-169.
518. Van Vliet BN, Chafe LL, Antic V, Schnyder-Candrian S, and Montani JP. Direct and indirect methods used to study arterial blood pressure. *J Pharmacol Toxicol.* 2000;44(2):361-373.
519. Kirschenlohr HL, Metcalfe JC, and Grainger DJ. Cultures of proliferating vascular smooth muscle cells from adult human aorta. *Human Cell Culture Protocols.* 1996:319-334.
520. Wang Z, Famulski K, Lee J, Das SK, Wang X, Halloran P, et al. TIMP2 and TIMP3 have divergent roles in early renal tubulointerstitial injury. *Kidney Int.* 2013.
521. Eguchi S, Dempsey PJ, Frank GD, Motley ED, and Inagami T. Activation of MAPKs by Angiotensin II in Vascular Smooth Muscle Cells Metalloprotease-dependent EGF receptor activation is required for activation of ERK and p38 MAPK but not for JNK. *Journal of Biological Chemistry.* 2001;276(11):7957-7962.
522. Saito Y, and Berk BC. Transactivation: a novel signaling pathway from angiotensin II to tyrosine kinase receptors. *Journal of molecular and cellular cardiology.* 2001;33(1):3-7.
523. Reynolds CM, Eguchi S, Frank GD, and Motley ED. Signaling mechanisms of heparin-binding epidermal growth factor-like growth factor in vascular smooth muscle cells. *Hypertension (Dallas, Tex : 1979).* 2002;39(2 Pt 2):525-529.
524. Prenzel N, Zwick E, Daub H, Leserer M, Abraham R, Wallasch C, et al. EGF receptor transactivation by G-protein-coupled receptors requires metalloproteinase cleavage of proHB-EGF. *Nature.* 1999;402(6764):884-888.
525. Mifune M, Ohtsu H, Suzuki H, Nakashima H, Brailoiu E, Dun NJ, et al. G protein coupling and second messenger generation are indispensable for metalloprotease-dependent, heparin-binding epidermal growth factor shedding through angiotensin II type-1 receptor. *The Journal of biological chemistry.* 2005;280(28):26592-26599.
526. Elliott KJ, Bourne AM, Takayanagi T, Takaguri A, Kobayashi T, Eguchi K, et al. ADAM17 silencing by adenovirus encoding miRNA-embedded siRNA revealed essential signal transduction by angiotensin II in vascular smooth muscle cells. *Journal of molecular and cellular cardiology.* 2013;62:1-7.
527. Global Health Statistics. Aortic Aneurysm: International Statistics on Mortality and Affected Populations. http://global-diseases.healthgrove.com/l/130/Aortic-Aneurysm#Global%20Impact&s=31QBqf. Accessed January 18, 2018.
528. Hiratzka LF, Bakris GL, Beckman JA, Bersin RM, Carr VF, Casey DE, Jr., et al. 2010 ACCF/AHA/AATS/ACR/ASA/SCA/SCAI/SIR/STS/SVM Guidelines for the diagnosis and management of patients with thoracic aortic disease. A Report of the American College of Cardiology Foundation/American Heart Association Task Force on Practice Guidelines, American Association for Thoracic Surgery, American College of Radiology,American Stroke Association, Society of Cardiovascular Anesthesiologists, Society for Cardiovascular Angiography and Interventions, Society of Interventional Radiology, Society of Thoracic Surgeons,and Society for Vascular Medicine. *J Am Coll Cardiol.* 2010;55(14):e27-e129.
529. Clouse WD, Hallett JW, Jr., Schaff HV, Gayari MM, Ilstrup DM, and Melton LJ, 3rd. Improved prognosis of thoracic aortic aneurysms: a population-based study. *Jama.* 1998;280(22):1926-1929.
530. Ruddy JM, Jones JA, Spinale FG, and Ikonomidis JS. Regional heterogeneity within the aorta: relevance to aneurysm disease. *J Thorac Cardiovasc Surg.* 2008;136(5):1123-1130.
531. Menghini R, Fiorentino L, Casagrande V, Lauro R, and Federici M. The role of ADAM17 in metabolic inflammation. *Atherosclerosis.* 2013;228(1):12-17.

532. White JV, Haas K, Phillips S, and Comerota AJ. Adventitial elastolysis is a primary event in aneurysm formation. *Journal of vascular surgery.* 1993;17(2):371-380; discussion 380-371.
533. Forde A, Constien R, Grone HJ, Hammerling G, and Arnold B. Temporal Cre-mediated recombination exclusively in endothelial cells using Tie2 regulatory elements. *Genesis.* 2002;33(4):191-197.
534. Moore L, Fan D, Basu R, Kandalam V, and Kassiri Z. Tissue inhibitor of metalloproteinases (TIMPs) in heart failure. *Heart Fail Rev.* 2012;17(4-5):693-706.
535. Pisano C, Balistreri CR, Ricasoli A, and Ruvolo G. Cardiovascular Disease in Ageing: An Overview on Thoracic Aortic Aneurysm as an Emerging Inflammatory Disease. *Mediators Inflamm.* 2017;2017:1274034.
536. Son BK, Sawaki D, Tomida S, Fujita D, Aizawa K, Aoki H, et al. Granulocyte macrophage colony-stimulating factor is required for aortic dissection/intramural haematoma. *Nat Commun.* 2015;6:6994.
537. Babamusta F, Rateri DL, Moorleghen JJ, Howatt DA, Li XA, and Daugherty A. Angiotensin II infusion induces site-specific intra-laminar hemorrhage in macrophage colony-stimulating factor-deficient mice. *Atherosclerosis.* 2006;186(2):282-290.
538. Mao N, Gu T, Shi E, Zhang G, Yu L, and Wang C. Phenotypic switching of vascular smooth muscle cells in animal model of rat thoracic aortic aneurysm. *Interactive cardiovascular and thoracic surgery.* 2015;21(1):62-70.
539. Ailawadi G, Moehle CW, Pei H, Walton SP, Yang Z, Kron IL, et al. Smooth muscle phenotypic modulation is an early event in aortic aneurysms. *J Thorac Cardiovasc Surg.* 2009;138(6):1392-1399.
540. Wang L, Zhang J, Fu W, Guo D, Jiang J, and Wang Y. Association of smooth muscle cell phenotypes with extracellular matrix disorders in thoracic aortic dissection. *Journal of vascular surgery.* 2012;56(6):1698-1709, 1709 e1691.
541. Doring Y, Noels H, van der Vorst EPC, Neideck C, Egea V, Drechsler M, et al. Vascular CXCR4 Limits Atherosclerosis by Maintaining Arterial Integrity: Evidence From Mouse and Human Studies. *Circulation.* 2017;136(4):388-403.
542. Bazzoni G, and Dejana E. Endothelial cell-to-cell junctions: molecular organization and role in vascular homeostasis. *Physiol Rev.* 2004;84(3):869-901.
543. Vestweber D. VE-cadherin: the major endothelial adhesion molecule controlling cellular junctions and blood vessel formation. *Arterioscler Thromb Vasc Biol.* 2008;28(2):223-232.
544. Sukriti S, Tauseef M, Yazbeck P, and Mehta D. Mechanisms regulating endothelial permeability. *Pulm Circ.* 2014;4(4):535-551.
545. Blomkalns AL, Gavrila D, Thomas M, Neltner BS, Blanco VM, Benjamin SB, et al. CD14 directs adventitial macrophage precursor recruitment: role in early abdominal aortic aneurysm formation. *Journal of the American Heart Association.* 2013;2(2):e000065.
546. Alexander MR, and Owens GK. Epigenetic control of smooth muscle cell differentiation and phenotypic switching in vascular development and disease. *Annu Rev Physiol.* 2012;74:13-40.
547. Prakash SK, LeMaire SA, Guo DC, Russell L, Regalado ES, Golabbakhsh H, et al. Rare copy number variants disrupt genes regulating vascular smooth muscle cell adhesion and contractility in sporadic thoracic aortic aneurysms and dissections. *American journal of human genetics.* 2010;87(6):743-756.
548. Lv X, Li Y, Qian M, Ma C, Jing H, Wen Z, et al. ADAM17 silencing suppresses the migration and invasion of non-small cell lung cancer. *Molecular medicine reports.* 2014;9(5):1935-1940.
549. Carter SL, Muller M, Manders PM, and Campbell IL. Induction of the genes for Cxcl9 and Cxcl10 is dependent on IFN-gamma but shows differential cellular expression in experimental autoimmune encephalomyelitis and by astrocytes and microglia in vitro. *Glia.* 2007;55(16):1728-1739.
550. Adair-Kirk TL, and Senior RM. Fragments of extracellular matrix as mediators of inflammation. *Int J Biochem Cell Biol.* 2008;40(6-7):1101-1110.
551. Maiellaro K, and Taylor WR. The role of the adventitia in vascular inflammation. *Cardiovascular research.* 2007;75(4):640-648.
552. Benigni A, Cassis P, and Remuzzi G. Angiotensin II revisited: new roles in inflammation, immunology and aging. *EMBO Mol Med.* 2010;2(7):247-257.
553. McMaster WG, Kirabo A, Madhur MS, and Harrison DG. Inflammation, immunity, and hypertensive end-organ damage. *Circ Res.* 2015;116(6):1022-1033.
554. Rudemiller NP, and Crowley SD. Interactions Between the Immune and the Renin-Angiotensin Systems in Hypertension. *Hypertension.* 2016;68(2):289-296.
555. Guzik TJ, Hoch NE, Brown KA, McCann LA, Rahman A, Dikalov S, et al. Role of the T cell in the genesis of angiotensin II induced hypertension and vascular dysfunction. *The Journal of experimental medicine.* 2007;204(10):2449-2460.

556. Marvar PJ, Thabet SR, Guzik TJ, Lob HE, McCann LA, Weyand C, et al. Central and peripheral mechanisms of T-lymphocyte activation and vascular inflammation produced by angiotensin II-induced hypertension. *Circ Res.* 2010;107(2):263-270.
557. Wenzel P, Knorr M, Kossmann S, Stratmann J, Hausding M, Schuhmacher S, et al. Lysozyme M-positive monocytes mediate angiotensin II-induced arterial hypertension and vascular dysfunction. *Circulation.* 2011;124(12):1370-1381.
558. Eguchi S, Iwasaki H, Ueno H, Frank GD, Motley ED, Eguchi K, et al. Intracellular signaling of angiotensin II-induced p70 S6 kinase phosphorylation at Ser(411) in vascular smooth muscle cells. Possible requirement of epidermal growth factor receptor, Ras, extracellular signal-regulated kinase, and Akt. *The Journal of biological chemistry.* 1999;274(52):36843-36851.
559. Eguchi S, Dempsey PJ, Frank GD, Motley ED, and Inagami T. Activation of MAPKs by angiotensin II in vascular smooth muscle cells. Metalloprotease-dependent EGF receptor activation is required for activation of ERK and p38 MAPK but not for JNK. *The Journal of biological chemistry.* 2001;276(11):7957-7962.
560. Takayanagi T, Kawai T, Forrester SJ, Obama T, Tsuji T, Fukuda Y, et al. Role of epidermal growth factor receptor and endoplasmic reticulum stress in vascular remodeling induced by angiotensin II. *Hypertension.* 2015;65(6):1349-1355.
561. Sriramula S, Haque M, Majid DS, and Francis J. Involvement of tumor necrosis factor-alpha in angiotensin II-mediated effects on salt appetite, hypertension, and cardiac hypertrophy. *Hypertension.* 2008;51(5):1345-1351.
562. Patel VB, Clarke N, Wang Z, Fan D, Parajuli N, Basu R, et al. Angiotensin II induced proteolytic cleavage of myocardial ACE2 is mediated by TACE/ADAM-17: a positive feedback mechanism in the RAS. *Journal of molecular and cellular cardiology.* 2014;66:167-176.
563. Wang W, McKinnie SM, Farhan M, Paul M, McDonald T, McLean B, et al. Angiotensin-Converting Enzyme 2 Metabolizes and Partially Inactivates Pyr-Apelin-13 and Apelin-17: Physiological Effects in the Cardiovascular System. *Hypertension.* 2016;68(2):365-377.
564. Cherepanova OA, Gomez D, Shankman LS, Swiatlowska P, Williams J, Sarmento OF, et al. Activation of the pluripotency factor OCT4 in smooth muscle cells is atheroprotective. *Nat Med.* 2016;22(6):657-665.
565. van der Vorst EP, Jeurissen M, Wolfs IM, Keijbeck A, Theodorou K, Wijnands E, et al. Myeloid A disintegrin and metalloproteinase domain 10 deficiency modulates atherosclerotic plaque composition by shifting the balance from inflammation toward fibrosis. *The American journal of pathology.* 2015;185(4):1145-1155.
566. Forrester SJ, Kawai T, O'Brien S, Thomas W, Harris RC, and Eguchi S. Epidermal Growth Factor Receptor Transactivation: Mechanisms, Pathophysiology, and Potential Therapies in the Cardiovascular System. *Annu Rev Pharmacol Toxicol.* 2016;56:627-653.
567. Poduri A, Rateri DL, Howatt DA, Balakrishnan A, Moorleghen JJ, Cassis LA, et al. Fibroblast Angiotensin II Type 1a Receptors Contribute to Angiotensin II-Induced Medial Hyperplasia in the Ascending Aorta. *Arterioscler Thromb Vasc Biol.* 2015;35(9):1995-2002.
568. Tieu BC, Ju X, Lee C, Sun H, Lejeune W, Recinos A, 3rd, et al. Aortic adventitial fibroblasts participate in angiotensin-induced vascular wall inflammation and remodeling. *J Vasc Res.* 2011;48(3):261-272.
569. Cerutti C, and Ridley AJ. Endothelial cell-cell adhesion and signaling. *Experimental cell research.* 2017;358(1):31-38.
570. Reglero-Real N, Colom B, Bodkin JV, and Nourshargh S. Endothelial Cell Junctional Adhesion Molecules: Role and Regulation of Expression in Inflammation. *Arterioscler Thromb Vasc Biol.* 2016;36(10):2048-2057.
571. Gavard J. Endothelial permeability and VE-cadherin: a wacky comradeship. *Cell Adh Migr.* 2013;7(6):455-461.
572. Yao L, Romero MJ, Toque HA, Yang G, Caldwell RB, and Caldwell RW. The role of RhoA/Rho kinase pathway in endothelial dysfunction. *J Cardiovasc Dis Res.* 2010;1(4):165-170.
573. Isselbacher EM. Thoracic and abdominal aortic aneurysms. *Circulation.* 2005;111(6):816-828.
574. Nordon IM, Hinchliffe RJ, Loftus IM, and Thompson MM. Pathophysiology and epidemiology of abdominal aortic aneurysms. *Nature reviews Cardiology.* 2011;8(2):92-102.
575. Li L, Miano JM, Cserjesi P, and Olson EN. SM22 alpha, a marker of adult smooth muscle, is expressed in multiple myogenic lineages during embryogenesis. *Circ Res.* 1996;78(2):188-195.
576. Li L, Miano JM, Mercer B, and Olson EN. Expression of the SM22alpha promoter in transgenic mice provides evidence for distinct transcriptional regulatory programs in vascular and visceral smooth muscle cells. *The Journal of cell biology.* 1996;132(5):849-859.
577. Basford JE, Moore ZW, Zhou L, Herz J, and Hui DY. Smooth muscle LDL receptor-related protein-1 inactivation reduces vascular reactivity and promotes injury-induced neointima formation. *Arterioscler Thromb Vasc Biol.* 2009;29(11):1772-1778.

578. Calvier L, Chouvarine P, Legchenko E, Hoffmann N, Geldner J, Borchert P, et al. PPARgamma Links BMP2 and TGFbeta1 Pathways in Vascular Smooth Muscle Cells, Regulating Cell Proliferation and Glucose Metabolism. *Cell Metab.* 2017;25(5):1118-1134.e1117.
579. Regan CP, Adam PJ, Madsen CS, and Owens GK. Molecular mechanisms of decreased smooth muscle differentiation marker expression after vascular injury. *J Clin Invest.* 2000;106(9):1139-1147.
580. Wamhoff BR, Hoofnagle MH, Burns A, Sinha S, McDonald OG, and Owens GK. A G/C element mediates repression of the SM22alpha promoter within phenotypically modulated smooth muscle cells in experimental atherosclerosis. *Circ Res.* 2004;95(10):981-988.
581. Majesky MW, Horita H, Ostriker A, Lu S, Regan JN, Bagchi A, et al. Differentiated Smooth Muscle Cells Generate a Subpopulation of Resident Vascular Progenitor Cells in the Adventitia Regulated by Klf4. *Circ Res.* 2017;120(2):296-311.
582. Chen XH, Ruan CC, Ge Q, Ma Y, Xu JZ, Zhang ZB, et al. Deficiency of Complement C3a and C5a Receptors Prevents Angiotensin II-Induced Hypertension via Regulatory T Cells. *Circ Res.* 2018;122(7):970-983.